UNIVERSITY OF
KWAZULU-NATAL

INYUVESI
YAKWAZULU-NATALI

Mycobacterium tuberculosis pili (MTP) modulates pathogen and host metabolomic changes in an A549 epithelial cell model of infection

KAJAL SOULAKSHANA REEDOY

Submitted in fulfilment of the requirements for the degree of
Masters in Medical Science (Medical Microbiology)

Discipline of Medical Microbiology
School of Laboratory Medicine and Medical Sciences
College of Health Sciences
University of KwaZulu-Natal
South Africa

2020

MANUSCRIPT AND PLAGIARISM DECLARATION

This Masters Dissertation consists of 2 manuscripts that are ready for submission. Author contributions are stipulated below.

Manuscript 1: Ashokcoomar, S*., Reedoy, K. S*., Senzani, S., Loots, D. T., Beukes, D., van Reenen, M., Pillay, B. and Pillay, M. *Mycobacterium tuberculosis* curli pili (MTP) deficiency is associated with alterations in cell wall biogenesis, fatty acid metabolism and amino acid synthesis**.**

*****Joint co-authors; submitted as Chapter 2 of respective Masters Dissertations.

Author contribution: MP conceptualized the study. MP, BP and DTL designed the study. SA and KSR contributed equally to the study, conducted experiments, analysed the data and drafted the manuscript. DB processed the samples and performed GCxGC-TOFMS. MVR conducted statistical bioinformatic analyses. SS provided RT-qPCR guidance and analytical support. All authors contributed to and approved the manuscript.

Manuscript 2: Reedoy, K. S., Loots, D. T., Beukes, D., van Reenen, M., Pillay, B., and Pillay, M. *Mycobacterium tuberculosis* curli pili (MTP) is associated with significant host metabolic pathways in an A549 epithelial cell infection model and contributes to the pathogenicity of *M. tuberculosis.*

Author contribution: MP conceptualised the study. MP, BP and DTL designed the study. KSR conducted experiments, analysed and interpreted the data, and drafted the manuscript. DB processed the samples and performed GCxGC-TOFMS. MVR conducted statistical bioinformatic analyses. All authors contributed to and approved the manuscript.

I, Kajal Soulakshana Reedoy, declare that the work presented hereby has not been submitted to the University of KwaZulu-Natal or any other university for the obtainment of an academic qualification. Any work performed by individuals other than myself has been duly acknowledged and referenced in this dissertation.

_____ _____

Kajal Soulakshana Reedoy Date

As the candidate's supervisor, and co-supervisor, we agree with all aspects of this Masters submission.

_____ _____

Supervisor: Professor Manormoney Pillay Date

_____ _____

Co-supervisor: Professor Balakrishna Pillay Date

PRESENTATIONS

School of Laboratory Medicine and Medical Sciences Research Day, Durban, South Africa.

6 September 2019

M. tuberculosis pili (MTP) modulates pathogen and host metabolomic changes in an A549 epithelial cell model of infection.

Oral presentation - 2nd place

DEDICATION

For my family, Krish, Devi and Akaash Reedoy

ACKNOWLEDGEMENTS

A heartfelt thank you goes out to my supervisor and co-supervisor, Professor Manormoney Pillay and Professor Balakrishna Pillay for your constant motivation, careful prioritisation and sound critique on every aspect of this project. I am truly grateful for your patience and support.

To our collaborators at North-West University, Professor Du Toit Loots, Ms. Mari van Reenen and Ms. Derylize Beukes, your warm approach and expert contributions are greatly appreciated. It was a pleasure working with your team.

I would like to thank the National Research Foundation (Grantholder-linked) and the UKZN College of Health Sciences for the bursary awards.

To my mentors and colleagues at Medical Microbiology, thank you for the laboratory training, imparting of scientific skills and techniques, and the countless words of wisdom. A special thank you goes out to Dr Sibusiso Senzani, Deepika Moti, Anisha Balgobin, Kimona Rampersadh, Sanisha Muniram, Dr Bestinee Naidoo and Tashmin Rampersad.

A sincere token of gratitude goes to my parents, Krish and Devi Reedoy, and my brother, Akaash Reedoy for your never-ending support, sacrifices and encouragement. To Karmen Naidoo, Shinese Ashokcoomar, Jenine Ramruthan, Tarien Naidoo and Nevlin Manicum, thank you for being my anchors.

Lastly and most importantly, I would like to thank God and the universe for always giving me the strength and determination, together with the limitless blessings, in completing my Masters degree.

TABLE OF CONTENTS

MANUSCRIPT AND PLAGIARISM DECLARATION i

PRESENTATIONS ii

DEDICATION iii

ACKNOWLEDGEMENTS iv

LIST OF TABLES viii

LIST OF FIGURES ix

LIST OF ABBREVIATIONS x

ABSTRACT xii

INTRODUCTION xv

Chapter 1: LITERATURE REVIEW 1

1.1 Epidemiology of TB 1
1.2 Drug resistance 2
1.3 General characteristics of *M. tuberculosis* 3

1.3.1 Lineages and strains of *M. tuberculosis* 4
1.3.2 *Mycobacterium tuberculosis* pathogenesis 4
1.3.3 Cell wall components 5

1.4 *Mycobacterium tuberculosis* adhesins 6
1.5 *Mycobacterium tuberculosis* curli pili identification and characterisation 7
1.6 The MTP adhesin as a potential diagnostic target 8
1.7 A459 epithelial cells 8

1.7.1 A549 cell identification and characterisation 8
1.7.2 The A549 epithelial cells and infection with M. tuberculosis 8

1.8 Functional genomics 9
1.9 Metabolomics 9

1.9.1 Techniques used in metabolomics 10
1.9.2 Applications of metabolomics 10
1.9.3 Metabolomic profiling and biomarker identification 11

1.10 Significance of work 12
1.11 References 13

Chapter 2: MANUSCRIPT 1 22

2.1 Abstract 22
2.2 Introduction 23
2.3 Materials and methods 25

2.3.1 Ethical Approval 25
2.3.2 Bacterial strains and culture conditions 25
2.3.3 Sample preparation 25
2.3.4 Sample extraction and derivatization 26
2.3.5 GCxGC-TOFMS analysis 26
2.3.6 Statistical data analysis 27
2.3.7 RT-qPCR validation of metabolomics data 29

2.4 Results 30
2.4.1 Statistical and practical significance of univariate results graphically represented in the volcano plot shows numerous metabolites with the ability to differentiate between groups. 30
2.4.2 PLS-DA data produced group separation amongst WT, Δ*mtp* and *mtp*-complement thereby confirming model validation 31
2.4.3 Spearman Correlation Plots show less correlation between WT and Δ*mtp*, and more correlation between WT and *mtp*-complement 32
2.4.4 Four selection criteria were used to tabulate biologically significant metabolites between WT and Δ*mtp* (Table 2.2), and between WT and *mtp*-complement (Table 2.3) 34
2.4.5 Gene expression data significantly correlates with metabolomics data 38
2.5 Discussion 38
2.5.1 The role of MTP and carbohydrates for cell wall biogenesis in *M. tuberculosis* 39
2.5.2 The role of MTP and the utilisation of fatty acids by *M. tuberculosis* 40
2.5.3 The role of MTP in amino acid and protein synthesis in *M. tuberculosis* 42
2.5.4 The role of MTP in peptidoglycan synthesis in *M. tuberculosis* 44
2.5.5 Complementation with *mtp* restoration 44
2.5.6 Functional analysis using RT-qPCR support metabolomics results 46
2.6 Conclusion 48
2.7 References 49
Chapter 3: MANUSCRIPT 2 56
3.1 Abstract 56
3.2 Introduction 57
3.3 Materials and methods 59
3.3.1 Ethical Approval 59
3.3.2 Bacterial strains and culture conditions 59
3.3.3 Culture and infection of A549 epithelial cells 59
3.3.4 Sample extraction and derivatization 60
3.3.5 GCxGC-TOFMS analysis 61
3.3.6 Statistical data analysis 61
3.4 Results 63
3.4.1 Volcano plots showing distribution of univariate data with the best spread of metabolites depicted in the WT-infected and Δ*mtp*-infected A549 cell model 63
3.4.2 PCA data revealed partial overlap across four models while complete group separation validated the WT-infected and Δ*mtp*-infected A549 epithelial cell statistical model 65
3.4.3 PLS-DA data revealed complete group separation between the WT-infected A549 cells and Δ*mtp*-infected A549 cells further confirming model validation 67
3.4.4 Biologically significant metabolites that met the selection criteria between WT-infected cells and Δ*mtp*-infected cells 68
3.5 Discussion 72
3.5.1 MTP and nucleic acid metabolism during *M. tuberculosis* infection 73
3.5.2 MTP and amino acid metabolism during *M. tuberculosis* infection. 74
3.5.3 MTP and glutathione metabolism during *M. tuberculosis* infection. 76
3.5.4 MTP and oxidative stress during *M. tuberculosis* infection 76
3.5.5 MTP and lipid metabolism during *M. tuberculosis* infection. 77
3.5.6 Implication of lanthionine detection in potential peptidoglycan anomaly 78
3.6 Conclusion 79

3.7 References 80
Chapter 4: SYNTHESIS OF RESEARCH FINDINGS 87
4.1 Review of the biomarker potential of MTP adhesin 87
4.2 Chapter 2: Manuscript 1 Synthesis 88
4.3 Chapter 2: Manuscript 1 Synthesis 89
4.4 Comparison of bacterial model and host-infection model 90
4.5 Limitations of the study 90
4.6 Recommendations for future research 91
4.7 Conclusion 92
4.8 References 92
Chapter 5: APPENDICES 94
Appendix A: BREC Approval 94
Appendix B: Media, solutions and reagents 95
Appendix C: Chapter 2 Supplementary Material 97
Appendix D: Chapter 3 Supplementary Material 112
Appendix E: Turnitin Reports 126

LIST OF TABLES

Table 2.1 Gene and primer sequences selected for gene expression analysis using RT-qPCR 30

Table 2.2 Most significant metabolites between *M. tuberculosis* WT and Δ*mtp* strains selected as per multivariate and univariate selection criteria together with their respective mean relative concentration and standard deviation, fold change with respect to the WT, PLS-DA VIP value, Cohen's d-value and BH-adjusted *p*-value 35

Table 2.3 Most significant metabolites between *M. tuberculosis* WT and Δ*mtp*-complemented strains selected as per multivariate and univariate selection criteria together with their respective mean relative concentration and standard deviation, fold change with respect to the WT, PLS-DA VIP value, Cohen's d-value and BH-adjusted *p*-value 36

Table 3.1 Most significant metabolites between WT-infected and Δ*mtp*-infected A549 epithelial cells selected as per multivariate and univariate selection criteria together with their respective mean relative concentration and standard deviation, fold change with respect to the WT, PLS-DA VIP value, Cohen's d-value and BH adjusted *p*-values from the independent samples *t*-test 70

LIST OF FIGURES

Figure 1.1 Estimated global TB incidence rates in 2018 (WHO, 2019). 1
Figure 1.2 Estimated global case fatality ratios (CFR) in 2018 (WHO, 2019). 2
Figure 1.3 Structural components of the mycobacterial cell wall (Brown et al., 2015). 6
Figure 2.1 Flow diagram depicting statistical workflow for data analysis including cut-off values used as selection criteria for shortlisting of metabolites. 28
Figure 2.2 Volcano plots showing scatter of metabolites for the (a) wild-type and Δ*mtp*, and (b) wild-type and *mtp*-complement. 30
Figure 2.3 A PLS-DA scores plot comparing the three bacterial strains highlight the variation associated with genotype. 30
Figure 2.4 Spearman Correlation Plots comparing the bacterial strains. 33
Figure 2.5 The validation of metabolomics data using RT-qPCR to assess gene expression of five genes (*glf, glmU, fadD32, fadE5* and *glpK*). 38
Figure 3.1 Volcano plots showing univariate spread of metabolites across *M. tuberculosis*-infected and uninfected A549 epithelial cell models. 64
Figure 3.2 Three-dimensional PCA scores plots for *M. tuberculosis*-infected and uninfected A549 epithelial cell models 66
Figure 3.3 A three-dimensional PLS-DA scores plot comparing the WT-infected A549 cells and Δ*mtp*-infected A549 cells 67

LIST OF ABBREVIATIONS

Abbreviation	Full name
ABC	Adenosine triphosphate-binding cassette
AIDS	Acquired Immunodeficiency Syndrome
APA	Alanine-proline-rich antigen
ATP	Adenosine triphosphate
BCG	Bacille Calmette Guerin
BH	Benjamini and Hochberg
cDNA	Complementary deoxyribonucleic acid
CFR	Case fatality ratio
CI	Confidence Interval
Cpn60.2	Chaperone protein 60.2
CTAB	Cetyl trimethylammonium bromide
DNA	Deoxyribonucleic acid
ES	Effective size
FBS	Fetal bovine serum
FC	Fold change
GABA	Gamma-aminobutyric acid
GCxGC-TOFMS	Two-dimensional gas chromatography time-of-flight mass spectrometry
GC	Gas chromatography
HBHA	Haemagglutinin adhesin
HIV	Human Immunodeficiency Virus
IFNγ	Interferon gamma
IgG	Immunoglobulin
kDa	Kilo Dalton
KEGG	Kyoto Encyclopedia of Genes and Genome
KZN	KwaZulu-Natal
LAM	Latin-American Mediterranean
LC	Liquid chromatography
LCP-MRM/MS	Liquid chromatography-mass spectrometric multiple reactions monitoring
LV	Latent variables
mAGP	Mycolic acid-arabinogalactan-peptidoglycan
MAIS	*Mycobacterium avium-Mycobacterium intracellulare-Mycobacerium scrofulaceum* complex
MDR	Multidrug-resistant
MDR/RR-TB	Multidrug-resistant or rifampicin-resistant tuberculosis

MS	Mass spectrometry
MTA	5'-Methylthioadenosine
MTBC	*M. tuberculosis* complex
MTP	*M. tuberculosis* curli pili
NMR	Nuclear magnetic resonance
OADC	Oleic acid-albumin-dextrose-catalase
OD	Optical density
PBS	Phosphate buffered saline
PCA	Principal Component Analysis
PIM	Phosphatidyl-myo-inositol mannoside
PLS-DA	Partial Least Squares Discriminant Analysis
QC	Quality control
RNA	Ribonucleic acid
RT-qPCR	Real-time quantitative polymerase chain reaction
TB	Tuberculosis
TDR	Totally drug-resistant
TEM	Transmission electron microscopy
tRNA	Transcriptional ribonucleic acid
VIP	Variable importance in projection
WHO	World Health Organization
WT	Wild-type
XDR	Extensively drug-resistant

ABSTRACT

Background/Aim: *Mycobacterium tuberculosis*, the causative organism of tuberculosis, continues to drive research efforts in the quest to develop novel diagnostics and therapeutics. The complexities associated with drug-resistant strains (multidrug-resistant (MDR), extensively drug-resistant (XDR) and totally drug-resistant tuberculosis (TDR-TB)) and co-infection with human immunodeficiency virus/acquired immune deficiency virus (HIV/AIDS) further cripple the fight against tuberculosis (TB). Hence, a comprehensive understanding of the *M. tuberculosis* genome, transcriptome, proteome and metabolome is required to gain different perspectives on potential target points, such as novel biomarkers, for intervention. The *M. tuberculosis* curli pili (MTP), a surface-located adhesin is involved in the first point of contact with the host cell, and has shown diagnostic and therapeutic potential based on previous genomic, transcriptomic and proteomic findings. Understanding the metabolome of *Mycobacterium tuberculosis* and its target host cell during infection will provide further insights into the role of MTP and its metabolic influence. This study aimed to determine the role of MTP in modulating bacterial and host metabolic pathways of *M. tuberculosis* and A549 epithelial cells, respectively, using a two-dimensional gas chromatography time-of-flight mass spectrometry (GCxGC-TOFMS) approach coupled with bioinformatic analyses.

Methods: The wild-type (WT), *mtp* deletion mutant (Δ*mtp*) and *mtp*-complemented strains were confirmed by genomic DNA extraction and PCR. For the pathogen model investigation, ten biological replicates of each of the three strains were individually cultured in supplemented Middlebrook 7H9 broth till an OD_{600} of 1 was reached. Cultures were centrifuged, subjected to a washing procedure and the resulting pellets were stored at - 80 °C. For the infection model investigation, A549 epithelial cells were grown till confluent, and seeded at a concentration of 5×10^5 cells/mL. A549 cells were infected with each *M. tuberculosis* strain at a multiplicity of infection of approximately 5. After the 2 hr infection period, cells underwent a washing procedure and the resulting pellets were stored at - 80°C prior to extraction for GCxGC-TOFMS metabolomic analysis. A whole metabolome extraction method was applied to extract metabolites from various metabolite classes using chloroform:methanol:water (1:3:1). The samples were analysed by GCxGC-TOFMS which underwent first and second dimensional separation. ChromaTOF software, MATLAB software along with the Eigenvector PLS_Toolbox 8.7 were used to identify differentiating metabolites. Parametric univariate analysis included independent samples *t*-test with its associated Cohen's d-value. Correcting for multiple testing was done by the Benjamini & Hochberg (BH) adjustment to control the rate of false discovery. Multivariate analyses included quality assurance based on Principal Component Analysis (PCA) and Partial Least Squares Discriminant Analysis (PLS-DA). Variable Importance in the Projection (VIP) values, BH-adjusted *p*-values, Cohen's d-values and fold changes were considered as criteria for shortlisting metabolites. In order to better understand the metabolomic changes at a transcriptomics level, RT-qPCR was performed

on the bacterial strains. The resulting gene expression data was normalised using 16S rRNA and analysed using the relative standard curve method. GraphPad Prism version 8 software was used to determine significance values.

Results/Discussion: The results from the bacterial model investigation were significant as 27 metabolites were found to be altered in concentration between the *mtp*-deficient cells and the WT, while 7 metabolites were deemed significantly different between the WT and *mtp*-complemented strains. Three of the 4 categories were produced in higher relative concentrations by Δ*mtp*; carbohydrates in cell wall biogenesis, fatty acid metabolism and peptidoglycan synthesis, indicating an overall reduced ability in the utilisation of these metabolites for natural cellular processes in the Δ*mtp* compared to the WT. Metabolites involved in amino acid and protein synthesis were produced in relatively lower concentrations in Δ*mtp*, again suggesting defective pathways in Δ*mtp*. The infection model analysis investigated five different *M. tuberculosis* infection models, of which only one validated. The first three models, which revealed minimal differences, were the infected and uninfected models of comparison to determine whether any significant differences existed in the *M. tuberculosis*-infected A549 cell model compared to the respective uninfected model. There were no major differences between the WT-infected and *mtp*-complement-infected strain showing functional restoration of *mtp*. Significant differences were observed between the WT-infected and Δ*mtp*-infected A549 cells. These included a total of 46 metabolites produced in significantly lower relative concentrations in the Δ*mtp*-infected cells. The deletion of the MTP adhesin led to a perturbation in nucleic acid metabolism, which was found to be less efficient in the Δ*mtp*-infected cells. A similar observation was seen for lysine metabolism and degradation. Nitrogen assimilation was also found to be less prominent in Δ*mtp*-infected cells arising from aspartate, alanine and glutamate metabolism. Metabolites involved in glutathione metabolism, oxidative stress and lipid metabolism were produced in lower relative concentration in Δ*mtp*-infected cells, potentially resulting in a compromised mycobacterial cell envelope in the deletion mutant. Lanthionine was an unusual metabolite detected in the present study. These metabolic alterations were indicative of lowered pathogenicity of the *M. tuberculosis* mutant strain, as a result of the absence of MTP.

Conclusion: The significant findings of this study confirm previous reports that MTP has potential as a biomarker that can be targeted for intervention. The first investigation revealed a total of 27 metabolites to be biologically significant between the Δ*mtp* and WT strains. These were associated with reduced cell wall biogenesis, fatty acid metabolism, amino acid and protein synthesis, and peptidoglycan synthesis. Between the WT and *mtp*-complemented strains, seven metabolites were biologically significant and corresponded with various cell envelope functions. In the second investigation, all 46 metabolites were produced in a relatively lower concentration by the Δ*mtp*-infected cells compared to the WT-infected cells and were associated with a decrease in nucleic acid synthesis,

amino acid metabolism, glutathione metabolism, oxidative stress, lipid metabolism and a peptidoglycan anomaly. The MTP adhesin is associated with various changes to the pathogen and host metabolome, highlighting its importance as a virulence factor that further substantiates its potential as a suitable biomarker for corrective intervention in the fight against TB.

INTRODUCTION

Approximately 1.7 billion people are infected with *Mycobacterium tuberculosis*, the etiological agent of tuberculosis (TB) (WHO, 2019). One of the Sustainable Development Goals for the year 2030 is to end the global TB epidemic (WHO, 2019). Currently, the global TB burden still poses a concern with an incidence of 10.0 million people while 1.2 million Human Immunodeficiency Virus (HIV)-negative people died from TB in 2018, in addition to the 251 000 deaths from those who were HIV-positive (WHO, 2019). South Africa ranks at eighth place in the world with the highest number of TB cases (WHO, 2019). Presently, much effort is focused towards the reduction of TB incidence and death rates with the currently available diagnostic and treatment options (Fogel, 2015). This, however, is a growing challenge owing to the delays in diagnosis/misdiagnosis and late initiation of treatment, emergence of drug resistant strains via chromosomal mutations, and the complexity associated with HIV- co-infections and co-morbidities such as diabetes (Otero et al., 2011; McGrath et al., 2014; Georghiou et al., 2017; Manson et al., 2017; Hameed et al., 2018). Additionally, the administration of incorrect drugs, the lack of effective drugs, or suitable vaccines further heightens these challenges (Hameed et al., 2018).

Research efforts on biomarker discovery aim to elucidate a particular measurable characteristic that is able to differentiate between a normal and pathological state (Wallis and Peppard, 2015). Biomarkers specific to *M. tuberculosis* during infection are detectable in sputum, blood and urine, and have shown better sensitivity than traditional culturing methods to detect pulmonary TB (Cannas et al., 2008; Cruz et al., 2011; Theron et al., 2014). Lipoarabinomannan, a cell wall component of *M. tuberculosis*, has been proposed as a TB biomarker, however it was shown to have poor sensitivity commercially (Minion et al., 2011). The *M. tuberculosis* antigen 85 complex is a group of three proteins (Ag85A, Ag85B and Ag85C) which facilitates binding between the cell wall arabinogalactan and mycolic acids (Ronning et al., 2000), and has also shown biomarker potential although at variable performances (Bentley-Hibbert et al., 1999; Kashyap et al., 2007). A transcriptional biomarker, interferon-gamma (IFNγ) is a popular indicator of TB disease, however, it is mostly indicative of active TB (Berry et al., 2010; Lesho et al., 2011; Maertzdorf et al., 2011). The search for a more robust biomarker is necessary, more importantly to indicate the presence of *M. tuberculosis* before disease progression to an active state (Goletti et al., 2016).

A comprehensive understanding of the pathogen's infectious cycle may provide vital information on potential targets for vaccine and therapeutic intervention (Sudhindra et al., 2011). The infection cycle of *M. tuberculosis* begins with the attachment of the bacterium to the host cell (Sasindran and Torrelles, 2011). The host-microbe interaction is facilitated by microbial cell surface structures, called adhesins, which mediate adherence to surface receptors on the host cell (Bermudez and Goodman, 1996). Govender et al. (2014) highlighted a number of *M. tuberculosis* adhesins significant to its pathogenesis,

namely; heparin-binding haemagglutinin adhesin, malate synthase, 19 kDa lipoprotein, alanine-proline-rich antigen, molecular chaperone protein 60.2, and lastly, *Mycobacterium tuberculosis* curli pili, the focus of the current study.

A major *M. tuberculosis* adhesin is the *Mycobacterium tuberculosis* curli pili (MTP) (Alteri et al., 2007). The MTP functions in the adherence to and invasion of epithelial cells (Ramsugit et al., 2016) and macrophages (Ramsugit and Pillay, 2014), and plays a role in *in vitro* biofilm formation (Ramsugit et al., 2013). A study by Naidoo et al. (2014) found that the *mtp* gene was absent in non-tuberculous mycobacteria and other respiratory organisms but was present in all tested clinical isolates belonging to the MTBC. A recent study investigated the ability of MTP to react with Immunoglobulin G (IgG) in serum or plasma samples from TB patients, including HIV-uninfected and co-infected patients (Naidoo et al., 2018). Using an MTP synthetic peptide in a slot blot assay, anti-MTP IgG antibodies were detected with a 97 % accuracy, confirming the expression of MTP during *M. tuberculosis* infection (Naidoo et al., 2018). Literature thus far suggests that the MTP adhesin could be useful as a biomarker and targeted for the development of rapid point-of-care diagnostics, more effective drugs, vaccines and immunotherapeutics (Naidoo et al., 2014; Naidoo et al., 2018). The role of MTP in TB metabolomics has yet to be investigated to elucidate its role in the regulation of pathogen and host metabolic pathways.

The systems biology approach together with metabolomics, and previously acquired data on genomics, transcriptomics and proteomics, achieves a more comprehensive and holistic view of *M. tuberculosis* and its biological role during pathogenesis (Meissner-Roloff et al., 2012; Swanepoel and Loots, 2014). Metabolomic profiling involves qualitative and quantitative analyses of small metabolites and is a useful tool for biomarker discovery (Zhong et al., 2016). Any change to a biological system will result in a change to the metabolomic profile of that system (Zhong et al., 2016), hence this is a powerful approach that can readily identify altered metabolic pathways and specific biomarkers in an altered/diseased state for early TB diagnosis/therapy (Sudhindra et al., 2011; Lau et al., 2015; Wallis and Peppard, 2015). Various platforms of mass spectrometry coupled to gas chromatography and liquid chromatography have been used to study TB metabolomics (Cha et al., 2009; Bisson et al., 2012; O'Sullivan et al., 2012; Loots et al., 2014; Pal et al., 2018). In particular, two-dimensional gas chromatography time-of-flight mass spectrometry (GCxGC-TOFMS) is a more sensitive technique that has been used in the search for TB biomarkers to better explain the metabolic state attributed to virulence (Meissner-Roloff et al., 2012; du Preez and Loots 2013; Loots et al., 2016).

Hence, the rationale of this study was to use GCxGC-TOFMS to further elucidate the role of MTP in TB pathogenesis by identifying adhesin-specific metabolites related to the pathogen and/or host using *mtp*-proficient, *mtp*-deficient, and complemented strains in an A549 epithelial cell model of infection. The MTP metabolite signatures identified in this study may provide further supporting evidence for this

major adhesin as an important diagnostic biomarker or vaccine candidate. Furthermore, the metabolomics signatures themselves may potentially serve as biomarkers for novel intervention strategies.

References

Alteri, C. J., Xicohténcatl-Cortes, J., Hess, S., Caballero-Olín, G., Girón, J. A. and Friedman, R. L. (2007). *Mycobacterium tuberculosis* produces pili during human infection. *Proceedings of the National Academy of Sciences, 104*(12), 5145-5150.

Bentley-Hibbert, S. I., Quan, X., Newman, T., Huygen, K. and Godfrey, H. P. (1999). Pathophysiology of antigen 85 in patients with active tuberculosis: antigen 85 circulates as complexes with fibronectin and immunoglobulin G. *Infection and Immunity, 67*(2), 581-588.

Bermudez, L. E. and Goodman, J. (1996). *Mycobacterium tuberculosis* invades and replicates within type II alveolar cells. *Infection and Immunity, 64*(4), 1400-1406.

Berry, M. P., Graham, C. M., McNab, F. W., Xu, Z., Bloch, S. A., Oni, T., et al. (2010). An interferon-inducible neutrophil-driven blood transcriptional signature in human tuberculosis. *Nature, 466*(7309), 973.

Bisson, G. P., Mehaffy, C., Broeckling, C., Prenni, J., Rifat, D., Lun, D. S., et al. (2012). Upregulation of the phthiocerol dimycocerosate biosynthetic pathway by rifampin-resistant, rpoB mutant *Mycobacterium tuberculosis*. *Journal of Bacteriology, 194*(23), 6441-6452.

Cannas, A., Goletti, D., Girardi, E., Chiacchio, T., Calvo, L., Cuzzi, G., et al. (2008). *Mycobacterium tuberculosis* DNA detection in soluble fraction of urine from pulmonary tuberculosis patients. *The International Journal of Tuberculosis and Lung Disease, 12*(2), 146-151.

Cha, D., Cheng, D., Liu, M., Zeng, Z., Hu, X. and Guan, W. (2009). Analysis of fatty acids in sputum from patients with pulmonary tuberculosis using gas chromatography-mass spectrometry preceded by solid-phase microextraction and post-derivatization on the fiber. *Journal of Chromatography A, 1216*(9), 1450-1457.

Cruz, H. L. A. D., Montenegro, R. D. A., Lima, J. F. D. A., Poroca, D. D. R., Lima, J. F. D. C., Montenegro, L. M. L., et al. (2011). Evaluation of a nested-PCR for mycobacterium tuberculosis detection in blood and urine samples. *Brazilian Journal of Microbiology, 42*(1), 321-329.

du Preez, I. and Loots, D. T. (2013). New sputum metabolite markers implicating adaptations of the host to *Mycobacterium tuberculosis*, and vice versa. *Tuberculosis (Edinb), 93*(3), 330-337.

Fogel, N. (2015). Tuberculosis: a disease without boundaries. *Tuberculosis, 95*, 527-531.

Georghiou, S. B., Seifert, M., Catanzaro, D. G., Garfein, R. S. and Rodwell, T. C. (2017). Increased tuberculosis patient mortality associated with *Mycobacterium tuberculosis* mutations conferring resistance to second-line antituberculous drugs. *Journal of Clinical Microbiology, 55*, 1928-1937.

Goletti, D., Petruccioli, E., Joosten, S. A. and Ottenhoff, T. H. (2016). Tuberculosis biomarkers: from diagnosis to protection. *Infectious Disease Reports, 8*(2), 6568.

Govender, V. S., Ramsugit, S. and Pillay, M. (2014). *Mycobacterium tuberculosis* adhesins: potential biomarkers as anti-tuberculosis therapeutic and diagnostic targets. *Microbiology, 160*(9), 1821-1831.

Hameed, H., Islam, M. M., Chhotaray, C., Wang, C., Liu, Y., Tan, Y., et al. (2018). Molecular targets related drug resistance mechanisms in MDR-, XDR-, and TDR-*Mycobacterium tuberculosis* strains. *Frontiers in Cellular and Infection Microbiology, 8*, 114.

Kashyap, R. S., Rajan, A. N., Ramteke, S. S., Agrawal, V. S., Kelkar, S. S., Purohit, H. J., et al. (2007). Diagnosis of tuberculosis in an Indian population by an indirect ELISA protocol based on detection of Antigen 85 complex: a prospective cohort study. *BMC Infectious Diseases, 7*(1), 74.

Lau, S. K., Lam, C.-W., Curreem, S. O., Lee, K.-C., Lau, C. C., Chow, W. N., et al. (2015). Identification of specific metabolites in culture supernatant of *Mycobacterium tuberculosis*

using metabolomics: exploration of potential biomarkers. *Emerging Microbes and Infections, 4*(1), e6.

Lesho, E., Forestiero, F. J., Hirata, M. H., Hirata, R. D., Cecon, L., Melo, F. F., et al. (2011). Transcriptional responses of host peripheral blood cells to tuberculosis infection. *Tuberculosis, 91*(5), 390-399.

Loots D, T. (2014). An altered *Mycobacterium tuberculosis* metabolome induced by katG mutations resulting in isoniazid resistance. *Antimicrobial Agents and Chemotherapy, 58*(4), 2144-2149.

Loots, D. T., Swanepoel, C. C., Newton-Foot, M. and Gey van Pittius, N. C. (2016). A metabolomics investigation of the function of the ESX-1 gene cluster in mycobacteria. *Microbial Pathogenesis, 100*, 268-275.

Maertzdorf, J., Repsilber, D., Parida, S. K., Stanley, K., Roberts, T., Black, G., et al. (2011). Human gene expression profiles of susceptibility and resistance in tuberculosis. *Genes and Immunity, 12*(1), 15.

Manson, A. L., Cohen, K. A., Abeel, T., Desjardins, C. A., Armstrong, D. T., Barry, C. E., et al. (2017). Genomic analysis of globally diverse *Mycobacterium tuberculosis* strains provides insights into emergence and spread of multidrug resistance. *Nature Genetics, 49*, 395-402.

McGrath, M., Gey Van Pittius, N. C., Van Helden, P. D., Warren, R. M. and Warner, D. F. (2014). Mutation rate and the emergence of drug resistance in *Mycobacterium tuberculosis*. *The Journal of Antimicrobial Chemotherapy,* 69, 292-302.

Meissner-Roloff, R. J., Koekemoer, G. and Warren, R. M. (2012). A metabolomics investigation of a hyper-and hypo-virulent phenotype of Beijing lineage *M. tuberculosis*. *Metabolomics, 8*(6), 1194-1203.

Minion, J., Leung, E., Talbot, E., Dheda, K., Pai, M. and Menzies, D. (2011). Diagnosing tuberculosis with urine lipoarabinomannan: systematic review and meta-analysis. *European Respiratory Journal, 38*(6), 1398-1405.

Naidoo, N., Ramsugit, S. and Pillay, M. (2014). *Mycobacterium tuberculosis* pili (MTP), a putative biomarker for a tuberculosis diagnostic test. *Tuberculosis (Edinb), 94*(3), 338-345.

Naidoo, N., Pillay, B., Bubb, M., Pym, A., Chiliza, T., Naidoo, K., et al. (2018). Evaluation of a synthetic peptide for the detection of anti-*Mycobacterium tuberculosis* curli pili IgG antibodies in patients with pulmonary tuberculosis. *Tuberculosis (Edinb), 109*, 80-84.

O'Sullivan, D. M., Nicoara, S. C., Mutetwa, R., Mungofa, S., Lee, O. Y., Minnikin, D. E., et al. (2012). Detection of *Mycobacterium tuberculosis* in sputum by gas chromatography-mass spectrometry of methyl mycocerosates released by thermochemolysis. *PloS One, 7*(3), e32836.

Otero, L., Krapp, F., Tomatis, C., Zamudio, C., Matthys, F., Gotuzzo, E., et al. (2011). High prevalence of primary multidrug resistant tuberculosis in persons with no known risk factors. *PLoS One, 6*(10), e26276.

Pal, R., Hameed, S., Sabareesh, V., Kumar, P., Singh, S. and Fatima, Z. (2018). Investigations into Isoniazid Treated *Mycobacterium tuberculosis* by Electrospray Mass Spectrometry Reveals New Insights into Its Lipid Composition. *Journal of Pathogens, 2018*, 1454316.

Ramsugit, S., Guma, S., Pillay, B., Jain, P., Larsen, M. H., Danaviah, S., et al. (2013). Pili contribute to biofilm formation *in vitro* in *Mycobacterium tuberculosis*. *Antonie Van Leeuwenhoek, 104*(5), 725-735.

Ramsugit, S. and Pillay, M. (2014). *Mycobacterium tuberculosis* Pili promote adhesion to and invasion of THP-1 macrophages. *Japanese Journal of Infectious Diseases, 67*(6), 476-478.

Ramsugit, S., Pillay, B. and Pillay, M. (2016). Evaluation of the role of *Mycobacterium tuberculosis* pili (MTP) as an adhesin, invasin, and cytokine inducer of epithelial cells. *Brazilian Journal of Infectious Diseases, 20*, 160-165.

Ronning, D. R., Klabunde, T., Besra, G. S., Vissa, V. D., Belisle, J. T. and Sacchettini, J. C. (2000). Crystal structure of the secreted form of antigen 85C reveals potential targets for mycobacterial drugs and vaccines. *Nature Structural & Molecular Biology, 7*(2), 141.

Sasindran, S. J. and Torrelles, J. B. (2011). *Mycobacterium Tuberculosis* Infection and Inflammation: what is Beneficial for the Host and for the Bacterium? *Frontiers in Microbiology, 2*, 2.

Sudhindra, A., Ochoa, R. and Santos, E. S. (2011). Biomarkers, prediction, and prognosis in non-small-cell lung cancer: a platform for personalized treatment. *Clinical Lung Cancer, 12*(6), 360-368.

Swanepoel, C. C. and Loots, D. T. (2014). The use of functional genomics in conjunction with metabolomics for *Mycobacterium tuberculosis* research. *Disease markers, 2014*, e124218.
Theron, G., Peter, J., Calligaro, G., Meldau, R., Hanrahan, C., Khalfey, H., et al. (2014). Determinants of PCR performance (Xpert MTB/RIF), including bacterial load and inhibition, for TB diagnosis using specimens from different body compartments. *Scientific reports, 4*, 5658.
Wallis, R. S. and Peppard, T. (2015). Early Biomarkers and regulatory innovation in multidrug-resistant tuberculosis. *Clinical Infectious Diseases, 61*, 160-163.
WHO, (2019). World Health Organization 2018 Global Statistics Report. http://www.who.int/tb/publications/global_report/en/. Accessed 30/11/2019.
Zhong, L., Zhou, J., Chen, X. and Yin, Y. (2016). Serum metabolomic study for the detection of candidate biomarkers of tuberculosis. *International Journal of Clinical and Experimental Pathology, 9*(3), 3256-3266.

Dissertation outline

This dissertation comprises of two manuscripts which are ready for publication. The first chapter reviews the relevant literature on the topic. Chapter 2 presents Manuscript 1, which investigated the role of MTP in modulating bacterial metabolic pathways in *M. tuberculosis* WT V9124, the Δ*mtp* deletion mutant and its complemented strain. Chapter 3 presents Manuscript 2, which investigated the role of MTP in an infection model using A549 epithelial cells infected with the three *M. tuberculosis* strains to determine significant modulations in metabolic pathways. Chapter 4 synthesises the important findings from Chapters 2 and 3, and highlights any limitations as well as future recommendations.

CHAPTER 1: LITERATURE REVIEW

1.1 Epidemiology of TB

Major global research efforts are directed at control and eradication of the airborne disease, tuberculosis (TB), caused by *Mycobacterium tuberculosis*. Co-infection with the human immunodeficiency virus and acquired immune deficiency syndrome (HIV/AIDS), multidrug-resistant (MDR), extensively drug-resistant (XDR) and totally drug-resistant (TDR) TB (Velayati et al., 2009), further contributes to these challenges in addition to factors such as patient noncompliance (Lange et al., 2014), poor drug efficacy (McGrath et al., 2014), poverty, and undernutrition (World Health Organization (WHO), 2019). Global statistical data have highlighted the major concerns emanating from this disease.

An estimated 1.2 million TB-related deaths in HIV-negative individuals were reported in 2018 alone (WHO, 2019). In the same year, approximately 10.0 million people became ill with TB with 11 % being children, 32 % being female and 8.6 % being people co-infected with HIV (WHO, 2019). The incidence rate differed among countries in 2018 (Fig. 1.1.) and varied from under 10 per 100 000 population in first world countries to between 150 – 400 per 100 000 population in high TB burden countries (WHO, 2019). It was also reported that the incidence rate was above 500 in certain countries such as Korea, Philippines, Lesotho and South Africa (WHO, 2019).

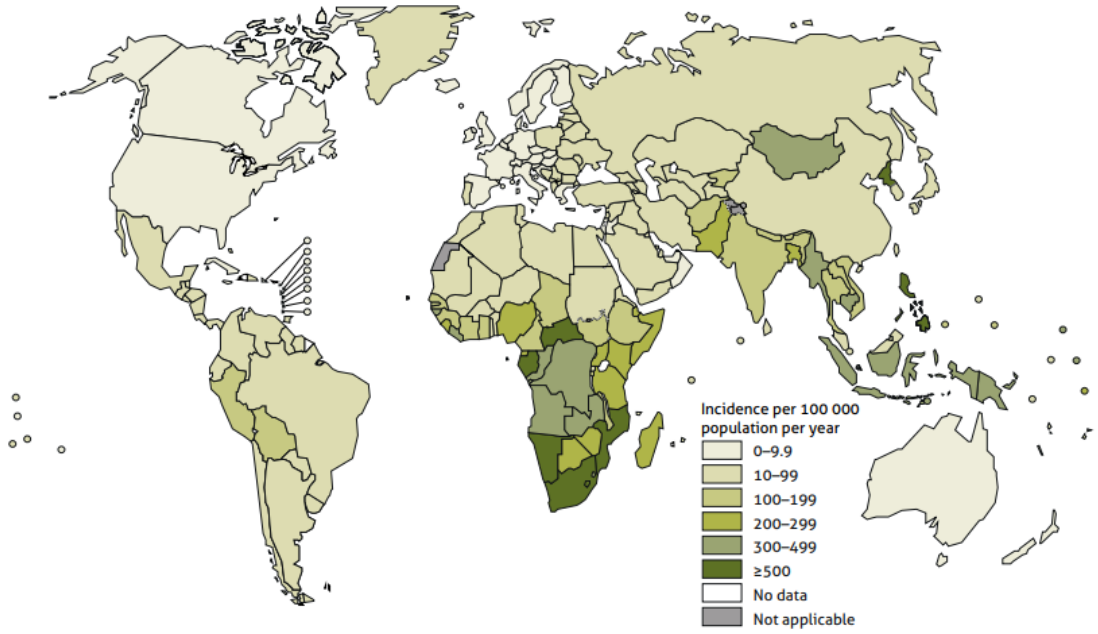

Figure 1.1 Estimated global TB incidence rates in 2018 (WHO, 2019).

The case fatality ratio (CFR) is calculated as the number of TB deaths relative to the number of new TB cases in that year and provides an indication of the proportion of people who die from TB in a given year (WHO, 2019). The CFR includes both the number of HIV-negative and HIV-positive people infected with TB. In 2018, the global CFR was 15 %, ranging from less than 5 % in a few countries to

over 20 % in most African countries (Fig. 1.2.). Part of the END TB Strategy is to reduce the global CFR to 10 % in 2020 (WHO, 2019). Hypothetically, the CFR would be low across all countries if infected individuals had access to early diagnosis, followed by timeous admission of the required treatment. This cross-country comparison emphasises the high CFRs centralised across Africa which calls for intensified efforts to develop more effective diagnostic methods and care regimens.

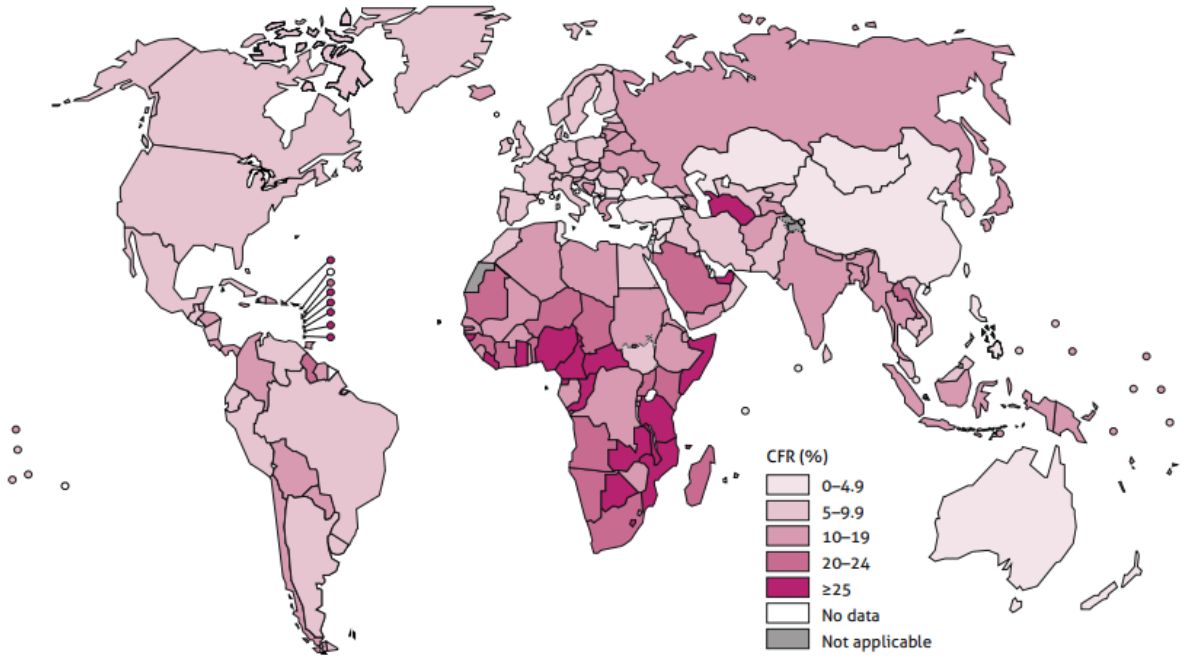

Figure 1.2 Estimated global case fatality ratios (CFR) in 2018 (WHO, 2019).

In South Africa, an estimated 301 000 people fell ill with TB in 2018 while 63 000 deaths were reported, of which 42 000 were HIV-positive individuals (WHO, 2019). South Africa ranks eighth worldwide in terms of absolute number of cases, harbouring 3 % of global TB cases (WHO, 2019).

KwaZulu-Natal (KZN) has one of the highest TB incidence rates in South Africa with 685 cases per 100 000 population in 2015 (Massyn, 2018). It was reported that during 2016/17, 78.3 % of individuals aged 5 and older who visited a public healthcare facility in KZN were symptomatic of TB after mandatory screening (Massyn, 2018).

1.2 Drug resistance

Drug resistance is an increasing occurrence owing to multiple factors that contribute to the emergence of this problem. Some of these factors include failure to obtain treatment, failure to complete treatment course, chromosomal mutations or the acquisition of a highly resistant strain within a high burden setting, where such strain has become virulent owing to high infectivity with low diagnostic/treatment facilities (Otero et al., 2011; McGrath et al., 2014; Georghiou et al., 2017; Manson et al., 2017). The

WHO reported an incidence of approximately 484 000 cases of multidrug-resistant or rifampicin-resistant TB (MDR/RR-TB), of which 214 000 people died in the year 2018 (WHO, 2019). Rifampicin and isoniazid are the two most efficacious drugs used to treat most TB patients but once a patient develops resistance to these drugs, they are classified as having acquired MDR-TB (Centers for Disease Control and Prevention (CDC), 2018; Hameed et al., 2018). In the same year, 6.2 % of MDR cases were reported as XDR (WHO, 2019). Extensively drug-resistant tuberculosis (XDR-TB) occurs when a patient is resistant to rifampicin and isoniazid, in addition to fluoroquinolones and at least one of the available second-line injectable drugs (capreomycin, kanamycin or amikacin) (CDC, 2018; Hameed et al., 2018). Worldwide, a total of 13 068 cases of XDR-TB was reported across 81 countries in 2018, with South Africa being one of the five countries with the largest number of cases (WHO, 2019). Totally drug-resistant tuberculosis (TDR-TB) occurs when there is resistance to first- and second-line drugs, rifabutin, clofazimine, dapsone, clarithromycin, and thiacetazone (Migliori et al., 2007), para-aminosalicylic acid (Klopper et al., 2013), and it was also reported that novel drugs such as bedaquiline and delamanid were also ineffective (Maeurer et al., 2014).

In South Africa, an estimated 11 000 cases of MDR/RR-TB were reported in 2018 (WHO, 2019). KZN is synonymous with the highest burdens of drug-resistant TB in South Africa (Kapwata et al., 2017), in addition to the Eastern Cape and the Western Cape (Klopper et al., 2013). Laboratory-confirmed cases of MDR-TB increased from 583 in 2004 to 6630 in 2012 stressing the need for case detection and immediate treatment roll-out in order to prevent the escalating spread of drug-resistant strains (Gandhi et al., 2012). Recent KZN statistics have shown that there was a prevalence of 22.9 % in 2016 amongst cases that were resistant to levofloxacin or pyrazinamide in addition to exhibiting rifampicin-resistance (WHO, 2019). A recent study conducted in KZN found that 250 individuals out of 318 were tested positive for XDR-TB and were found to harbour the F15/LAM4/KZN strain (Brown et al., 2019). Reports of TDR-TB in South Africa have been made although recent statistical data is unavailable (Velayati et al., 2009; Klopper et al., 2013).

1.3 General characteristics of *M. tuberculosis*

Mycobacterium tuberculosis is a pathogenic bacterium that was first discovered in 1882 by Robert Koch and is classified under the phylum and family of *Actinobacteria* and *Mycobacteriaceae*, respectively. Microscopically, the cells can be viewed using Ziehl-Neelsen staining as short, rod-shaped cells and has been shown to have a length of 1 – 4 µm and a width of 0.2 – 0.5 µm via electron microscopy (James et al., 2000; Sakamoto, 2012). This bacteriumis a facultative anaerobe, non-spore forming and non-motile (Parish and Stoker, 1999; Wilson et al., 1999). In culture, this bacteriumhas a slow growth rate and generally has a doubling time of approximately 14 – 24 hours (James et al., 2000), which can vary depending on its strain, resistance mechanisms and virulence (Dunn and North, 1995).

Mycobacterium tuberculosis forms part of the *M. tuberculosis* complex (MTBC) which consists of ten mycobacterial members namely; *M. tuberculosis*, *M. microti*, *M. africanum*, *M. bovis*, *M. caprae*, *M. canettii*, *M. orygis*, *M. suricattae*, *M. pinnipedii*, and *M. mungi* (Frothingham et al., 1994; Alexander et al., 2010; van Ingen et al., 2012; Sinha et al., 2016). *M. tuberculosis* is mainly responsible for TB in humans, while *M. bovis* and *M. avium* causes TB in animals (Hlokwe et al., 2017). A study by Wirth et al. (2008) utilised Bayesian statistics together with the data obtained from mycobacterial markers from infected TB patients and found that the estimated age of the MTBC is 40 000 years (Wirth et al., 2008). This shows that the MTBC is an evolutionarily successful group of pathogens that still holds relevance today.

1.3.1 Lineages and strains of M. tuberculosis

Whole-genome sequencing has been instrumental in reconstructing the evolution of the MTBC (Comas et al., 2013). Bioinformatic analyses have clustered mycobacterial genomes into seven geographically restricted lineages which are listed in the order from Lineage 1 to Lineage 7; Indo-Oceanic, East Asian (which includes the Beijing strain), Central Asian (CAS), Euro-American (which includes the Latin-American Mediterranean (LAM), X type and T families), West African 1, West African 2, and Lineage 7 (Comas et al., 2013; Yimer et al., 2015).

Various strain families of *M. tuberculosis* have been reported to be responsible for causing MDR- and XDR-TB. Drug-susceptible TB has been found to be caused by the W/Beijing, T and S families across South Africa (Mlambo et al., 2008; Stavrum et al., 2009; Gandhi et al., 2014). The W/Beijing strain has also been found to be implicated in cases of MDR- and XDR-TB along with the F15/KZN/LAM strain which has been commonly found to be the cause amongst cases in KZN (Pillay and Sturm, 2007). The F15/KZN/LAM strain has the spoligotype ST60 (Filliol et al., 2003). Pillay and Sturm (2007) reported that this strain was initially found as early as 1994 to be in a drug-susceptible and MDR form, and subsequently developed additional resistance mechanisms, transforming into XDR-TB. This strain caused the outbreak in 2005 at the Church of Scotland Hospital in Tugela Ferry, KZN (Gandhi et al., 2006).

1.3.2 Mycobacterium tuberculosis pathogenesis

A person can become infected with TB via the inhalation of aerosol droplets that harbour this pathogenic bacterium, followed by being deposited into alveolar sacs of the lung (Sasindran and Torrelles, 2011). Alveolar macrophages and dendritic cells are phagocytic cells that engulf *M. tuberculosis* (Bermudez et al., 2002; Sasindran and Torrelles, 2011). Alveolar epithelial cells, which are non-professional phagocytes, have been found to be involved in bacterial recognition and uptake, hence play a significant role in pathogenesis (Garcia-Perez et al., 2012). The formation of a granuloma occurs as a result of a

multitude of signalling events and the recruitment of immune cells in an effort to contain and eliminate the infection (Silva Miranda et al., 2012). Granuloma formation can lead to caseous necrosis, creating an adverse environment for *M. tuberculosis* survival, and through its metabolic network, *M. tuberculosis* has evolved to cope with these challenges (Shleeva et al., 2002; Eoh, 2014).

1.3.3 Cell wall components

The cell wall of *M. tuberculosis* (Fig. 1.3) is a complex arrangement of unique features that differentiate it from Gram-positive and Gram-negative bacteria (Catalão and Pimentel, 2018). The cell membrane assumes the same functionality and lipid bilayer properties as in other bacteria. Surrounding this membrane is the cell wall which is comprised of three major components; mycolic acid, arabinogalactan and peptidoglycan (Brennan and Nikaido, 1995). This aggregation of components is termed the mycolyl-arabinogalactan-peptidoglycan complex (mAGP) and is known as the cell wall core (Catalão and Pimentel, 2018). Peptidoglycan is covalently linked to the polymer arabinogalactan, which is a major branched-chain polysaccharide in the cell wall that is attached to muramic residues via phosphodiester linkages, to which mycolic acids are then linked (Lederer et al., 1975). The mycolic acids are orientated perpendicular to the plane of the plasma membrane (Nikaido et al., 1993). The components of arabinogalactan namely, arabinose and galactose, are found to be in the furanose configuration which is different to other bacterial polysaccharides as it contains clear structural motifs, a lack of repeating units and exists in its elemental form (Vilkas et al., 1973; Daffe et al., 1990). The cell envelope polymers such as lipoarabinomannan can be found anchored to the cell membrane by diacylglycerol (Brown et al., 2015). Other glycolipids such as lipomannan, polyacyltrehalose, sulfolipids and trehalose-6,6'-dimycolate form part of the array of unique lipids that confer survival advantages to this pathogen (Nikaido et al., 1993; Ghazaei, 2018).

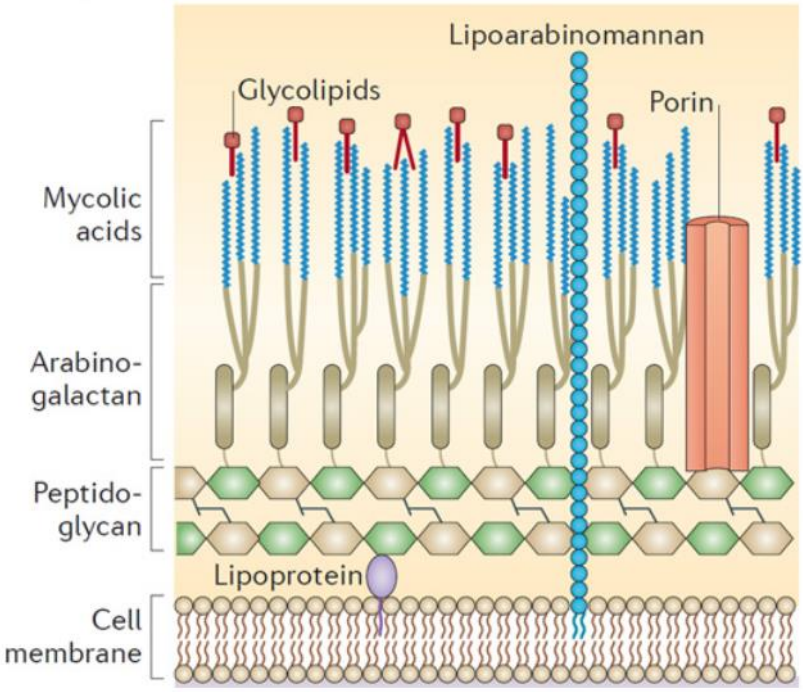

Figure 1.3 Structural components of the mycobacterial cell wall (Brown et al., 2015).

1.4 *Mycobacterium tuberculosis* adhesins

The initial host-microbe interaction is initiated by microbial cell surface structures, called adhesins, which mediate adherence to host cell surface receptors (Bermudez and Goodman, 1996). A number of *M. tuberculosis* adhesin molecules have been found to bind to and interact with mammalian host cells and tissues (Menozzi et al., 1998; Diaz-Silvestre et al., 2005; Singh et al., 2005; Alteri et al., 2007; Dunn et al., 2009). Only a few of these adhesins are well-characterized with potential functions. Govender et al. (2014) listed the following adhesins as significant owing to their major role in *M. tuberculosis* pathogenesis: heparin-binding haemagglutinin adhesin (HBHA), malate synthase, 19 kDa lipoprotein, alanine-proline-rich antigen (Apa), molecular chaperone protein 60.2 (Cpn60.2), and *Mycobacterium tuberculosis* curli pili.

Heparin-binding haemagglutinin adhesin is the most well-defined and primary adhesin of *M. tuberculosis* which adheres to epithelial cells (Menozzi et al., 1998). Heparin-binding haemagglutinin adhesin functions in the infection of lung epithelial cells and facilitates extrapulmonary dissemination of this pathogen (Sohn et al., 2011). This adhesin is a 28 kDa methylated protein (Delogu and Brennan, 1999) that enables heparin binding due to the presence of lysine-rich repeats located at its carboxyl terminal (Pethe et al., 2000).

Malate synthase is the second enzyme of the glyoxylate cycle and is encoded by the glycolate B (*glcB*) gene (Dunn et al., 2009). This enzyme serves to catabolize carbon assimilation through the shunt by converting glyoxylate using an acetyl group from acetyl-CoA to produce malate and adenosine

triphosphate (ATP) for the bacterium (Dunn et al., 2009). A study performed by Kinhikar et al. (2006) indicated that malate synthase binds to laminin and fibronectin, which are human extracellular proteins. Antibodies targeted to this domain resulted in an interference between malate synthase and these proteins which reduced the adherence between *M. tuberculosis* and A549 epithelial cells (Kinhikar et al., 2006).

The 19 kDa lipoprotein antigen (*Rv3763*) is also a cell wall-associated protein and has been found bound to THP-1 macrophage-like cells (Diaz-Silvestre et al., 2005). The glycoprotein Apa (*Rv1860*) previously classified as secreted, also resides on the cell wall and aids attachment to the pulmonary surfactant protein A (Singh et al., 2005). The Cpn60.2 molecular chaperone protein (*Rv0440*) confers pathology due to its immunogenicity and the associated activation of human monocytes as well as vascular endothelial cells in the host during infection (van Eden et al., 1998; Stokes et al., 2004).

1.5 *Mycobacterium tuberculosis* curli pili identification and characterisation

Previously, it was thought that pili production in mycobacteria did not exist. However, Alteri (2005) reported that *M. tuberculosis* does produce two different types of pili, which include type IV and curli pili using transmission electron microscopy (TEM) of negatively stained *M. tuberculosis*. In addition, Alteri et al. (2007) confirmed that *M. tuberculosis* produces curli pili (MTP) encoded by the *Rv3312A* gene, utilizing an *mtp* mutant of *M. tuberculosis* H37*Rv* and CDC1551 strains. The authors also showed that sera from recovering TB patients contained antibodies that react to these particular organelles and that MTP binds *in vitro* to laminin, an extracellular matrix protein, with negligible binding to fibronectin or Type IV collagen (Alteri et al., 2007). The MTP adhesin expression was further confirmed by Ramsugit et al. (2013) by TEM and real-time quantitative polymerase chain reaction (RT-qPCR) using ribonucleic acid (RNA) extracted from an *mtp*-knockout mutant strain relative to the *M. tuberculosis* V9124 wild-type strain.

The MTP adhesin functions in the adherence to and invasion of epithelial cells (Ramsugit et al., 2016) and macrophages (Ramsugit and Pillay, 2014), and plays a role in *in vitro* biofilm formation (Ramsugit et al., 2013). Ramsugit et al. (2016) also assessed the role of MTP in cytokine induction and found that this adhesin does not significantly influence the overall cytokine response of epithelial cells infected with *M. tuberculosis*. However, since a slightly elevated cytokine response was observed by the MTP deletion mutant, the authors speculated a dampening of the host immune response by MTP, as a protective mechanism to enable replication and survival of the pathogen (Ramsugit et al., 2016).

1.6 The MTP adhesin as a potential diagnostic target

A study conducted by Naidoo et al. (2014) investigated the potential of the *mtp*-encoded pilin subunit protein as a diagnostic biomarker. The authors found that the *mtp* gene was absent in non-tuberculous mycobacteria and other respiratory organisms but was found to be present in all tested clinical isolates belonging to the MTBC. It was hence deduced that the pilin subunit protein of *M. tuberculosis* could be used as a suitable biomarker for point of care diagnostics (Naidoo et al., 2014). A recent study investigated the ability of MTP to react with Immunoglobulin G (IgG) in TB patients, including HIV-uninfected and co-infected patients, for future evaluation in a point of care test (Naidoo et al., 2018). Serum or plasma samples were screened using an MTP synthetic peptide in a slot blot assay revealing an accuracy of 97 % in the detection of anti-MTP IgG antibodies thereby, confirming the expression of MTP during *M. tuberculosis* infection (Naidoo et al., 2018). Recently, data from our research group demonstrated that MTP modulates the host immune response by significantly inducing immune response genes, pathways and networks in infected A549 pulmonary epithelial cells (Dlamini, 2017), and in a mouse infection model (Nyawo, 2016). Collectively, data thus far suggests that this adhesin could be a useful biomarker for the development of rapid point of care diagnostics, more effective drugs, vaccines and immunotherapeutics.

1.7 A459 epithelial cells

1.7.1 The A549 cell identification and characterisation

The A549 cells are an alveolar human-derived lung cancer cell line that was first described by Giard et al. (1973) via the harvesting of Type II cancerous lung tissue from a 58 year-old Caucasian male. These cells are squamous or cuboidal in appearance and grow as adherent, monolayer cultures on the surface of tissue culture flasks *in vitro* (Swain et al., 2010; Mao et al., 2015). The A549 cells are non-phagocytic and non-antigen presenting, and are involved in the synthesis of lecithins, phospholipids, multilamellar inclusion bodies and surfactant (Lieber et al., 1976; Nardone and Andrews, 1979). The advantages of using this cell line include its high rate of proliferation and lifespan in a research-based setting, as well as the ability to maintain the cell phenotype in culture (Clover and Gowen, 1994; Swain et al., 2010). Its use in research serves as a Type II human alveolar epithelium cell model to develop methods of drug delivery to the lung to treat diseases of this organ, to study drug metabolism, viral infections and *M. tuberculosis* in order to better understand mechanisms of infection and pathogenesis (Foster et al., 1998; Lin et al., 1998; Swain et al., 2010).

1.7.2 The A549 epithelial cells and infection with M. tuberculosis

When *M. tuberculosis* is first inhaled into the alveolus, it is initially taken up by alveolar macrophages (Maertzdorf et al., 2018). However, the presence of Type II alveolar epithelial cells far outnumbers macrophages as each alveolus consists of approximately 30 000 alveolar epithelial cells and 50 alveolar

macrophages (Lubman et al., 1997; Schneeberger and Lynch, 1997). *Mycobacterium tuberculosis* deoxyribonucleic acid (DNA) within alveolar epithelial cells was initially detected in latently infected TB individuals (Hernandez-Pando et al., 2000). A number of studies have investigated *M. tuberculosis* infection within A549 epithelial cells (McDonough and Kress, 1995; Bermudez and Goodman, 1996; Birkness et al., 1999; Dobos et al., 2000; Bermudez et al., 2002; Castro-Garza et al., 2002;Chapeton-Montes et al., 2008). In addition, animal models have provided evidence suggesting that alveolar epithelial cells can provide a niche for *M. tuberculosis* invasion and expansion where phagocytosis is evaded, thereby establishing a systemic infection (Chackerian et al., 2002; McMurray, 2003; Wolf et al., 2008). Further, transcriptomics evidence has shown that *M. tuberculosis* within Type II alveolar epithelial cells exhibit an aerobic state which is actively replicative (Ryndak et al., 2015). Collectively, it is evident that alveolar epithelial cells function as a reservoir for *M. tuberculosis* replication prior to dissemination. Hence, inhibiting the interaction between host cell and pathogen may limit progression to an active infection.

1.8 Functional genomics

The systems biology approach interrogates the different 'omics' of biology which include genomics, transcriptomics, proteomics and metabolomics. Swanepoel and Loots (2014) discussed the complexity of the *M. tuberculosis* genome that genomics and transcriptomics have failed to extensively characterise. By incorporating the newly emerging 'omics' approach, namely metabolomics, with previously acquired data on genomics, transcriptomics and proteomics, researchers will be able to achieve a more comprehensive and holistic view of *M. tuberculosis* and its biological role in pathogenesis (Meissner-Roloff et al., 2012; Swanepoel and Loots, 2014). Integrating metabolomics data with functional genomics will enhance our understanding of functionality at the phenotypic level.

1.9 Metabolomics

Metabolomics is the in-depth study of analytical compounds found within a biological sample and can be used as a tool to characterize molecular phenotypes (Clish, 2015). The metabolome can be described as the metabolite complement of living tissue and its exploration can better explain the molecular complexity of biological systems (Wagner et al., 2003). There are two types of methodological approaches to metabolomic studies; a targeted or an untargeted approach. A targeted approach is when known compounds or groups of compounds that are chemically and biochemically characterised are specifically selected for and measured. In contrast, an untargeted approach is where all detectable analytes in a sample, known and unknown, are measured (Roberts et al., 2012). A targeted approach is used when a specific class of compounds is being tested, in conjunction with a comprehensive understanding of the specific metabolic pathways, enzymes and end products being targeted (Roberts et al., 2012). Untargeted metabolomics is used to obtain a holistic view of metabolism in a given

biological specimen where pathways, mechanisms and functionality are not completely understood (Patti et al., 2012). The main disadvantage of an untargeted approach is the copious amounts of data that are generated which require streamlined statistical analyses such as multivariate tests in order to reduce the dataset to a smaller more manageable one (Roberts et al., 2012).

1.9.1 Techniques used in metabolomics

Analytical techniques employed for metabolomic studies include nuclear magnetic resonance (NMR), liquid chromatography-mass spectrometry (LC-MS), gas chromatography-mass spectrometry (GC-MS), gas chromatography-flame ionization detection (GC-FID) and direct infusion-mass spectrometry (DI-MS), to name a few (Roberts et al., 2012). Mass spectrometry is the preferred technique as detection is simple and less time consuming, compared to NMR where spectra are complex to analyse due to the great diversity and concentrations of metabolites obtained (Kim et al., 2011).

Bioinformatics tools can provide a visual representation of the copious amount of mass spectrometry data generated through the processing of raw analytical data, integrating and annotating data as well as mathematic modelling (Duran et al., 2003; Eoh, 2014). Bioinformatics, coupled with metabolomics, can provide a useful platform to differentiate biological systems and possibly link potential biomarkers that are specific to these systems (Lau et al., 2015).

1.9.2 Applications of metabolomics

Metabolomics has found itself to be useful across numerous fields to better characterise the extensive network of complex biochemical interactions. Metabolomics can be used in a number of ways which include the identification of novel therapeutic targets, biomarker selection to be used in diagnostics or it can even be used as a means to monitor levels of a therapeutic agent in a biological sample to monitor therapy (Clish, 2015). Understanding *M. tuberculosis* metabolism is fundamental in ascertaining its role as a pathogen and how it influences the metabolism of its target host cell. Approximately one quarter of the *M. tuberculosis* genome encodes proteins that are associated with metabolism (Rienksma et al., 2014).

Mycobacterium tuberculosis relies on cholesterol and fatty acid metabolism inside its host cell and as a result, a subfield of metabolomics called lipidomics has emerged which aims to identify lipid metabolites to better characterise the lipid profile of *M. tuberculosis* and its role in virulence (Chow and Cox, 2011; Mirsaeidi et al., 2015). A number of studies have utilised mass spectrometry and nuclear magnetic resonance to quantify *M tuberculosis* lipids highlighting that each bacterial strain possesses a unique lipidome (Jain et al., 2007; Mahrous et al., 2008; Portevin et al., 2014). Studies conducted on patients' sputum samples showed that GC-MS and LC-MS can be used as a sensitive platform to

differentiate TB-infected from uninfected patients based on fatty acid composition (Cha et al., 2009; O'Sullivan et al., 2012; Pal et al., 2018). Due to the specificity of metabolomics, it has been useful in drug resistance studies where altered metabolic profiles were identified in the case of rifampin-resistant *M. tuberculosis* strains carrying *rpoB* mutations (Bisson et al., 2012) and isoniazid-resistant strains carrying *katG* mutations (Loots, 2014). An interesting study by Halouska et al. (2014) used NMR metabolomics to investigate D-cycloserine, a last resort drug used to treat MDR- and XDR-TB, which causes serious neurological effects. The aim of their study was to gain more insight on the antimicrobial activity of this drug in order to advocate the production of safer next-generation antibiotics (Halouska et al., 2014). Moreover, pharmacometabolomics is a subfield that aims to examine metabolites in drug development studies against TB (Mehta et al., 2011) where the metabolome can be monitored before and after drug administration to better understand biological processes during treatment (Kaddurah-Daouk et al., 2008). This could contribute towards personalised medicine where metabolomics can effectively be used to detect prognostic information through drug interactions which will result in improved patient response to treatment (Sudhindra et al., 2011).

Two-dimensional gas chromatography-time-of-flight mass spectrometry (GCxGC-TOFMS) is more advantageous than conventional GC-MS as it has an increased capacity to analyse complex samples, and the sensitivity to detect far more compounds in a relatively small sample is high (Welthagen et al., 2004; Weckwerth and Morgenthal, 2005). This technique was used in a study by du Preez and Loots (2013) where 22 metabolite markers were identified in sputum samples from TB-infected patients. Important findings from this study support the citramalate cycle and it was found that during pulmonary TB infection, there was an increased utilisation of fatty acids and glutamate as a carbon source (du Preez and Loots, 2013). Another study using GCxGC-TOFMS investigated the hyper- and hypo-virulent phenotypes of the Beijing lineage of *M. tuberculosis* where the hyper-virulent strain was found to be associated with metabolite markers related to increased metabolic activity, cell wall activity and virulence (Meissner-Roloff et al., 2012). A study by Loots et al. (2016) utilised metabolomics to investigate the homeobox protein ESX1, also known as ESX-1 gene cluster in *Mycobacterium smegmatis.* The ESX-1 gene cluster plays a role in mycolic acid synthesis and cell wall synthesis, and these functions were significantly affected in ESX-1 gene knockout mutants after the metabolic profiles showed an overabundance of fatty acids, amino acids and carbohydrates compared to the wild-type (Loots et al., 2016). This study by Loots et al. (2016) shows that metabolomics can be used to further validate and/or provide novel insights into the functionality of genes with the use of knockout mutants.

1.9.3 Metabolomic profiling and biomarker identification

Metabolomic profiling involves qualitative and quantitative analyses of small metabolites and is a useful tool for the identification of analytes and for biomarker discovery (Zhong et al., 2016).

Thousands of metabolites that play different roles in cell function are generated from normal metabolic activities in a biological system. Hence, it is expected that any change to a biological system will result in a change to the metabolomic profile of that system (Zhong et al., 2016). This is a powerful approach that can readily identify altered metabolic pathways and specific biomarkers in the diseased state for early TB diagnosis/therapeutics (Lau et al., 2015).

A biomarker is an invaluable indicator that can differentiate between a normal and pathological state, providing information regarding disease status, risk of disease and progression (Mahapatra et al., 2014). Tuberculosis biomarkers are necessary to overcome the lack of suitable diagnostic tests and the lack of detecting *M. tuberculosis* in host samples within an adequate amount of time. The ultimate aim of ongoing TB metabolomics research efforts is to identify significant metabolites from TB-infected host samples such as urine, sputum or serum to assemble a metabolic signature to be used for simple, non-invasive and rapid diagnostic practices (Eoh, 2014; Mahapatra et al., 2014; Zhong et al., 2016). The entry of this pathogen into its host, specifically via adhesins, may accompany numerous metabolic adaptations to survive in the host environment, however, knowledge on these specific metabolite changes is lacking, hence requires further exploration (Eoh, 2014).

1.10 Significance of work

Our research group has previously conducted numerous studies in the fields of TB genomics (Naidoo and Pillay, 2017), and transcriptomics (Mvubu et al., 2016a, 2016b; Kuvar, 2017; Dlamini, 2017; Nyawo, 2017; Rampersadh, 2019; Moodley, 2019). In recent years, much focus has leaned towards *M. tuberculosis* adhesins. The construction of the Δ*mtp*-gene-knockout mutant and its complemented strain by members of our group has opened up an array of research questions to further elucidate the role of this adhesin in an infection model. Because the only difference between the wild-type strain and the gene-knockout mutant is the gene encoding the adhesin, the significance of using this approach will provide critical information on the impact on the metabolomics profile attributed to the adhesin in question. On the basis of our knowledge, no such investigation has been previously reported. Hence, the rationale of this study was to further elucidate the role of MTP in TB pathogenesis by identifying adhesin-specific metabolites using *mtp*-proficient, *mtp*-deficient and complemented strains in an A549 epithelial host infection model. The MTP metabolite signatures identified in this study, may provide further supporting evidence for this major adhesin as an important diagnostic biomarker or vaccine candidate. Furthermore, the metabolomics signatures themselves may potentially serve as biomarkers for novel intervention strategies.

Aim of study

A GCxGC-TOFMS approach to metabolomics was used to investigate the role of MTP in modulating *M. tuberculosis* and A549 epithelial host cell metabolic pathways.

Objectives of study

1. To culture the wild-type, Δ*mtp* and *mtp*-complemented strains of *M. tuberculosis*, and to collect the bacterial pelleted wet mass.
2. To infect A549 epithelial cells with the 3 strains, and to collect infected pelleted wet mass.
3. To extract metabolites from the pelleted wet mass.
4. To use GCxGC-TOF mass spectrometry to perform metabolomic analysis.
5. To use statistical and bioinformatics tools to evaluate metabolomic profiles.
6. To perform RT-qPCR on bacterial strains to analyse gene expression profiles of significantly affected metabolic pathways.

1.11 References

Alexander, K. A., Laver, P. N., Michel, A. L., Williams, M., van Helden, P. D., Warren, R. M., et al. (2010). Novel *Mycobacterium tuberculosis* complex pathogen, *M. mungi*. *Emerging Infectious Diseases, 16*(8), 1296-1299.

Alteri, C. J. (2005). Novel pili of *Mycobacterium tuberculosis*. PhD thesis. University of Arizona Tucson.

Alteri, C. J., Xicohténcatl-Cortes, J., Hess, S., Caballero-Olín, G., Girón, J. A. and Friedman, R. L. (2007). *Mycobacterium tuberculosis* produces pili during human infection. *Proceedings of the National Academy of Sciences, 104*(12), 5145-5150.

Bermudez, L. E. and Goodman, J. (1996). *Mycobacterium tuberculosis* invades and replicates within type II alveolar cells. *Infection and Immunity, 64*(4), 1400-1406.

Bermudez, L. E., Sangari, F. J., Kolonoski, P., Petrofsky, M. and Goodman, J. (2002). The efficiency of the translocation of *Mycobacterium tuberculosis* across a bilayer of epithelial and endothelial cells as a model of the alveolar wall is a consequence of transport within mononuclear phagocytes and invasion of alveolar epithelial cells. *Infection and Immunity, 70*(1), 140-146.

Birkness, K. A., Deslauriers, M., Bartlett, J. H., White, E. H., King, C. H. and Quinn, F. D. (1999). An *in vitro* tissue culture bilayer model to examine early events in *Mycobacterium tuberculosis* infection. *Infection and Immunity, 67*(2), 653-658.

Bisson, G. P., Mehaffy, C., Broeckling, C., Prenni, J., Rifat, D., Lun, D. S., et al. (2012). Upregulation of the phthiocerol dimycocerosate biosynthetic pathway by rifampin-resistant, rpoB mutant *Mycobacterium tuberculosis*. *Journal of Bacteriology, 194*(23), 6441-6452.

Brennan, P. J. and Nikaido, H. (1995). The envelope of mycobacteria. *Annual Review of Biochemistry, 64*, 29-63.

Brown, L., Wolf, J. M., Prados-Rosales, R. and Casadevall, A. (2015). Through the wall: extracellular vesicles in Gram-positive bacteria, mycobacteria and fungi. *Nature Reviews Microbiology, 13*(10), 620-630.

Brown, T. S., Challagundla, L., Baugh, E. H., Omar, S. V., Mustaev, A., Auld, S. C., et al. (2019). Pre-detection history of extensively drug-resistant tuberculosis in KwaZulu-Natal, South Africa. *Proceedings of the National Academy of Sciences of the United States of America, 116*(46), 23284–23291.

Castro-Garza, J., King, C. H., Swords, W. E. and Quinn, F. D. (2002). Demonstration of spread by *Mycobacterium tuberculosis* bacilli in A549 epithelial cell monolayers. *FEMS Microbiology Letters, 212*(2), 145-149.

Catalão, M. J. and Pimentel, M. (2018). Mycobacteriophage lysis enzymes: targeting the mycobacterial cell envelope. *Viruses, 10*(8), 428.

Centers for Disease Control and Prevention, (2018). Tuberculosis (TB) Data and Statistics for Centers for Disease Control. https://www.cdc.gov/tb/statistics/default.htm. Accessed 05/06 2018.

Cha, D., Cheng, D., Liu, M., Zeng, Z., Hu, X. and Guan, W. (2009). Analysis of fatty acids in sputum from patients with pulmonary tuberculosis using gas chromatography-mass spectrometry preceded by solid-phase microextraction and post-derivatization on the fiber. *Journal of Chromatography A, 1216*(9), 1450-1457.

Chackerian, A. A., Alt, J. M., Perera, T. V., Dascher, C. C. and Behar, S. M. (2002). Dissemination of *Mycobacterium tuberculosis* is influenced by host factors and precedes the initiation of T-cell immunity. *Infection and Immunity, 70*(8), 4501-4509.

Chapeton-Montes, J. A., Plaza, D. F., Barrero, C. A. and Patarroyo, M. A. (2008). Quantitative flow cytometric monitoring of invasion of epithelial cells by *Mycobacterium tuberculosis*. *Frontiers in Bioscience, 13*, 650-656.

Chow, E. D. and Cox, J. S. (2011). TB lipidomics--the final frontier. *Chemistry and Biology, 18*(12), 1517-1518.

Clish, C. B. (2015). Metabolomics: an emerging but powerful tool for precision medicine. *Cold Spring Harbor Molecular Case Studies, 1*(1), a000588.

Clover, J. and Gowen, M. (1994). Are MG-63 and HOS TE85 human osteosarcoma cell lines representative models of the osteoblastic phenotype? *Bone, 15*(6), 585-591.

Comas, I., Coscolla, M., Luo, T., Borrell, S., Holt, K. E., Kato-Maeda, M., et al. (2013). Out-of-Africa migration and Neolithic coexpansion of *Mycobacterium tuberculosis* with modern humans. *Nature Genetics, 45*(10), 1176-1182.

Daffe, M., Brennan, P. J. and McNeil, M. (1990). Predominant structural features of the cell wall arabinogalactan of *Mycobacterium tuberculosis* as revealed through characterization of oligoglycosyl alditol fragments by gas chromatography/mass spectrometry and by 1H and 13C NMR analyses. *Journal of Biological Chemistry, 265*(12), 6734-6743.

Delogu, G. and Brennan, M. J. (1999). Functional domains present in the mycobacterial hemagglutinin, HBHA. *Journal of Bacteriology, 181*(24), 7464-7469.

Diaz-Silvestre, H., Espinosa-Cueto, P., Sanchez-Gonzalez, A., Esparza-Ceron, M. A., Pereira-Suarez, A. L., Bernal-Fernandez, G. et al. (2005). The 19-kDa antigen of *Mycobacterium tuberculosis* is a major adhesin that binds the mannose receptor of THP-1 monocytic cells and promotes phagocytosis of mycobacteria. *Microbial pathogenesis, 39*(3), 97-107.

Dlamini, M. T. (2017). Whole transcriptome analysis to elucidate the role of MTP in gene regulation of pulmonary epithelial cells infected with *Mycobacterium tuberculosis.* Masters thesis. University of KwaZulu-Natal. Durban.

Dobos, K. M., Spotts, E. A., Quinn, F. D. and King, C. H. (2000). Necrosis of lung epithelial cells during infection with *Mycobacterium tuberculosis* is preceded by cell permeation. *Infection and Immunity, 68*(11), 6300-6310.

du Preez, I. and Loots, D. T. (2013). New sputum metabolite markers implicating adaptations of the host to *Mycobacterium tuberculosis*, and vice versa. *Tuberculosis (Edinb), 93*(3), 330-337.

Dunn, P. L. and North, R. J. (1995). Virulence ranking of some *Mycobacterium tuberculosis* and *Mycobacterium bovis* strains according to their ability to multiply in the lungs, induce lung pathology, and cause mortality in mice. *Infection and Immunity, 63*(9), 3428-3437.

Dunn, M. F., Ramirez-Trujillo, J. A. and Hernández-Lucas, I. (2009). Major roles of isocitrate lyase and malate synthase in bacterial and fungal pathogenesis. *Microbiology, 155*(10), 3166-3175.

Duran, A. L., Yang, J., Wang, L. and Sumner, L. W. (2003). Metabolomics spectral formatting, alignment and conversion tools (MSFACTs). *Bioinformatics, 19*(17), 2283-2293.

Eoh, H. (2014). Metabolomics: A window into the adaptive physiology of *Mycobacterium tuberculosis*. *Tuberculosis, 94*(6), 538-543.

Filliol, I., Driscoll, J. R., van Soolingen, D., Kreiswirth, B. N., Kremer, K., Valetudie, G., et al. (2003). Snapshot of moving and expanding clones of *Mycobacterium tuberculosis* and their global distribution assessed by spoligotyping in an international study. *Journal of Clinical Microbiology, 41*(5), 1963-1970.

Foster, K. A., Oster, C. G., Mayer, M. M., Avery, M. L. and Audus, K. L. (1998). Characterization of the A549 cell line as a type II pulmonary epithelial cell model for drug metabolism. *Experimental Cell Research, 243*(2), 359-366.

Frothingham, R., Hills, H. G. and Wilson, K. H. (1994). Extensive DNA sequence conservation throughout the *Mycobacterium tuberculosis* complex. *Journal of Clinical Microbiology, 32*(7), 1639-1643.

Gandhi, N. R., Moll, A., Sturm, A. W., Pawinski, R., Govender, T., Lalloo, U., et al. (2006). Extensively drug-resistant tuberculosis as a cause of death in patients co-infected with tuberculosis and HIV in a rural area of South Africa. *Lancet, 368*(9547), 1575-1580.

Gandhi, N. R., Andrews, J. R., Brust, J. C., Montreuil, R., Weissman, D., Heo, M., et al. (2012). Risk factors for mortality among MDR- and XDR-TB patients in a high HIV prevalence setting. *International Journal of Tuberculosis and Lung Disease, 16*(1), 90-97.

Gandhi, N. R., Brust, J. C. M., Moodley, P., Weissman, D., Heo, M., Ning, Y., et al. (2014). Minimal diversity of drug-resistant *Mycobacterium tuberculosis* strains, South Africa. *Emerging Infectious Diseases, 20*(3), 426-437.

Garcia-Perez, B. E., Castrejon-Jimenez, N. S. and Luna-Herrera, J. (2012). The role of non-phagocytic cells in mycobacterial infections. *Understanding tuberculosis-Analyzing the origin of Mycobacterium tuberculosis pathogenicity, 6*, 151-178.

Georghiou, S. B., Seifert, M., Catanzaro, D. G., Garfein, R. S. and Rodwell, T. C. (2017). Increased tuberculosis patient mortality associated with *Mycobacterium tuberculosis* mutations conferring resistance to second-line antituberculous drugs. *Journal of Clinical Microbiology, 55*, 1928-1937.

Ghazaei, C. (2018). *Mycobacterium tuberculosis* and lipids: Insights into molecular mechanisms from persistence to virulence. *Journal of Research in Medical Sciences: The Official Journal of Isfahan University of Medical Sciences, 23*, 63-63.

Giard, D. J., Aaronson, S. A., Todaro, G. J., Arnstein, P., Kersey, J. H., Dosik, H., et al. (1973). *In vitro* cultivation of human tumors: establishment of cell lines derived from a series of solid tumors. *Journal of the National Cancer Institute, 51*(5), 1417-1423.

Govender, V. S., Ramsugit, S. and Pillay, M. (2014). *Mycobacterium tuberculosis* adhesins: potential biomarkers as anti-tuberculosis therapeutic and diagnostic targets. *Microbiology, 160*(9), 1821-1831.

Halouska, S., Fenton, R. J., Zinniel, D. K., Marshall, D. D., Barletta, R. G. and Powers, R. (2014). Metabolomics analysis identifies d-Alanine-d-Alanine ligase as the primary lethal target of d-Cycloserine in mycobacteria. *Journal of Proteome Research, 13*(2), 1065-1076.

Hameed, H., Islam, M. M., Chhotaray, C., Wang, C., Liu, Y., Tan, Y., et al. (2018). Molecular targets related drug resistance mechanisms in MDR-, XDR-, and TDR-*Mycobacterium tuberculosis* strains. *Frontiers in Cellular and Infection Microbiology, 8*, 114.

Hernandez-Pando, R., Jeyanathan, M., Mengistu, G., Aguilar, D., Orozco, H., Harboe, M., et al. (2000). Persistence of DNA from *Mycobacterium tuberculosis* in superficially normal lung tissue during latent infection. *Lancet, 356*(9248), 2133-2138.

Hlokwe, T. M., Said, H. and Gcebe, N. (2017). *Mycobacterium tuberculosis* infection in cattle from the Eastern Cape Province of South Africa. *BMC Veterinary Research, 13*(1), 299.

Jain, M., Petzold, C. J., Schelle, M. W., Leavell, M. D., Mougous, J. D., Bertozzi, C. R., et al. (2007). Lipidomics reveals control of *Mycobacterium tuberculosis* virulence lipids via metabolic coupling. *Proceedings of the National Academy of Sciences of the United States of America, 104*(12), 5133-5138.

James, B. W., Williams, A. and Marsh, P. D. (2000). The physiology and pathogenicity of *Mycobacterium tuberculosis* grown under controlled conditions in a defined medium. *Journal of Applied Microbiology, 88*(4), 669-677.

Kaddurah-Daouk, R., Kristal, B. S. and Weinshilboum, R. M. (2008). Metabolomics: a global biochemical approach to drug response and disease. *Annual Review of Pharmacology and Toxicology, 48*, 653-683.

Kapwata, T., Morris, N., Campbell, A., Mthiyane, T., Mpangase, P., Nelson, K. N., et al. (2017). Spatial distribution of extensively drug-resistant tuberculosis (XDR TB) patients in KwaZulu-Natal, South Africa. *PloS One, 12*(10), e0181797-e0181797.

Kim, H. K., Choi, Y. H. and Verpoorte, R. (2011). NMR-based plant metabolomics: where do we stand, where do we go? *Trends in Biotechnology, 29*(6), 267-275.

Kinhikar, A. G., Vargas, D., Li, H., Mahaffey, S. B., Hinds, L., Belisle, J. T. and Laal, S. (2006). *Mycobacterium tuberculosis* malate synthase is a laminin-binding adhesin. *Molecular Microbiology, 60*(4), 999-1013.

Klopper M., Warren R. M., Hayes C., Gey Van Pittius N. C., Streicher E. M., Müller B., et al. (2013). Emergence and spread of extensively and totally drug-resistant tuberculosis, South Africa. *Emerging Infectious Diseases, 19*, 449-455.

Kuvar, S. (2017). The role of *hbhA* in gene regulation *in vivo* using a *hbhA* knockout mutant of *M. tuberculosis*. Masters dissertation. University of KwaZulu-Natal. Durban.

Lau, S. K., Lam, C.-W., Curreem, S. O., Lee, K.-C., Lau, C. C., Chow, W. N., et al. (2015). Identification of specific metabolites in culture supernatant of *Mycobacterium tuberculosis* using metabolomics: exploration of potential biomarkers. *Emerging Microbes and Infections, 4*(1), e6.

Lange, C., Abubakar, I., Alffenaar, J. W., Bothamley, G., Caminero, J. A., Carvalho, A. C., et al. (2014). Management of patients with multidrug-resistant/extensively drug-resistant tuberculosis in Europe: a TBNET consensus statement. *The European Respiratory Journal*, *44*(1), 23-63.

Lederer, E., Adam, A., Ciorbaru, R., Petit, J. F. and Wietzerbin, J. (1975). Cell walls of Mycobacteria and related organisms; chemistry and immunostimulant properties. *Molecular and Cellular Biochemistry, 7*(2), 87-104.

Lieber, M., Smith, B., Szakal, A., Nelson-Rees, W. and Todaro, G. (1976). A continuous tumor-cell line from a human lung carcinoma with properties of type II alveolar epithelial cells. *International Journal of Cancer, 17*(1), 62-70.

Lin, Y., Zhang, M. and Barnes, P. F. (1998). Chemokine production by a human alveolar epithelial cell line in response to *Mycobacterium tuberculosis*. *Infection and Immunity, 66*(3), 1121-1126.

Loots D, T. (2014). An altered *Mycobacterium tuberculosis* metabolome induced by katG mutations resulting in isoniazid resistance. *Antimicrobial Agents and Chemotherapy, 58*(4), 2144-2149.

Loots, D. T., Swanepoel, C. C., Newton-Foot, M. and Gey van Pittius, N. C. (2016). A metabolomics investigation of the function of the ESX-1 gene cluster in mycobacteria. *Microbial Pathogenesis, 100*, 268-275.

Lubman, R., Kim, K. and Crandall, E. (1997). Alveolar epithelial barrier properties. The Lung: Scientific Foundations., 2nd ed., *Crystal, R. G., West, J. B., Weibel, E. R., Barnes, P. J*., Eds., Lippincott-Raven, Philadelphia.

Maertzdorf, J., Tönnies, M., Lozza, L., Schommer-Leitner, S., Mollenkopf, H., Bauer, T. T. and Kaufmann, S. (2018). *Mycobacterium tuberculosis* invasion of the human lung: First contact. *Frontiers in Immunology, 9*, 1346.

Maeurer, M., Schito, M. and Zumla, A. (2014). Totally-drug-resistant tuberculosis: hype versus hope. *Lancet Respiritory Medicine, 2*, 256-257.

Mahapatra, S., Hess, A. M., Johnson, J. L., Eisenach, K. D., DeGroote, M. A., Gitta, P., et al. (2014). A metabolic biosignature of early response to anti-tuberculosis treatment. *BMC Infectious Diseases, 14*(1), 53.

Mahrous, E. A., Lee, R. B. and Lee, R. E. (2008). A rapid approach to lipid profiling of mycobacteria using 2D HSQC NMR maps. *Journal of Lipid Research, 49*(2), 455-463.

Manson, A. L., Cohen, K. A., Abeel, T., Desjardins, C. A., Armstrong, D. T., Barry, C. E., et al. (2017). Genomic analysis of globally diverse *Mycobacterium tuberculosis* strains provides insights into emergence and spread of multidrug resistance. *Nature Genetics, 49*, 395-402.

Mao, P., Wu, S., Li, J., Fu, W., He, W., Liu, X., et al. (2015). Human alveolar epithelial type II cells in primary culture. *Physiological Reports, 3*(2), e12288.

Massyn, N., Padarath, A., Peer, N. and Day, C. (2018). District Health Barometer 2016/17. *Health Trust Systems* (12th ed.).

McDonough, K. A. and Kress, Y. (1995). Cytotoxicity for lung epithelial cells is a virulence-associated phenotype of *Mycobacterium tuberculosis*. *Infection and Immunity, 63*(12), 4802-4811.

McGrath, M., Gey Van Pittius, N. C., Van Helden, P. D., Warren, R. M. and Warner, D. F. (2014). Mutation rate and the emergence of drug resistance in *Mycobacterium tuberculosis*. *The Journal of Antimicrobial Chemotherapy*, 69, 292-302.

McMurray, D. N. (2003). Hematogenous reseeding of the lung in low-dose, aerosol-infected guinea pigs: unique features of the host-pathogen interface in secondary tubercles. *Tuberculosis (Edinb), 83*(1-3), 131-134.

Mehta, R., Jain, R. K. and Badve, S. (2011). Personalized medicine: the road ahead. *Clinical Breast Cancer, 11*(1), 20-26.

Meissner-Roloff, R. J., Koekemoer, G. and Warren, R. M. (2012). A metabolomics investigation of a hyper-and hypo-virulent phenotype of Beijing lineage *M. tuberculosis*. *Metabolomics, 8*(6), 1194-1203.

Menozzi, F. D., Bischoff, R., Fort, E., Brennan, M. J. and Locht, C. (1998). Molecular characterization of the mycobacterial heparin-binding hemagglutinin, a mycobacterial adhesin. *Proceedings of the National Academy of Sciences of the United States of America*, *95*(21), 12625-12630.

Migliori G. B., Ortmann J., Girardi E., Besozzi G., Lange C., Cirillo D. M., et al. (2007). Extensively drug-resistant tuberculosis, Italy and Germany. *Emerging Infectious Diseases, 13*, 780-782.

Minion, J., Leung, E., Talbot, E., Dheda, K., Pai, M. and Menzies, D. (2011). Diagnosing tuberculosis with urine lipoarabinomannan: systematic review and meta-analysis. *European Respiratory Journal*, *38*(6), 1398-1405.

Mirsaeidi, M., Banoei, M. M., Winston, B. W. and Schraufnagel, D. E. (2015). Metabolomics: applications and promise in mycobacterial disease. *Annals of the American Thoracic Society, 12*(9), 1278-1287.

Mlambo, C. K., Warren, R. M., Poswa, X., Victor, T. C., Duse, A. G. and Marais, E. (2008). Genotypic diversity of extensively drug-resistant tuberculosis (XDR-TB) in South Africa. *The International Journal of Tuberculosis and Tung Disease*, *12*(1), 99-104.

Moodley, S. (2019). The role of heparin binding haemagglutinin adhesin and curli pili on the pathogenicity of *Mycobacterium tuberculosis.* PhD thesis. University of KwaZulu-Natal. Durban.

Mvubu, N. E., Pillay, B., Gamieldien, J., Bishai, W. and Pillay, M. (2016a). Canonical pathways, networks and transcriptional factor regulation by clinical strains of *Mycobacterium tuberculosis* in pulmonary alveolar epithelial cells. *Tuberculosis (Edinb), 97*, 73-85.

Mvubu, N. E., Pillay, B., Gamieldien, J., Bishai, W. and Pillay, M. (2016b). *Mycobacterium tuberculosis* strains exhibit differential and strain-specific molecular signatures in pulmonary epithelial cells. *Developmental and Comparative Immunology, 65*, 321-329.

Naidoo, N., Ramsugit, S. and Pillay, M. (2014). *Mycobacterium tuberculosis* pili (MTP), a putative biomarker for a tuberculosis diagnostic test. *Tuberculosis (Edinb), 94*(3), 338-345.

Naidoo, C. and Pillay, M. (2017). Fitness-compensatory mutations facilitate the spread of drug-resistant F15/LAM4/KZN and F28 *Mycobacterium tuberculosis* strains in KwaZulu-Natal, South Africa. *Journal of Genetics, 96*(4), 599-612.

Naidoo, N. and Pillay, M. (2017). Bacterial pili, with emphasis on *Mycobacterium tuberculosis* curli pili: potential biomarkers for point-of care tests and therapeutics. *Biomarkers, 22*(2), 93-105.

Naidoo, N., Pillay, B., Bubb, M., Pym, A., Chiliza, T., Naidoo, K., et al. (2018). Evaluation of a synthetic peptide for the detection of anti-*Mycobacterium tuberculosis* curli pili IgG antibodies in patients with pulmonary tuberculosis. *Tuberculosis (Edinb), 109*, 80-84.

Nardone, L. L. and Andrews, S. B. (1979). Cell line A549 as a model of the type II pneumocyte. Phospholipid biosynthesis from native and organometallic precursors. *Biochimica et Biophysica Acta - Molecular and Cell Biology of Lipids, 573*(2), 276-295.

Nikaido, H., Kim, S. H. and Rosenberg, E. Y. (1993). Physical organization of lipids in the cell wall of *Mycobacterium chelonae*. *Molecular Microbiology, 8*(6), 1025-1030.

Nyawo, G. (2016). The role of *Mycobacterium tuberculosis* pili in pathogenesis: growth and survival kinetics, gene regulation and host immune response, and in vitro growth kinetics. Masters thesis. University of KwaZulu-Natal. Durban.

O'Sullivan, D. M., Nicoara, S. C., Mutetwa, R., Mungofa, S., Lee, O. Y., Minnikin, D. E., et al. (2012). Detection of *Mycobacterium tuberculosis* in sputum by gas chromatography-mass spectrometry of methyl mycocerosates released by thermochemolysis. *PloS One, 7*(3), e32836.

Otero, L., Krapp, F., Tomatis, C., Zamudio, C., Matthys, F., Gotuzzo, E., et al. (2011). High prevalence of primary multidrug resistant tuberculosis in persons with no known risk factors. *PLoS One*, *6*(10), e26276.

Pal, R., Hameed, S., Sabareesh, V., Kumar, P., Singh, S. and Fatima, Z. (2018). Investigations into Isoniazid Treated *Mycobacterium tuberculosis* by Electrospray Mass Spectrometry Reveals New Insights into Its Lipid Composition. *Journal of Pathogens, 2018*, 1454316.

Parish, T. and Stoker, N. G. (1999). Mycobacteria: bugs and bugbears (two steps forward and one step back). *Molecular Biotechnology, 13*(3), 191-200.

Patti, G. J., Yanes, O. and Siuzdak, G. (2012). Metabolomics: the apogee of the omics trilogy. [Perspective]. *Nature Reviews Molecular Cell Biology, 13*, 263.

Pethe, K., Aumercier, M., Fort, E., Gatot, C., Locht, C. and Menozzi, F. D. (2000). Characterization of the heparin-binding site of the mycobacterial heparin-binding hemagglutinin adhesin. *Journal of Biological Chemistry, 275*(19), 14273-14280.

Pillay, M. and Sturm, A. W. (2007). Evolution of the extensively drug-resistant F15/LAM4/KZN strain of *Mycobacterium tuberculosis* in KwaZulu-Natal, South Africa. *Clinical Infectious Diseases, 45*(11), 1409-1414.

Portevin, D., Sukumar, S., Coscolla, M., Shui, G., Li, B., Guan, X. L., et al. (2014). Lipidomics and genomics of *Mycobacterium tuberculosis* reveal lineage-specific trends in mycolic acid biosynthesis. *Microbiologyopen, 3*(6), 823-835.

Rampersadh, K. (2019). Whole genome transcript analysis to elucidate the role of *Mycobacterium tuberculosis* HBHA in host response of THP-1 macrophages. Masters dissertation. University of KwaZulu-Natal. Durban.

Ramsugit, S., Guma, S., Pillay, B., Jain, P., Larsen, M. H., Danaviah, S., et al. (2013). Pili contribute to biofilm formation *in vitro* in *Mycobacterium tuberculosis*. *Antonie Van Leeuwenhoek, 104*(5), 725-735.

Ramsugit, S. and Pillay, M. (2014). *Mycobacterium tuberculosis* Pili promote adhesion to and invasion of THP-1 macrophages. *Japanese Journal of Infectious Diseases, 67*(6), 476-478.

Ramsugit, S., Pillay, B. and Pillay, M. (2016). Evaluation of the role of *Mycobacterium tuberculosis* pili (MTP) as an adhesin, invasin, and cytokine inducer of epithelial cells. *Brazilian Journal of Infectious Diseases, 20*, 160-165.

Rienksma, R. A., Suarez-Diez, M., Spina, L., Schaap, P. J. and Martins dos Santos, V. A. (2014). Systems-level modeling of mycobacterial metabolism for the identification of new (multi-) drug targets. *Semininars in Immunology, 26*(6), 610-622.

Roberts, L. D., Souza, A. L., Gerszten, R. E. and Clish, C. B. (2012). Targeted Metabolomics. *Current Protocols in Molecular Biology*, Unit 30.32.

Ryndak, M. B., Singh, K. K., Peng, Z. and Laal, S. (2015). Transcriptional profile of *Mycobacterium tuberculosis* replicating in type II alveolar epithelial cells. *PloS One, 10*(4), e0123745-e0123745.

Sakamoto, K. (2012). The pathology of *Mycobacterium tuberculosis* infection. *Veterinary Pathology, 49*(3), 423-439.

Sasindran, S. J. and Torrelles, J. B. (2011). *Mycobacterium Tuberculosis* Infection and Inflammation: what is Beneficial for the Host and for the Bacterium? *Frontiers in Microbiology, 2*, 2.

Schneeberger, E. and Lynch, R. (1997). Airway and alveolar epithelial cell junctions. The Lung. Scientific Foundations, 2nd ed., *Crystal, R. G., West, J. B., Weibel, E. R., Barnes, P. J.*, Eds., Lippincott-Raven, Philadelphia.

Shleeva, M., Bagramyan, K., Telkov, M., Mukamolova, G., Young, M., Kell, D., et al. (2002). Formation and resuscitation of 'non-culturable'cells of *Rhodococcus rhodochrous* and *Mycobacterium tuberculosis* in prolonged stationary phase. *Microbiology, 148*(5), 1581-1591.

Silva Miranda, M., Breiman, A., Allain, S., Deknuydt, F. and Altare, F. (2012). The tuberculous granuloma: an unsuccessful host defence mechanism providing a safety shelter for the bacteria? *Clinical and Developmental Immunology, 2012*, e139127.

Singh, K. K., Dong, Y., Belisle, J. T., Harder, J., Arora, V. K. and Laal, S. (2005). Antigens of *Mycobacterium tuberculosis* recognized by antibodies during incipient, subclinical tuberculosis. *Clinical and Diagnostic Laboratory Immunology, 12*(2), 354-358.

Sinha, P., Gupta, A., Prakash, P., Anupurba, S., Tripathi, R. and Srivastava, G. N. (2016). Differentiation of *Mycobacterium tuberculosis* complex from non-tubercular mycobacteria by nested multiplex PCR targeting IS6110, MTP40 and 32kD alpha antigen encoding gene fragments. *BMC Infectious Diseases, 16*, 123.

Sohn, H., Kim, J. S., Shin, S. J., Kim, K., Won, C. J., Kim, W. S., et al. (2011). Targeting of *Mycobacterium tuberculosis* heparin-binding hemagglutinin to mitochondria in macrophages. *PLoS Pathogenesis, 7*(12), e1002435.

Stavrum, R., Mphahlele, M., Øvreås, K., Muthivhi, T., Fourie, P. B., Weyer, K. and Grewal, H. M. (2009). High diversity of *Mycobacterium tuberculosis* genotypes in South Africa and preponderance of mixed infections among ST53 isolates. *Journal of Clinical Microbiology, 47*(6), 1848-1856.

Stokes, R. W., Norris-Jones, R., Brooks, D. E., Beveridge, T. J., Doxsee, D. and Thorson, L. M. (2004). The glycan-rich outer layer of the cell wall of *Mycobacterium tuberculosis* acts as an antiphagocytic capsule limiting the association of the bacterium with macrophages. *Infection and Immunity, 72*(10), 5676-5686.

Sudhindra, A., Ochoa, R. and Santos, E. S. (2011). Biomarkers, prediction, and prognosis in non-small-cell lung cancer: a platform for personalized treatment. *Clinical Lung Cancer, 12*(6), 360-368.

Swain, R. J., Kemp, S. J., Goldstraw, P., Tetley, T. D. and Stevens, M. M. (2010). Assessment of cell line models of primary human cells by raman spectral phenotyping. *Biophysical Journal, 98*(8), 1703-1711.

Swanepoel, C. C. and Loots, D. T. (2014). The use of functional genomics in conjunction with metabolomics for *Mycobacterium tuberculosis* research. *Disease markers, 2014*, e124218.

van Eden, W., van der Zee, R., Paul, A. G., Prakken, B. J., Wendling, U., Anderton, S. M., et al. (1998). Do heat shock proteins control the balance of T-cell regulation in inflammatory diseases? *Immunology Today, 19*(7), 303-307.

van Ingen, J., Rahim, Z., Mulder, A., Boeree, M. J., Simeone, R., Brosch, R., et al. (2012). Characterization of *Mycobacterium orygis* as *M. tuberculosis* complex subspecies. *Emerging Infectious Diseases, 18*(4), 653-655.

Velayati, A. A., Masjedi, M. R., Farnia, P., Tabarsi, P., Ghanavi, J., Ziazarifi, A. H. and Hoffner, S. E. 2009. Emergence of new forms of totally drug-resistant tuberculosis bacilli: super extensively drug-resistant tuberculosis or totally drug-resistant strains in Iran. *Chest*, 136**,** 420-425.

Vilkas, E., Amar, C., Markovits, J., Vliegenthart, J. F. G. and Kamerling, J. P. (1973). Occurrence of a galactofuranose disaccharide in immunoadjuvant fractions of *Mycobacterium tuberculosis* (cell walls and wax D). *Biochim Biophys Acta, 297*, 423-435.

Wagner, C., Sefkow, M. and Kopka, J. (2003). Construction and application of a mass spectral and retention time index database generated from plant GC/EI-TOF-MS metabolite profiles. *Phytochemistry, 62*(6), 887-900.

Welthagen, W., Shellie, R.A., Spranger, J., Ristow, M., Zimmermann, R. and Fiehng, O. (2004). Comprehensive two-dimensional gas chromatography time-of-flight mass spectrometry (GCxGCTOF) for high resolution metabolomics: biomarker discovery on spleen tissue extracts of obese NZO compared to lean C57BL/6 mice. *Metabolomics, 1*(1), 65-73.

Weckwerth, W. and Morgenthal, K. (2005). Metabolomics: from pattern recognition to biological interpretation. *Drug Discovery Today, 10*(22), 1551-1558.

WHO, (2019). World Health Organization 2018 Global Statistics Report. http://www.who.int/tb/publications/global_report/en/. Accessed 30/11/2019.

Wilson, R. J., Pillay, D. G. and Sturm, A. W. (1999). *Mycobacterium tuberculosis* is not an obligate aerobe. *Journal of Infection, 38*(3), 197-198.

Wirth, T., Hildebrand, F., Allix-Beguec, C., Wolbeling, F., Kubica, T., Kremer, K., et al. (2008). Origin, spread and demography of the *Mycobacterium tuberculosis* complex. *PLoS Pathogenesis, 4*(9), e1000160.

Wolf, A. J., Desvignes, L., Linas, B., Banaiee, N., Tamura, T., Takatsu, K., et al. (2008). Initiation of the adaptive immune response to *Mycobacterium tuberculosis* depends on antigen production in the local lymph node, not the lungs. *Journal of Experimental Medicine, 205*(1), 105-115.

Yimer, S. A., Norheim, G., Namouchi, A., Zegeye, E. D., Kinander, W., Tonjum, T., et al. (2015). *Mycobacterium tuberculosis* lineage 7 strains are associated with prolonged patient delay in seeking treatment for pulmonary tuberculosis in Amhara Region, Ethiopia. *Journal of Clinical Microbiology, 53*(4), 1301-1309.

Zhong, L., Zhou, J., Chen, X. and Yin, Y. (2016). Serum metabolomic study for the detection of candidate biomarkers of tuberculosis. *International Journal of Clinical and Experimental Pathology, 9*(3), 3256-3266.

The first chapter reported on the existing and current literature on the TB burden, *M. tuberculosis* characteristics and pathogenesis, *M. tuberculosis* adhesins with the focus on MTP, A549 epithelial cells and its role in infection, and lastly, metabolomics and its importance in TB research. Chapter 2 investigated the role of MTP in modulating bacterial metabolic pathways in *M. tuberculosis* wild-type V9124, the Δ*mtp* deletion mutant and its complemented strain.

CHAPTER 2: MANUSCRIPT 1

Mycobacterium tuberculosis curli pili (MTP) deficiency is associated with alterations in cell wall biogenesis, fatty acid metabolism and amino acid synthesis

Ashokcoomar, S[1#]., Reedoy, K. S[1#]., Senzani, S[1]., Loots, D. T[3]., Beukes, D[3]., van Reenen, M[3]., Pillay, B[2]. and Pillay, M[1].*

[1]Medical Microbiology, School of Laboratory Medicine and Medical Sciences, College of Health Sciences, University of KwaZulu-Natal, 1st floor Doris Duke Medical Research Institute, Congella, Private Bag 7, Durban, 4013, South Africa.

[2]School of Life Sciences, College of Agriculture, Engineering and Science, University of KwaZulu-Natal, Westville Campus, Private Bag X54001, Durban, 4000, South Africa.

[3]Centre for Human Metabolomics, North-West University, Potchefstroom, Private Bag x6001, Box 269, 2531, South Africa.

Joint first authors

*Corresponding author
Prof. Manormoney Pillay, PhD.
Medical Microbiology, School of Laboratory Medicine and Medical Sciences, College of Health Sciences, University of KwaZulu-Natal, 1st floor Doris Duke Medical Research Institute, Congella, Private Bag 7, Durban, 4013, South Africa.
Tel: +2731 260 4059
E-mail: pillayc@ukzn.ac.za

Funding: This study was funded by a NRF Grantholder-linked bursary (105841) and a UKZN College of Health Sciences scholarship.
Authors Conflict of Interest Statement: The authors of this study declare no conflicts of interest.
Authors Contribution Statement: MP conceptualized the study. MP, BP and DTL designed the study. SA and KSR contributed equally to the study, conducted experiments, analysed the data and drafted the manuscript. DB processed the samples and performed GCxGC-TOFMS. MVR conducted statistical bioinformatic analyses. SS provided RT-qPCR guidance and analytical support. All authors contributed to and approved the manuscript.

2.1 Abstract

In an effort to find alternative therapeutic interventions to combat tuberculosis, a more refined understanding of the pathophysiology of *Mycobacterium tuberculosis* is required. The *M. tuberculosis* curli pili (MTP) adhesin is found on the surface of this pathogen and has previously been shown, using functional genomics and global transcriptomics, to play a vital role in establishing infection, bacterial aggregation, and modulating a host response *in vitro*. This investigation aimed to determine the role of MTP in modulating the metabolism of *M. tuberculosis*, using an *mtp* gene-knockout mutant strain and metabolomics. Untargeted GCxGC-TOFMS metabolomics, coupled with bioinformatic analyses, was used to identify significant differences in the metabolite profiles in the wild-type, Δ*mtp* mutant and *mtp*-complemented strains. A total of 27 metabolites was found to be biologically significant when comparing the Δ*mtp* mutant and the wild-type strains, and explains the reduced cell wall biogenesis, fatty acid metabolism, amino acid and protein synthesis, and peptidoglycan synthesis seen in the Δ*mtp* mutant. An additional seven significant metabolites were identified when comparing the wild-type and *mtp*-complemented strain, all of which are associated with cell envelope functionality. These results suggest that the lack of the MTP adhesin characterized by the Δ*mtp* mutant, resulted in various cell wall alterations and related metabolic changes. This study highlights the importance of MTP as a virulence

factor and further substantiates its potential use as a suitable biomarker for the development of diagnostic tools and intervention therapeutics against TB.

Keywords: *M. tuberculosis curli pili*; *mtp*; adhesin; GCxGC-TOFMS; metabolomics

2.2 Introduction

Tuberculosis (TB), caused by *Mycobacterium tuberculosis*, still poses a threat, not only to health, but also to socio-economics, particularly in low and middle income countries around the globe (WHO, 2019). An estimated 10 million incident cases of TB, 1.2 million deaths among HIV-negative people and 251 000 deaths in HIV-co-infected individuals were reported in 2018 (WHO, 2019). Globally, TB drug-resistance has amplified this public health crisis as 3.5% of incident cases and 18% of previously treated cases, demonstrate multidrug-resistant or rifampicin-resistant (MDR/RR) TB (WHO, 2019). Extensively drug-resistant (XDR) TB was reported in 13 068 cases in 2018 (WHO, 2019), while cases of totally drug-resistant (TDR) TB are also on the rise globally; 10.3% of all TB in Middle Eastern countries (Velayati et al., 2009), 4 patients from India (Udwadia et al., 2012), and 20% of all TB cases in the Eastern Cape region of South Africa (Klopper et al., 2013). Although good TB diagnostics and treatment strategies for TB exist, there is still much to do towards improving these strategies. This process starts by gaining a better understanding of *M. tuberculosis* physiology and pathogenicity, and by identifying bacterial determinants of infection, rather of those associated with survival (Smith, 2003; Forrellad et al., 2013).

TB primarily manifests as a pulmonary infection, once *M. tuberculosis* bacilli enter the host's respiratory tract and evades host defence mechanisms (Dannenberg Jr. and Rook, 1994). In order to invade host cells and establish infection, the bacteria first need to establish contact with the target cells, which include macrophages, epithelial cells and dendritic cells (Bussi and Gutierrez, 2019). This is followed by adherence, which is mediated by extracellular surface molecules or appendages termed adhesins (Bermudez and Goodman, 1996). Adhesins not only promote bacterial interaction with host cell receptors, but also prevent removal by shear stress, in addition to the activation of key virulence factors that lead to invasion of the host cell for the manipulation of host cell signalling (Kline et al., 2009; Stones and Krachler, 2015). These events collectively promote the spread of the pathogen and evasion of the host immune response (Stones and Krachler, 2015).

M. tuberculosis curli pili (MTP) is an important adhesin for the pathogen. The open reading frame, assigned as Rv3312A in *M. tuberculosis*, encodes pilin subunits (Alteri et al., 2007). The *mtp* gene is highly conserved amongst clinical isolates, and unique to *M. tuberculosis* complex strains (Naidoo et al., 2014). The aggregative and insoluble structures of MTP contain a large number of glycine and proline residues, resulting in its hydrophobic nature, which is a common characteristic of pilins (Alteri

et al., 2007). In addition to functioning as an adherence factor, MTP acts as an invasin (Ramsugit and Pillay, 2014). Unlike the *mtp* knockout mutant, the wild-type *M. tuberculosis* H37Rv was able to bind *in vitro* to an extracellular matrix protein, laminin (Alteri et al., 2007). Differences in adherence and invasion levels in THP-1 macrophages (Ramsugit and Pillay, 2014) and A549-pulmonary epithelial cells (Ramsugit et al., 2016) have been demonstrated when comparing *mtp*-deficient and *mtp*-proficient strains of *M. tuberculosis*. While MTP was shown to elicit minimal influence on the cytokine response of infected A549 epithelial cells (Ramsugit et al., 2016), global transcriptomics data demonstrated that this adhesin modulates host immune responses in epithelial cells and THP-1 macrophages (Nyawo, 2016; Dlamini, 2017). Furthermore, a synthetic MTP peptide, has demonstrated 97 % accuracy in detecting anti-MTP IgG antibodies in serum samples of HIV-uninfected, as well as co-infected patients (Naidoo et al., 2018). Subsequently, MTP has potential as a suitable biomarker that is involved in the initial infection process.

Metabolomics, a relatively new research approach, analyses all the metabolites produced or influenced by an organism with altered gene expression and environmental or an external stimulus (Meissner-Roloff et al., 2013). Differences in the specific composition of metabolites including: amino acids, fatty acids, lipids and sugars, can be attributed to a particular perturbation in the biological system. These can be quantified by the various types of analytical techniques, including the hyphenated two-dimensional gas chromatography coupled with time-of-flight mass spectrometry (GCxGC-TOFMS), that combines chromatographic and spectral technologies to identify metabolites (Patel et al., 2010). This robust and powerful technique allows for both group-type and within-group separations of metabolites (Haglund et al., 2013). Metabolomics has been used in a number of studies to investigate *M. tuberculosis* physiology and metabolic pathways, in order to better understand carbon, lipid and amino acid metabolism (de Carvalho et al., 2010; Chow and Cox, 2011; Beste et al., 2013; Eoh, 2014; Halouska et al., 2014; Warner, 2014). It has also found use to better characterise active TB infection (Cha et al., 2009; Mirsaeidi et al., 2015; Collins et al., 2018) and to identify significant biomarkers as indicators of virulence (Meissner-Roloff et al., 2012; Meissner-Roloff et al., 2013; Swanepoel and Loots, 2014; Lau et al., 2015; Loots et al., 2016) as well as indicators of TB disease detectable in sera (Zhong et al., 2016) and in urine (Mahapatra et al., 2014), all in an effort to develop simple, non-invasive and rapid diagnostic or novel therapeutics.

While much of the research on MTP supports it being a crucial determinant to the onset of the TB infection cycle, the metabolite changes associated with this adhesin have not been previously reported. Hence, this study reports on the use of a GCxGC-TOFMS metabolomics research approach, in the identification of novel biomarkers better describing the role of MTP in modulating *M. tuberculosis* metabolism and associated functions. Furthermore, an understanding of these metabolic pathways

involved in the infection cascade, would serve to further validate the use of the adhesin as a suitable biomarker for the advancement of intervention strategies against TB.

2.3 Materials and methods

2.3.1 Ethical Approval

The study was approved by the Biomedical Research Ethics Council (BE255/17).

2.3.2 Bacterial strains and culture conditions

The wild-type (WT) *M. tuberculosis* V9124 from the F15/LAM4/KZN family was previously isolated in Medical Microbiology, University of KwaZulu-Natal, from Tugela Ferry, KwaZulu-Natal, South Africa (Gandhi et al., 2006). This strain has been used in a previous study to construct the *mtp* deletion mutant (Δ*mtp*) using the protocol described by Bardorov et al. (2002), and the *mtp*-complemented strain (Ramsugit et al., 2013). Briefly, the Δ*mtp* strain was constructed via specialized transduction, during which the *mtp* gene was replaced with a hygromycin-resistance (hyg^R)–sacB cassette (Bardarov et al., 2002). The Δ*mtp* was subsequently complemented by electrotransformation with a non-integrating plasmid pMV261, containing the *mtp* gene, following the protocol by Bardarov et al. (2002) (Ramsugit et al., 2013). The strains were confirmed by genomic deoxyribonucleic acid (DNA) extraction using the InstaGene Matrix (Bio-Rad) and Polymerase Chain Reaction (PCR) (Appendix: C1). These strains were cultured on Middlebrook 7H11 or 7H9 (Difco, Becton-Dickinson, Franklin Lakes, NJ, USA) media at 37˚C supplemented with 10% (v/v) oleic albumin dextrose catalase (OADC) (Becton–Dickinson, Franklin Lakes, NJ, USA) and 0.5% (v/v) glycerol (Sigma-Aldrich, St. Louis, MO, USA). Broth cultures were grown with additional supplementation with Tween-80 (Sigma-Aldrich, St. Louis, MO, USA) (0.05%) and shaking (I-26 Shaking Incubator, New Brunswick Scientific, Canada) at 100 rpm for 7 – 8 days.

2.3.3 Sample preparation

Prior to sample preparation, the inoculum for each strain was standardized by 10-fold serial dilutions of OD_{600nm} 1 (equivalent to ~$1x10^8$ CFU/mL; Larsen et al., 2007) cultures, and were plated onto 7H11 (Difco, Becton-Dickinson, Franklin Lakes, NJ, USA) agar and incubated (Shel Lab CO_2 Incubator, Cornelius, OR, USA) at 37˚C for about 3 weeks to determine the colony forming units (CFU) (Appendix: C2). GraphPad Prism version 8 software (GraphPad Software, La Jolla, CA, USA) was used to determine any significant differences between the strains based on CFU/mL counts (Appendix: C2). Thereafter, ten biological replicates of each of the three strains were individually cultured (n = 30) in 40 mL Middlebrook 7H9 (Difco, Becton-Dickinson, Franklin Lakes, NJ, USA) supplemented broth. Each biological replicate was standardized to an OD_{600} of 0.015 (Appendix: C3) and incubated (Shel Lab CO_2 Incubator, Cornelius, OR, USA) at 37°C with shaking (I-26 Shaking Incubator, New

Brunswick Scientific, Canada) at 100 rpm. Once an OD_{600} of between 0.95 – 1.1 was reached, 22 mL and 17 mL of culture from each sample was used for pellet collection and RNA extraction, respectively. Cultures were centrifuged (Mikro 200R, Hettich Zentrifugen, Tuttlingen, Germany) at 4°C at 1 792 x *g* for 30 min. The pellets for RNA extraction were resuspended in 1 mL TriZol reagent (Ambion, Life Technologies, USA) and stored at - 80°C until used. The pellets for metabolite extraction were resuspended in 500 µL of phosphate buffered saline (PBS) (Appendix B) obtained from Merck (Darmstadt,Germany) and centrifuged (Mikro 200R, Hettich Zentrifugen, Tuttlingen, Germany) in Lobind microcentrifuge tubes (Sigma-Aldrich) at 4°C at 21 952 x *g* for 10 min. This wash step was repeated twice more and at the end of the third wash, PBS (Merck, Darmstadt, Germany) was removed via aspiration, and the resulting pellets were stored at - 80°C for GCxGC-TOFMS.

2.3.4 Sample extraction and derivatization

At the Centre for Human Metabolomics (North-West University), samples were thawed and centrifuged (Mikro 200R, Hettich Zentrifugen, Tuttlingen, Germany) at 4°C at 21 952 x *g* for 10 min to remove any residual PBS. Eight milligrams of pelleted wet cell mass were weighed into a 1.5 mL Eppendorf tube for each sample. The remainder of the sample volumes were used in the constitution of a pooled quality control (QC) sample. This was made up by combining 8 mg of one randomly selected sample from each of the sample groups. A whole metabolome extraction method (Beukes et al., 2019) was applied to extract metabolites from various metabolite classes. In short, 50 µL of 3-phenylbutyric acid (0.13125 mg/mL; Sigma-Aldrich, St. Louis, MO, USA) internal standard solution and 1 mL extraction solvent comprising ultra-pure Burdick & Jackson brand (Honeywell International Inc., Muskegon, MI, USA) chloroform:methanol:water (1:3:1) were added to the microcentrifuge tubes (Honeywell International Inc., Muskegon, MI, USA). After the addition of a 3 mm tungsten carbide bead (Qiagen, Veno, The Netherlands), the samples were extracted in a vibration mill with shaking in a MM400 mixer mill (Retsch GmbH & co. KG, Haan, Germany) at a frequency of 30 Hz for 5 min on each side. Following centrifugation (4°C at 21 952 x *g* for 10 min), the supernatant was transferred to a GC-MS sample vial (Thermo Fisher Scientific, Waltham, MA, USA) and dried under a light stream of nitrogen (Sigma-Aldrich, St. Louis, MO, USA). Subsequently, samples were derivatised using 50 µL of methoxyamine hydrochloride (Sigma-Aldrich, St. Louis, MO, USA) in pyridine (15 mg/mL; Merck, Darmstadt, Germany) at 50°C for 90 min, followed by 40 µL of N,O-Bis(trimethylsilyl)trifluoroacetamide (BSTFA) (Sigma-Aldrich, St. Louis, MO, USA) with 1% trimethylchlorosilane (TMCS) (Sigma-Aldrich, St. Louis, MO, USA) at 60°C for 60 min. The extracts were transferred to a 0.1 mL insert in a sample vial (Thermo Fisher Scientific, Waltham, MA, USA) and capped prior to GCxGC-TOFMS analysis.

2.3.5 GCxGC-TOFMS analysis

The samples were analysed using a Pegasus 4D GCxGC-TOFMS (Leco Corporation, St. Joseph, MI, USA). One microliter of sample was injected in a two-split ratio on an Agilent 7890A GC (Agilent, Atlanta, GA) coupled to a time of flight mass spectrometer (Leco Corporation, St. Joseph, MI, USA) equipped with a Gerstel Multi-Purpose Sampler (MPS) (Gerstel GmbH & co. KG, Eberhard-Gerstel-Platz 1, D-45473 Mülheim an der Ruhr). First dimensional separation was achieved with a Rxi-5Sil MS primary column (28.759 m, 0.25 mm internal diameter, 0.25 μm film thickness) (Restch GmbH & co. KG, Haan, Germany) and a Rxi-17 capillary column (1.380 m, 0.25 mm internal diameter, 0.25 μm film thickness) was fitted as the secondary column (Restch GmbH & co. KG, Haan, Germany). The front inlet temperature was held at a constant 270°C for the entire run, ensuring rapid vaporization. For the primary oven, an initial GC oven temperature was set at 70°C for 2 min followed by an initial increase in oven temperature of 4°C/min to a final temperature of 300°C, which was maintained for 2 min. The secondary column oven temperature was set at 85°C for 2 min, then increased by 4°C /min, until a final temperature of 300°C. The initial temperature of the modulator was 100°C for 2 min, followed by a 4°C/min increase to a final temperature of 310°C held for 12 min. To control the effluent from the primary onto the secondary column, cryomodulation and a hot pulse of nitrogen gas of 0.7 s, every 3 s was used. The acquisition delay for each sample was 400 s and the transfer line temperature was held at a constant 270°C, with the ion source temperature at a constant 200°C. The detector voltage was adjusted to 1600 V with the filament bias - 70 eV. Spectra were collected from 50 - 800 m/z at an acquisition rate of 200 spectra per second. Peak finding and mass spectral deconvolution was achieved using ChromaTOF (Leco Corporation) software (version 4.51.6.0). Conditions were set as follows; signal to noise ratio of 100 and a minimum of 5 apexing peaks. Mass fragmentation patterns and their respective retention times screened against commercially available National Institute of Standards and Technology (NIST) spectral libraries (mainlib, replib) for peak identification. Level 3 identification was performed (Schymanski et al., 2014).

2.3.6 Statistical data analysis

A total of 30 experimental samples and 12 QC samples were included in the statistical analysis. Samples were randomized to 3 batches and quantified across 731 metabolites. For data pre-processing, a zero filter was applied removing 189 metabolites, thereby retaining 542 metabolites. Zero value replacement was performed for each variable independently with zeros replaced by random numbers below the observed minimum. QC samples were injected intermittently throughout the GCxGC-TOFMS analysis to ensure analytical repeatability. The analysis was considered successful as the variability between experimental samples far exceeded the variability between QC sample analyses (Appendix: C6). Both parametric uni- and multivariate methods were employed to identify metabolites with discriminatory ability. Log transformation of the metabolomics data was required to achieve normality, as this is an assumption of parametric methods. In addition, auto-scaling was required to ensure all metabolites are regarded as equally important by multivariate models (van den Berg et al., 2006). Fold change (FC)

values were calculated to assess the magnitude of differences on average. The independent samples *t*-test was used to determine the statistical significance of differences between groups for each metabolite. To supplement the findings of the *t*-test, Cohen's d-value was used as an effect size indicating practical significance of differences (Sullivan and Feinn, 2012). Note that though analysis of variance or ANOVA models are generally considered more appropriate when comparing more than two groups, each pairwise comparison was required to interpret differences from a biological point of view. In ANOVA, post-hoc test control for inflation of Type I error rate by default, and adjustments were made subsequent to analyses. Corrections for multiple testing was effected by the Benjamini & Hochberg (BH) adjustment to control the rate of false discovery and applied to the *p*-value resulting from the independent samples *t*-test. Multivariate analyses incorporated PCA scores plots and associated power values; scores plots and associated Variable Importance in the Projection or VIP values produced by the supervised modelling technique Partial Least Squares Discriminant Analysis (PLS-DA); and correlation analysis using Spearman's Rho VIP and power values rank metabolites according to their importance in explaining the variation summarized by the PLS-DA and PCA models, respectively. Figure 2.1 summarizes the above workflow and indicates metabolite selection criteria. All of the criteria indicated in Figure 2.1 had to be met for a metabolite to be considered for further interpretation. MATLAB (MATLAB with Statistics Toolbox (2019), version 9.5.0 (R2018b) software (Natick, Massachusetts: The MathWorks Inc) along with the Eigenvector PLS_Toolbox 8.7 (Wenatchee, WA: Eigenvector Research Inc. Software available at http://www.eigenvector.com) was used to identify metabolites with the potential to differentiate among the three strains.

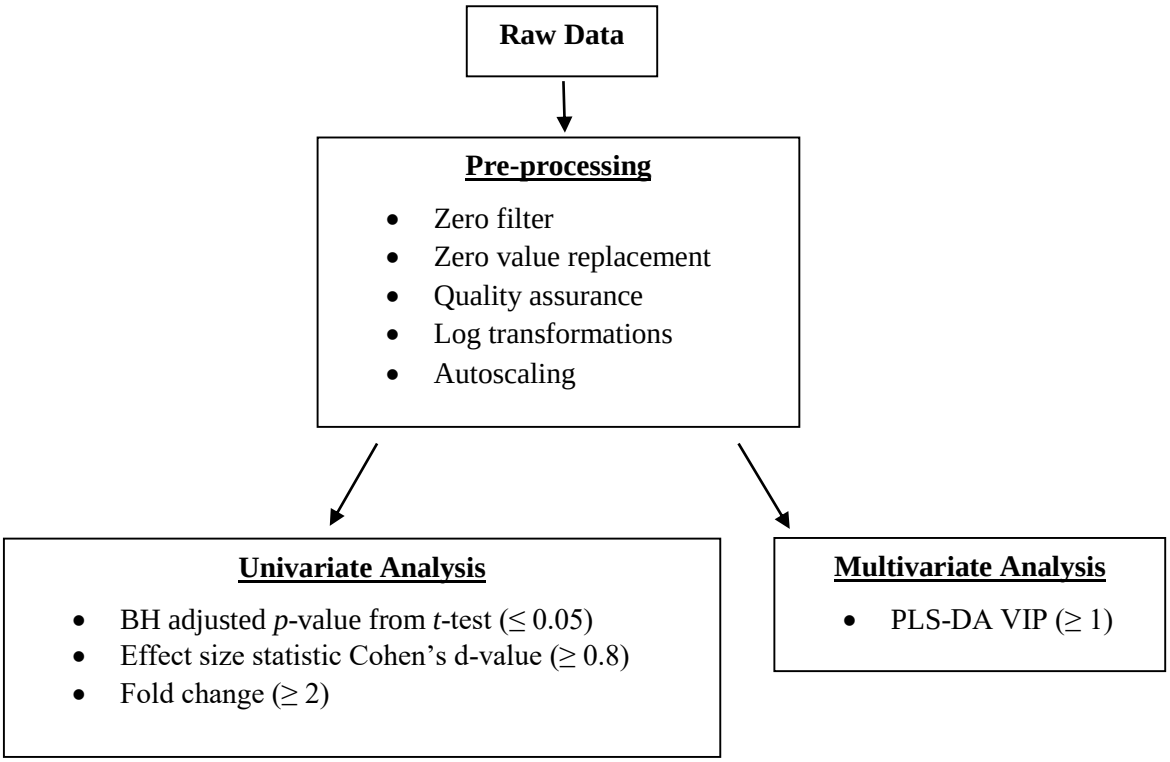

Figure 2.1 Flow diagram depicting statistical workflow for data analysis including cut-off values used as selection criteria for shortlisting of metabolites.

2.3.7 Real-time quantitative polymerase chain reaction (RT-qPCR) validation of metabolomics data

In order to better understand the metabolomic changes at a transcriptomics level, RT-qPCR was performed on the three bacterial strains (WT, Δ*mtp* and *mtp*-complement) to assess gene expression levels as a result of the *mtp* gene deletion. Upon closer inspection of the metabolic pathways that were found to be significant in this study, five randomly selected genes were chosen for amplification using primers listed in Table 2.1. The FASTA format for each gene was obtained from the Kyoto Encyclopedia of Genes and Genomes (KEGG) database (Kanehisa et al., 2017) and Primer3Plus (Untergasser et al., 2007) was used to select the best primer set. The RNA was extracted from the same broth cultures of WT, Δ*mtp* and *mtp*-complement that were used for metabolomics analysis. TriZol (Ambion) was used for RNA extraction using a method by Larson et al. (2007), with the modification of performing the 70 % ethanol wash step twice for better RNA quality. An additional modification was the use of a Precellys 24 lysis and homogenisation machine (Bertin Technologies, Montigny-le-Bretonneux, France), coupled to a Cryolys (Bertin Technologies, Montigny-le-Bretonneux, France) advanced temperature controller. The RNA concentrations were standardised to 100 µg/µL prior to DNase treatment (Thermo Fisher Scientific, Waltham, MA, USA). The cDNA conversion using the High-Capacity cDNA Reverse Transcription kit (Roche Applied Sciences, Penzberg, Germany) was conducted as per the Manufacturer's instructions. Primer efficiencies were tested for all primer sets prior to RT-qPCR. The Ssoadvanced Universal SYBR Green Supermix kit (Bio-Rad, Hercules, CA, USA) was used to perform RT-qPCR using a total reaction volume of 10 µL, in a 7500 RT-qPCR Detection System (Applied Biosystems, Foster City, CA, USA). Cycling conditions were as follows for a total of 40 cycles; holding stage at 95˚C for 30 s, cycling stage at 95˚C for 5 s with an annealing temperature of 60˚C for 30 s. Melt curve analysis was measured as continuous fluorescence set at 95˚C for 15 s, 60˚C for 1 min, 95˚C for 30 s, and 60˚C for 15 s. The resulting gene expression data was normalised using 16S rRNA and was analysed using the relative standard curve method. Four biological replicates and three technical replicates were performed for each strain. Parametric, unpaired *t*-test analyses were performed using GraphPad Prism version 8 software to determine significance values.

Table 2.1 Gene and primer sequences selected for gene expression analysis using RT-qPCR

Gene	Primer sequence
glf	Forward primer: 5'-cgttttgacctttcgtcgt-3'
	Reverse primer: 5'-ccgtacttgtggacctcgat-3'
glmU	Forward primer: 5'-gcacccaggatcacgaagtc-3'
	Reverse primer: 5'-gtggctggcatgtacggtct-3'
fadD32	Forward primer: 5'-cttttccaccgaacgagacg-3'
	Reverse primer: 5'-agtagagggcgccgaagaag-3'
fadE5	Forward primer: 5'-cagaagaagtgggcggtcct-3'
	Reverse primer: 5'-ccagcaccaggtggaagatg-3'
glpK	Forward primer: 5'-taccaaccaacgtgagacga-3'
	Reverse primer: 5'-cttgccgccagagaaataag-3'

2.4 Results

2.4.1 Statistical and practical significance of univariate results graphically represented in the volcano plot shows numerous metabolites with the ability to differentiate between groups.

The univariate discriminatory ability of metabolites produced by the different strains were summarized in volcano plots when comparing WT to Δ*mtp* (Figure 2.2a) and WT to Δ*mtp*-complement (Figure 2.2b). The volcano plots used here scatters the $-\log_{10}$ scaled *p*-values from the independent samples *t*-test (prior to correcting for multiple testing) against Cohen's d-values. A large number of metabolites showed some ability to differentiate between the two groups considered.

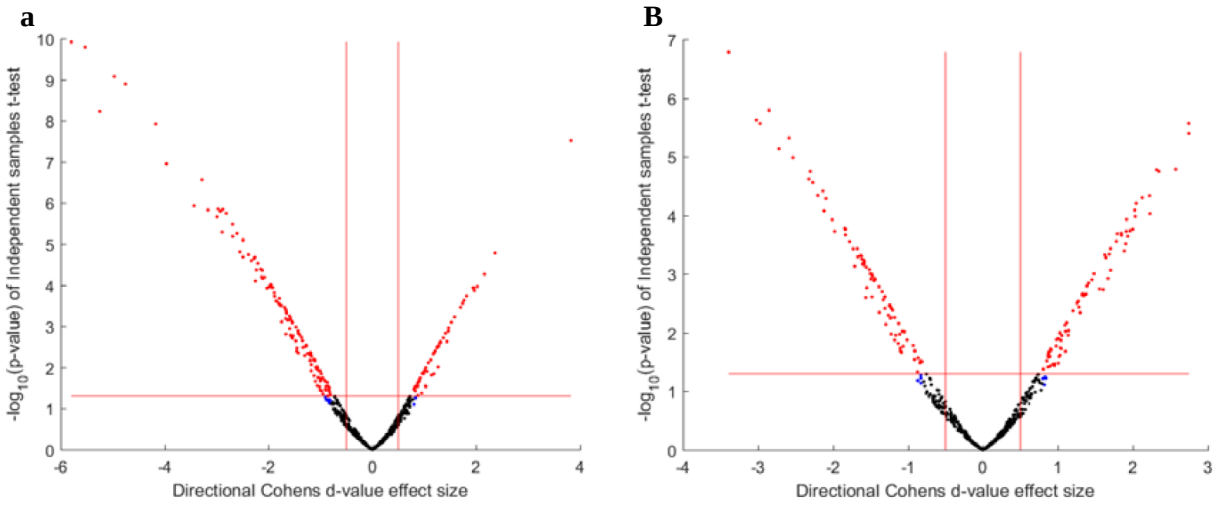

Figure 2.2 Volcano plots showing scatter of metabolites for (a) wild-type and Δ*mtp*, and (b) wild-type and *mtp*-complement (b). The dots display practical significance (blue); statistical and practical significance (red); or neither (black). Metabolites are displayed as red dots beyond the red thresholds differ statistically as well as practically between groups.

2.4.2 PLS-DA data produced group separation amongst WT, Δmtp and mtp-complement thereby confirming model validation

PLS-DA is a supervised technique that was used to identify combinations of metabolites that can differentiate between the WT, Δ*mtp* and *mtp*-complemented strains. The PLS-DA models produced VIP values, ranking metabolites according to their joint ability to explain the group structure. A VIP value greater than and equal to 1 was used as one of the selection criteria for metabolites to be considered for further interpretation. The supervised nature of PLS-DA makes this modelling approach prone to overfit and thus less likely to be reproducible. To guard against the biased use of PLS-DA VIP values, models were validated using a leave-one-out (LOO) approach. Hence, to understand the extent of overfit, the R^2 value (indicative of the proportion of variation in the grouping variable explained by the model) and Q^2 value (the LOO counterpart of R^2), were compared. The models produced R^2 and Q^2 values of 99 % and 92 % for WT versus Δ*mtp*, and 99 % and 85 % for WT versus *mtp*-complement, respectively, indicating good predictive ability or group separation which was not sensitive to case reduction. Furthermore, since the LOO approach has been known to underestimate overfit and given the small groups and no other validation was possible, univariate and multivariate criteria were used in combination to select important metabolites. In addition, scores plots from the PCA models required ellipsoidal separation as well (Appendix: C7). The PLS-DA scores plot incorporated all three experimental groups (Figure 2.3), however, VIP values were generated for the separate comparisons listed above to aid interpretation. Figure 2.3 placed emphasis on group information and ensured the variation associated with genotype was accurately captured. Similar variation between the WT and the Δ*mtp* as between the WT and the *mtp*-complement can be seen (Figure 2.3).

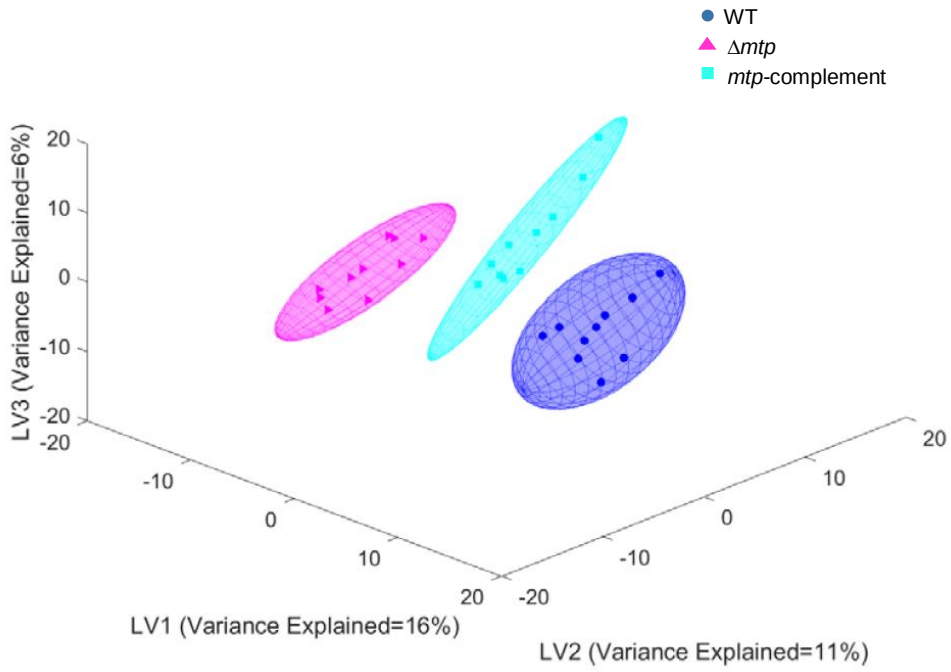

Figure 2.3 A PLS-DA scores plot comparing the three bacterial strains highlighting the variation associated with genotype. Dots represents cases projected onto the new lower-dimensional space considering their group association (indicated in the figure key) generated by the PLS-DA model within. Ellipsoids represent a 90 % confidence interval (CI) of score centroids for each group. The percentage of the overall variation explained by each latent variable (a linear combination of the metabolites which forms a new dimension in the modelled subspace), is indicated in brackets along each axis.

2.4.3 Spearman Correlation Plots show less correlation between WT and Δmtp, and more correlation between WT and mtp-complement

Figure 2.4 shows the Spearman Correlation Plots based on subsets of data; WT and either Δ*mtp or mtp*-complement. Correlations observed between metabolites when considering only WT and Δ*mtp* cases (Figure 2.4a) were mostly of no real significance with some exceptions. Interestingly, when considering WT and *mtp*-complement cases (Figure 2.4b) stronger associations can be observed. This is evident from the dominant green colouring in the WT versus Δ*mtp* plot (Figure 2.4a), indicating low correlation values, compared to the more orange/red colouring seen in the WT versus *mtp*-complement plot (Figure 2.4b). This was an expected result as the *mtp*-complement will have returned to a similar, if not identical phenotype to the parental WT strain.

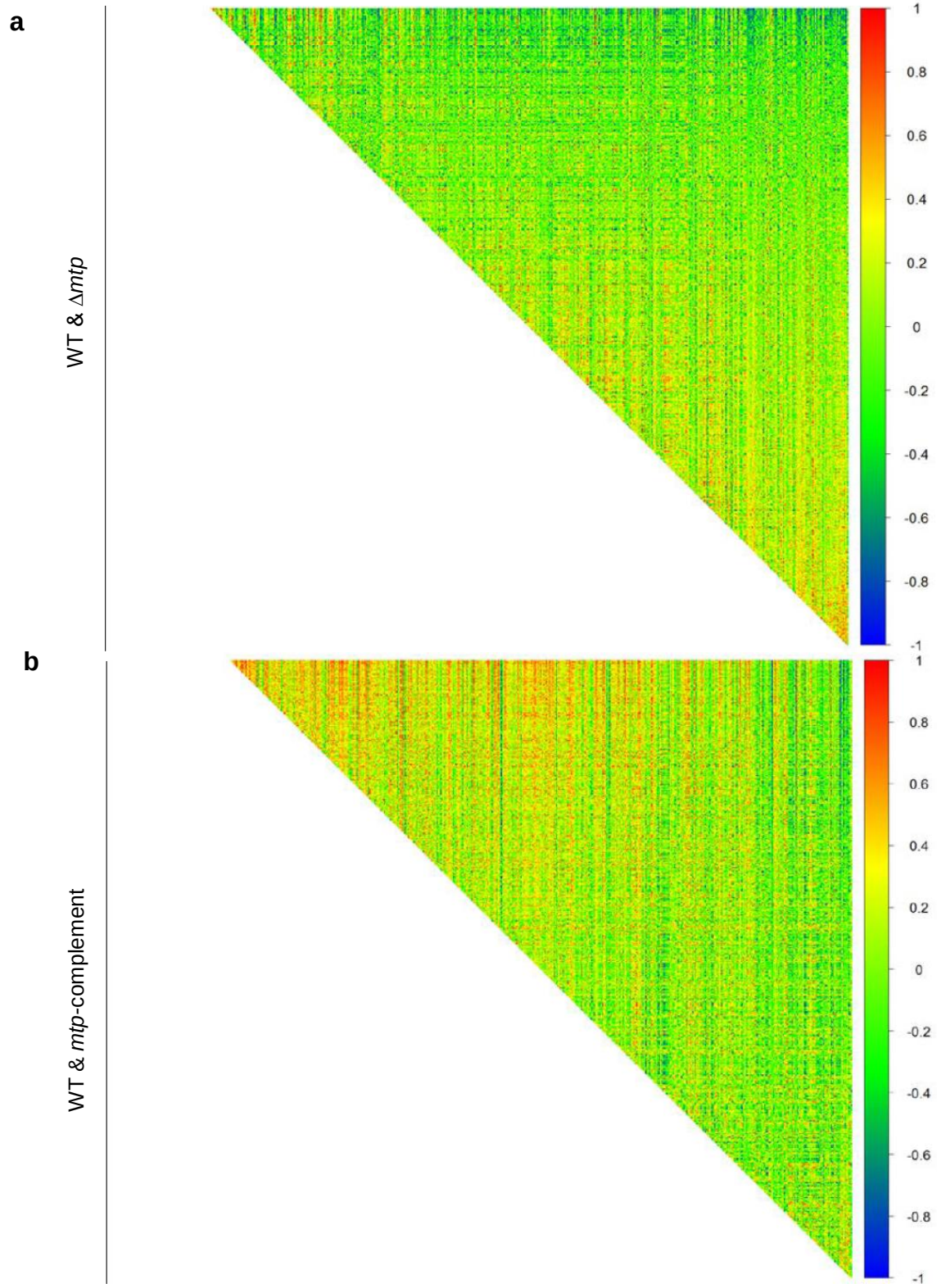

Figure 2.4 Spearman Correlation Plots comparing the bacterial strains. (a) considering WT and Δ*mtp* cases showing a poor degree of correlation with the abundance of green colouration. (b) considering WT and *mtp*-complement cases showing a greater degree of correlation as observed by the more evident orange/red colouration. Low correlation values, closer to 0, are associated with the green colouring and high correlation values, closer to 1 or -1, are associated with the red or dark blue colouring, respectively.

2.4.4 Four selection criteria were used to tabulate biologically significant metabolites between WT and Δmtp (Table 2.2), and between WT and mtp-complement (Table 2.3)

After data clean-up, 542 metabolites were detected amongst all three strains. Metabolites were shortlisted using the selection criteria; *t*-test *p*-value (after BH adjustment) ≤ 0.05, Cohen's d-value ≥ 0.8, PLS-DA VIP ≥ 1, and fold change ≥ 2. Metabolites were included in the shortlist if one or more of the criteria were met, resulting in 202 metabolites with discriminatory ability between WT and Δ*mtp*, and 180 metabolites between WT and *mtp*-complement. The shortlist was further refined by selecting the metabolites that met all four criteria. A total of 49 metabolites met all criteria between WT and Δ*mtp* (Appendix C8: Table C8.1), however, only 27 of these (Table 2.2) were deemed biologically significant based on supporting literature and analysis of metabolites and pathways using PubChem (Kim et al., 2019) and/or KEGG (Kanehisa et al., 2017). The metabolites that were of statistical and practical significance, when comparing WT to Δ*mtp,* were categorized according to biological relevance. Overall, three of the fourcategories were produced in greater quantity by Δ*mtp* than WT; carbohydrates in cell wall biogenesis, fatty acid metabolism and peptidoglycan synthesis. One of the four categories, amino acid and protein synthesis, was mostly produced in lower relative concentration in Δ*mtp* compared to WT. There were eight carbohydrates associated with cell wall biogenesis, seven of which were increased in the Δ*mtp*. D-Galactofuranose was the only metabolite in the group that was decreased in the Δ*mtp* compared to the WT. All six metabolites associated with fatty acid metabolism had a higher relative concentration in Δ*mtp* compared to WT. For the amino acid and protein synthesis category, eight of the 10 metabolites had a higher relative concentration in the WT cells except for dl-2-aminoadipic acid and cadaverine. All three metabolites associated with peptidoglycan synthesis were produced in higher relative concentrations in Δ*mtp*. A total of 16 metabolites met all criteria between WT and *mtp*-complement (Appendix C8: Table C8.2). Only seven of these metabolites were of biologically relevance (Table 2.3), five of which were found in higher relative concentrations in the WT, except for α-D-Glucopyranoside and 11-eicosenoic acid which were increased in Δ*mtp.*

Table 2.2 Most significant metabolites between *M. tuberculosis* WT and Δ*mtp* strains selected as per multivariate and univariate selection criteria together with their respective mean relative concentration and standard deviation, fold change with respect to the WT, PLS-DA VIP value, Cohen's d-value and BH-adjusted *p*-value

Category	Metabolite	Mean relative concentration and standard deviation (ng/mg cells)		Fold change	PLS-DA VIP	d-value	*p*-value
		WT	Δ*mtp*				
Carbohydrates in cell wall biogenesis	D-Galactose	3.52E-03 (1.22E-03)	1.63E-02 (4.08E-03)	4.635	7.867	3.164	<0.001
	D-Glucose	2.95E-04 (1.96E-04)	1.87E-03 (7.93E-04)	6.350	2.334	1.989	0.001
	D-Mannose	3.87E-03 (2.13E-03)	9.58E-03 (2.57E-03)	2.479	2.143	2.231	<0.001
	Glucopyranose	2.30E-03 (8.98E-04)	9.13E-03 (2.95E-03)	3.977	2.375	2.328	<0.001
	D-Mannopyranose	8.64E-05 (5.07E-05)	5.21E-04 (2.04E-04)	6.035	1.899	2.129	0.001
	D-Galactofuranose	2.82E-04 (1.24E-04)	1.36E-04 (3.03E-05)	-2.073	3.511	1.175	0.022
	D-Ribofuranose	2.70E-04 (1.87E-04)	6.74E-04 (2.43E-04)	2.495	1.348	1.665	0.005
	D-Erythro-pentofuranose	2.44E-03 (8.09E-04)	0.014 (6.25E-03)	5.554	1.036	1.780	0.003
Metabolites associated with fatty acid metabolism	Docosanoic acid	3.37E-04 (1.16E-04)	1.01E-03 (1.13E-04)	2.988	5.057	5.796	<0.001
	Hexacosanoic acid	1.63E-03 (4.69E-04)	4.63E-03 (1.03E-03)	2.834	4.289	2.926	<0.001
	Tetracosanoic acid	5.12E-04 (1.23E-04)	1.33E-03 (2.74E-04)	2.591	3.593	2.970	<0.001
	Linolenic acid	2.65E-04 (1.00E-04)	6.07E-04 (1.91E-04)	2.288	1.100	1.789	0.002
	9-Octadecenoic acid	8.15E-04 (2.71E-04)	2.00E-03 (8.28E-04)	2.452	3.768	1.429	0.009
	Myo-inositol	0.022 (0.007)	0.059 (0.008)	2.701	4.593	1.757	0.003

Table 2.3 Most significant metabolites between *M. tuberculosis* WT and Δ*mtp* strains selected as per multivariate and univariate selection criteria together with their respective mean relative concentration and standard deviation, fold change with respect to the WT, PLS-DA VIP value, Cohen's d-value and BH-adjusted *p*-value

Category	Metabolite	Mean relative concentration and standard deviation (ng/mg cells)		Fold change	PLS-DA VIP	d-value	*p*-value
		WT	Δ*mtp*				
Metabolites involved in amino acid and protein synthesis	L-Aspartic acid	0.092 (0.028)	0.027 (0.011)	-3.365	4.651	2.364	<0.001
	N-Acetylaspartic acid	5.14E-04 (4.10E-04)	7.18E-05 (1.99E-05)	-7.163	3.899	1.079	0.033
	Tryptophan	4.01E-03 (1.42E-03)	1.43E-03 (7.12E-04)	-2.800	4.110	1.815	0.002
	L-Proline	1.10E-03 (4.60E-04)	5.21E-04 (1.93E-04)	-2.110	3.079	1.257	0.017
	L-Threonine	4.47E-03 (5.92E-03)	1.47E-03 (7.44E-04)	-3.043	1.855	1.47	0.008
	dl-2-Aminoadipic acid	2.84E-04 (1.52E-04)	1.30E-03 (9.19E-04)	4.589	4.790	1.11	0.029
	Cadaverine	4.82E-05 (2.19E-05)	1.03E-04 (4.69E-05)	2.138	2.377	1.19	0.022
	2-Hydroxyisovaleric acid	4.43E-04 (2.48E-04)	1.48E-04 (6.1E-05)	-2.996	3.336	1.19	0.022
	Propanetriol	8.46E-04 (2.70E-04)	3.16E-04 (4.92E-05)	-2.678	3.157	1.96	0.002
	Methylcitric acid	9.54E-04 (3.78E-04)	4.58E-04 (9.15E-05)	-2.082	2.807	1.31	0.014
Involvement of some metabolites in peptidoglycan synthesis	N-Acetyl-D-glucosamine	1.38E-04 (4.23E-05)	6.10E-04 (1.19E-04)	4.414	6.958	3.96	<0.001
	D-Fructose	3.92E-03 (1.68E-03)	0.010 (0.002)	2.564	3.254	2.69	<0.001
	Phosphoric acid	0.005 (0.001)	0.013 (0.002)	2.485	6.720	4.75	<0.001

WT: wild-type; Δ*mtp*: *mtp*-gene knockout mutant; PLS-DA VIP: Partial Least Squares Discriminatory Analysis Variable in Projection value; Positive fold change = higher concentration in Δ*mtp*; Negative fold change = higher concentration in WT.Table 2.4 Most significant metabolites between *M. tuberculosis* WT and

***mtp*-complemented strains selected as per multivariate and univariate selection criteria together with their respective mean relative concentration and standard deviation, fold change with respect to the WT, PLS-DA VIP value, Cohen's d-value and BH-adjusted *p*-value**

Metabolite	Mean relative concentration and standard deviation (ng/mg cells)		Fold change	PLS-DA VIP	d-value	*p*-value
	WT	*mtp*-complement				
11-Eicosenoic acid	8.08E-05 (3.15E-05)	4.83E-04 (2.33E-04)	5.977	5.306	1.730	0.005
α-D-Glucopyranose	0.020 (0.007)	0.007 (0.001)	-2.956	5.112	2.032	0.002
α-D-Glucopyranoside	8.14E-04 (3.36E-04)	0.002 (7.57E-04)	2.372	2.411	1.478	0.008
2-Hydroxyisovaleric acid	4.43E-04 (2.48E-04)	1.66E-04 (1.01E-04)	-2.664	3.082	1.116	0.034
Alanine	0.002 (0.001)	6.87E-04 (6.48E-04)	-3.523	2.988	1.454	0.009
5'-S-Methyl-5'-thioadenosine	9.04E-04 (2.19 E-04)	3.02 E-04 (1.67E-04)	-2.995	3.482	2.744	<0.001
Adenosine	0.001 (4.39E-04)	4.63E-04 (4.68E-04)	-2.686	0.995	1.668	0.009

WT: wild-type; *mtp*-complement: *mtp*-complemented strain; PLS-DA VIP: Partial Least Squares Discriminatory Analysis Variable in Projection value; Positive fold change = higher concentration in *mtp*-complement; Negative fold change = higher concentration in WT.

2.4.5 Gene expression data significantly correlates with metabolomics data

The Δ*mtp* strain expressed the highest level of all genes except *fadE5* compared to the WT and *mtp*-complement (Figure 2.5). This pattern in the transcriptomics data was supported by the metabolomics data for the respective metabolite pathways where the Δ*mtp* strain produced various metabolites in increased concentrations compared to the WT strain.

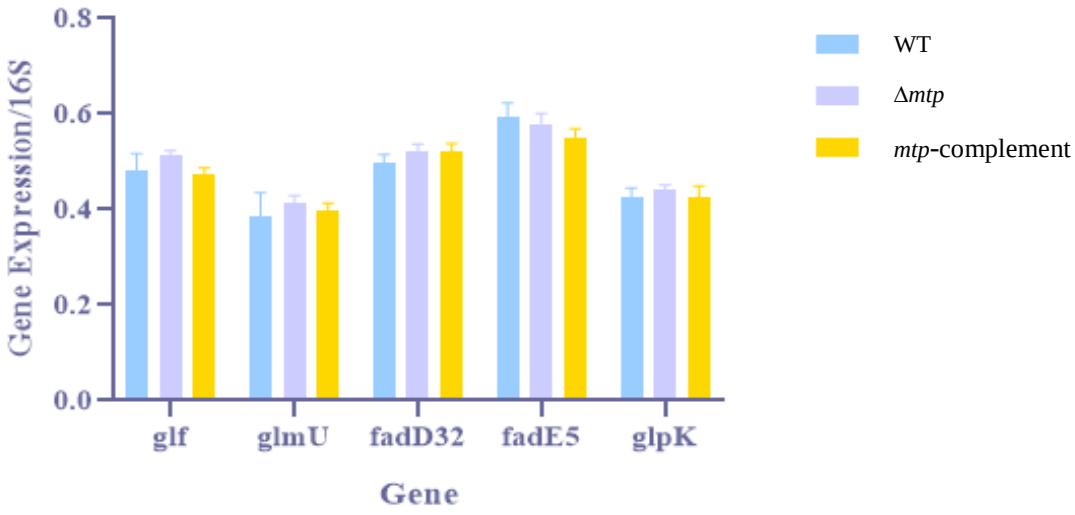

Figure 2.5 The validation of metabolomics data using real-time quantitative PCR to assess gene expression of five genes (*glf, glmU, fadD32, fadE5* and *glpK*). The relative standard curve method of interpretation was used for assessment of RT-qPCR data. The results were represented as gene expression levels normalised to 16S rRNA for each gene of interest. Significance levels were established using the unpaired sample *t*-test for parametric data between the WT and Δ*mtp* strains, and for the WT and *mtp*-complement strains. Between the WT and Δ*mtp*, 4 of the genes displayed statistical significance; *glf* ($p = 0.0033$), *glmU* ($p = 0.0068$), *fadD32* ($p = 0.001$) and *glpK* ($p = 0.0247$). The gene *fadE5* was non-significant ($p = 0.1723$). Expression levels of four of the genes in the Δ*mtp*-complement were restored to the WT levels; *glf* ($p = 0.9777$), *glmU* ($p = 0.1792$), *fadD32* ($p = 0.1195$) and *glpK* ($p = 0.4181$) while the gene *fadE5* was significantly expressed, compared to the WT ($p = 0.0093$).

2.5 Discussion

Previous studies have demonstrated that the surface-located adhesin, MTP, plays an important role as the first point of contact during the host-pathogen interaction (Alteri et al., 2007; Ramsugit and Pillay, 2014; Ramsugit et al., 2016). Functional genomics clarified the involvement of MTP in adhesion and invasion of A549 pulmonary epithelial cells and THP-1 macrophages, as well as in biofilm formation (Ramsugit et al., 2013; Ramsugit and Pillay, 2014; Ramsugit et al., 2016). MTP was further suggested to dampen cytokine/chemokine induction in epithelial cells, as a survival strategy (Ramsugit et al.,

2016). Global transcriptomics in an epithelial cell and mouse model, produced further evidence of the involvement of MTP in inducing significant host immune response genes, pathways and networks (Nyawo, 2016; Dlamini, 2017). These findings collectively indicated that MTP are potentially suitable as a TB diagnostic target and vaccine candidate. This provided the impetus for the current study, which hypothesised that MTP contributes to the regulation of the metabolome of *M. tuberculosis*, and to identify potential metabolic pathways and/or specific metabolites that could be exploited as intervention targets.

A number of metabolites, including carbohydrates, fatty acids and amino acids were detected, and found to be significantly differentially produced by the strains compared in this study. The majority of these metabolites were elevated in the Δ*mtp* strain compared to the WT strain, while fewer differences were observed between the WT and *mtp*-complement strains. These findings suggest that the deletion of *mtp* resulted in a significant perturbation of the *M. tuberculosis* metabolome while gene complementation returned the metabolome to a state similar to the WT. The 27 practically and biologically significant metabolites identified in the Δ*mtp* strain, compared to the WT strain, were categorised into four groups based on functional relevance (Table 2.2) and their potential roles in various metabolic pathways are discussed, according to KEGG analysis (Kanehisa et al., 2017). The seven biologically significant metabolites that were detected when comparing the *mtp*-complement strains to that of WT strains (Table 2.3) could not be categorised although their potential involvement in metabolism is explained.

2.5.1 The role of MTP and the utilization of carbohydrates for cell wall biogenesis in M. tuberculosis.

D-galactose, along with D-arabinose, make up arabinogalactan, a *Mycobacterium* cell wall polymer that facilities covalent attachment of peptidoglycan and mycolic acids (Azuma et al., 1970; Ramakrishnan et al., 1972; Brennan and Nikaido, 1995). Arabinomannan, another cell wall polymer, is composed of galactose and mannose (Azuma et al., 1970; Titgemeyer et al., 2007). The accumulation of galactose and mannose, indicated by their elevated levels in the Δ*mtp* strain in the current study, may suggest a reduction of arabinogalactan and arabinomannan as demonstrated in an ESX-1 knockout mutant compared to its WT strain (Loots et al., 2016). In the present study, the elevated relative concentrations of D-glucose observed in the Δ*mtp* strain, suggests reduced utilization of this substrate for cell wall synthesis. Similarly, a hypo-virulent Beijing strain of *M. tuberculosis* previously showed a similar increase in D-galactose, D-mannose and D-glucose, compared to the hyper-virulent strain (Meissner-Roloff et al., 2012). These findings collectively indicated that these metabolites are more efficiently used for energy production for cell wall synthesis in the faster growing WT or hyper-virulent strains in the aforementioned metabolomics investigations, and similarly explain their increased growth rates in the WT strain compared to the slower growing Δ*mtp* mutant strains used in the current investigation

(Nyawo, 2016; Govender, 2019). Furthermore, since both D-mannopyranose and glucopyranose play an important role in cell wall biosynthesis as carbohydrate precursors (Pathak et al., 2004; Kanehisa et al., 2017), reduced relative concentrations of these metabolites in the WT allude to a more efficient integration of these metabolites into the cell wall compared to the Δ*mtp* strain.

The mycolic acid-arabinogalactan-peptidoglycan (mAGP) complex, composed of mycolic acid lipids, arabinofuranose and galactofuranose residues (Mikusová et al., 2005; Wesener et al., 2017), is a crucial glycoconjugate structure that forms the major structural element of the mycobacterial cell wall (Joe and Lowary, 2016; Completo and Lowary, 2019). Drug development research for anti-mycobacterial agents, could in the future target the specific inhibition of the mAGP complex, thereby crippling the proliferation of *M. tuberculosis* (Joe and Lowary, 2016). The metabolomics findings in the current investigation, demonstrated greater utilisation of the D-galactofuranose (reduced relative concentrations) in the Δ*mtp* strain compared to the WT strain. While this finding was unexpected, it may suggest a potential increased requirement for D-galactofuranose to compensate for the cell wall alteration due to the loss of the MTP adhesin, or an impaired synthesis of the metabolite which may have a cascading effect on the glycoconjugate structure and ultimately on the cell wall synthesis of the pathogen due to the loss of MTP, all of which supports the aforementioned mechanisms related to the role of MTP.

The metabolite decaprenylphosphoryl-β-d-ribofuranose, a form of D-ribofuranose present in *M. tuberculosis*, is converted via a series of reactions to decaprenylphosphoryl-β-d-arabinofuranose, which ultimately serves as the precursor for the synthesis of arabinan (Mikusová et al., 2005; Alderwick et al., 2015; Rogacki et al., 2018). D-Erythro-pentofuranose is commonly found in *M. tuberculosis* in the form of decaprenylphosphoryl-2-keto-β-d-erythro-pentofuranose and decaprenylphosphoryl-2-keto-beta-D-erythro-pentose reductase (Mikusová et al., 2005). Both D-ribofuranose and D-erythro-pentofuranose are major cell wall components that were found in elevated relative concentrations in the Δ*mtp* strain compared to the WT. The accumulation of these metabolites in the Δ*mtp* are indicative of a reduced arabinan synthesis (Mikusová et al., 2005; Alderwick et al., 2015; Rogacki et al., 2018) in the absence of MTP. It is important to note, that these metabolites were present in similar relative concentrations in the WT and complemented strains, and therefore, the above findings collectively suggest that MTP plays a vital role in the efficient uptake of specific carbohydrates in cell wall biogenesis.

2.5.2 The role of MTP and the utilisation of fatty acids by M. tuberculosis

Docosanoic acid, linolenic acid and oleic acid are involved in the biosynthesis of unsaturated fatty acids (Kim et al., 2019). Fatty acid biosynthesis is essential for the formation of cell wall components such as mycolic acids in mycobacteria (Kinsella et al., 2003). The metabolite, 9-octadecenoic acid, is a chemical derivative of oleic acid and is formed when the 9,10 double bond of oleic acid undergoes

stereospecific hydration (Baker and Gunstone, 1963; Niehaus et al., 1970). It is a major fatty acid constituent found in most strains of mycobacteria along with hexadecanoic acid (Lambert et al., 1986). These metabolites form part of fatty acid metabolism that is necessary for mycobacterial survival where fatty acids are accumulated and stored in globules functioning as a reservoir for access to a carbon energy source (Schaefer and Lewis, 1965). Elevated relative concentrations of docosanoic acid, linolenic acid and 9-octadecenoic acid, were found in the Δ*mtp* strain compared to the WT, indicating dysfunctionality of the Δ*mtp* strain for utilizing these fatty acids in the integration of their respective lipid by-products into the cell wall. Tetracosanoic acid, also known as lignoceric acid, is a 24-carbon straight-chain saturated fatty acid found mostly in extracellular cytoplasmic locations, membranes or peroxisomes of all living organisms (Wishart et al., 2018). This metabolite, in combination with hexacosanoic acid, have been previously used for TB diagnostic applications. Members belonging to the *M. tuberculosis* complex (MTBC) were differentiated from the mycobacterial members of the *M. avium-M. intracellulare-M. scrofulaceum* (MAIS) complex by gas chromatography, by a mean hexacosanoic acid content of 4 % and trace amounts, and a mean tetracosanoic acid content of 1 % and 5 %, respectively (Jantzen et al., 1989). Similarly, tetracosanoic acid and hexacosanoic acid have shown promise for use as diagnostic markers to differentiate *M. fortuitum* from *M. genavense* using gas-liquid chromatography (Chou et al., 1998). In the current study, the relative concentration of these two metabolites were significantly lower in the WT strain as compared to the Δ*mtp* strain, with the accumulation in the Δ*mtp* strain suggesting abnormal incorporation into the cell wall, and /or cell signalling (Chou et al., 1998). Furthermore, this reduction may also suggest a reduced energy production capacity and hence a reduced virulence in the Δ*mtp* strain (Meissner-Roloff et al., 2012).

Myo-inositol was first discovered in the phospholipids of mycobacterium cell envelopes in the form of phosphatidyl-myo-inositol glycosides, more specifically phosphatidyl-myo-inositol mannosides (PIMs) (Vilkas and Lederer, 1960). The PIMs are unique glycolipids located in the inner and outer membranes of *Mycobacterium* cell envelopes and are considered crucial for maintaining membrane structure (Sancho-Vaello et al., 2017). The PIMs are also precursors of lipomannan and lipoarabinomannan, which are lipoglycans involved in host and pathogen interaction (Sancho-Vaello et al., 2017), and hence considered important virulence factors and essential components in the survival of these pathogens. There is also particular interest in this PIM biosynthetic pathway in terms of targeted TB drug discovery, owing to its exclusivity to mycobacteria (Boldrin et al., 2014) and other human pathogens such as *Pseudomonas aeruginosa*, *Streptococcus pneumoniae* and *Staphylococcus aureus* (Berg et al., 2001; Lind et al., 2007; Boldrin et al., 2014). In the present study, the comparatively elevated relative concentrations of myo-inositol in the Δ*mtp*, indicates inhibition of PIM in this strain. Similarly, myo-inositol was also found in elevated relative concentrations in the hypo-virulent strain when compared to a hyper-virulent strain of *M. tuberculosis* (Meissner-Roloff et al., 2012), and subsequently the higher relative concentrations in the Δ*mtp* strain in the current study suggests a reduced

ability to utilise this lipid in synthesising the characteristic lipid-rich cell wall and also suggests that MTP plays a role in the pathogenicity of *M. tuberculosis* by promoting the utilization of key fatty acids in cell wall biogenesis.

2.5.3 The role of MTP in amino acid and protein synthesis in M. tuberculosis

Aspartic acid, N-acetylaspartic acid and threonine were seen to be significantly reduced in the Δ*mtp* strain comparatively. N-Acetylaspartic acid is a precursor of aspartic acid (Kanehisa et al., 2017), a non-essential amino acid that is known to play a role in the synthesis of nucleotides and other amino acids, including threonine, proline, alanine, isoleucine, glycine, serine and glutamate (Kanehisa et al., 2017; Kim et al., 2019). Similarly to the present study, aspartic acid was also significantly reduced in the hypo-virulent compared to the hyper-virulent Beijing strains (Meissner-Roloff et al., 2012). These results collectively demonstrate a role for MTP in inducing a more efficient production of aspartic acid, N-acetylaspartic acid and threonine, and the impact this has on a variety of other amino acid metabolic pathways in *M. tuberculosis*.

Tryptophan is an amino acid that is important in protein synthesis and is synthesized *de novo* by *M. tuberculosis* (Zhang et al., 2013). This characteristic is useful for *M. tuberculosis* to overcome tryptophan starvation during infection. Host immune cells such as CD4 T cells, prevent invasion of some pathogens via tryptophan starvation by which tryptophan is catabolized by the enzyme indoleamine 2,3-dioxygenase (Zelante et al., 2009). The significantly reduced relative concentrations of tryptophan in the Δ*mtp* strain, suggests that MTP confers an advantage to the pathogen by aiding host immune evasion.

The amino acid L-proline, a building block in protein synthesis, also participates in arginine and proline metabolism, ATP-binding cassette (ABC) transportation and aminoacyl-tRNA biosynthesis (Kim et al., 2019). It is a well-known carbon and nitrogen source for most bacteria (Zhang et al., 2015), and is found near the N-terminus of both proline-glutamate and proline-proline-glutamate proteins (Akhter et al., 2012). Proline can be synthesized from glutamate (Zhang et al., 2015) and serves as a significant organic compatible solute. Proline facilitates the maintenance of cellular osmotic pressure necessary for bacterial growth (Csonka, 1989). In the current study, comparatively low relative concentrations of proline were detected for Δ*mtp* compared to the WT, as had also been reported in the hypo-virulent strain of *M. tuberculosis* (Meissner-Roloff et al., 2012). This is suggestive of decreased cell wall synthesis, metabolic activity, rate of replication and an altered antioxidant capacity (Meissner-Roloff et al., 2013). The relatively lower concentration of this metabolite in the Δ*mtp* strain might also suggest that this amino acid is synthesized in lower concentrations in contrast to the WT where it may be involved in an alternate function such as protein synthesis as previously mentioned (Meissner-Roloff et al., 2013). Interestingly, protein analyses have shown that the MTP consists of proline and glycine

residues, characteristic of pilin proteins (Alteri et al., 2007). Hence, the increased levels of proline (Table 2.2) and glycine (WT = 0.018 ng/mg cells; Δ*mtp* = 0.004 ng/mg cells; did not meet shortlist criteria) may indicate that the WT is able to assemble the MTP protein due to sufficiently available levels of these two amino acids in contrast to the Δ*mtp* strain.

The metabolite, dL-2-aminoadipic acid, also referred to as L-2-aminoadipate is an intermediate in lysine degradation and biosynthesis (Kim et al., 2019). Elevated levels of dL-2-aminoadipic acid was found in Δ*mtp* compared to the WT strain. High levels of dL-2-aminoadipic acid were also found in the hypo-virulent Beijing strain of *M. tuberculosis* in comparison to the hyper-virulent strain (Meissner-Roloff et al., 2012) suggesting that the lysine biosynthesis pathway is upregulated in the less virulent strain possibly as a compensatory mechanism.

Cadaverine, synthesised from lysine, regulates acid tolerance, membrane permeability, RNA synthesis, glutathione metabolism, and tropane, piperidine and pyridine alkaloid biosynthesis (Kamio et al., 1981; Neely and Olson, 1996; Samartzidou and Delcour, 1998; Kim et al., 2019). In *Escherichia coli*, cadaverine was reported to induce porin closure, which in turn reduces the cellular uptake of numerous metabolites (Samartzidou and Delcour, 1998). The elevated cadaverine in the Δ*mtp* strain, most likely resulting in the closure of the *M. tuberculosis* porins, leads to a reduced uptake of nutrients through its porin structures of the cell, significantly lowering metabolic and growth rates. Similar results were seen previously in the hypo-virulent Beijing strain (Meissner-Roloff et al., 2012), and the ESX-1 knockout mutant strains of *M. tuberculosis*, which are known to have an altered cell envelope composition and reduced levels of nutrient influx (Loots et al., 2016). Furthermore, cadaverine also functions as a direct radical scavenger, and was previously reported to be upregulated in *M. tuberculosis* experiencing elevated oxidative stress (Loots, 2014).

The metabolite, 2-hydroxyisovaleric acid (also known as β-hydroxy-β-methylbutyric acid (Wishart et al., 2018)), is a hydroxyl fatty acid product of the isoleucine degradation pathway, most commonly reported in humans (Landaas, 1975; Mobley et al., 2014; Ehling and Reddy, 2015). Elevated relative concentrations of 2-hydroxyisovaleric acid however, have also been identified in *M. phlei*, grown under hypoxic conditions. In the current study, the reduced relative concentrations of this metabolite in the Δ*mtp* strain possibly indicates either a reduced availability of isoleucine for growth, or reduced capacity of the Δ*mtp* strain for metabolising isoleucine (Landaas, 1975; Ehling and Reddy, 2015), with the former being the more likely cause. Furthermore, the metabolism of isoleucine allows for the synthesis of propionic acid, which in turn serves as a precursor for the methylcitric acid cycle of *M. tuberculosis* (Kanehisa et al., 2017). This furthermore, explains the reduced levels of methylcitric acid in the Δ*mtp* strain comparatively.

Propanetriol (or glycerol), a supplement commonly used in the growth media to culture *M. tuberculosis*, serves as a carbon source for growth and is taken up by the cells via passive diffusion (Cook et al., 2009). It is then converted via phosphorylation to glycerol-3-phosphate by action of glycerol kinase after which it participates in central carbon metabolism (Cook et al., 2009). However, it has been reported that during the course of infection, *M. tuberculosis* switches from carbon metabolism (using glycerol or glucose) to lipid metabolism (using fatty acids and host lipids) (Cook et al., 2009). In the present study, the reduced relative concentrations of propanetriol observed in the Δ*mtp* strain comparatively, indicate a greater utilisation of this metabolite as a carbon source for growth as a compensatory mechanism to the reduced fatty acid catabolism seen, in combination to a reduced uptake, due to elevated cadaverine resulting in porin closure (Samartzidou and Delcour, 1998).

The elevated levels of most of the significantly detected amino acids with the exception of dL-2-aminoadipic acid and cadaverine, in the WT strain, may reflect its propensity to favour amino acid and protein synthesis in the presence of MTP. The potential impact of the relatively lower concentrations of these amino acids present in the Δ*mtp* strain was manifested by its significantly decreased growth rate compared to the WT during log phase culture in Middlebrook 7H9 broth in a previous study by the same research group (Nyawo, 2016; Govender, 2019).

2.5.4 The role of MTP in peptidoglycan synthesis in M. tuberculosis

The metabolite, N-acetyl-D-glucosamine, is involved in amino sugar and nucleotide sugar metabolism, ABC transport and the phototransferase system, apart from playing an important role in the structure of bacterial peptidoglycan (Schleifer and Kandler, 1972; Kim et al., 2019). Although there are differences in the chemistry of the glycans among bacteria, the glycan chains are generally mostly composed of alternating, β-1,4-linked N-acetylglucosamine and N-acetylmuramic acid subunits (Schleifer and Kandler, 1972). Cellular D-fructose occurring as D-fructose-6-phosphate, plays a role in peptidoglycan synthesis in mycobacteria (Alderwick et al., 2015). Phosphoric acid, is also involved in oxidative phosphorylation, peptidoglycan biosynthesis and ABC transporter systems (Kim et al., 2019). In the present study, the accumulation of N-acetyl-D-glucosamine, D-fructose and phosphoric acid in the Δ*mtp* strain, is indicative that these metabolites were not integrated as efficiently into the peptidoglycan of its cell wall comparatively, and the role of MTP in peptidoglycan synthesis.

2.5.5 Complementation with mtp largely restores the altered metabolomics profile of the Δmtp strain to that of the WT strain

This study focused on identifying significant metabolites that were perturbed by the absence of MTP. The complemented strain or *mtp*-complement, in which the MTP production was restored, was also investigated to confirm whether phenotypical alterations observed in the Δ*mtp* was due to the genotypic

differences caused by deletion of the *mtp* gene specifically. The *mtp*-complement was expected to phenotypically react similarly, if not identically, to the WT. As depicted in Table 2.3, the metabolites produced by *mtp*-complement differed from the WT by only seven (0.96 %) of 731 statistically and biologically significant metabolites of the overall metabolite profile, hence indicating that the metabolomes of the WT and *mtp*-complement are in essence almost identical. These minor differences in the metabolite profile of *mtp*-complement may be due to complementation via the insertion of a non-integrating plasmid (Ramsugit et al., 2013), or analytical variation in the metabolomics analyses. Interestingly, the metabolites that were found in relatively higher concentrations in the *mtp*-complement compared to the WT included 11-eicosenoic acid and alpha-D-glucopyranoside, which are associated with cell envelopes. The elevated production of these metabolites in the *mtp*-complement are most likely due to the presence of the over-expressing *mtp* following complementation (Ramsugit et al., 2013), further substantiating the role of MTP in cell envelope structure. The metabolite, 11-eicosenoic acid, a monounsaturated fatty acid has been previously reported in two relatives of *M. tuberculosis; M. aurum* and *M. smegmatis.* In *M. aurum*, eicosenoic acid is present in the methyl-branched fatty acids 2-L, 4-L-dimethyl-11-eicosenoic acid and 2-L, 4-L-dimethyl-14-eicosenoic acid (Rafidinarivo et al., 1982). Similarly, 2,4-dimethyl-2-eicosenoic acid is a major lipooligosacharide located within deeper compartments of the cell envelope of *M. smegmatis* (Etienne et al., 2009). Eicosenoic acid had not previously been identified in *M. tuberculosis* potentially due to its complex location. However, in the current study, the relative concentrations were 8.08×10^{-5}, 0.000245 and 0.000483 ng/mg in the WT, Δ*mtp* and *mtp*-complement, respectively. The elevated concentrations of this metabolite in the *mtp*-complement, points toward its decreased utilisation and thereby, resulting in a possibly altered fatty acid cell envelope composition in the *mtp*-complement relative to the WT.

Alpha-D-glucopyranose and alpha-D-glucopyranoside, also present in the cell envelope of *M. tuberculosis* (Angala et al., 2014), are derivatives of glucose produced during fructose and mannose degradation, galactose metabolism, gluconeogenesis and glycolysis (Kim et al., 2019). A comparatively lower relative concentration of alpha-D-glucopyranose (pyranose form of glucose) and a higher relative concentration of alpha-D-glucopyranoside (glycoside of glucopyranose), were observed in the *mtp*-complemented strain compared to the WT. This indicates a slight dysfunctionality in these pathways perhaps in the *mtp*-complemented strain, and while this is unexpected, may be explained by pili overexpression in this strain.

The relatively lower concentrations of 2-hydroxyisovaleric acid, involved in the isoleucine degradation pathway, and alanine that is part of peptidoglycan synthesis within *M. tuberculosis* (Bruning et al., 2011), indicates that the *mtp*-complement is still slightly impaired in the production of these metabolites compared to the WT .

The metabolite, 5'-S-methyl-5'-thioadenosine (MTA), is hydrolysed by MTA nucleosidase to form adenine and 5'-methylthioribose (Buckoreelall et al., 2012; Namanja-Magliano et al., 2017). Adenine can then be utilised in the purine salvage pathway where adenine nucleotides can be formed, and 5'-methylthioribose proceeds to the methionine salvage pathway after it has been phosphorylated to 5'-methylthioribose-1-phosphate (Buckoreelall et al., 2012). The lower levels of these 2 metabolites may be suggestive of marginally defective pathways in the *mtp*-complement relative to the WT.

Adenosine has additional roles and derivatives other than its incorporation into DNA or RNA. In *M. tuberculosis*, adenosine is phosphorylated to adenosine monophosphate via the catalytic activity of adenosine kinase during the purine salvage pathway (Long et al., 2003). A study using *M. smegmatis* identified the enzyme, 5′-methylthioadenosine phosphorylase, that is responsible for the cleavage of adenosine into adenine in a degradative pathway (Buckoreelall et al., 2011). In the present study, the relatively lower concentration of adenosine in the *mtp*-complement suggests decreased synthesis, and hence lower availability of this metabolite in the degradative pathway compared to the WT strain.

It must be noted that the unexpected findings that four metabolites were produced greater than 2-fold and two less than 2-fold in the WT compared to the *mtp*-complement, and which may have impacted on their respective metabolic pathways in the latter represents minor, only 0.96 % of the 731 detected metabolites of the overall metabolite profile.

2.5.6 Functional analysis using RT-qPCR support metabolomics results

The gene *glf,* encodes a UDP-galactopyranose mutase, which is involved in galactose metabolism and plays a role in cell wall biosynthesis (Kim et al., 2019). The metabolite, UDP-galactofuranose, and galactose residues are vital components of arabinogalactan (Azuma et al., 1970; Brennan and Nikaido, 1995) that connect the peptidoglycan and the mycolic acids, making it essential for cell viability (Halouska et al., 2014). The metabolomics data demonstrated a higher relative concentration of galactose (0.016312 ng/mg cells), consistent with the significantly higher gene expression in the Δ*mtp* ($p = 0.0033$) than the WT (0.003519 ng/mg cells). Gene function was restored in the *mtp*-complement as demonstrated by the lack of a significant difference ($p = 0.9777$) in the expression levels of this gene compared to the WT, with a corresponding 0.004692 ng/mg cells of galactose measured in the former strain.

Similar results were observed for the expression of the other 3 genes, *glpK*, *glmU* and fadD32. The gene, *glpK,* encodes a glycerol kinase that degrades glycerol during glycerolipid metabolism (Kim et al., 2019). This enzyme regulates glycerol metabolism and uptake to yield sn-glycerol 3-phosphate after phosphorylation of glycerol (Cook et al., 2009). The metabolomics data revealed lower relative concentrations of propanetriol (or glycerol) in the Δ*mtp* (0.000316 ng/mg cells) compared to WT

(0.000846 ng/mg cells). This was supported by the significantly higher expression (p = 0.0247) of *glpK* in Δ*mtp* when compared to the WT and may indicate a more rapid degradation of glycerol by the mutant to be used as a carbon source compared to the WT (Cook et al., 2009) or a reduced uptake as previously described. Complementation revealed no significant difference to the WT (p = 0.418).

The bifunctional N-acetyltransferase/uridylyltransferase encoded by *glmU*, catalyzes the final two steps in the UDP-N-acetyl-D-glucosamine biosynthesis I pathway to finally produce N-acetyl-D-glucosamine (Titgemeyer et al., 2007, Kim et al., 2019). Hence, *glmU* is essential for optimal growth of *M. tuberculosis*, since N-acetyl-D-glucosamine is an integral component of peptidoglycan. The metabolomics data revealed higher relative concentrations of this metabolite in Δ*mtp* (0.00061 ng/mg cells) when compared to the WT (0.000138 ng/mg cells) and is supported by the significantly increased *glmU* expression levels of the former (p=0.0068). This suggests that the deletion of *mtp* compensates by up-regulating the expression of *glmU*, resulting in the accumulation of N-acetyl-D-glucosamine in the mutant, and potentially hindering its utilization in peptidoglycan synthesis.

The genes *fadD32* and *fadE5*, encoding an acyl-CoA synthetase and an acyl-CoA dehydrogenase, respectively, are involved in fatty acid β-oxidation (lipid metabolism) which each splits into individual routes of breakdown (Kim et al., 2019). The catabolism of fatty acids proceeds via several routes, depending on the length of the acids, whether the number of carbons is odd or even, and whether they are saturated or unsaturated (Chow and Cox, 2011). The metabolites detected in this study, associated with fatty acid metabolism, were all increased in the mutant strain compared to the WT. This indicates an overall accumulation of these fatty acids in the mutant, suggestive of a slower breakdown of these lipids into their by-products. In support of this, the *fadD32* was significantly expressed at a higher level by the Δ*mtp* compared to the WT (p = 0.001), while the complemented strain was not significantly different from the WT. In contrast to *fadD32*, no significant difference was observed in the expression of *fadE5* between the WT and Δ*mtp*, although the complemented strain differed significantly from the WT (p = 0.0093). The gene expression findings suggest that the *fadD32* route of lipid breakdown, is utilised preferentially over the *fadE5* route by the WT. They further suggest that lipid metabolism should be efficient in Δ*mtp*. However, the metabolomics data has indicated this not to be the case. This points towards the possibility that a different gene/enzyme in this pathway may be downregulated, and needs to be investigated.

Ten of the 27 biologically relevant metabolites that differed significantly between the mutant and WT strains in this study, were identical to those reported by Meissner-Roloff et al. (2012) in an investigation comparing a hyper- and hypo-virulent strain of the Beijing lineage of *M. tuberculosis*. These metabolites include N-acetylaspartic acid, L-proline, dL-aminoadipic acid, tetracosanoic acid, myo-inositol, D-galactose, mannose, glucose, N-acetyl-D-glucosamine and cadaverine. The majority of these

metabolites are involved in cell wall synthesis and virulence, substantiating the possible association of the MTP adhesin with virulence.

In another similar study by Loots et al. (2016), the metabolomic changes associated with the ESX-1 gene cluster were investigated between an ESX-1 gene knockout mutant and the WT strain of *M. smegmatis*. A total of 4 out of 27 metabolites from the current study were found to be identical to those reported by Loots et al. (2016). These metabolites include D-galactose, mannose, phosphoric acid and cadaverine. Interestingly, these metabolites were also found to be associated with cell wall alterations and virulence attributes. The current study has demonstrated that the MTP adhesin has a strong association with cell envelope modification which may affect virulence and propagation of *M. tuberculosis* cells that lack this adhesin.

A limitation of this study is that the use of only a single *M. tuberculosis* strain makes it difficult to extrapolate the findings to all clinical strains. However, since metabolomics analyses in general are expensive, labour intensive, and time consuming, the testing of multiple, virulent clinical *M. tuberculosis* strains is challenging. Other factors that may affect metabolomic data is variation from the sample preparation techniques, and instrumentation. In the current study, this limitations were overcome by subjecting each sample and control to identical experimental conditions using rapid and accurate techniques to minimise variation, and by making use of quality controls and internal standards to ensure reproducibility and excellent quality reads. Another potential limitation stems from bioinformatics analyses as a range of approaches can be taken to analyse a given set of data. This limitation was mitigated by streamlining the selection of analyses for the current study according to the study design, aim and objectives of this investigation in order to produce the most ideal set of data necessary to answer the research question. A difficulty experienced in the current study was the lack of annotated *M. tuberculosis* pathways and metabolites that were identifiable with this bacterium. Nevertheless, studies like these can provide compelling metabolomics evidence to support hypotheses to help grow the already existing reservoir of genomics, transcriptomics and proteomics data. Future work should include phenotypic assays to investigate the various metabolic pathways that were perturbed, e.g. cell wall biogenesis and peptidoglycan synthesis using transmission electron microscopy (TEM) in order to elucidate possible cell envelope anomalies. *M. tuberculosis* has numerous adhesins on its cell surface, hence, the effect of those using functional metabolomics would prove invaluable in understanding their role in TB pathogenesis.

2.6 Conclusion

Apart from being an adhesin and invasin, and modulator of cytokine/chemokine response, the current study demonstrates that MTP also facilitated changes to the *M. tuberculosis* metabolome. Using functional metabolomics, the metabolites detected in this study provided greater insight to the effect of

the MTP deletion, on various metabolic pathways. The Δ*mtp* was associated with an altered cell wall composition as seen by the decreased utilisation of carbohydrates in cell wall biogenesis, a reduced efficiency in the breakdown of fatty acids, decreased amino acid biosynthesis, a reduction in peptidoglycan synthesis, which collectively may explain the mechanisms driving the previously reported growth retardation compared to the WT. The elevation of the majority of the metabolites (18 out of 27) in the Δ*mtp* strain compared to the WT, points towards an overall reduced ability for the utilisation of these metabolites for biological processes in the Δ*mtp* strain. Taken together, these metabolomic findings further validate the MTP adhesin as an important contributor to TB pathogenesis, and therefore, an important biomarker for the design of a diagnostic tool and intervention therapy.

2.7 References

Akhter, Y., Ehebauer, M. T., Mukhopadhyay, S. and Hasnain, S. E. (2012). The PE/PPE multigene family codes for virulence factors and is a possible source of mycobacterial antigenic variation: perhaps more? *Biochimie, 94*(1), 110-116.

Alderwick, L. J., Harrison, J., Lloyd, G. S. and Birch, H. L. (2015). The mycobacterial cell wall - peptidoglycan and arabinogalactan. *Cold Spring Harbor Perspectives in Medicine, 5*(8), a021113-a021113.

Alteri, C. J., Xicohténcatl-Cortes, J., Hess, S., Caballero-Olín, G., Girón, J. A. and Friedman, R. L. (2007). *Mycobacterium tuberculosis* produces pili during human infection. *Proceedings of the National Academy of Sciences, 104*(12), 5145-5150.

Angala, S. K., Belardinelli, J. M., Huc-Claustre, E., Wheat, W. H. and Jackson, M. (2014). The cell envelope glycoconjugates of *Mycobacterium tuberculosis*. *Critical Reviews in Biochemistry and Molecular Biology, 49*(5), 361-399.

Azuma, I., Ajisaka, M. and Yamamura, Y. (1970). Polysaccharides of *Mycobacterium bovis* Ushi 10, *Mycobacterium smegmatis, Mycobacterium phlei*, and atypical *Mycobacterium* P1. *Infection and Immunity, 2*(3), 347-349.

Baker, C. and Gunstone, F. (1963). Fatty Acids. Chapter 11. Synthesis of 9D-Hydroxy-Octadecanoic Acid: Royal Society Chemistry Thomas Graham House, Science Park, Milton Rd, Cambridge, 759.

Bardarov, S., Bardarov, S. Jr., Pavelka, M. S. Jr., Sambandamurthy, V., Larsen, M., Tufariello, J., et al. (2002). Specialized transduction: an efficient method for generating marked and unmarked targeted gene disruptions in *Mycobacterium tuberculosis, M. bovis* BCG and *M. smegmatis. Microbiology, 148*(10), 3007-3017.

Berg, S., Edman, M., Li, L., Wikstrom, M. and Wieslander, A. (2001). Sequence properties of the 1,2-diacylglycerol 3-glucosyltransferase from *Acholeplasma laidlawii* membranes. Recognition of a large group of lipid glycosyltransferases in eubacteria and archaea. *Journal of Biological Chemistry, 276*(25), 22056-22063.

Bermudez, L. E. and Goodman, J. (1996). *Mycobacterium tuberculosis* invades and replicates within type II alveolar cells. *Infection and Immunity, 64*(4), 1400-1406.

Beste, D. J., Nöh, K., Niedenführ, S., Mendum, T. A., Hawkins, N. D., Ward, J. L., et al. (2013). 13C-flux spectral analysis of host-pathogen metabolism reveals a mixed diet for intracellular *Mycobacterium tuberculosis*. *Chemistry and Biology, 20***,** 1012-1021.

Beukes, D., Du Preez, I. and Loots, D. T. (2019). Total metabolome extraction from mycobacterial cells for GC-MS metabolomics analysis. *Microbial Metabolomics, 1859*, 121-131.

Boldrin, F., Ventura, M., Degiacomi, G., Ravishankar, S., Sala, C., Svetlikova, Z., et al. (2014). The phosphatidyl-myo-inositol mannosyltransferase PimA is essential for *Mycobacterium tuberculosis* growth *in vitro* and *in vivo*. *Journal of Bacteriology, 196*(19), 3441-3451.

Brennan, P. J. and Nikaido, H. (1995). The envelope of mycobacteria. *Annual Review of Biochemistry, 64*, 29-63.

Bruning, J. B., Murillo, A. C., Chacon, O., Barletta, R. G. and Sacchettini, J. C. (2011). Structure of the *Mycobacterium tuberculosis* D-alanine:D-alanine ligase, a target of the antituberculosis drug D-cycloserine. *Antimicrobial Agents and Chemotherapy, 55*(1), 291-301.

Buckoreelall, K., Wilson, L. and Parker, W. B. (2011). Identification and characterization of two adenosine phosphorylase activities in *Mycobacterium smegmatis*. *Journal of Bacteriology, 193*(20), 5668.

Buckoreelall, K., Sun, Y., Hobrath, J. V., Wilson, L. and Parker, W. B. (2012). Identification of Rv0535 as methylthioadenosine phosphorylase from *Mycobacterium tuberculosis. Tuberculosis (Edinburgh), 92*(2), 139-147.

Bussi, C. and Gutierrez, M. G. (2019). *Mycobacterium tuberculosis* infection of host cells in space and time. *FEMS Microbiology Reviews, 43*(4), 341-361.

Cha, D., Cheng, D., Liu, M., Zeng, Z., Hu, X. and Guan, W. (2009). Analysis of fatty acids in sputum from patients with pulmonary tuberculosis using gas chromatography-mass spectrometry preceded by solid-phase microextraction and post-derivatization on the fiber. *Journal of Chromatography A, 1216***,** 1450-1457.

Chou, S., Chedore, P. and Kasatiya, S. (1998). Use of gas chromatographic fatty acid and mycolic acid cleavage product determination to differentiate among *Mycobacterium genavense, Mycobacterium fortuitum, Mycobacterium simiae*, and *Mycobacterium tuberculosis*. *Journal of Clinical Microbiology, 36*(2), 577-579.

Chow, E. D. and Cox, J. S. (2011). TB lipidomics - the final frontier. *Chemistry and Biology, 18***,** 1517-1518.

Collins, J. M., Walker, D. I., Jones, D. P., Tukvadze, N., Liu, K. H., Tran, V. T., et al. (2018). High-resolution plasma metabolomics analysis to detect *Mycobacterium tuberculosis*-associated metabolites that distinguish active pulmonary tuberculosis in humans. *PloS One, 13*(10), e0205398.

Completo, G. and Lowary, T. (2008). Synthesis of galactofuranose-containing acceptor substrates for mycobacterial galactofuranosyltransferases. *Journal of Organic Chemistry, 73*(12), 4513-4525.

Cook, G. M., Berney, M., Gebhard, S., Heinemann, M., Cox, R. A., Danilchanka, O., et al. (2009). Physiology of mycobacteria. *Advances in Microbial Physiology, 55*, 81-319.

Csonka, L. N. (1989). Physiological and genetic responses of bacteria to osmotic stress. *Microbiological Reviews, 53*(1), 121-147.

Dannenberg Jr, A. M. and Rook, G. A. (1994). Pathogenesis of pulmonary tuberculosis: an interplay of tissue-damaging and macrophage-activating immune responses - dual mechanisms that control bacillary multiplication. *Tuberculosis.* American Society of Microbiology. 459-483.

de Carvalho, L. P., Fischer, S. M., Marrero, J., Nathan, C., Ehrt, S. and Rhee, K. Y. (2010). Metabolomics of *Mycobacterium tuberculosis* reveals compartmentalized co-catabolism of carbon substrates. *Chemistry and Biology, 17***,** 1122-1131.

Dlamini, M. T. (2017). Whole transcriptome analysis to elucidate the role of MTP in gene regulation of pulmonary epithelial cells infected with *Mycobacterium tuberculosis.* Masters thesis. University of KwaZulu-Natal. Durban.

Ehling, S. and Reddy, T. M. (2015). Direct analysis of leucine and its metabolites beta-hydroxy-beta-methylbutyric acid, alpha-ketoisocaproic acid, and alpha-hydroxyisocaproic acid in human breast milk by liquid chromatography-mass spectrometry. *Journal of Agricultural and Food Chemistry, 63*(34), 7567-7573.

Eoh, H. (2014). Metabolomics: A window into the adaptive physiology of *Mycobacterium tuberculosis*. *Tuberculosis, 94*(6), 538-543.

Etienne, G., Malaga, W., Laval, F., Lemassu, A., Guilhot, C. and Daffé, M. (2009). Identification of the polyketide synthase involved in the biosynthesis of the surface-exposed lipooligosaccharides in mycobacteria. *Journal of Bacteriology, 191*(8), 2613-2621.

Forrellad, M. A., Klepp, L. I., Gioffré, A., Sabio y García, J., Morbidoni, H. R., de la Paz Santangelo, M., et al. (2013). Virulence factors of the *Mycobacterium tuberculosis* complex. *Virulence, 4*(1), 3–66.

Gandhi, N .R., Moll, A., Sturm, A.W., Pawinski, R., Govender, T., Lalloo, U., et al. (2006). Extensively drug-resistant tuberculosis as a cause of death in patients co-infected with tuberculosis and HIV in a rural area of South Africa. *The Lancet*, *368*(9547), 1575-1580.

Govender, V. S. (2019). Investigating the *in vitro* roles played by the major adhesins HBHA and MTP in the pathogenesis of *M. tuberculosis*, in a novel double gene-knockout mutant strain. PhD thesis. University of KwaZulu-Natal. Durban.

Haglund, P. S., Löfstrand, K., Siek, K., and Asplund, L. (2013). Powerful GC-TOF-MS techniques for screening, identification and quantification of halogenated natural products. *Mass Spectrometry*, *2*(Special_Issue), S0018-S0018.

Halouska, S., Fenton, R. J., Zinniel, D. K., Marshall, D. D., Barletta, R. G. and Powers, R. (2014). Metabolomics analysis identifies d-alanine-d-alanine ligase as the primary lethal target of d-cycloserine in mycobacteria. *Journal of Proteome Research*, *13*(2), 1065–1076.

Jantzen, E., Tangen, T. and Eng, J. (1989). Gas chromatography of mycobacterial fatty acids and alcohols: diagnostic applications. *Apmis*, *97*(11), 1037-1045.

Joe, M. and Lowary, T. (2016). Synthesis of a homologous series of galactofuranose-containing mycobacterial arabinogalactan fragments. *Canadian Journal of Chemistry*, *94*(11), 976-988.

Kamio, Y., Itoh, Y. and Terawaki, Y. (1981). Chemical structure of peptidoglycan in Selenomonas ruminantium: cadaverine links covalently to the D-glutamic acid residue of peptidoglycan. *Journal of Bacteriology*, *146*(1), 49-53.

Kanehisa, M., Furumichi, M., Tanabe, M., Sato, Y., and Morishima, K. (2017). KEGG: new perspectives on genomes, pathways, diseases and drugs. *Nucleic Acids Research*, *45*(D1), D353-d361.

Kim, S., Chen, J., Cheng, T., Gindulyte, A., He, J., He, S., et al. (2019). PubChem 2019 update: improved access to chemical data. *Nucleic Acids Research*, *47*(D1), D1102-D1109.

Kinsella, R. J., Fitzpatrick, D. A., Creevey, C. J. and McInerney, J. O. (2003). Fatty acid biosynthesis in *Mycobacterium tuberculosis*: lateral gene transfer, adaptive evolution, and gene duplication. *Proceedings of the National Academy of Sciences of the United States of America*, *100*(18), 10320-10325.

Kline, K. A., Fälker, S., Dahlberg, S., Normark, S., and Henriques-Normark, B. (2009). Bacterial adhesins in host-microbe interactions. *Cell Host and Microbe*, *5*(6), 580-592.

Klopper, M., Warren, R. M., Hayes, C., Gey van Pittius, N. C., Streicher, E. M., Müller, B., et al. (2013). Emergence and spread of extensively and totally drug-resistant tuberculosis, South Africa. *Emerging Infectious Diseases*, *19*, 449-455.

Lambert, M. A., Moss, C. W., Silcox, V. A. and Good, R. C. (1986). Analysis of mycolic acid cleavage products and cellular fatty acids of *Mycobacterium* species by capillary gas chromatography. *Journal of Clinical Microbiology*, *23*(4), 731.

Landaas, S. (1975). Accumulation of 3-hydroxyisobutyric acid, 2-methyl-3-hydroxybutyric acid and 3-hydroxyisovaleric acid in ketoacidosis. *International Journal of Clinical Chemistry*, *64*(2), 143-154.

Larsen, M. H., Biermann, K., Tandberg, S., Hsu, T., and Jacobs Jr, W. R. (2007). Genetic manipulation of Mycobacterium tuberculosis. *Current Protocols in Microbiology*, *6*(1), 10A-2.

Lau, S. K., Lam, C. W., Curreem, S. O., Lee, K. C., Lau, C. C., Chow, W. N., et al. (2015). Identification of specific metabolites in culture supernatant of *Mycobacterium tuberculosis* using metabolomics: exploration of potential biomarkers. *Emerging Microbes and Infections*, *4*(1), e6.

Lind, J., Ramo, T., Klement, M. L., Barany-Wallje, E., Epand, R. M., Epand, R. F., et al. (2007). High cationic charge and bilayer interface-binding helices in a regulatory lipid glycosyltransferase. *Biochemistry*, *46*(19), 5664-5677.

Long, M. C., Escuyer, V. and Parker, W. B. (2003). Identification and characterization of a unique adenosine kinase from *Mycobacterium tuberculosis*. *Journal of Bacteriology*, *185*(22), 6548-6555.

Loots, D. T. (2014). An altered *Mycobacterium tuberculosis* metabolome induced by katG mutations resulting in isoniazid resistance. *Antimicrobial Agents and Chemotherapy*, *58*(4), 2144–2149.

Loots, D. T., Swanepoel, C. C., Newton-Foot, M., and Gey van Pittius, N. C. (2016). A metabolomics investigation of the function of the ESX-1 gene cluster in mycobacteria. *Microbial Pathogenesis, 100*, 268-275.

Mahapatra, S., Hess, A. M., Johnson, J. L., Eisenach, K. D., DeGroote, M. A., Gitta, P., et al. (2014). A metabolic biosignature of early response to anti-tuberculosis treatment. *BMC Infectious Diseases, 14*(1), 53.

Meissner-Roloff, R. J., Koekemoer, G. and Warren, R. M. (2012). A metabolomics investigation of a hyper-and hypo-virulent phenotype of Beijing lineage *M. tuberculosis*. *Metabolomics, 8*(6), 1194-1203.

Meissner-Roloff, R. J., Newton-Foot, M. and van Pittius, N. C. G. (2013). A metabolomics approach exploring the function of the ESX-3 type VII secretion system of *M. smegmatis*. *Metabolomics, 9*(3), 631-641.

Mikusová, K., Huang, H., Yagi, T., Holsters, M., Vereecke, D., D'Haeze, W., et al. (2005). Decaprenylphosphoryl arabinofuranose, the donor of the D-arabinofuranosyl residues of mycobacterial arabinan, is formed via a two-step epimerization of decaprenylphosphoryl ribose. *Journal of Bacteriology, 187*(23), 8020-8025.

Mirsaeidi, M., Banoei, M. M., Winston, B. W. and Schraufnagel, D. E. (2015). Metabolomics: Applications and Promise in Mycobacterial Disease. *Annals of the American Thoracic Society, 12*(9), 1278–1287.

Mobley, C. B., Fox, C. D., Ferguson, B. S., Amin, R. H., Dalbo, V. J., Baier, S., et al. (2014). L-leucine, beta-hydroxy-beta-methylbutyric acid (HMB) and creatine monohydrate prevent myostatin-induced Akirin-1/Mighty mRNA down-regulation and myotube atrophy. *Journal of the International Society of Sports Nutrition, 11*, 38-38.

Naidoo, N., Ramsugit, S. and Pillay, M. (2014). *Mycobacterium tuberculosis* pili (MTP), a putative biomarker for a tuberculosis diagnostic test. *Tuberculosis, 94*(3), 338-345.

Naidoo, N., Pillay, B., Bubb, M., Pym, A., Chiliza, T., Naidoo, K., et al. (2018). Evaluation of a synthetic peptide for the detection of anti-*Mycobacterium tuberculosis* curli pili IgG antibodies in patients with pulmonary tuberculosis. *Tuberculosis (Edinburgh, Scotland), 109*, 80–84.

Namanja-Magliano, H. A., Evans, G. B., Harijan, R. K., Tyler, P. C. and Schramm, V. L. (2017). Transition state analogue inhibitors of 5'-deoxyadenosine/5'-methylthioadenosine nucleosidase from *Mycobacterium tuberculosis*. *Biochemistry, 56*(38), 5090-5098.

Neely, M. N. and Olson, E. R. (1996). Kinetics of expression of the *Escherichia coli* cad operon as a function of pH and lysine. *Journal of Bacteriology, 178*(18), 5522-5528.

Niehaus, W. G., Kisic, A., Torkelson, A., Bednarczyk, D. and Schroepfer, G. (1970). Stereospecific hydration of the Δ9 double bond of oleic acid. *Journal of Biological Chemistry, 245*(15), 3790-3797.

Nyawo, G. (2016). The role of *Mycobacterium tuberculosis* pili in pathogenesis: growth and survival kinetics, gene regulation and host immune response, and in vitro growth kinetics. Masters thesis. University of KwaZulu-Natal. Durban.

Patel, K. N., Patel, J. K., Patel, M. P., Rajput, G. C. and Patel, H. A. (2010). Introduction to hyphenated techniques and their applications in pharmacy. *Pharmaceutical Methods, 1*(1), 2-13.

Pathak, A. K., Pathak, V., Riordan, J. M., Gurcha, S. S., Besra, G. S. and Reynolds, R. C. (2004). Synthesis of mannopyranose disaccharides as photoaffinity probes for mannosyltransferases in *Mycobacterium tuberculosis*. *Carbohydrate Research,, 339*(3), 683-691.

Rafidinarivo, E., Savagnac, A., Lacave, C. and Prome, J. C. (1982). Branched fatty acids from *Mycobacterium aurum. Biochimica et Biophysica Acta, 711*(2), 266-271.

Ramakrishnan, T., Murthy, P. S. and Gopinathan, K. P. (1972). Intermediary metabolism of mycobacteria. *Bacteriological Reviews, 36*(1), 65-108.

Ramsugit, S., Guma, S., Pillay, B., Jain, P., Larsen, M. H., Danaviah, S., et al. (2013). Pili contribute to biofilm formation *in vitro* in *Mycobacterium tuberculosis*. *Antonie Van Leeuwenhoek, 104*(5), 725-735.

Ramsugit, S. and Pillay, M. (2014). *Mycobacterium tuberculosis* pili promote adhesion to and invasion of THP-1 macrophages. *Japanese Journal of Infectious Diseases, 67*(6), 476-478.

Ramsugit, S., Pillay, B. and Pillay, M. (2016). Evaluation of the role of *Mycobacterium tuberculosis* pili (MTP) as an adhesin, invasin, and cytokine inducer of epithelial cells. The *Brazilian Journal of Infectious Diseases, 20*(2), 160-165.

Rogacki, M. K., Pitta, E., Balabon, O. B., Huss, S., Lopez-Roman, E. M., Argyrou, A., et al. (2018). Identification and profiling of hydantoins - a novel class of potent antimycobacterial DprE1 inhibitors. *Journal of Medicinal Chemistry, 61*(24), 11221-11249.

Samartzidou, H. and Delcour, A. H. (1998). *E. coli* PhoE porin has an opposite voltage-dependence to the homologous OmpF. *The Embo Journal, 17*(1), 93-100.

Sancho-Vaello, E., Albesa-Jové, D., Rodrigo-Unzueta, A. and Guerin, M. E. (2017). Structural basis of phosphatidyl-myo-inositol mannosides biosynthesis in mycobacteria. *Biochimica et Biophysica Acta (BBA) - Molecular and Cell Biology of Lipids, 1862*(11), 1355-1367.

Schaefer, W. B. and Lewis, C. W., Jr. (1965). Effect of oleic acid on growth and cell structure of mycobacteria. *Journal of Bacteriology, 90*(5), 1438-1447.

Schleifer, K. H. and Kandler, O. (1972). Peptidoglycan types of bacterial cell walls and their taxonomic implications. *Bacteriological Reviews, 36*(4), 407-477.

Schymanski, E. L., Jeon, J., Gulde, R., Fenner, K., Ruff, M., Singer, H. P., & Hollender, J. (2014). Identifying small molecules via high resolution mass spectrometry: communicating confidence. *Environmental Science and Technology, 48*, 2097-2098.

Smith, I. (2003). *Mycobacterium tuberculosis* pathogenesis and molecular determinants of virulence. *Clinical Microbiology Reviews*, *16*(3), 463-496.

Stones, D. H. and Krachler, A. M. (2015). Fatal attraction: how bacterial adhesins affect host signaling and what we can learn from them. *International Journal of Molecular Sciences, 16*(2), 2626-2640.

Sullivan, G. M. and Feinn, R. (2012). Using effect size—or why the P value is not enough. *Journal of Graduate Medical Education, 4*(3), 279-282.

Swanepoel, C. C. and Loots, D. T. (2014). The use of functional genomics in conjunction with metabolomics for *Mycobacterium tuberculosis* research. *Disease Markers, 2014*, 124218.

Titgemeyer, F., Amon, J., Parche, S., Mahfoud, M., Bail, J., Schlicht, M., et al. (2007). A genomic view of sugar transport in *Mycobacterium smegmatis* and *Mycobacterium tuberculosis. Journal of Bacteriology, 189*(16), 5903-5915.

Udwadia, Z. F., Amale, R. A., Ajbani, K. K., and Rodrigues, C. (2012). Totally drug-resistant tuberculosis in India. *Clinical Infectious Diseases, 54*(4), 579-581.

Untergasser, A., Nijveen, H., Rao, X., Bisseling, T., Geurts, R., and Leunissen, J. A. (2007). Primer3Plus, an enhanced web interface to Primer3. *Nucleic Acids Research, 35* (Web Server issue), W71–W74.

van den Berg, R. A., Hoefsloot, H. C., Westerhuis, J. A., Smilde, A. K. and van der Werf, M. J. (2006). Centering, scaling, and transformations: improving the biological information content of metabolomics data. *BMC Genomics*, *7*(1), 142.

Velayati, A. A., Masjedi, M. R., Farnia, P., Tabarsi, P., Ghanavi, J., Ziazarifi, A. H. and Hoffner, S. E. (2009). Emergence of new forms of totally drug-resistant tuberculosis bacilli: super extensively drug-resistant tuberculosis or totally drug-resistant strains in Iran. *Chest, 136***,** 420-425.

Vilkas, E. and Lederer, E. (1960). On the structure of phosphatidylinosito-dimannoside of *Mycobacterium tuberculosis*, *Bulletin de Societe Chimique Biologique (Paris), 42*, 1013-1022.

Warner D. F. (2014). *Mycobacterium tuberculosis* metabolism. *Cold Spring Harbor Perspectives in Medicine*, *5*(4), a021121.

Wesener, D. A., Levengood, M. R. and Kiessling, L. L. (2017). Comparing galactan biosynthesis in *Mycobacterium tuberculosis* and *Corynebacterium diphtheriae*. *Journal of Biological Chemistry, 292*(7), 2944-2955.

Wishart, D. S., Feunang, Y. D., Marcu, A., Guo, A. C., Liang, K., Vazquez-Fresno, R., et al. (2018). HMDB 4.0: the human metabolome database for 2018. *Nucleic Acids Research, 46*(D1), D608-d617.

World Health Organization (2019). WHO 2018 Global Statistics Report. http://www.who.int/tb/publications/global_report/en/. Accessed 30/11/2019.

Zelante, T., Fallarino, F., Bistoni, F., Puccetti, P. and Romani, L. (2009). Indoleamine 2,3-dioxygenase in infection: the paradox of an evasive strategy that benefits the host. *Microbes and Infection, 11*(1), 133-141.

Zhang, Y. J., Reddy, M. C., Ioerger, T. R., Rothchild, A. C., Dartois, V., Schuster, B. M., et al. (2013). Tryptophan biosynthesis protects mycobacteria from CD4 T-cell-mediated killing. *Cell, 155*(6), 1296-1308.

Zhang, L., Alfano, J. R. and Becker, D. F. (2015). Proline metabolism increases katG expression and oxidative stress resistance in *Escherichia coli*. *Journal of Bacteriology, 197*(3), 431-440.

Zhong, L., Zhou, J., Chen, X. and Yin, Y. (2016). Serum metabolomic study for the detection of candidate biomarkers of tuberculosis. *International Journal Of Clinical And Experimental Pathology, 9*(3), 3256-3266.

Chapter 2 investigated the role of MTP in a bacterial model using *M. tuberculosis* V9124, the Δ*mtp* deletion mutant and its complemented strain. Significant metabolic perturbations were observed in the *mtp*-deficient *M. tuberculosis* strain compared to *mtp*-proficient strain. Gene function was mostly restored in the complemented strain. Chapter 3 aimed to investigate the role of MTP in an infection model using A549 epithelial cells infected with these *M. tuberculosis* strains to determine any significant modulation in metabolic pathways.

CHAPTER 3: MANUSCRIPT 2

Mycobacterium tuberculosis curli pili (MTP) is associated with significant host metabolic pathways in an A549 epithelial cell infection model and contributes to the pathogenicity of *M. tuberculosis*

Reedoy, K. S[1]., Loots, D. T[3]., Beukes, D[3]., van Reenen, M[3]., Pillay, B[2]. and Pillay, M[1].*

[1]Medical Microbiology, School of Laboratory Medicine and Medical Sciences, College of Health Sciences, University of KwaZulu-Natal, 1st floor Doris Duke Medical Research Institute, Congella, Private Bag 7, Durban 4013, South Africa.

[2]School of Life Sciences, College of Agriculture, Engineering and Science, University of KwaZulu-Natal, Westville Campus, Private Bag X54001, Durban. 4000

[3]Centre for Human Metabolomics, North-West University, Potchefstroom, Private Bag x6001, Box 269, 2531, South Africa.

*Corresponding author
Medical Microbiology,
School of Laboratory Medicine and Medical Sciences,
College of Health Sciences, University of KwaZulu-Natal,
1st floor Doris Duke Medical Research Institute,
Congella, Private Bag 7, Durban 4013, South Africa
E-mail: pillayc@ukzn.ac.za
Tel: +2731 260 4059

Funding: This study was funded by a NRF Grantholder-linked bursary (105841) and a UKZN College of Health Sciences scholarship.
Authors Conflict of Interest Statement: The authors of this study declare no conflicts of interest.
Authors Contribution Statement: MP conceptualised the study, MP, BP and DTL designed the study. KSR conducted experiments, analysed and interpreted the data and drafted the manuscript. DBM processed the samples and performed GCxGC-TOFMS. MVR conducted statistical bioinformatic analyses. All authors contributed to and approved the manuscript.

3.1 Abstract

A clear understanding of the metabolome of *Mycobacterium tuberculosis* and its target host cell during infection is fundamental for the development of novel diagnostic tools, effective drugs and vaccines required to combat tuberculosis. The surface-located *Mycobacterium tuberculosis* curli pili (MTP) adhesin forms initial contact with the host cell and is therefore considered critical for the establishment of infection. The aim of this investigation was to determine the role of MTP in modulating pathogen and host metabolic pathways in A549 epithelial cells infected with MTP proficient and deficient strains of *M. tuberculosis*. Uninfected, and A549 epithelial cells infected with *M. tuberculosis* V9124 wild-type strain, Δ*mtp* and the *mtp*-complemented strains were subjected to metabolite extraction, GCxGC-TOFMS and bioinformatic analyses. Univariate and multivariate statistical tests were used to identify metabolites that were significantly and differentially produced for the validated WT-infected and Δ*mtp*-infected A549 epithelial cell model. Overall, the 46 metabolites significantly occurring in lower relative concentrations in the Δ*mtp*-infected cells, indicated a reduction in nucleic acid synthesis, amino acid metabolism, glutathione metabolism, oxidative stress, lipid metabolism and a peptidoglycan anomaly, compared to those cells infected with the WT strain. In conclusion, the absence of MTP was associated with significant changes to the host metabolome, suggesting that this adhesin is an important contributor

to the pathogenicity of *M. tuberculosis*, and supports previous findings of its potential as a suitable drug, vaccine and diagnostic target.

Keywords: *M. tuberculosis* curli pili; A549 epithelial cells; *mtp*; adhesin; GCxGC-TOFMS; metabolomics

3.2 Introduction

Mycobacterium tuberculosis, one of the top 10 death-causing organisms by a single infectious entity, is the etiological agent of the worldwide epidemic tuberculosis (TB) (Centrs for Disease Control and Prevention (CDC), 2018). In 2018 alone, of the approximately 10.0 million people diagnosed with TB, 11% were children, 32% were female and 8.6% were co-infected with HIV (World Health Organization (WHO), 2019). Despite the currently available diagnostic and treatment regimens, the growing emergence of multi-, extensively and totally drug-resistant *M. tuberculosis* strains (Dheda et al., 2014; Hameed et al., 2018) and the HIV/AIDS pandemic (Abdool Karim et al., 2009; Naidoo et al., 2019), have significantly contributed to the challenges faced by health professionals in controlling this infectious disease. The development of more effective and rapid diagnostic or therapeutic interventions towards TB control requires further insights into the pathogenesis of TB by the identification of novel biomarkers.

Bacterial adhesins function as the first point-of-contact between bacterium and host cell receptor (Kline et al., 2009). Upon adhesion, key virulence factors that trigger events leading to host cell invasion are activated (Alberts et al., 2002). This series of events warrants exploration from a metabolomics perspective to better understand the role of adhesins in modulating metabolic pathways upon infection. *Mycobacterium tuberculosis* curli pili (MTP), encoded by Rv3312A (Alteri et al., 2007), is a surface-located adhesin, and previous studies have documented its importance in TB pathogenesis *in vitro* as an adhesin/invasin, biofilm producer and cytokine modulator (Ramsugit et al., 2013; Ramsugit and Pillay, 2014; Ramsugit et al., 2016). The *mtp* gene is specific to the *M. tuberculosis* complex members (Naidoo et al., 2014), and a synthetic MTP peptide yielded a 97% accuracy in anti-MTP IgG antibody detection within patients' sera (Naidoo et al., 2018). Research has demonstrated through functional genomics and global transcriptomics that MTP modulates transcriptional host immune responses in A549 epithelial cells (Dlamini, 2017), as well as in THP-1 macrophages (Moodley, 2019).

Extensive research has provided insights into the interactions between *M. tuberculosis* and A549 epithelial cells (Bermudez and Goodman, 1996; Birkness et al., 1999; Bermudez et al., 2002), the role of lung epithelium using A549 epithelial cells during *M. tuberculosis* pathogenesis (Castro-Garza et al., 2002; Chapeton-Montes et al., 2008) and cytotoxicity of epithelial cells (McDonough and Kress, 1995; Dobos et al., 2000). Upon inhalation, *M. tuberculosis* comes into contact with the vast numbers of

alveolar epithelial cells (approximately 100 fold more than alveolar macrophages), which comprise the lining of the alveolus (Lubman et al., 1997; Schneeberger and Lynch, 1997; Ryndak et al,. 2015). *M. tuberculosis* was shown to rapidly replicate in Type II alveolar epithelial A549 cells, thus aiding the continuation of the infection process by facilitating subsequent dissemination (Ryndak et al., 2015). The pathogenicity of *M. tuberculosis* is further enhanced by exploiting its host environment through host metabolic networks (de Carvalho et al., 2010). The transcriptional profile of A549 cells infected with *M. tuberculosis* demonstrated that significantly upregulated genes were associated with an active metabolic state as well as increased virulence (Ryndak et al., 2015). Global transcriptomics of *M. tuberculosis*-infected A549 cells, with and without *mtp*, demonstrated that MTP differentially regulated gene expression associated with cell communication, response to lipids and signal transduction (Dlamini, 2017). The metabolomic profile associated with these MTP transcriptomic findings on infection, would undoubtedly shed further insight into the infection process.

Two-dimensional gas chromatography time-of-flight mass spectrometry (GCxGC-TOFMS) metabolomics, is a sensitive and powerful approach that can readily identify altered metabolic pathways and specific biomarkers in the diseased state for early diagnosis and therapeutics (Shellie et al., 2001). Metabolomics has been used to further validate and/or provide novel insights into the functionality of genes and metabolites (Eoh, 2014; Mahapatra et al., 2014; Zhong et al., 2016). Infection with *M. tuberculosis* can alter the host's metabolic networks resulting in a variation of the types and quantity of metabolites in a sample or cell (du Preez and Loots, 2013). The complex metabolism of *M. tuberculosis* calls for more research to elucidate the pathways utilised by thisbacterium, to explore its role in virulence, and to target potential metabolic pathways and/or specific metabolites for subsequent interrogation in the inhibition of the success of this pathogen (de Carvalho et al., 2010; Warner, 2014).

As mentioned previously, adhesion activates key virulence factors resulting in host cell invasion (Alberts et al., 2002). Functional metabolomics would provide an understanding of the metabolic perturbations that may arise upon deletion of an adhesin gene, thus, elucidating its role in the host's response to infection. The metabolomic changes associated with MTP in *M. tuberculosis*, has been previously documented (Ashokcoomar and Reedoy et al., 2020; unpublished). However, metabolite changes to the host, triggered by MTP during infection, has not been previously reported. Hence, the rationale of this study was to investigate the role of MTP in modulating pathogen and host metabolic pathways in A549 epithelial cells infected with an *mtp* gene-knockout mutant strain, compared to that when infected with a WT strain with fully functioning MTP. The findings of this study provide further evidence of the potential of MTP, as well as the associated metabolite biosignatures, for use as suitable TB diagnostic targets and vaccine candidates.

3.3 Materials and methods

3.3.1 Ethical Approval

The study was approved by the Biomedical Research Ethics Council (BE255/17).

3.3.2 Bacterial strains and culture conditions

Mycobacterium tuberculosis wild type (WT) strain V9124, and the previously constructed Δ*mtp* mutant and Δ*mtp* complemented strains (Ramsugit et al., 2013) were propagated in 10 mL Middlebrook 7H9 broth (Difco, Becton-Dickinson, Franklin Lakes, NJ, USA), supplemented with 10% (v/v) oleic acid-albumin-dextrose-catalase (OADC) supplement (Becton-Dickinson, Franklin Lakes, NJ, USA), 0.5% (v/v) glycerol (Sigma-Aldrich, St. Louis, MO, USA), and 0.05% (v/v) Tween-80 (Sigma-Aldrich, St. Louis, MO, USA). These cultures were incubated at 37˚C with shaking (I-26 Shaking Incubator, New Brunswick Scientific, Canada) at 100 rpm for 7 – 8 days, until an OD_{600nm} (Lightwave II, Biochrom, Cambridge, UK) of 1 was reached, using 7H9 as a blank, equivalent to approximately $1x10^8$ colony forming units (CFU)/mL (Larsen et al., 2007).

3.3.3 Culture and infection of A549 epithelial cells

A total of five models were investigated in the study. Three of the five models were investigated for differences between the infected and uninfected A549 epithelial cells for each strain; WT-infected and WT-uninfected cells, Δ*mtp*-infected and Δ*mtp*-uninfected cells, and the *mtp*-complement-infected and *mtp*-complement-uninfected cells. Two of the five models investigated differences in infection between the strains; WT-infected and Δ*mtp*-infected cells, and WT-infected and *mtp*-complement-infected cells.

The A549 human type II alveolar epithelial cell line (ATCC CCL-185) was grown in Eagle's Minimum Essential Medium (EMEM)(Lonza, Basel, Switzerland) with L-glutamine supplemented with 10% (v/v) fetal bovine serum (FBS) (BioWest, Nuaille, France) in tissue culture flasks (Nest Biotechnology, Jiangsu, China) at 37ºC in 5% CO_2 (Shel Lab CO_2 Incubator, Cornelius, OR, USA) until 70% to 90% confluent. After 3 washes with phosphate buffered saline (PBS) (Merck, Darmstadt, Germany) (Appendix B), adherent cells were detached with 2 mL trypsin (Lonza) at 37˚C for 3 – 5 minutes. Trypsinization was stopped by the addition of 2 mL neat FBS. This was followed by the trypan blue (Lonza, Basel, Switzerland) exclusion assay (Strober, 1997) using a hemocytometer (Neubauer 1/10 mm, Boeco, Germany) to perform cell counts. Flasks were seeded at a concentration of 5×10^5 cells/mL and incubated (Shel Lab CO_2 Incubator, Cornelius, OR, USA) at 37ºC for 24 hrs in 5% CO_2.

Once the optimal time point for infection was determined in a pilot study (Appendix: D1), 10 replicates of each of the three strains (n = 30) were cultured in 25 mL supplemented Middlebrook 7H9 (Difco, Becton-Dickinson, Franklin Lakes, NJ, USA) broth. Each biological replicate was standardized

(Appendix: C3) to an OD_{600nm} (Lightwave II, Biochrom, Cambridge, UK) of 0.015 and incubated (Shel Lab CO_2 Incubator, Cornelius, OR, USA) at 37°C with shaking at 100 rpm until an OD_{600} (Lightwave II, Biochrom, Cambridge, UK) of between 0.9 – 1.1 was reached. Mid-log phase mycobacterial cultures were centrifuged at 2000 g for 10 min and resuspended in approximately 30 mL fresh EMEM (Lonza, Basel, Switzerland) media to obtain an inoculum that measured an OD_{600nm} (Lightwave II, Biochrom, Cambridge, UK) of 1. A multiplicity of infection (MOI) of approximately five was used. The flasks were incubated (Shel Lab CO_2 Incubator, Cornelius, OR, USA) at 37˚C with 5% CO_2 and 95% humidity for 2 hrs.

Thereafter, cells were washed twice with 500 µL PBS (Sigma-Aldrich, St. Louis, MO, USA) (Appendix B), trypsinized (Lonza, Basel, Switzerland) and centrifuged (Mikro 200R, Hettich Zentrifugen, Tuttlingen, Germany) at 200 x *g* for 10 min. Resuspension of pellets were done in 500 µL of PBS (Sigma-Aldrich, St. Louis, MO, USA) and transferred into Microcentrifuge tubes (Sigma-Aldrich, St. Louis, MO, USA). Infected cells were washed three times with 500 µL of PBS (Sigma-Aldrich, St. Louis, MO, USA), centrifuged (Mikro 200R, Hettich Zentrifugen, Tuttlingen, Germany) at 4°C at 21 952 x *g* for 10 min and stored at - 80°C prior to metabolite extraction. Uninfected A549 epithelial cells in 10 flasks (Nest Biotechnology, Jiangsu, China) subjected to identical conditions were used as a control. An additional 10 flasks (Nest Biotechnology, Jiangsu, China) were also infected, identical to the 10 experimental flasks, to determine CFU/mL at 2 hrs post-infection. After the 2 hr infection period, the flasks were decanted, and epithelial cells were lysed with 20 mL of 0.1% Triton-X100 (Millipore, Merck, Dermstadt, Germany) for 20 min at 37˚C. Ten-fold serial dilutions were plated in triplicate and incubated (Shel Lab CO_2 Incubator, Cornelius, OR, USA) at 37°C for 3 weeks, after which, colonies were counted to determine CFU/mL for each strain (Appendix: D2). The initial inoculum of each strain was treated similarly to determine the CFU/mL prior to the infection of A549 epithelial cells (Appendix: D2).

3.3.4 Sample extraction and derivatization

Samples were prepared and extracted as mentioned previously (Beukes et al., 2019; Ashokcoomar and Reedoy et al., 2020; unpublished). Briefly, after the removal of residual PBS (Sigma-Aldrich, St. Louis, MO, USA) (Appendix B) by centrifugation (Mikro 200R, Hettich Zentrifugen, Tuttlingen, Germany) at 4 ^{o}C, metabolites from various metabolite classes were extracted from 8 mg of pelleted wet cell mass using a whole metabolome extraction method (Beukes et al., 2019). A pooled quality control (QC) sample was made up by combining 8 mg of one randomly selected sample from each of the sample groups, since the volumes were too low to allow for pooling across all samples. The internal standard used was 0.13125 mg/mL 3-phenylbutyric acid (Sigma-Aldrich, St. Louis, MO, USA). Metabolites were extracted using a 1:3:1 ratio of chloroform:methanol:water (Burdick & Jackson; Honeywell International Inc., Muskegon, MI, USA). A MM400 mixer mill (Retsch GmbH & co. KG, Haan,

Germany) was used for extraction. The samples were centrifuged (Mikro 200R, Hettich Zentrifugen, Tuttlingen, Germany) and the supernatant was transferred to a GC-MS vial (Thermo Fisher Scientific, Waltham, MA, USA) where it was dried under a light stream of nitrogen (Sigma-Aldrich, St. Louis, MO, USA). Derivatisation was performed using 50 µL methoxyamine hydrochloride (Sigma-Aldrich, St. Louis, MO, USA) in 15 mg/mL pyridine (Merck, Darmstadt, Germany), N,O-Bis(trimethylsilyl)trifluoroacetamide (BSTFA) with 1 % trimethylchlorosilane (TMCS) (Sigma-Aldrich, St. Louis, MO, USA). Derivatised metabolites were decanted into an insert within a sample vial (Thermo Fisher Scientific, Waltham, MA, USA) and capped.

3.3.5 GCxGC-TOFMS analysis

The prepared samples were subjected to GCxGC-TOFMS analysis as described previously (Ashokcoomar and Reedoy et al., 2020) using a Pegasus 4D instrument (Leco Corporation, St. Joseph, MI, USA). Briefly, a three-split ratio of 1 µL of sample was injected into an Agilent 7890A GC (Agilent, Atlanta, GA) coupled to a time of flight mass spectrometer (Leco Corporation, St. Joseph, MI, USA) which was equipped with a Gerstel Multi-Purpose Sampler (Gerstel GmbH & co. KG, Eberhard-Gerstel- Platz 1, D-45473 Mülheim an der Ruhr). Primary and secondary columns of various temperatures were used to produce first dimensional and second dimensional separation, respectively, with some modifications. A Restek RTX-1ms (Leco Africa) primary column (30 m length; 250 µM diameter; 0.25 µM filament thickness) and a Restek RTX-17 (Leco Africa) secondary column (1.4 m length; 250 µM diameter; 0.25 µM filament thickness) was used. The oven (Leco Corporation, St. Joseph, MI, USA) conditions remained the same with the following modifications; initial oven temperature was 50°C; a rate of 4.5°C /min for 4.5 min was used for the secondary column; hot pulse time of nitrogen gas was 0.5 s; ion source temperature was set at 220°C; detector voltage was 1400 V. Peak finding and mass spectral deconvolution was performed using Leco Corporation (St. Joseph, MI, USA) ChromaTOF software (version 4.51.6.0). Processing of the data was achieved by baseline removal, offset to 1, using the 'spanning' tracking method followed by automatic smoothing. Peaks with 5 apexing masses were detected using a signal-to-noise ratio of 100 and an expected 2D peak width of 50 (5 s x 10 modulations; and 1 s on the second dimension). Peak identities were determined by combining MS-generated mass fragmentation patterns, and their GC retention times. These properties were then matched to the data within NIST spectral libraries (mainlib, replib). A spectral match of 80% similarity resulted in a level 3 identity (Schymanski et al., 2014). Peak alignment and data matric formation was done using Statistical Compare.

3.3.6 Statistical data analysis

GraphPad Prism version 8 software (GraphPad Software, La Jolla, CA, USA) was used to assess whether any significant differences existed among the three strains pre- or post-infection based on the

CFU counts. MATLAB (MATLAB with Statistics Toolbox (2019), version 9.5.0 (R2018b) software (Natick, Massachusetts: The MathWorks Inc) along with the Eigenvector PLS_Toolbox 8.7 (Wenatchee, WA: Eigenvector Research Inc. Software available at http://www.eigenvector.com) was used to identify differentiating metabolites amongst the three strains. After GCxGC-TOFMS, statistical analysis was performed on 54 experimental samples, 9 from each group (WT, Δ*mtp* and *mtp*-complement, both infected and uninfected groups), following quality assurance on 50 QC observations. The QC samples were injected intermittently throughout GCxGC-TOFMS analysis to ensure analytical repeatability. The statistical analysis strategy focused on specific biological questions hence, WT was compared to Δ*mtp* and *mtp*-complement, respectively and separately. Data pre-processing included a zero and QC coefficient of variation (CV) filter, excluding metabolites with 50 % or more zero-valued observations in both experimental groups, or CV values for QCs above 1. This was followed by zero value replacement by random numbers below the minimum observed variable. Normality was achieved via log transformation and the data was auto-scaled to ensure the metabolites were regarded as equally important by multivariate models (van den Berg et al., 2006). Pre-processing preceded quality assurance performed by comparing variation between experimental samples to variation between QC observations as presented in the latent variables of a Principal Component Analysis (PCA). The variability observed between the experimental samples far exceeded the variability observed between the QC sample analyses, indicating a favourable outcome (Appendix: D3). Outlier removal could not be justified owing to small group sizes. Filtering removed 1275, 1290 and 1271 metabolites, retaining 218, 203 and 222 for WT, Δ*mtp* and *mtp*-complement strains, respectively. The independent samples *t*-test was used to determine the statistical significance of differences between groups for each metabolite. To supplement the findings of the *t*-test, Cohen's d-value was used as an effect size indicating practical significance of differences (Sullivan, 2012). Although analysis of variance or ANOVA models are generally considered more appropriate when comparing more than two groups, each pairwise comparison was required to interpret differences from a biological point of view. In ANOVA, post-hoc tests control for inflation of Type I error rate by default. Adjustments were made subsequent to analyses. Multiple testing correction was conducted on the independent samples *t*-test *p*-values and adjusted to a 5 % significance level using Benjamini & Hochberg (BH) adjustment, which controls the rate of false discovery. Fold change (FC) values provided an additional measure of practical relevance in relation to the magnitude of differences based on group averages. PCA and Partial Least Squares Discrimant Analysis (PLS-DA) are unsupervised and supervised techniques of multivariate analyses, respectively. Variation was summarised using PCA and the observation of ellipsoidal separation was considered supportive to PLS-DA model validation, where the main source of variation stems from group structure. If no ellipsoidal separation was present, the model did not validate and no further reporting or testing was required, although the overlap and variation observed may be useful. In some instances, the groupings provided explained less variation than other unknown factors, resulting in PCA separation between groups only on lower components than the preferred first three. PLS-DA was used to identify potential biomarkers

based on the two defined groups using Variable in Projection (VIP) values. To validate the PLS-DA model, a leave-one-out cross-validation approach was used to test the sensitivity of prediction accuracy to changes in the data provided. The resulting R^2 (prediction accuracy given all data) and Q^2 (cross-validated prediction accuracy) values provide rigour and confidence to the metabolites of the model. Significant metabolites were selected using a combination of univariate and multivariate significance i.e. an adjusted *p*-value (≤ 0.05), Cohen's d-value (≥ 0.8), VIP value (≥ 1) (given a valid PLS-DA model), and fold change (≥ 2).

3.4 Results

Three of the five models in the study were investigated for differences between the uninfected epithelial cells and the WT-infected, Δ*mtp*-infected and *mtp*-complement-infected. The remaining two models investigated the infection models between the strains; WT-infected and Δ*mtp*-infected A549 cells, and WT-infected and *mtp*-complement-infected A549 cells. Overall, only the WT-infected and Δ*mtp*-infected A549 cell model was fully validated by statistical testing and the resulting metabolites were tabulated. The other models did not validate, as explained in further detail below, hence testing up until PCA scores plots was conducted.

3.4.1 Volcano plots showing distribution of univariate data with the best spread of metabolites depicted in the WT-infected and Δmtp-infected A549 cell model

The metabolites produced by the infected and/or uninfected A549 cells are graphically represented in order to determine whether there are any significant differences in their profiles (Figure 3.1). The –log10 scaled p-values (prior to correcting for multiple testing) from the independent samples t-test were scattered against the Cohen's d-values. Very few statistical and practical significant metabolites (red dots) were observed between the WT-infected and WT-uninfected A549 cells (Figure 3.1a), the Δ*mtp*-infected and Δ*mtp*-uninfected A549 cells (Figure 3.1b), and the *mtp*-complement-infected and *mtp*-complement-uninfected A549 cells (Figure 3.1c), while the majority of metabolites were found to be non-significant (black dots). In contrast, the best spread of statistically and practically significant metabolites were observed between the WT-infected and Δ*mtp*-infected A549 cells (Figure 3.1d). The majority of metabolites between the WT-infected and *mtp*-complement-infected A549 cells (Figure 3.1e), were neither statistically nor practically significant, although a few metabolites that were significant were scattered above the threshold.

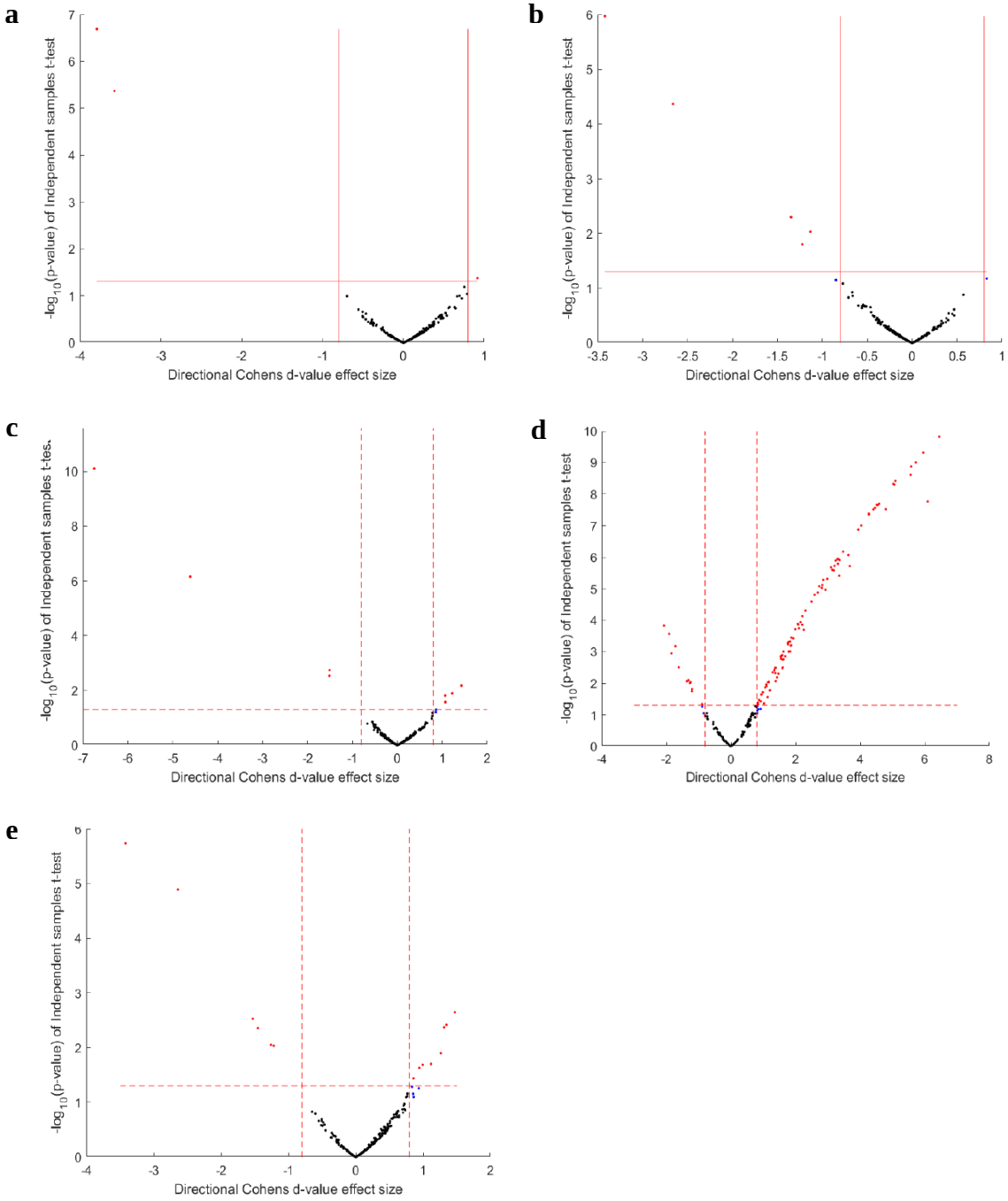

Figure 3.1 Volcano plots showing univariate spread of metabolites across *M. tuberculosis*-infected and uninfected A549 epithelial cell models. Practical (blue), statistical and practical (red) or neither (black) significance is depicted by the dots. The horizontal threshold represents a 5 % significance level (prior to correcting for multiple testing), while the vertical thresholds represent a |Cohen's d-value| = 0.5. These models compared WT-infected and WT-uninfected A549 cells (a), Δ*mtp*-infected and Δ*mtp*-uninfected A549 cells (b), *mtp*-complement-infected and *mtp*-complement-uninfected A549 cells (c), WT-infected and Δ*mtp*-infected A549 cells (d), and lastly, WT-infected and *mtp*-complement-infected A549 cells (e). Most of the statistically and practically significant metabolites were observed between WT-infected and Δ*mtp*-infected A549 cells (d), followed by (e), while very few were seen in the infected and uninfected comparisons (a - c).

3.4.2 PCA data revealed partial overlap across four models while complete group separation validated the WT-infected and Δmtp-infected A549 epithelial cell statistical model

This unsupervised technique makes use of a multivariate parametric projection approach to summarise the variation from a large dataset in order to produce a graph projecting observations onto fewer components (Figure 3.2). Ellipsoids represent 95% confidence intervals of score centroids of each group. The percentage of variation, explained by each principal component (PC) is indicated in brackets along each axis. Overall, ellipsoidal overlap was observed for four of the five models, leading to model invalidation, while the WT-infected and Δ*mtp*-infected A549 cell model showed complete separation, thereby satisfying model validation.

Between the WT-infected and WT-uninfected A549 cells (Figure 3.2a), there was some discrimination across PC's 7 to 9 showing the best separation, although complete separation was not achieved. Only 4% (sum of the PC's) of the variation is related to group structure for this cell model. For the Δ*mtp*-infected and Δ*mtp*-uninfected A549 cell model (Figure 3.2b), almost complete overlap was observed with a total variation of 83% across PC's 1 to 3 indicating that the variation is strongly related to the total metabolome. Partial overlap between the *mtp*-complement-infected and *mtp*-complement-uninfected A549 cells (Figure 3.2c) was seen, amounting to a total variation of 4% across PC's 7 to 9, an almost identical observation to the WT-infected and WT-uninfected A549 cell model. The observed variation in Figures 3.2a and 3.2c indicate that only a small part (4%) of the total metabolome is affected. The top 3 components, with a total variation of 74%, in the WT-infected and Δ*mtp*-infected A549 cell model (Figure 3.2d) best describe the data showing complete separation of ellipsoids. The power values emanating from this model analysis provide high confidence when selecting discriminatory values for the selection of statistically significant metabolites. Lastly, the WT-infected and *mtp*-complement-infected A549 cell model (Figure 3.2e) depicts a partial overlap of ellipsoids with a total variation of 11% across PC's 4 to 6. This indicates that 89 % of the metabolome between these two cell models were identical, highlighting the restoration of *mtp* gene function in the *mtp*-complemented strain. Because the 4 models did not validate, subsequent interrogation (i.e. PLS-DA) was considered to be unnecessary.

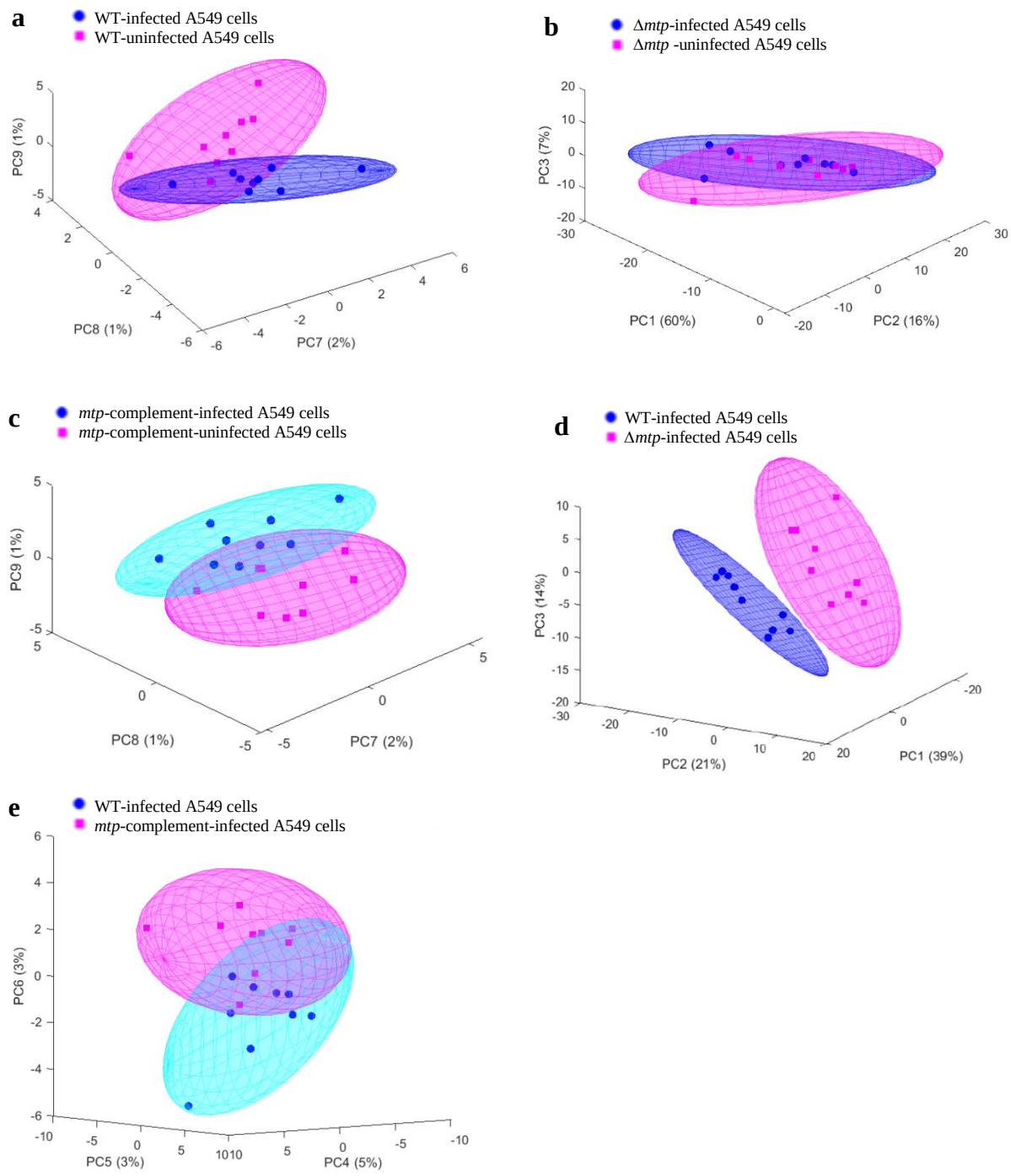

Figure 3.2 Three-dimensional PCA scores plots for *M. tuberculosis*-infected and uninfected A549 epithelial cell models. Ellipsoidal overlap was observed between (a) WT-infected and WT-uninfected A549 cells, (b) Δ*mtp*-infected and Δ*mtp*-uninfected A549 cells, (c) *mtp*-complement-infected and *mtp*-complement-uninfected A549 cells, and (e) WT-infected and *mtp*-complement-infected A549 cells, while WT-infected and Δ*mtp*-infected A549 cells (d) displayed complete ellipsoidal separation. PC = Principal component.

3.4.3 PLS-DA data revealed complete group separation between the WT-infected A549 cells and Δmtp-infected A549 cells further confirming model validation

The PLS-DA identifies combinations of metabolites that differentiate between groups. The PLS-DA models are known to not replicate well given previously unseen data. Therefore, models must validate before they can be interpreted with confidence. In this study, leave-one-out cross-validation of the prediction accuracy and PCA separation were used as validation. Hence, only the WT-infected A549 cells and Δ*mtp*-infected A549 cell model is reported. A VIP value is produced which is used to rank metabolites jointly to best describe the model as a whole. Ellipsoids represent a 95 % confidence interval (CI) of score centroids of each group. The percentage of the overall variation in the groups (Y) as well as the metabolites observed (X), as explained by each component, are indicated in brackets along each latent variable (LV) axis. Complete ellipsoidal separation was observed between the WT-infected A549 cells and Δ*mtp*-infected A549 cells (Figure 3.3). R^2 and Q^2 values were 98 % and 94 %, respectively. Along with the observed PCA separation (Figure 3.2d), the PLS-DA model met the validation criteria for the shortlisting of discriminatory metabolites with VIP scores greater than or equal to 1.

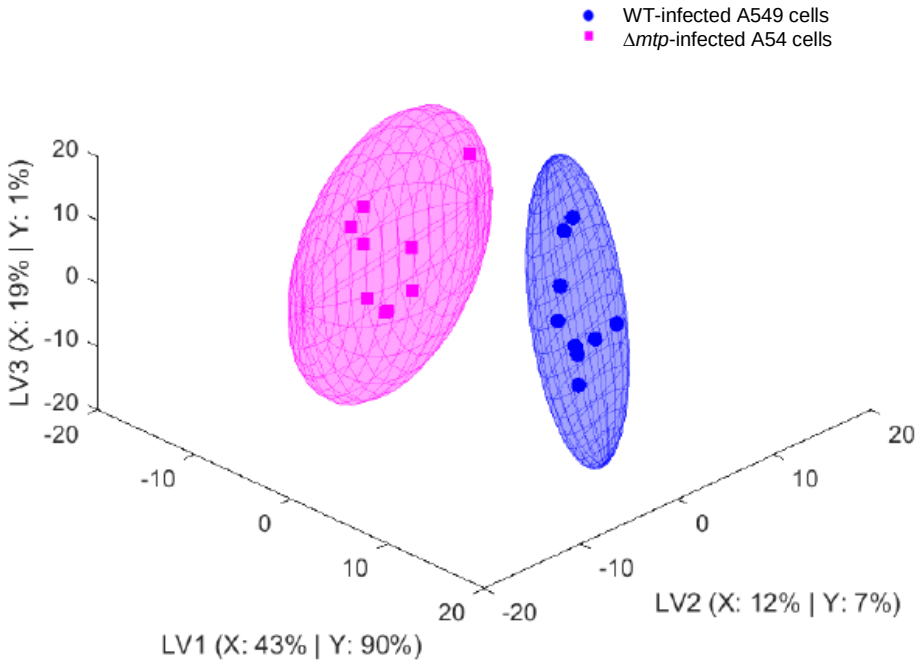

Figure 3.3 A three-dimensional PLS-DA scores plot comparing the WT-infected A549 cells and Δ*mtp*-infected A549 cells. Dots represents cases projected onto the new lower-dimensional space considering their group association generated by the PLS-DA model. Complete ellipsoidal separation between the two cell models were observed. The percentage of the overall variation in the groups (Y) as well as the metabolites observed (X), as explained by each component, are indicated in brackets along each latent variable (LV) axis.

3.4.4 Biologically significant metabolites that met the selection criteria between WT-infected cells and Δmtp-infected cells

The selection criteria were as follows; *t*-test *p*-value (after BH adjustment) ≤ 0.05, Cohen's d-value ≥ 0.8, PLS-DA (3D) VIP ≥ 1, and fold change ≥ 2. Only the metabolites that met either both univariate criteria or had a VIP ≥ 1 were included, resulting in 107 metabolites (Appendix D4: Table D4.5) with discriminatory ability between the two cell models. A total of 68 metabolites met all 3 criteria, resulting in a final shortlist of 62 metabolites after the fold change criterion was applied. A total of 46 biologically-relevant metabolites met all criteria between the two cell models (Table 3.1), while the remaining 16 had limited or no biological function (Appendix D4: Table D4.5). The metabolites that were statistically significant between the WT-infected cells and Δ*mtp*-infected cells were categorized in Table 3.1 according to biological relevance using PubChem (Kim et al., 2019) and/or KEGG (Kanehisa et al., 2017). These included metabolites involved in nucleic acid synthesis, amino acid metabolism (lysine biosynthesis and degradation; aspartate, alanine and glutamate metabolism; proline metabolism), glutathione metabolism, oxidative stress, lipid metabolism and a peptidoglycan anomaly.

Overall, all the metabolites were produced at a lower relative concentration in the Δ*mtp*-infected cells compared to the WT-infected cells. The category with the largest number of metabolites was aspartate, alanine and glutamate metabolism with 13 metabolites. N-Acetylglutamic acid had the highest fold change of 32.00 and urea had the lowest fold change of 2.27. Glutathione metabolism had eight metabolites in total with a fold change of 76.89 for L-cystine while L-threose had a fold change of 3.21. A metabolite of note in this category was butanoic acid as it was only detectable in the WT-infected cells. Three categories had a total of seven metabolites each; nucleic acid synthesis, lysine biosynthesis and degradation, and lipid metabolism. The nucleic acid synthesis category had the metabolite with the highest fold change in the study, namely 5'-methylthioadenosine, with a fold change of 100.39. The other metabolites in the category ranged from 2.00 (uracil) to 27.66 (pyrimidinedione). For the lysine biosynthesis and degradation category, 6-aminocaproic acid had the highest fold change value of 16.31 while pimelic acid had the lowest fold change value of 3.30. The metabolites detected in the lipid metabolism category ranged from a fold change of 2.31 to 13.64 with scyllo-inositol being the metabolite with the highest fold change. The oxidative stress category had two metabolites; timonacic and deoxyglucose with fold changes of 8.50 and 5.79, respectively. L-hydroxyproline with a fold change of 7.81 was the only detected metabolite for proline metabolism while lanthionine (10.78) was the only metabolite detected for peptidoglycan synthesis.

A total of six metabolites were identical to those detected in the previous investigation by Ashokcoomar and Reedoy et al. (2020; unpublished) where *M. tuberculosis* bacterial metabolites were identified using

the same strains. These metabolites were 2-aminoadipic acid, N-acetylaspartic acid, L-aspartic acid, cadaverine, 2-hydroxyisovaleric acid and myo-inositol.

Four of the five models tested in this investigation did not validate. A few metabolites were detected (Appendix: D4), however, they lacked statistical rigour to be classified as potential biomarkers and were omitted from the discussion section. These metabolites included aucubin and niacin for all 4 models, in addition to, 1,2,3-butanetriol and allonic acid between the Δ*mtp*-infected and Δ*mtp*-uninfected A549 cell model, 5-dodecenoic acid between the *mtp*-complement-infected and *mtp*-complement-uninfected A549 cell model, and 5-dodecenoic acid, hydracrylic acid and L-aspartic between the WT-infected and *mtp*-complement-infected A549 cells.

Table 3.1 Most significant metabolites between WT-infected and Δ*mtp*-infected A549 epithelial cells selected as per multivariate and univariate selection criteria together with their respective mean relative concentration and standard deviation, fold change with respect to the WT, PLS-DA VIP value, Cohen's d-value and BH adjusted *p*-values from the independent samples *t*-test

Category	Metabolite	Mean relative concentration and standard deviation (ng/mg cells)		Fold change	PLS-DA VIP	d-value	*p*-value
		WT-infected A549	Δ*mtp*-infected A549				
Lysine biosynthesis and degradation	2-Aminoadipic acid	6.420 (1.690)	0.641 (0.496)	-10.019	2.228	5.05	<0.001
	6-Aminocaproic acid	3.630 (0.959)	0.223 (0.274)	-16.309	1.969	5.58	<0.001
	Pimelic acid	0.759 (0.333)	0.230 (0.182)	-3.299	1.115	1.63	<0.001
	5-Aminovaleric acid	47.396 (16.653)	4.801 (2.400)	-9.871	2.131	4.51	<0.001
	Cadaverine	11.653 (4.917)	1.499 (1.266)	-7.775	1.472	3.63	<0.001
	Pentanedioic acid	7.605 (2.482)	1.668 (0.218)	-4.560	1.931	3.68	<0.001
	Pipecolic acid	47.579 (31.565)	13.908 (21.284)	-3.421	1.453	1.35	0.019
Aspartate, alanine and glutamate metabolism	N-Acetylaspartic acid	59.416 (34.156)	4.568 (3.256)	-13.007	2.071	3.31	<0.001
	Aspartic acid	2202.024 (711.363)	568.271 (218.263)	-3.875	1.473	3.10	<0.001
	Fumaric acid	34.824 (9.226)	13.242 (3.157)	-2.630	1.555	3.21	<0.001
	Alanine	4009.529 (1777.720)	1507.353 (642.839)	-2.660	1.154	1.93	0.001
	Malic acid	40.843 (11.0547)	16.7380 (3.866)	-2.440	1.370	2.74	<0.001
	N-Acetylalanine	7.827 (4.157)	1.873 (1.635)	-4.179	1.137	1.37	0.017
	á-Alanine	380.368 (232.880)	38.089 (26.995)	-9.986	1.270	3.19	<0.001
	Pantothenic acid	19.253 (5.161)	7.362 (2.902)	-2.615	1.075	2.07	<0.001
	Pyroglutamic-Acid	4000.010 (1041.297)	850.264 (228.117)	-4.704	2.007	5.72	<0.001
	N-Acetylglutamic acid	6.835 (2.572)	0.214 (0.339)	-32.005	1.994	4.79	<0.001
	Glutamine	182.574 (33.690)	71.281 (30.888)	-2.561	1.080	1.37	<0.001
	4-Aminobutanoic acid	97.8290 (37.374)	11.171 (4.594)	-8.757	1.812	4.41	<0.001
	Urea	55.503 (22.440)	24.4710 (3.253)	-2.268	1.189	1.10	0.040
Proline metabolism	Hydroxyproline	93.516 (24.917)	11.974 (5.008)	-7.810	2.085	4.54	<0.001

WT: wild-type; Δ*mtp*: *mtp*-gene knockout mutant; PLS-DA VIP: Partial Least Squares Discriminatory Analysis Variable in Projection value; Positive fold change = higher concentration in Δ*mtp*-infected cells; Negative fold change = higher concentration in WT-infected cells.

Table 3.2 Most significant metabolites between WT-infected and Δ*mtp*-infected A549 epithelial cells selected as per multivariate and univariate selection criteria together with their respective mean relative concentration and standard deviation, fold change with respect to the WT, PLS-DA VIP value, Cohen's d-value and BH adjusted *p*-values from the independent samples *t*-test

Category	Metabolite	Mean relative concentration and standard deviation (ng/mg cells)		Fold change	PLS-DA VIP	d-value	*p*-value
		WT-infected A549	Δ*mtp*-infected A549				
Glutathione metabolism	Cystine	335.928 (191.086)	4.369 (5.376)	-76.895	2.0347	4.27	<0.001
	Glycine	4.887 (2.368)	0.303 (0.479)	-16.116	1.896	3.37	<0.001
	Putrescine	298.385 (102.733)	54.242(29.823)	-5.501	1.620	2.85	<0.001
	Cysteine	1431.354 (447.301)	244.865 (116.430)	-5.845	1.587	2.82	<0.001
	Spermine	15.636 (8.174)	4.049 (2.871)	-3.862	1.349	2.10	0.002
	2-Aminobutanoic acid	82.387(26.688)	9.970 (6.172)	-8.264	1.621	2.83	<0.001
	Threose	30.220 (9.454)	9.419 (2.200)	-3.208	1.066	3.24	<0.001
	Butanoic acid	1.2136 (0.510)	0.000	-	1.577	2.21	0.008
Nucleic acid synthesis	5'-Methylthioadenosine	16.223 (5.746)	0.162 (0.324)	-100.389	2.490	6.09	<0.001
	Pyrimidinedione	11.334 (4.529)	0.410 (0.5630)	-27.660	2.009	5.96	<0.001
	Uracil	5066.375 (1293.552)	2528.215 (499.946)	-2.004	1.403	2.50	<0.001
	Ribonic acid	19.092 (8.001)	2.818 (1.939)	-6.775	1.360	3.33	<0.001
	Pentitol	2.879 (1.392)	0.115 (0.229)	-24.969	1.244	2.93	<0.001
	Methyl à-D-ribofuranoside	25.105 (11.612)	3.872 (2.293)	-6.484	1.148	3.14	<0.001
	Guanosine	37.694 (27.697)	4.654 (10.348)	-8.100	1.107	1.87	0.008
Oxidative stress	Deoxyglucose	27.852 (7.891)	4.813 (1.397)	-5.787	2.217	5.09	<0.001
	Timonacic	144.044 (80.701)	16.950 (11.973)	-8.498	1.491	2.16	0.002
Peptidoglycan	Lanthionine	18.044 (8.605)	1.674 (1.681)	-10.781	1.495	3.48	<0.001
Lipid metabolism	5-Dodecenoic acid	21.972 (9.504)	2.742 (1.209)	-8.013	1.979	3.30	<0.001
	Scyllo-Inositol	37.565 (11.641)	2.754 (1.386)	-13.642	1.880	5.03	<0.001
	Decanoic acid	19.115 (12.794)	3.906 (1.291)	-4.893	1.289	1.55	0.008
	Myo-Inositol	1761.324 (431.925)	394.299 (98.898)	-4.467	1.248	5.56	<0.001
	D-Glucopyranuronic acid	15.882 (9.334)	2.161 (1.577)	-7.351	1.156	1.57	0.011
	Ethanolamine	2047.569 (906.272)	884.518 (480.229)	-2.315	1.144	1.43	0.014
	2-Hydroxyisovaleric acid	4.227 (3.183)	0.554 (0.741)	-7.632	1.315	1.29	0.031

WT: wild-type; Δ*mtp*: *mtp*-gene knockout mutant; PLS-DA VIP: Partial Least Squares Discriminatory Analysis Variable in Projection value; Positive fold change = higher concentration in Δ*mtp*-infected cells; Negative fold change = higher concentration in WT-infected cells.

3.5 Discussion

A recent functional metabolomics study comparing the *mtp* knockout and a fully functioning WT *M. tuberculosis* strain, elucidated the role of MTP in the metabolomic profile of *M. tuberculosis* during logarithmic growth in Middlebrook 7H9 broth (Ashokcoomar and Reedoy et al., 2020; unpublished). Deletion of *mtp* resulted in metabolite signatures significantly associated with a deleterious effect on cell wall composition, fatty acid metabolism, and amino acid and peptidoglycan biosynthesis in *M. tuberculosis*. These findings supported previous reports (Ramsugit et al., 2013; Naidoo et al., 2014; Ramsugit and Pillay, 2014; Ramsugit et al., 2016; Naidoo et al., 2018) that alluded to MTP as an important contributor to the pathogenicity of *M. tuberculosis*, and thus, provided validation of this adhesin as a target for the design of TB diagnostics and therapeutics. The current study provided further supporting evidence of the role of MTP in modulating the host metabolome during *in vitro* infection of A549 pulmonary epithelial cells.

The present study investigated five different infection models, however, only one model validated and formed the focus of this investigation from which the shortlist of metabolites was produced. The first 3 models were infected and uninfected models of comparison. These were tested to determine whether there were any significant differences observed in the *M. tuberculosis*-infected A549 cell model compared to the respective uninfected model to identify potential metabolites perturbed by the specific infecting strain, as any observed changes would be attributed to adhesion/invasion events. Between the WT-infected and WT-uninfected A549 cells, Δ*mtp*-infected and Δ*mtp*-uninfected A549 cells, and the *mtp*-complement-infected and *mtp*-complement-uninfected A549 cells, only 2 – 4 metabolites were detected but not validated, indicating very slight differences due to infection. This may suggest that *M. tuberculosis* exerts minimal metabolomic disturbances to enable successful establishment of the pathogen during the initial host pathogen interaction.

The *mtp*-complemented strain was investigated to assess functional restoration. The PCA scores plots (Figure 3.2a and 3.2c) of the WT-infected and WT-uninfected A549 cells, and the *mtp*-complement-infected and *mtp*-complement-uninfected A549 cells, demonstrated highly similar metabolomes, with only a 4% variation detected for both models, indicating that only a minimal percentage of their metabolome were altered, while the remaining 96% remained unchanged. The PCA scores plot (Figure 3.2e) comparing the WT-infected cells and *mtp*-complement-infected cell model revealed only 11% variation of the total metabolome, inferring an 89% metabolome similarity between the groups. This was supported by the differential detection of 19 (8.56%) of the total 222 metabolites, of which only 5 (2.25%) metabolites met the statistical selection criteria, however could not be validated (Appendix: D4). Moreover, the fold change differences when comparing these groups were small, ranging between 2 and 3, with the exception of aspartic acid which had a fold change of 6 (Appendix: D4). Overall, no major perturbation of the metabolic pathways was demonstrated when comparing the metabolome of

A549 cells infected with the WT and *mtp*-complement strains, confirming that the *mtp* function was restored close to that of the WT.

It must be noted that the metabolites detected in the current study could be attributed to either 1) *M. tuberculosis* metabolism and the changes that may occur within the bacterial metabolic network due to infection, as elucidated by the use of an uninfected control; or 2) the changes that may occur within an A549 epithelial cell model of infection, in response to the infecting *M. tuberculosis* (du Preez and Loots, 2013). All 46 identified metabolites were produced in significantly higher quantities in WT-infected cells compared to the *Δmtp*-infected cells, and the major metabolic pathways differences were seen in: nucleic acid synthesis, amino acid metabolism, glutathione metabolism, oxidative stress, lipid metabolism and a peptidoglycan anomaly, as will be described in detail below.

3.5.1 MTP and nucleic acid metabolism during M. tuberculosis infection.

The metabolite, 5'-methylthioadenosine (MTA), synthesised from methionine, is involved in the polyamine biosynthetic pathway, where adenine is one of the resultant products (Kim et al. 2019). In addition to being found in mammalian tissue, this pathway is also well-known to *M. tuberculosis* (Berger and Knodel, 2003; Venos et al., 2004). This metabolite has been found to influence cell proliferation and differentiation (Avila et al., 2004). Since the WT-infected cells in this study exhibited an approximate 10-fold increase in the levels of this metabolite and fold change of approximately 100, compared to the Δ*mtp*-infected cells, this implicates the role of MTP in this purine synthesis pathway during infection. Since MTA is detectable in human urine also, it could possibly be investigated as metabolite biomarker for TB infection/disease (Mills and Mills, 1985). Furthermore, there was an 8-fold increase in the purine metabolite guanosine in the WT infected cells comparatively. Pyrimidinedione and uracil, were also both detected in significantly higher relative concentrations in the WT-infected cells compared to the Δ*mtp*-infected cells, indicating an inability of the latter to synthesise not only purine, but also pyrimidines nucleotides, required by the infecting *M. tuberculosis* for propagation (Ehrt et al., 2018). Substantiating this, were the elevated levels of various purine and pyrimidine metabolism intermediates in the WT infected cells, including: ribonic acid (a product of a reaction involving D-ribose, NADP+ and water (Kim et al., 2019)), pentitol (a sugar alcohol formed as a result of ribose reduction), methyl à-D-ribofuranoside (a derivative of D-ribose (Kim et al., 2019)), glycine, aspartic acid, fumaric and glutamine (Voet et al., 2016). Collectively, this indicates a less efficient nucleic acid metabolism in the Δ*mtp*-infected cells compared to the WT-infected cells. The metabolites could be both pathogen- and host-derived, the former of which gears up replicative machinery for microbial expansion, and the latter which drives an immune response to eradicate the infecting organism (Passalacqua et al., 2016; Ehrt et al., 2018).

3.5.2 MTP and amino acid metabolism during M. tuberculosis infection.

3.5.2.1 Lysine biosynthesis and degradation

Bacterial organisms primarily utilise the *meso*-diaminopimelate pathway for lysine biosynthesis (Scapin and Blanchard, 1998). This pathway begins with aspartic acid, and progresses through a series of reactions and intermediates including pimelic acid (Scapin and Blanchard, 1998; Kim et al., 2019). Lysine degradation on the other hand proceeds via 6-aminocaproic acid, which then produces 2-aminoadipic acid, followed by a series of other metabolic intermediates (Kanehisa et al., 2017; Karlsson et al., 2018). Bacterial lysine also serves as a substrate for the synthesis of cadaverine which in turn can be catabolized to 5-aminovaleric acid, via the breakdown of 5-aminopentanal (Kanehisa et al., 2017; Kim et al., 2019). Pentanedioic acid, also known as glutaric acid, (Kanehisa et al., 2017; Wishart et al., 2018) and pipecolic acid (Kanehisa et al., 2017) are further catabolism intermediates of lysine. All of the aforementioned lysine synthesis intermediates, and catabolism intermediates were seen to be elevated in the WT strain comparatively, which points towards a greater yield and utilisation of these metabolic pathways in the WT infected cells. Additionally, although not selected via the strict statistical marker selection protocol selected, lysine itself (Appendix: D4) was also detected in a higher relative concentration in the WT infected cells comparatively, however the fold change was below the set cut-off value. Since lysine is an essential amino acid that cannot be synthesised by humans, hence the above-mentioned metabolites can be assumed to be derived from the infecting *M. tuberculosis* (Gillner et al., 2013).

In mycobacteria, lysine biosynthesis is necessary for subsequent peptidoglycan formation (Pavelka and Jacobs, 1996) and lysine degradation also fuels the citrate cycle since it serves as a metabolic substrate for acetyl-CoA (Kanehisa et al., 2017). Both of these processes are vital for pathogen survival and propagation (Gillner et al., 2013). The fold changes of the associated metabolites in lysine biosynthesis and degradation ranged from - 16.3 to - 3.4 (Table 3.1) in the Δ*mtp* -infected cells which signifies less efficient lysine metabolism in this group comparatively. Since lysine biosynthesis and degradation are specific to the bacteria, as opposed to the host cells, these pathways could be ideal targets for antimicrobial therapeutics. This hypothesis was substantiated by (Pavelka and Jacobs, 1996), who determined that the deletion of the genes coding for a key enzyme in this pathway, *N*-succinyl-L,L-diaminopimelic acid desuccinylase, was lethal to *M. smegmatis*. Lysine auxotrophs have also been used in vaccine studies which further highlight the necessity of this pathway for *M. tuberculosis* survival (Pavelka et al., 2003; Larsen et al., 2009). In the aforementioned study, two doses of the lysine auxotrophic mutant of *M. tuberculosis* H37Rv in a mouse model, using an aerosol immunisation strategy, showed a boosting effect to the Bacille Calmette Guerin (BCG) vaccine (Pavelka et al., 2003). After this successful immunisation in mice and guinea pigs (Sambandamurthy et al., 2005;

Sambandamurthy et al., 2006), the safety and efficacy of two double deletion *M. tuberculosis* vaccine strains; mc^2 6020 and mc^2 6030 were established in non-human primates, namely (cynomolgus macaques), however, protection levels were not as high as the compared BCG vaccine (Larsen et al., 2009).

3.5.2.2 Aspartate, alanine and glutamate metabolism

The metabolite, N-acetylaspartic acid is a precursor to aspartic acid, which in turn serves as a substrate for fumaric acid, malic acid and alanine (Kanehisa et al., 2017). *Mycobacterium tuberculosis* assimilates aspartic acid from its host, and the absence of the *M. tuberculosis* aspartic acid transporter; AnsP1, has been shown to reduce its pathogenesis (Gouzy et al., 2013). All of the aforementioned metabolites were detected in elevated relative concentrations in the WT-infected cells comparatively, showing a more efficient assimilation of aspartic acid, synthesis of alanine and the resulting citrate cycle metabolites, all of which supports the role of MTP in *M. tuberculosis* pathogenesis Furthermore, L-aspartic acid is converted to pantothenic acid (Kanehisa et al., 2017), and ultimately to coenzyme A (coA) after a series of reactions. Also known as vitamin B5, pantothenic acid is considered essential in fatty acid metabolism and the functioning of the citric acid cycle (Jackowski and Rock, 1996). An *M. tuberculosis* auxotroph of this metabolite was shown to provide immunogenicity in vaccinated mice, further highlighting the importance of pantothenic acid in *M. tuberculosis* survival and pathogenicity (Sambandamurthy et al., 2002). A double auxotroph with pantothenic acid and lysine have shown success in vaccine studies using non-human primates (Larsen et al., 2009). Human-derived cells are unable to secrete pantothenic acid (White et al., 2001), hence this metabolite is of bacterial origin.

Urea is a by-product of amino acid metabolism, however more closely associated with the metabolism of arginine (Kanehisa et al., 2017), and is used as a nitrogen source by *M. tuberculosis* (Lin et al., 2012). The elevated relative concentrations of the aforementioned in the WT-infected cells comparatively, indicated the role of MTP in nitrogen assimilation. This was further supported by the elevated level of all metabolites associated with glutamine/glutamate metabolism (pyroglutamic acid, N-acetylglutamic acid, 4-aminobutanoic acid/gamma-amino butyric acid (GABA)) (Table 3.1) (Kanehisa et al., 2017), in the WT-infected cells in the current study. The GABA has also previously been shown to play a role in *M. tuberculosis* host cell infection, by serving as a proton-quencher, regulating the pH of the immediate *M. tuberculosis* environment and reducing oxidative stress (Rizvi et al., 2019). The metabolite, L-glutamate, is not only associated with nitrogen metabolism but also glutathione metabolism and butanoate metabolism (Kanehisa et al., 2017). In summary, MTP plays a role in aspartate, alanine and glutamate metabolism, all of which participate in nitrogen assimilation during pathogenesis (Gouzy et al., 2013; Rizvi et al., 2019).

3.5.2.3 Proline metabolism

The metabolite, L-Hydroxyproline, a precursor to proline synthesis (Kanehisa et al., 2017) can be used as an indicator of fibrogenesis in the lung and liver following infection with mycobacteria (Shkurupiy et al., 2013). In the aforementioned study, the authors observed that the concentrations of hydroxyproline correlated with an increase in granuloma and resident fibroblast synthesis (Shkurupiy et al., 2013). The current study revealed a 7-fold decrease in L-hydroxyproline in the Δ*mtp*-infected cells, which indicates that the production of this metabolite is less efficient in the deletion mutant, emphasising the role of MTP in the pathogenesis of *M. tuberculosis* and the role of hydroxyproline in this process.

3.5.3 MTP and glutathione metabolism during M. tuberculosis infection.

Cysteine (derived from cysteine), threose (a metabolite of ascorbate), glycine, cadaverine, putrescine, spermine (Table 3.1) and glutamic acid (Appendix: D4) are major metabolites contributors involved in the glutathione metabolism (Kanehisa et al., 2017). All of the aforementioned metabolites were once again elevated in the WT-infected cells, indicating the role of MTP in glutathione synthesis and the latter role in infection of host cells. L-Glutamate is converted to butanoic acid via a series of reactions (Kanehisa et al., 2017). Butanoic acid (derived from L-glutamic acid) serves as a carbon source for *M. tuberculosis*, hence it appears that the mutant strain (in which this metabolite was at a relative concentration below detectable levels), has a reduced capacity for carbon assimilation via this route, and subsequently derives carbon from other metabolic sources during infection (de Carvalho et al., 2010; Early et al., 2016). Considering this, during infection, *M. tuberculosis* experiences reductive stress as a result of host defences, cofactor reduction and hypoxia (Mavi et al., 2019). Metabolic adaptations to these adverse environments may result in a toxic host cell environment, hence glutathione metabolism plays a crucial role for host cells in order to confer protection against infection (Morris et al., 2013), and the aforementioned explains the role in MTP for *M. tuberculosis* survival.

3.5.4 MTP and oxidative stress during M. tuberculosis infection.

Deoxyglucose, an analogue of glucose, is a competitive inhibitor of hexokinase II, an enzyme participating in the first step in glycolysis (Zhang et al., 2014; Cumming et al., 2018). This metabolite was reported to increase oxidative stress and cause cell apoptosis in specific types of cancer cells (Zhang et al., 2014). An alteration in glucose metabolism, known as the Warburg effect, is a common observation in cancer cells (Warburg et al., 1927), and has also been noted in mycobacterial granulomas caused by *M. avium* infection (Appelberg et al., 2015). This phenomenon is accompanied by an elevated cellular glucose uptake by the host cell (Warburg et al., 1927; Appelberg et al., 2015). The origin of deoxyglucose is unknown, but it can be hypothesised that it is a host response to *M. tuberculosis* infection by interrupting glycolysis. Furthermore, du Preez and Loots (2013), indicated this to be a host

adaptation, subsequently producing hydrogen peroxide driven oxidative stress within the cell, killing *M. tuberculosis* at the site of infection, and/or programmed cell death. Timonacic, alternately known as thiazolidine-4-carboxylic acid, is a condensation product of cysteine and formaldehyde (Weber et al., 1982). It functions as a proline analogue, also called thioproline, where it mimics proline and is subsequently incorporated into proteins in place of proline, an occurrence which results in perturbed growth of an organism, as seen in *E. coli* K-12 (Unger and DeMoss, 1966). This metabolite was also demonstrated to have potential therapeutic action, since it inhibits the growth of infecting pathogens (Magdaleno et al., 2009). It is unclear as to whether this metabolite is of bacterial origin, but it is most likely also a host-derived response, to prevent growth and halt subsequent propagation of the invading *M. tuberculosis* cells by creating an environment of oxidative stress. The fold changes of deoxyglucose (- 5.8) and timonacic acid (- 8.5) indicate that the Δ*mtp*-infected cells exhibited significantly lower relative concentrations of these metabolites, pointing towards a reduced state of oxidative stress in this cell model of infection, most likely due to a compromised infection mechanism due to the absence of MTP.

3.5.5 MTP and lipid metabolism during M. tuberculosis infection.

It is well known that the unique mycobacterial lipid components contribute to the success of this pathogen, and subsequently this has been a drug therapy target for years (Barry et al., 1998; Kinsella et al., 2003). A number of altered lipid metabolites were detected in the current study. The metabolite, 2-hydroxyisovaleric acid is a hydroxyl fatty acid and is also known by its alternative name as β-hydroxy-β-methylbutyric acid (Wishart et al., 2018). This metabolite is a leucine degradation pathway product and is commonly found as a human metabolite (Landaas, 1975; Mobley et al., 2014; Ehling and Reddy, 2015). The metabolite, 5-dodecenoic acid is a medium-chain fatty acid also present as a human metabolite (Wishart et al., 2018). Decanoic acid is a straight-chain saturated fatty acid that plays a role in fatty acid biosynthesis, and the breakdown of pimelic acid is also involved in the same pathway (Kanehisa et al., 2017). Scyllo-inositol and myo-inositol are isomers of inositol (Wishart et al., 2018). Inositol is found in mycobacterial cell envelopes where it anchors lipomannan, lipoarabinomannan and phosphatidylinositol mannosides (Jackson et al., 2000). The metabolite, D-Glucopyranuronic acid, also known as glucuronic acid, is one of the byproducts of myo-inositol breakdown (Kim et al., 2019) and is found in mycobacteria as glycopeptidolipids (Chatterjee et al., 1987). Ethanolamine is part of glycerophospholipid metabolism (Kanehisa et al., 2017) and is used as a source of carbon and nitrogen, especially during bacterial pathogenesis (Garsin, 2010). Collectively, these metabolites are involved in the production of fatty acids necessary for cell envelope biogenesis, possibly due to pathogen expansion for the continuation of infection. The Δ*mtp*-infected cells exhibited relatively lower concentrations of these lipid metabolites compared to the WT-infected cells, most likely leading to a compromised mycobacterial cell envelope during the infection process, as was highlighted in Chapter 2 of this dissertation (Ashokcoomar and Reedoy et al., 2020; unpublished).

3.5.6 Implication of lanthionine detection in potential peptidoglycan anomaly

Lanthionine, a thioether dimer of cysteine, is known to be a non-proteinogenic amino acid and was first reported in *Fusobacterium nucleatum*, as a constituent of peptidoglycan (Kato et al., 1979). The natural substitution of lanthionine for 3-hydroxy m-DAP in the peptidoglycan layer of some bacteria has been documented (Inoue et al., 1979; Vasstrand et al., 1980; Kawamoto et al., 1981). Uridine diphosphate (UDP)-MurNAc-tripeptide ligase (MurE), responsible for the addition of meso-diaminopimelic acid (m-DAP) into peptidoglycan in *M. tuberculosis*, demonstrated similar activity with DL-lanthionine as m-DAP (Basavannacharya et al., 2010). This finding, consistent with that in *E. coli* mutants (Mengin-Lecreulx et al., 1994) and *M. smegmatis* (Consaul et al., 2005), reportedly demonstrated MurE specificity for the meso-isomer (Basavannacharya et al., 2010). Lanthionine was surprisingly detected in the A549 epithelial cells infected with *M. tuberculosis* in the present study. While it is not known whether this metabolite is of host or pathogen origin, this is a confounding observation, and the implications for proposed treatment of drug-resistant TB with lantibiotics (Monteville et al., 1999; Sosunov et al., 2007; Carroll et al, 2010; Donaghy, 2010) is unclear, especially in the context of lanthionine incorporation resulting in peptidoglycan instability leading to increased antibiotic susceptibility, as well as the presence of lanthionine in this class of antibiotics itself (van Kraaij et al., 1999; Guder et al., 2000). The exact mechanism by which lanthionine is synthesised intracellularly is unknown, but it is hypothesised that it is produced from high concentrations of cysteine (Richaud et al., 1993; Consaul et al., 2005), which in turn is synthesized from cystine (Kanehisa et al., 2007). In the present study, cystine and cysteine were coincidentally detected at about 77- fold and 6-fold higher relative concentrations in the WT than Δ*mtp* infected cells respectively. The fold change of 10.8 higher relative concentration of lanthionine in the WT-infected cells than the Δ*mtp*-infected cells, indicates a possible major perturbation of the peptidoglycan composition in the latter.

A previous gas chromatography mass spectrometry investigation of the metabolic perturbations during infection of A549 lung epithelial cells by *Cryptococcus neoformans*, demonstrated high similarity to the affected pathways in the current study: alanine, aspartate and glutamate metabolism, glutathione metabolism, proline metabolism, glycine metabolism, inositol phosphate metabolism, citrate cycle and pantothenate biosynthesis (Liew et al., 2016). Furthermore, a previous liquid chromatography-mass spectrometric multiple reactions monitoring (LC-MRM/MS) to study the cellular metabolome of host macrophages infected with *M. tuberculosis,* showed that the most affected pathways were nucleotide metabolism, amino acid metabolism and central carbon metabolism (Rizvi et al., 2019), also confirming the results in the current study.

A limitation of this study is that *in vitro* conditions may not accurately represent the metabolites detected during human pulmonary infection, however it does provide an indication of the changes in metabolic

pathways that may result. Additionally, the study design did not permit accurate identification of metabolites of host or pathogen origin. Sample preparation, processing time and instrumentation limitations such as reproducibility, detection limit and accuracy, are potential factors that could serve as limitations. In the current study, these limitations were overcome by using identical experimental conditions for experiments and controls, with the use of meticulous technique and adherence to specific brands of consumables to minimise variation. Inoculum, OD_{600nm} and pellet mass standardisation, as well as quality controls, and internal standards, were utilised to ensure reproducibility, reliability and excellent quality reads. The choice of approach for bioinformatics analyses may serve as a limitation as a range of approaches are available. This was overcome by selecting a set of analyses for the current study according to the study design to produce the ideal set of data to best answer the aim of the investigation. The limitation of discriminating between host- and pathogen-derived metabolites, may be overcome by ^{13}C-labelling of *M. tuberculosis* cells in conjunction with a mass spectrometric platform to track the metabolic interactions of the pathogen during host infection (Beste et al., 2013).

Since the relative MTA concentration was significantly reduced by approximately 100 times in the mutant compared to the WT, the three pathways used in the synthesis of MTA (Kanehisa et al., 2017) could be investigated further in order to determine which gene is significantly downregulated in the absence of the *mtp* gene and to target this for the design of intervention therapy. Since MTA has been targeted as a urine biomarker for diabetes and cancer, it would also be interesting to design studies to elucidate whether the non-invasive detection of this metabolite would be useful for TB diagnosis. The metabolites of the pathogen-specific lysine metabolism and degradation pathway that was less efficient in the Δ*mtp*-infected cells, are worthy of further investigation as targets for TB therapeutics or diagnostics. To further validate the metabolomics data regarding nitrogen assimilation, the Δ*mtp*-infected cells can be grown in minimal media containing a sole nitrogen source (such as urea, glutamine, glutamate or aspartic acid) to determine whether there are any growth defects compared to the WT-infected cells (Gouzy et al., 2013). Similarly, since butanoic acid was not detected in the Δ*mtp*-infected cells, these cells can be grown in media where butanoic acid serves as a sole carbon source for *M. tuberculosis* to assess growth compared to WT-infected cells. The association between the high levels of cystine and cysteine (FC of 77 and 6, respectively) higher in the WT than mutant, and the detection of lanthionine in *M. tuberculosis* infected A549 cells deserves further research, as lanthionine has been reported to be produced due to elevated levels of L-cysteine.

3.6 Conclusion

This study highlighted significant differential metabolomic profiles in both WT-infected and Δ*mtp*-infected A549 epithelial cell models of infection. Nucleic acid metabolism in the Δ*mtp*-infected cells was less efficient compared to the WT-infected cells most likely owing to a less virulent phenotype that may be associated with the deletion of the MTP adhesin. Lysine biosynthesis and degradation was also

less efficient in the Δ*mtp*-infected cells, and since this pathway is pathogen-specific, metabolites of this pathway may serve as ideal targets for therapeutics or diagnostics in TB infection. Nitrogen assimilation was less prominent in Δ*mtp*-infected cells arising from aspartate, alanine and glutamate metabolism. Glutathione metabolism, oxidative stress and lipid metabolism were less regulated in Δ*mtp*-infected cells potentially due to the compromised mycobacterial cell envelope in the deletion mutant which contributes to lower pathogenicity. Lastly, lanthionine was an unusually detected metabolite, and sheds potentially new insight into the peptidoglycan composition of the *M. tuberculosis* strain used in the current study. Taken together, these findings show that the absence of MTP can be associated with significant changes to the host metabolome, suggesting that this adhesin may be an important contributor to the pathogenicity of *M. tuberculosis*, and supports previous findings of its potential as a suitable drug, vaccine and diagnostic target.

3.7 References

Abdool Karim, S. S., Churchyard, G. J., Karim, Q. A. and Lawn, S. D. (2009). HIV infection and tuberculosis in South Africa: an urgent need to escalate the public health response. *Lancet (London, England), 374*(9693), 921–933.

Alberts, B., Johnson, A., Lewis, J., Walter, P., Raff, M. and Roberts, K. (2002). Molecular Biology of the Cell 4th Edition: International Student Edition. Routledge.

Alteri, C. J., Xicohténcatl-Cortes, J., Hess, S., Caballero-Olín, G., Girón, J. A. and Friedman, R. L. (2007). *Mycobacterium tuberculosis* produces pili during human infection. *Proceedings of the National Academy of Sciences, 104*(12), 5145-5150.

Appelberg, R., Moreira, D., Barreira-Silva, P., Borges, M., Silva, L., Dinis-Oliveira, R. J., et al. (2015). The Warburg effect in mycobacterial granulomas is dependent on the recruitment and activation of macrophages by interferon-γ. *Immunology, 145*(4), 498-507.

Ashokcoomar, S. and Reedoy, K. S. (2020). *M. tuberculosis* curli pili (MTP) deficiency is associated with alterations in cell wall biogenesis, fatty acid metabolism and amino acid synthesis (Unpublished). Manuscript soon to be submitted for publication. University of KwaZulu-Natal. Durban.

Avila, M. A., Garcia-Trevijano, E. R., Lu, S. C., Corrales, F. J. and Mato, J. M. (2004). Methylthioadenosine. *International Journal of Biochemistry and Cell Biology, 36*(11), 2125-2130.

Barry, C. E., 3rd, Lee, R. E., Mdluli, K., Sampson, A. E., Schroeder, B. G., Slayden, R. A., et al. (1998). Mycolic acids: structure, biosynthesis and physiological functions. *Progress in Lipid Research, 37*(2-3), 143-179.

Basavannacharya, C., Robertson, G., Munshi, T., Keep, N. H. and Bhakta, S. (2010). ATP-dependent MurE ligase in *Mycobacterium tuberculosis*: biochemical and structural characterisation. *Tuberculosis, 90*(1), 16-24.

Berger, B. J. and Knodel, M. H. (2003). Characterisation of methionine adenosyltransferase from *Mycobacterium smegmatis* and *M. tuberculosis*. *BMC Microbiology, 3*(1), 12.

Bermudez, L. E. and Goodman, J. (1996). *Mycobacterium tuberculosis* invades and replicates within type II alveolar cells. *Infection and Immunity, 64*(4), 1400-1406.

Bermudez, L. E., Sangari, F. J., Kolonoski, P., Petrofsky, M. and Goodman, J. (2002). The efficiency of the translocation of *Mycobacterium tuberculosis* across a bilayer of epithelial and endothelial cells as a model of the alveolar wall is a consequence of transport within mononuclear phagocytes and invasion of alveolar epithelial cells. *Infection and Immunity, 70*(1), 140-146.

Beste, D. J., Nöh, K., Niedenführ, S., Mendum, T. A., Hawkins, N. D., Ward, J. L., et al. (2013). 13C-flux spectral analysis of host-pathogen metabolism reveals a mixed diet for intracellular *Mycobacterium tuberculosis*. *Chemistry and Biology, 20*(8), 1012-1021.

Beukes, D., Du Preez, I. and Loots, D. T. (2019). Total metabolome extraction from mycobacterial cells for GC-MS metabolomics analysis. *Microbial Metabolomics, 1859*, 121-131.

Birkness, K. A., Deslauriers, M., Bartlett, J. H., White, E. H., King, C. H. and Quinn, F. D. (1999). An *in vitro* tissue culture bilayer model to examine early events in *Mycobacterium tuberculosis* infection. *Infection and Immunity, 67*(2), 653-658.

Carroll, J., Draper, L. A., O'Connor, P. M., Coffey, A., Hill, C., Ross, R. P., et al. (2010). Comparison of the activities of the lantibiotics nisin and lacticin 3147 against clinically significant mycobacteria. *International Journal of Antimicrobial Agents, 36*(2), 132-136.

Castro-Garza, J., King, C. H., Swords, W. E. and Quinn, F. D. (2002). Demonstration of spread by *Mycobacterium tuberculosis* bacilli in A549 epithelial cell monolayers. *FEMS Microbiology Letters, 212*(2), 145-149.

CDC (2018). Tuberculosis (TB) Data and Statistics. https://www.cdc.gov/tb/statistics/default.htm. Accessed 05/06 2018.

Chapeton-Montes, J. A., Plaza, D. F., Barrero, C. A. and Patarroyo, M. A. (2008). Quantitative flow cytometric monitoring of invasion of epithelial cells by *Mycobacterium tuberculosis. Frontiers in Bioscience, 13*, 650-656.

Chatterjee, D., Aspinall, G. and Brennan, P. (1987). The presence of novel glucuronic acid-containing, type-specific glycolipid antigens within *Mycobacterium* spp. Revision of earlier structures. *Journal of Biological Chemistry, 262*(8), 3528-3533.

Consaul, S. A., Wright, L. F., Mahapatra, S., Crick, D. C. and Pavelka, M. S., Jr. (2005). An unusual mutation results in the replacement of diaminopimelate with lanthionine in the peptidoglycan of a mutant strain of *Mycobacterium smegmatis*. *Journal of Bacteriology, 187*(5), 1612-1620.

Cumming, B. M., Addicott, K. W., Adamson, J. H. and Steyn, A. J. (2018). *Mycobacterium tuberculosis* induces decelerated bioenergetic metabolism in human macrophages. *eLife, 7*, e39169.

de Carvalho, L. P., Fischer, S. M., Marrero, J., Nathan, C., Ehrt, S. and Rhee, K. Y. (2010). Metabolomics of *Mycobacterium tuberculosis* reveals compartmentalized co-catabolism of carbon substrates. *Chemistry and Biology, 17*(10), 1122-1131.

Dheda, K., Gumbo, T., Gandhi, N. R., Murray, M., Theron, G., Udwadia, Z. et al. (2014). Global control of tuberculosis: from extensively drug-resistant to untreatable tuberculosis. *The Lancet. Respiratory Medicine, 2*(4), 321–338.

Dlamini, M. T. (2017). Whole transcriptome analysis to elucidate the role of MTP in gene regulation of pulmonary epithelial cells infected with *Mycobacterium tuberculosis.* Masters thesis. University of KwaZulu-Natal. Durban.

Dobos, K. M., Spotts, E. A., Quinn, F. D. and King, C. H. (2000). Necrosis of lung epithelial cells during infection with *Mycobacterium tuberculosis* is preceded by cell permeation. *Infection and Immunity, 68*(11), 6300-6310.

Donaghy, J. (2010). Lantibiotics as prospective antimycobacterial agents. *Bioengineered Bugs, 1*(6), 437–439.

du Preez, I. and Loots, D. T. (2013). New sputum metabolite markers implicating adaptations of the host to *Mycobacterium tuberculosis*, and vice versa. *Tuberculosis (Edinb), 93*(3), 330-337.

Early, J. V., Casey, A., Martinez-Grau, M. A., Gonzalez Valcarcel, I. C., Vieth, M., Ollinger, J., et al. (2016). Oxadiazoles Have Butyrate-Specific Conditional Activity against *Mycobacterium tuberculosis*. *Antimicrobial Agents and Chemotherapy, 60*(6), 3608-3616.

Ehling, S. and Reddy, T. M. (2015). Direct analysis of leucine and its metabolites beta-hydroxy-beta-methylbutyric acid, alpha-ketoisocaproic acid, and alpha-hydroxyisocaproic acid in human breast milk by liquid chromatography-mass spectrometry. *Journal of Agricultural and Food Chemistry, 63*(34), 7567-7573.

Ehrt, S., Schnappinger, D. and Rhee, K. Y. (2018). Metabolic principles of persistence and pathogenicity in *Mycobacterium tuberculosis*. *Nature Reviews. Microbiology, 16*(8), 496-507,.

Eoh, H. (2014). Metabolomics: A window into the adaptive physiology of *Mycobacterium tuberculosis*. *Tuberculosis, 94*(6), 538-543.

Garsin, D. A. (2010). Ethanolamine utilization in bacterial pathogens: roles and regulation. *Nature Reviews. Microbiology, 8*(4), 290-295.

Gillner, D. M., Becker, D. P. and Holz, R. C. (2013). Lysine biosynthesis in bacteria: a metallodesuccinylase as a potential antimicrobial target. *Journal of Biological Inorganic Chemistry, 18*(2), 155-163.

Gouzy, A., Larrouy-Maumus, G., Wu, T. D., Peixoto, A., Levillain, F., Lugo-Villarino, G., et al. (2013). *Mycobacterium tuberculosis* nitrogen assimilation and host colonization require aspartate. *National Chemical Biology, 9*(11), 674-676.

Guder, A., Wiedemann, I. and Sahl, H. G. (2000). Posttranslationally modified bacteriocins—the lantibiotics. *Peptide Science, 55*(1), 62-73.

Hameed, H., Islam, M. M., Chhotaray, C., Wang, C., Liu, Y., Tan, Y., et al. (2018). Molecular targets related drug resistance mechanisms in MDR-, XDR-, and TDR-*Mycobacterium tuberculosis* strains. *Frontiers in Cellular and Infection Microbiology, 8*, 114.

Inoue, M., Hamada, S., Ooshima, T., Kotani, S. and Kato, K. (1979). Chemical composition of *Streptococcus mutans* cell walls and their susceptibility to *Flavobacterium* L-11 enzyme. *Microbiology and Immunology, 23*(5), 319-328.

Jackowski, S. and Rock, C. (1996). *Escherichia coli* and *Salmonella typhimurium. Cellular and Molecular Biology, 2nd ed., edited by FC Neidhardt*, 687-694.

Jackson, M., Crick, D. C. and Brennan, P. J. (2000). Phosphatidylinositol is an essential phospholipid of mycobacteria. *Journal of Biological Chemistry, 275*(39), 30092-30099.

Kanehisa, M., Furumichi, M., Tanabe, M., Sato, Y. ans Morishima, K. (2017). KEGG: new perspectives on genomes, pathways, diseases and drugs. *Nucleic Acids Research, 45*(D1), D353-d361.

Karlsson, E., Shin, J. H., Westman, G., Eriksson, L. A., Olsson, L. and Mapelli, V. (2018). *In silico* and *in vitro* studies of the reduction of unsaturated α,β bonds of trans-2-hexenedioic acid and 6-amino-trans-2-hexenoic acid - Important steps towards biobased production of adipic acid. *PloS One, 13*(2), e0193503-e0193503.

Kato, K., Umemoto, T., Sagawa, H. and Kotani, S. (1979). Lanthionine as an essential constituent of cell wall peptidoglycan of *Fusobacterium nucleatum*. *Current Microbiology, 3*(3), 147-151.

Kawamoto, I., Oka, T. and Nara, T. (1981). Cell wall composition of *Micromonospora olivoasterospora*, *Micromonospora sagamiensis*, and related organisms. *Journal of Bacteriology, 146*(2), 527-534.

Kim, S., Chen, J., Cheng, T., Gindulyte, A., He, J., He, S., et al. (2019). PubChem 2019 update: improved access to chemical data. *Nucleic Acids Research, 47*(D1), D1102-D1109.

Kinsella, R. J., Fitzpatrick, D. A., Creevey, C. J. and McInerney, J. O. (2003). Fatty acid biosynthesis in *Mycobacterium tuberculosis*: lateral gene transfer, adaptive evolution, and gene duplication. *Proceedings of the National Academy of Sciences of the United States of America, 100*(18), 10320-10325.

Kline, K. A., Fälker, S., Dahlberg, S., Normark, S. and Henriques-Normark, B. (2009). Bacterial adhesins in host-microbe interactions. *Cell Host and Microbe, 5*(6), 580-592.

Landaas, S. (1975). Accumulation of 3-hydroxyisobutyric acid, 2-methyl-3-hydroxybutyric acid and 3-hydroxyisovaleric acid in ketoacidosis. *Clinica Chimica Acta; International Journal of Clinical Chemistry, 64*(2), 143-154.

Larsen, M. H., Biermann, K., Chen, B., Hsu, T., Sambandamurthy, V. K., Lackner, A. A., et al. (2009). Efficacy and safety of live attenuated persistent and rapidly cleared *Mycobacterium tuberculosis* vaccine candidates in non-human primates. *Vaccine, 27*(34), 4709-4717.

Liew, K. L., Jee, J. M., Yap, I. and Yong, P. V. C. (2016). *In vitro* analysis of metabolites secreted during infection of lung epithelial cells by *Cryptococcus neoformans*. *PloS One, 11*(4), e0153356-e0153356.

Lin, W., Mathys, V., Ang, E. L. Y., Koh, V. H. Q., Martínez Gómez, J. M., Ang, M. L. T., et al. (2012). Urease activity represents an alternative pathway for *Mycobacterium tuberculosis* nitrogen metabolism. *Infection and Immunity, 80*(8), 2771-2779.

Lubman, R., Kim, K. and Crandall, E. (1997). Alveolar epithelial barrier properties. The Lung: Scientific Foundations., 2nd ed., *Crystal, R. G., West, J. B., Weibel, E. R., Barnes, P. J.*, Eds., Lippincott-Raven, Philadelphia.

Magdaleno, A., Ahn, I.-Y., Paes, L. S. and Silber, A. M. (2009). Actions of a proline analogue, L-thiazolidine-4-carboxylic acid (T4C), on Trypanosoma cruzi. *PloS One, 4*(2), e4534-e4534.

Mahapatra, S., Hess, A. M., Johnson, J. L., Eisenach, K. D., DeGroote, M. A., Gitta, P., et al. (2014). A metabolic biosignature of early response to anti-tuberculosis treatment. *BMC Infectious Diseases, 14*(1), 53.

Mavi, P. S., Singh, S. and Kumar, A. (2019). Reductive stress: new insights in physiology and drug tolerance of *Mycobacterium*. *Antioxidants and Redox Signaling*, doi:10.1089/ars.2019.7867 [ePub ahead of print].

McDonough, K. A. and Kress, Y. (1995). Cytotoxicity for lung epithelial cells is a virulence-associated phenotype of *Mycobacterium tuberculosis*. *Infection and Immunity, 63*(12), 4802-4811.

Mengin-Lecreulx, D., Blanot, D. and van Heijenoort, J. (1994). Replacement of diaminopimelic acid by cystathionine or lanthionine in the peptidoglycan of Escherichia coli. *Journal of Bacteriology, 176*(14), 4321-4327.

Mills, G. C. and Mills, J. S. (1985). Urinary excretion of methylthioadenosine in immunodeficient children. *Clinica Chimica Acta International Journal of Clinical Chemistry, 147*(1), 15-23.

Mobley, C. B., Fox, C. D., Ferguson, B. S., Amin, R. H., Dalbo, V. J., Baier, S., et al. (2014). L-leucine, beta-hydroxy-beta-methylbutyric acid (HMB) and creatine monohydrate prevent myostatin-induced Akirin-1/Mighty mRNA down-regulation and myotube atrophy. *Journal of the International Society of Sports Nutrition, 11*, 38-38.

Monteville, T. J., Chung, H., Chikindas, M. L. and Chen, Y. (1999). Nisin A depletes intracellular ATP and acts in bactericidal manner against *Mycobacterium smegatis*. *Letters in Applied Microbiology, 28*(3), 189-191.

Moodley, S. (2019). The role of heparin binding haemagglutinin adhesin and curli pili on the pathogenicity of *Mycobacterium tuberculosis.* PhD thesis. University of KwaZulu-Natal. Durban.

Morris, D., Khurasany, M., Nguyen, T., Kim, J., Guilford, F., Mehta, R., et al. (2013). Glutathione and infection. *Biochimica et Biophysica Acta (BBA) - Molecular and Cell Biology of Lipids, 1830*(5), 3329-3349.

Naidoo, N., Ramsugit, S. and Pillay, M. (2014). *Mycobacterium tuberculosis* pili (*mtp*), a putative biomarker for a tuberculosis diagnostic test. *Tuberculosis, 94*(3), 338-345.

Naidoo, N., Pillay, B., Bubb, M., Pym, A., Chiliza, T., Naidoo, K.,et al. (2018). Evaluation of a synthetic peptide for the detection of anti-*Mycobacterium tuberculosis* curli pili IgG antibodies in patients with pulmonary tuberculosis. *Tuberculosis (Edinburgh, Scotland), 109*, 80–84.

Naidoo, K., Gengiah, S., Yende-Zuma, N., Padayatchi, N., Barker, P., Nunn, A., et al. (2019). Addressing challenges in scaling up TB and HIV treatment integration in rural primary healthcare clinics in South Africa (SUTHI): a cluster randomized controlled trial protocol (vol 12, 129, 2017). *Implementation Science, 14*.

Passalacqua, K. D., Charbonneau, M.-E. and O'Riordan, M. X. D. (2016). Bacterial metabolism shapes the host-pathogen interface. *Microbiology Spectrum, 4*(3), 15-41.

Pavelka, M. S., Jr. and Jacobs, W. R., Jr. (1996). Biosynthesis of diaminopimelate, the precursor of lysine and a component of peptidoglycan, is an essential function of *Mycobacterium smegmatis*. *Journal of Bacteriology, 178*(22), 6496-6507.

Pavelka, M. S., Jr., Chen, B., Kelley, C. L., Collins, F. M. and Jacobs, W. R., Jr. (2003). Vaccine efficacy of a lysine auxotroph of *Mycobacterium tuberculosis*. *Infection and Immunity, 71*(7), 4190-4192.

Ramsugit, S., Guma, S., Pillay, B., Jain, P., Larsen, M. H., Danaviah, S. and Pillay, M. (2013). Pili contribute to biofilm formation *in vitro* in *Mycobacterium tuberculosis*. *Antonie Van Leeuwenhoek, 104*(5), 725-735.

Ramsugit, S., and Pillay, M. (2014). *Mycobacterium tuberculosis* pili promote adhesion to and invasion of THP-1 macrophages. *Japanese Journal of Infectious Diseases, 67*(6), 476-478.

Ramsugit, S., Pillay, B. and Pillay, M. (2016). Evaluation of the role of *Mycobacterium tuberculosis* pili (MTP) as an adhesin, invasin, and cytokine inducer of epithelial cells. The *Brazilian Journal of Infectious Diseases, 20*(2), 160-165.

Richaud, C., Mengin-Lecreulx, D., Pochet, S., Johnson, E. J., Cohen, G. N. and Marliere, P. (1993). Directed evolution of biosynthetic pathways. Recruitment of cysteine thioethers for

constructing the cell wall of Escherichia coli. *Journal of Biological Chemistry, 268*(36), 26827-26835.

Rizvi, A., Shankar, A., Chatterjee, A., More, T. H., Bose, T., Dutta, A., et al. (2019). Rewiring of metabolic network in *Mycobacterium tuberculosis* during adaptation to different stresses. *Frontiers in Microbiology, 10*, 2417.

Ryndak, M. B., Singh, K. K., Peng, Z. and Laal, S. (2015). Transcriptional profile of *Mycobacterium tuberculosis* replicating in type II alveolar epithelial cells. *PloS One, 10*(4), e0123745-e0123745.

Sambandamurthy, V. K., Wang, X., Chen, B., Russell, R. G., Derrick, S., Collins, F. M., et al. (2002). A pantothenate auxotroph of *Mycobacterium tuberculosis* is highly attenuated and protects mice against tuberculosis. *Nature Medicine Journal, 8*(10), 1171-1174.

Sambandamurthy, V. K., Derrick, S. C., Jalapathy, K. V., Chen, B., Russell, R. G., Morris, S. L., et al. (2005). Long-term protection against tuberculosis following vaccination with a severely attenuated double lysine and pantothenate auxotroph of *Mycobacterium tuberculosis*. *Infection and Immunity, 73*(2), 1196-203.

Sambandamurthy, V. K., Derrick, S. C., Hsu, T., Chen, B., Larsen, M. H., Jalapathy, K. V., et al. (2006). *Mycobacterium tuberculosis* DeltaRD1 DeltapanCD: a safe and limited replicating mutant strain that protects immunocompetent and immunocompromised mice against experimental tuberculosis. *Vaccine, 24*(37–39), 6309-20.

Scapin, G. and Blanchard, J. S. (1998). Enzymology of bacterial lysine biosynthesis. *Advances in Enzymology and Related Areas of Molecular Biology, 72*, 279-324.

Schneeberger, E. and Lynch, R. (1997). Airway and alveolar epithelial cell junctions. The Lung. Scientific Foundations, 2nd ed., *Crystal, R. G., West, J. B., Weibel, E. R., Barnes, P. J*., Eds., Lippincott-Raven, Philadelphia.

Shellie, R., Marriott, P. and Morrison, P. (2001). Concepts and preliminary observations on the triple-dimensional analysis of complex volatile samples by using GC× GC− TOFMS. *Analytical Chemistry, 73*(6), 1336-1344.

Shkurupiy, V. A., Kim, L. B., Nikonova, I. K., Potapova, O. V., Cherdantseva, L. A. and Sharkova, T. V. (2013). Hydroxyproline content and fibrogenesis in mouse liver and lungs during the early stages of BCG granulomatosis. *Bulletin of Experimental Biology and Medicine, 154*(3), 299-302.

Schymanski, E. L., Jeon, J., Gulde, R., Fenner, K., Ruff, M., Singer, H. P. and Hollender, J. (2014). Identifying small molecules via high resolution mass spectrometry: communicating confidence. *Environmental Science and Technology, 48*, 2097-2098.

Sosunov, V., Mischenko, V., Eruslanov, B., Svetoch, E., Shakina, Y., Stern, N., et al. (2007). Antimycobacterial activity of bacteriocins and their complexes with liposomes. *Journal of Antimicrobial Chemotherapy, 59*(5), 919-925.

Strober, W. (2015). Trypan blue exclusion test of cell viability. *Current Protocols in Immunology, 111*(1), A3-B.

Sullivan, G. M. and Feinn, R. (2012). Using effect size—or why the P value is not enough. *Journal of Graduate Medical Education, 4*(3), 279-282.

Unger, L. and DeMoss, R. D. (1966). Action of a proline analogue, l-thiazolidine-4-carboxylic acid, in *Escherichia coli*. *Journal of Bacteriology, 91*(4), 1556-1563.

van den Berg, R. A., Hoefsloot, H. C., Westerhuis, J. A., Smilde, A. K. and van der Werf, M. J. (2006). Centering, scaling, and transformations: improving the biological information content of metabolomics data. *BMC Genomics, 7*(1), 142.

van Kraaij, C., de Vos, W. M., Siezen, R. J. and Kuipers, O. P. (1999). Lantibiotics: biosynthesis, mode of action and applications. *Natural Product Reports, 16*(5), 575-587.

Vasstrand, E., Jensen, H. B. and Miron, T. (1980). Microbore single-column analysis of amino acids and amino sugars specific to bacterial cell wall eptidoglycans. *Analytical Biochemistry, 105*(1), 154-158.

Venos, E. S., Knodel, M. H., Radford, C. L. and Berger, B. J. (2004). Branched-chain amino acid aminotransferase and methionine formation in *Mycobacterium tuberculosis. BMC Microbiology, 4*, 39.

Voet, D., Voet, J. G. and Pratt, C. W. (2016). *Fundamentals of Biochemistry: Life at the Molecular Level*: John Wiley & Sons.

Warburg, O., Wind, F. and Negelein, E. (1927). The metabolism of tumors in the body. *Journal of General Physiology, 8*(6), 519-530.

Warner, D. F. (2014). *Mycobacterium tuberculosis* metabolism. *Cold Spring Harbor Perspectives in Medicine, 5*(4), a021121.

Weber, H. U., Fleming, J. F. and Miquel, J. (1982). Thiazolidine-4-carboxylic acid, a physiologic sulfhydryl antioxidant with potential value in geriatric medicine. *Archives of Gerontology and Geriatrics, 1*(4), 299-310.

White, W. H., Gunyuzlu, P. L. and Toyn, J. H. (2001). *Saccharomyces cerevisiae* is capable of de novo pantothenic acid biosynthesis involving a novel pathway of β-alanine production from spermine. *Journal of Biological Chemistry, 276*(14), 10794-10800.

WHO (2019). Global Tuberculosis Report 2019. https://apps.who.int/iris/bitstream/handle/10665/329368/9789241565714-eng.pdf?ua=1. Accessed 29/10 2019.

Wishart, D. S., Feunang, Y. D., Marcu, A., Guo, A. C., Liang, K., Vazquez-Fresno, R., et al. (2018). HMDB 4.0: the human metabolome database for 2018. *Nucleic Acids Research, 46*(D1), D608-d617.

Zhang, D., Li, J., Wang, F., Hu, J., Wang, S. and Sun, Y. (2014). 2-Deoxy-D-glucose targeting of glucose metabolism in cancer cells as a potential therapy. *Cancer Letters, 355*(2), 176-183.

Zhong, L., Zhou, J., Chen, X. and Yin, Y. (2016). Serum metabolomic study for the detection of candidate biomarkers of tuberculosis. *International Journal of Clinical and Experimental Pathology, 9*(3), 3256-3266.

Chapter 3 investigated the role of MTP in an infection model using A549 epithelial cells infected with *M. tuberculosis* (WT, Δ*mtp* and *mtp*-complemented strains) to determine significant modulations in metabolic pathways. It was found that 46 metabolites were significantly lowered in relative concentration in the Δ*mtp*-infected A549 cells compared to the WT-infected A549 cells. Chapter 4 synthesises the important findings from Chapters 2 and 3. Limitations and future recommendations are also suggested.

CHAPTER 4: SYNTHESIS OF RESEARCH FINDINGS

Tuberculosis, caused by *M. tuberculosis*, continues to affect more than a fourth of the global population (WHO, 2019). The treatment of this curable disease is further complicated by the emergence of drug-resistant strains (MDR-, XDR- and TDR-TB) (Udwadia, 2012) and co-infection with HIV/AIDS (Karim et al., 2009; Naidoo et al., 2019). Despite the availability of efficacious treatment regimens and the Bacille Calmette-Guerin (BCG) vaccine, both children and adults continue to contract TB (Gupta et al., 2018). The search for novel biomarkers becomes imperative in order to develop more effective diagnostic tools, therapeutics and a vaccine to better control this epidemic. Hence, the focus of this study was on *M. tuberculosis* curli pili (MTP), a surface-located adhesin that is involved in the first point of contact with the host, and has shown diagnostic and therapeutic potential based on previous findings (Ramsugit et al., 2013; Naidoo et al., 2014; Ramsugit and Pillay, 2014; Ramsugit et al., 2016; Naidoo et al., 2018). The aim of this study was to further substantiate the biomarker potential of MTP by investigating its role in modulating the metabolome in the bacterium and within a host infection model using A549 pulmonary epithelial cells.

4.1 Review of the biomarker potential of MTP adhesin

Previously, a number of studies have demonstrated that MTP forms an important part of the host-pathogen interaction. Alteri et al. (2007) first discovered that *M. tuberculosis* produces MTP, recognisable by IgG antibodies from active TB patients' sera. The open reading frame designated as Rv3312A in *M. tuberculosis* encodes pilin subunits comprising of glycine and proline residues (Alteri et al., 2007). The MTP harbours properties resembling curli amyloid fibres and it was found that the wild-type *M. tuberculosis* H37Rv was able to bind *in vitro* to an extracellular matrix protein, laminin, suggestive of its adhesive ability (Alteri et al., 2007). Subsequent research on its adhesive properties demonstrated that adhesion and invasion rates of the *mtp*-deficient strain to THP-1 macrophages and A549 pulmonary epithelial cells were markedly reduced by 42.16% and 69.02% (Ramsugit and Pillay, 2014), and 69.39% and 56.20% (Ramsugit et al., 2016), respectively, compared to the *mtp*-proficient WT strain. Complementation restored the *mtp* gene function to WT levels in both of these studies (Ramsugit and Pillay, 2014; Ramsugit et al., 2016). The biofilm producing ability of the Δ*mtp* strain showed a 68.4 % reduction in biofilm mass compared to the WT ($p = 0.002$). Complementation of the *mtp* gene showed a restoration of the WT biofilm phenotype (Ramsugit et al., 2013). The *mtp* gene was further suggested to dampen cytokine/chemokine induction in epithelial cells, as a survival strategy (Ramsugit et al., 2016). Global transcriptomics in epithelial cells, THP-1 cells and mouse model by the same research group (Nyawo, 2016; Dlamini, 2017) produced further evidence of the involvement of MTP in inducing significant host immune response genes, pathways and networks. The *mtp* gene was found to be specific to *M. tuberculosis* complex members, with high degree of conservation in clinical strains of *M. tuberculosis* (Naidoo et al., 2014). Moreover, while *mtp* shared 60% homology with a

sequence of unknown function in *M. marinum*, this non-tuberculous mycobacterial organism does not cause disease in humans, and therefore, does not pose an obstacle to TB diagnostics (Naidoo et al., 2014). A synthetic MTP peptide demonstrated 97% accuracy in detecting anti-MTP IgG antibodies in patients' serum samples, including HIV-uninfected as well as co-infected patients (Naidoo et al., 2018). Collectively, MTP has shown significant potential as a suitable biomarker in the initial infection process through studies involving functional genomics and transcriptomics. The metabolic changes associated with this adhesin have not been previously investigated, hence provided impetus for elucidation in the current study.

4.2 *Mycobacterium tuberculosis* curli pili (MTP) deficiency is associated with alterations in cell wall biogenesis, fatty acid metabolism and amino acid synthesis: Ashokcoomar, S., Reedoy, K. S., Senzani, S., Loots, D. T., Beukes, D., van Reenen, M., Pillay, B. and Pillay, M.

The first investigation, with joint first authorship with S. Ashokcoomar, investigated the role of MTP in modulating the metabolome in an *in vitro* bacterial model. This was a comparative analysis to assess any changes between the WT and Δ*mtp* strains, and to assess restoration of gene function of *mtp*-complemented strain to that of the WT. Hence, this study aimed to determine any metabolic perturbations in Middlebrook 7H9 broth cultures of *mtp*-deficient compared to *mtp*-proficient *M. tuberculosis* strains using a GCxGC-TOFMS approach.

The results from this investigation were significant as 27 metabolites were found to be altered in relative concentration between the *mtp*-deficient cells and the WT, while seven metabolites were deemed significantly different between the WT and *mtp*-complemented strains. Briefly, a total of four metabolic categories were affected. Three of the four categories were produced in relatively higher concentrations by Δ*mtp*, indicating an overall reduced ability in the utilisation of these metabolites for natural cellular processes in this strain compared to the WT. These included carbohydrates in cell wall biogenesis, metabolites in fatty acid metabolism and peptidoglycan synthesis. Amino acid and protein synthesis, the fourth category, was produced in lower relative concentration in Δ*mtp*, again suggesting defective pathways in this strain compared to the WT. In addition, the RT-qPCR transcriptomics data supported the metabolomics data which revealed a similar pattern, where the Δ*mtp* strain produced various metabolites, related to the respective pathways associated with *glf, glmU, fadD32* and *glpK*, in increased concentrations compared to the WT strain. The gene *fadE5* was found to be non-significant, indicating a more preferential route of lipid breakdown by *fadD32*. This, however, requires further confirmatory investigation.

Overall, Δ*mtp* was found to be associated with an altered cell wall composition due to the decreased utilisation of carbohydrates in cell wall biogenesis. It was also observed that there was a reduced efficiency in the breakdown of fatty acids, a decrease in amino acid biosynthesis, and a reduction in peptidoglycan synthesis. In the current bacterial model, the effect of the MTP deletion significantly affected various metabolic pathways specific to *M. tuberculosis* and its metabolism. This highlights the role of MTP in *M. tuberculosis* metabolism and TB pathogenesis, which further validates its biomarker potential in TB diagnostics, and vaccine and drug development.

4.3 *Mycobacterium tuberculosis* curli pili (MTP) is associated with significant host metabolic pathways in an A549 epithelial cell infection model and contributes to the pathogenicity of *M. tuberculosis*: Reedoy, K. S., Loots, D. T., Beukes, D., van Reenen. M., Pillay, B. and Pillay, M.

The significant metabolic changes demonstrated in the bacterial model in the first investigation warranted further exploration to determine whether the absence of MTP would result in any significant metabolomics changes during *in vitro* host infection. The aim of the second investigation was to elucidate any metabolic changes that may arise from the infection of A549 pulmonary epithelial cells with *M. tuberculosis* using a GCxGC-TOFMS approach.

The study investigated five different infection models, of which only one validated as explained hereafter. The first three models were the infected vs. uninfected models of comparison to determine whether there were any significant differences observed in the *M. tuberculosis*-infected A549 cell model compared to the respective uninfected model to identify any metabolomic changes associated with the infecting strain. Very slight differences were observed for the WT-infected and WT-uninfected A549 cells, Δ*mtp*-infected and Δ*mtp*-uninfected A549 cells, and the *mtp*-complement-infected and *mtp*-complement-uninfected A549 cells, suggesting undisturbed metabolomes for these infection models. There were also slight differences between the WT-infected and *mtp*-complement-infected strain showing functional restoration of *mtp*. Significant differences were observed in the metabolomics profile between the WT-infected vs. Δ*mtp*-infected A549 cells. A total of 46 metabolites were produced in significantly lower relative concentrations in the latter.

In summary, the deletion of the MTP adhesin led to a perturbation in nucleic acid metabolism, found to be less efficient in the Δ*mtp*-infected cells compared to the WT-infected cells. A number of amino acid pathways were affected. Lysine metabolism and degradation were less efficient in the Δ*mtp*-infected cells. Interestingly, the metabolites associated with lysine metabolism are specific to the bacterium hence, metabolites of this pathway can be targeted for TB therapeutics or diagnostics. Nitrogen assimilation was also found to be less prominent in Δ*mtp*-infected cells arising from aspartate, alanine

and glutamate metabolism. Metabolites involved in glutathione metabolism, oxidative stress and lipid metabolism were produced in lower relative concentration in Δ*mtp*-infected cells, potentially resulting in a compromised mycobacterial cell envelope in the deletion mutant. These metabolic alterations are indicative of lowered pathogenicity of *M. tuberculosis*, as a result of the absence of MTP. Lanthionine was an unusual metabolite detected in the present study which raises questions with regards to its association to lantibiotics and its possible association with *M. tuberculosis*. It is unknown at this stage whether it is of bacterial or host origin.

The current study revealed that the deletion of MTP does have a deleterious effect on important metabolic pathways and thus, affects the infection process. Therefore, it can be deduced that the absence of MTP results in attenuated virulence, highlighting the importance of this adhesin in regulating the metabolome of infected A549 pulmonary epithelial cells, and further validating its biomarker potential.

4.4 Comparison of bacterial model and host-infected model reveals minor similarity in amino acid metabolism, peptidoglycan synthesis and lipid metabolism.

A total of six metabolites was found to be identical when the metabolomes of the bacterial and the host infection models were compared. These metabolites were 2-aminoadipic acid, N-acetylaspartic acid, L-aspartic acid, cadaverine, 3-hydroxyisovaleric acid and myo-inositol, and were detected in relatively higher concentrations in the infection model compared to the bacterial model. This may be due to the possibility that these metabolites were produced by the host in addition to the pathogen, or that they could be produced in relatively higher concentrations by the bacterium alone during infection. Between the two studies, the similarly affected metabolite pathways were amino acid metabolism, peptidoglycan synthesis and lipid metabolism. It must be noted that there could be more metabolites that are identical in both models investigated, but only those that were deemed significant were identified in this study. It is difficult to differentiate between the metabolites that were solely produced by *M. tuberculosis* and those that were host-derived in response to infection.

4.5 Limitations of the study

A limitation of this study is that the use of only a single *M. tuberculosis* strain makes it difficult to extrapolate the findings to all clinical strains and infection models. However, since metabolomics analyses in general are expensive, labour intensive, and time consuming, the testing of multiple, virulent clinical *M. tuberculosis* strains is challenging, and was not within the scope of this Masters study. While *in vitro* conditions may not accurately represent the metabolites detected during human pulmonary infection, they may provide an indication of the changes in metabolic pathways that may result. In addition, the study design did not permit accurate identification of metabolites of host or pathogen origin. Other factors that may affect metabolomic data such as concentration include sample

preparation, time taken to process samples and instrumentation limitations such as reproducibility, detection limit and accuracy. In the current study, these limitations were overcome by treating every sample and control in the same way, by subjecting each sample to identical experimental conditions using rapid and accurate techniques to minimise variation, and by making use of quality controls and internal standards to ensure reproducibility and excellent quality reads. Another potential limitation stems from bioinformatics analyses as a range of approaches can be taken to analyse a given set of data as well as the limits of selection criteria. This limitation was mitigated by streamlining the selection of analyses for the current study according to the study design, aim and objectives of this investigation in order to produce the most ideal set of data necessary to answer the research question. Another difficulty that was beyond the control of the current study was the lack of annotated *M. tuberculosis* pathways and metabolites that are identifiable with this bacterium which may hinder associations made from the results obtained in an investigation. Nevertheless, studies like these can provide compelling metabolomics evidence to support hypotheses to help grow and understand the already existing reservoir of genomics, transcriptomics and proteomics data, especially, the host-pathogen interactions at the cellular level. Furthermore, a broader understanding of the metabolic perturbations associated with an altered phenotype can be achieved which can further explain mechanisms of pathogenesis in *M. tuberculosis.*

4.6 Recommendations for future research

The findings of this global metabolomics study serve as a platform for further validation studies in order to better understand the specific perturbations. *Mycobacterium tuberculosis* has numerous adhesins on its cell surface, hence, the effect of those using functional metabolomics would prove invaluable in understanding their role in TB pathogenesis. Future work should include phenotypic assays to investigate the various metabolic pathways that were perturbed, e.g. cell wall biogenesis and peptidoglycan synthesis using transmission electron microscopy in order to elucidate possible cell envelope anomalies. To overcome the limitation of discriminating between host- and pathogen-derived metabolites, ^{13}C-labelling of *M. tuberculosis* cells can be used with a mass spectrometric platform to track the metabolic interactions of the pathogen during host infection (Beste et al., 2013). Since MTA was present in 100x higher relative concentration in the WT than mutant, MTA can be further investigated to determine which gene is significantly downregulated in the absence of the *mtp* gene. Since MTA is detectable in urine, studies to elucidate whether the non-invasive detection of this metabolite would be significant for TB diagnosis. The detected metabolites of the lysine metabolism and degradation pathway warrant further investigation as targets for TB therapeutics or diagnostics since these metabolites are pathogen-specific. Nitrogen assimilation can be tested by growing the Δ*mtp*-infected cells in minimal media containing a sole nitrogen source (such as urea, glutamine, glutamate or aspartic acid) to determine whether there would be any growth defects compared to the WT-infected cells (Gouzy et al., 2013). Using a similar study design, Δ*mtp*-infected cells can be grown in media

where butanoic acid serves as a sole carbon source to assess growth compared to WT-infected cells since there were no detectable levels of butanoic acid in the mutant strain. Lastly, because lanthionine has been reported to be associated with elevated levels of L-cysteine (Richaud et al., 1993; Consaul et al., 2005), the association between the high levels of cystine and cysteine (FC of 77 and 6, respectively) higher in the WT than mutant in the present study, should be further investigated.

4.7 Conclusion

The findings of this study confirm previous reports that MTP has promise as a crucial bacterial adhesin and a biomarker that can be targeted for intervention. The first investigation revealed a total of 27 metabolites to be biologically significant between the Δ*mtp* mutant and the WT strains. These were associated with reduced cell wall biogenesis, fatty acid metabolism, amino acid and protein synthesis, and peptidoglycan synthesis. Between the WT and *mtp*-complemented strains, seven metabolites were biologically significant and corresponded with various cell envelope functions. In the second investigation, all 46 metabolites were produced in a lower relative concentration by the Δ*mtp*-infected cells compared to the WT-infected cells and were associated with a decrease in nucleic acid synthesis, amino acid metabolism, glutathione metabolism, oxidative stress, lipid metabolism and a peptidoglycan anomaly. Not only does the absence of this gene bring about bacterial metabolic changes but it also has an effect on the host metabolome of an A549 epithelial cell infection model. *Mycobacterium tuberculosis* metabolism is important during the infection process, and this study has provided further insight to better understand the changes that may occur on a metabolomic level due to the knockout of the *mtp* gene, further substantiating the biomarker potential of MTP in the fight against TB.

4.8 References

Alteri, C. J., Xicohténcatl-Cortes, J., Hess, S., Caballero-Olín, G., Girón, J. A. and Friedman, R. L. (2007). *Mycobacterium tuberculosis* produces pili during human infection. *Proceedings of the National Academy of Sciences, 104*(12), 5145-5150.

Beste, D. J., Nöh, K., Niedenführ, S., Mendum, T. A., Hawkins, N. D., Ward, J. L., et al. (2013). 13C-flux spectral analysis of host-pathogen metabolism reveals a mixed diet for intracellular *Mycobacterium tuberculosis*. *Chemistry and Biology, 20*(8), 1012-1021.

Consaul, S. A., Wright, L. F., Mahapatra, S., Crick, D. C. and Pavelka, M. S. (2005). An unusual mutation results in the replacement of diaminopimelate with lanthionine in the peptidoglycan of a mutant strain of *Mycobacterium smegmatis. Journal of Bacteriology, 187*(5), 1612-1620.

Dlamini, M. T. (2017). Whole transcriptome analysis to elucidate the role of MTP in gene regulation of pulmonary epithelial cells infected with *Mycobacterium tuberculosis.* Masters thesis. University of KwaZulu-Natal. Durban.

Gouzy, A., Larrouy-Maumus, G., Wu, T. D., Peixoto, A., Levillain, F., Lugo-Villarino, G., et al. (2013). *Mycobacterium tuberculosis* nitrogen assimilation and host colonization require aspartate. *Nature Chemical and Biology, 9*(11), 674-676.

Gupta, N., Garg, S., Vedi, S., Kunimoto, D. Y., Kumar, R. and Agrawal, B. (2018). Future path toward TB vaccine development: boosting BCG or re-educating by a new subunit vaccine. *Frontiers in Immunology, 9*, 2371.

Karim, S. S. A., Churchyard, G. J., Karim, Q. A. and Lawn, S. D. (2009). HIV infection and tuberculosis in South Africa: an urgent need to escalate the public health response. *The Lancet, 374*(9693), 921-933.

Naidoo, K., Gengiah, S., Yende-Zuma, N., Padayatchi, N., Barker, P., Nunn, A., et al. (2019). Addressing challenges in scaling up TB and HIV treatment integration in rural primary healthcare clinics in South Africa (SUTHI): a cluster randomized controlled trial protocol (vol 12, 129, 2017). *Implementation Science, 14*.

Naidoo, N., Ramsugit, S. and Pillay, M. (2014). *Mycobacterium tuberculosis* pili (MTP), a putative biomarker for a tuberculosis diagnostic test. *Tuberculosis, 94*(3), 338-345.

Naidoo, N., Pillay, B., Bubb, M., Pym, A., Chiliza, T., Naidoo, K., et al. (2018). Evaluation of a synthetic peptide for the detection of anti-*Mycobacterium tuberculosis* curli pili IgG antibodies in patients with pulmonary tuberculosis. *Tuberculosis, 109*, 80-84.

Naidoo, K., Gengiah, S., Yende-Zuma, N., Padayatchi, N., Barker, P., Nunn, A., et al. (2019). Addressing challenges in scaling up TB and HIV treatment integration in rural primary healthcare clinics in South Africa (SUTHI): a cluster randomized controlled trial protocol (vol 12, 129, 2017). *Implementation Science, 14*.

Nyawo, G. (2016). The role of *Mycobacterium tuberculosis* pili in pathogenesis: growth and survival kinetics, gene regulation and host immune response, and in vitro growth kinetics. Masters thesis. University of KwaZulu-Natal. Durban.

Ramsugit, S., Guma, S., Pillay, B., Jain, P., Larsen, M. H., Danaviah, S., and Pillay, M. (2013). Pili contribute to biofilm formation in vitro in *Mycobacterium tuberculosis*. *Antonie Van Leeuwenhoek, 104*(5), 725-735.

Ramsugit, S. and Pillay, M. (2014). *Mycobacterium tuberculosis* pili promote adhesion to and invasion of THP-1 macrophages. *Japanese Journal of Infectious Diseases, 67*(6), 476-478.

Ramsugit, S., Pillay, B. and Pillay, M. (2016). Evaluation of the role of *Mycobacterium tuberculosis* pili (MTP) as an adhesin, invasin, and cytokine inducer of epithelial cells. *Brazilian Journal of Infectious Diseases, 20*(2), 160-165.

Richaud, C., Mengin-Lecreulx, D., Pochet, S., Johnson, E. J., Cohen, G. N. and Marliere, P. (1993). Directed evolution of biosynthetic pathways. Recruitment of cysteine thioethers for constructing the cell wall of *Escherichia coli*. *Journal of Biological Chemistry, 268*(36), 26827-26835.

Udwadia, Z. F. (2012). MDR, XDR, TDR tuberculosis: ominous progression. *Thorax, 67*, 286-288.

World Health Organization (2019). WHO 2018 Global Statistics Report. http://www.who.int/tb/publications/global_report/en/. Accessed 30/11/2019.

CHAPTER 5:APPENDICES

Appendix A: BREC Approval

UNIVERSITY OF
KWAZULU-NATAL
INYUVESI
YAKWAZULU-NATALI
RESEARCH OFFICE
Biomedical Research Ethics Administration
Westville Campus, Govan Mbeki Building
Private Bag X 54001
Durban
4000
KwaZulu-Natal, SOUTH AFRICA
Tel: 27 31 2604769 - Fax: 27 31 2604609
Email: BREC@ukzn.ac.za
Website http://research.ukzn.ac.za/Research-Ethics/Biomedical-Research-Ethics.aspx

07 February 2020

Ms KS Reedoy (213505224)
Medical Microbiology and Infection control
1st Floor DDMRI Building
NRMSM
213505224@stu.ukzn.ac.za

Dear Ms Reedoy

Title: Metabolomic profiling to elucidate the in vitro of Mycobacterium tuberculosis HBHA and MTP in an epithelial cell model of infection.
Degree: MMedSc
BREC Ref No: BE255/17
New Title: M. Tuberculosis pili (MTP) modulates pathogen and host metabolomic changes in an A549 epithelial cell model of infection

We wish to advise you that your correspondence received on 09 January 2020 submitting and application for Amendments to change the title to the above and other amendments for the above study has been **noted and approved** by a sub-committee of the Biomedical Research Ethics Committee.

The committee will be notified of the above approval at its next meeting to be held on 10 March 2020.

Yours sincerely

Professor V Rambiritch
Chair: Biomedical Research Ethics Committee

cc supervisor: taylor@ukzn.ac.za cc postgraduate administrator: arumig amdg.ukzn.ac.za

Appendix B: Media, solutions and reagents

1. Middlebrook 7H9 broth (1 L)

   4.7 g Middlebrook 7H9 powder (Difco, Becton-Dickinson, Franklin Lakes, NJ, USA)
   900 mL distilled water
   10 mL 50% (w/v) glycerol (Sigma-Aldrich, St. Louis, MO, USA)
   100 mL OADC (Becton-Dickinson, Franklin Lakes, NJ, USA)
   2.5 mL 20% Tween-80 (Sigma-Aldrich, St. Louis, MO, USA)
   Middlebrook 7H9 powder was dissolved in distilled water and autoclaved at 121°C for 15 min. Glycerol, OADC and Tween-80 were added aseptically after cooling at 56°C in a water bath. Media was mixed well and stored at 4°C.

2. Middlebrook 7H11 agar (1 L)

   21 g Middlebrook 7H11 powder (Difco, Becton-Dickinson, Franklin Lakes, NJ, USA)
   900 mL distilled water
   5 mL 100% glycerol (Sigma-Aldrich, St. Louis, MO, USA)
   100 mL OADC (Becton-Dickinson, Franklin Lakes, NJ, USA)
   Middlebrook 7H11 powder was dissolved in distilled water and autoclaved at 121°C for 15 min. Glycerol and OADC were added aseptically after cooling at 56°C in a water bath. A volume of 10 mL was aliquotted into sterile 65 mm petri dishes.

3. Phosphate buffered saline (PBS); pH 7.4

   5 PBS tablets (Sigma-Aldrich, St. Louis, MO, USA)
   1000 mL distilled water
   PBS tablets were dissolved in distilled water. The solution was autoclaved at 121°C for 15 min, and thereafter decanted into 50 mL aliquots and stored at4 °C.

4. Diethylpyrocarbonate (DEPC)

   1 mL 0.1 % DEPC (Sigma-Aldrich, St. Louis, MO, USA)
   1 L distilled water
   DEPC was added to the distilled water, mixed well and left at room temperature overnight. Thereafter, the water was autoclaved at 121°C for 15 min and allowed to cool prior to use.

5. 0.5 M EDTA

   9.305 g EDTA (Sigma-Aldrich, St. Louis, MO, USA)
   40 mL DEPC water

EDTA was dissolved in DEPC water (prepared from Point 4 above) and brought to 50 mL volume with DEPC water. Thereafter, the solution was autoclaved 121°C for 15 min and allowed to cool prior to use.

6. 37% Formaldehyde

   1.85 g paraformaldehyde (Sigma-Aldrich, St. Louis, MO, USA)

   3.5 mL H2O (Sigma-Aldrich, St. Louis, MO, USA)

   90 µL 1 N NaOH (Sigma-Aldrich, St. Louis, MO, USA)

   Water was added to paraformaldehyde and heated in a boiling water bath. NaOH was added and the mixture was agitated for ~1 min. Thereafter, it was cooled and sterilized by filtration through a 0.22 µM membrane

7. 10 X MOPs Buffer (1 L)

   41.9 g MOPS (Sigma-Aldrich, St. Louis, MO, USA)

   8.2 g Sodium acetate. $3H_20$ (Sigma-Aldrich, St. Louis, MO, USA)

   3.72 g EDTA (Sigma-Aldrich, St. Louis, MO, USA)

   DEPC-treated water

   The MOPS, sodium acetate and EDTA were dissolved in 800 mL DEPC-treated water, and the volume made up to 1 L with DEPC-treated water. Thereafter, the solution was autoclaved for 121°C for 15 min and aliquoted in 200 mL amounts.

8. MOPS gel

   2 g agarose (SeaKem, Lonza, Basel, Switzerland)

   144 mL DEPC-treated water

   20 mL 10X MOPS buffer

   36 mL 37% Formaldehyde (Sigma-Aldrich, St. Louis, MO, USA)

   DEPC-treated water was added to the agarose and gently swirled to mix. The mixture was heated in a microwave until dissolved, and cooled to 60°C, after which the 10X MOPS buffer was added. Thereafter, formaldehyde was added to this mixture in a fume hood. The gel was poured into a casting tray, avoiding air bubbles, and allowed to set for 30 min.

9. 0.01 % Triton X-100

   100 µL Triton X-100 (Millipore, Merck, Dermstadt, Germany)

   9.999 mL dH_2O

   Triton X-100 was diluted into dH_2O to make up 0.01% working solutions. Working solutions were filtered through a 0.22 µM membrane and stored at 4°C until used.

Appendix C: Chapter 2 Supplementary Material

C1. PCR confirmation of bacterial strains

InstaGene Matrix (Bio-Rad, Hercules, CA, USA) was used to perform total DNA extraction for all strains. This method was selected based on standardizing the DNA extraction for the inclusion of both genomic and plasmid DNA given how the mutant and complemented strains were constructed. Therefore, crude DNA from each strain was used to perform conventional PCR reactions using the specific primers and their respective annealing temperatures reported in Table C1. The expected PCR product of 300 bp and 731 bp was observed in Figure 1a and b, respectively. This indicated the presence of the Hygromycin resistance (hyg^R) cassette and allelic exchange substrate (AES) in both Δ*mtp* (lane 4) and *mtp*-complement samples (lane 5), respectively. The wild-type (lane 2) in Figure 1a and b shows no banding which was expected it lacks the hyg^R cassette and AES, respectively. The expected PCR product of 436 bp was seen in Figure C1c for the wild-type (lane 2) and *mtp*-complement (lane 5) samples indicative of the presence of the *mtp* gene which is absent in the Δ*mtp* (lane 4). All negative controls (Figure C1a, b and c; lane 5) were clear of any contaminants.

Table C1. PCR target and primer sequences used for confirmation of three strains (Ramsugit et al., 2013)

PCR target	Primers	Annealing temperature (°C)
Region of hyg^R cassette	Hyg-F: 5'-ACC CCC CAT TCC GAG GTC TT-3' Hyg-R: 5'-CCG GAA GGC GTT GAG ATG CA-3'	55
Upstream allelic exchange substrate (AES)	Mtp-LL: 5'- TTTTTTTTGCATAAATTGCTCACGATTCATGCCGGTGAG-3' Universal uptag 5'GATGTCTCACTGAGGTCTCTs3'	50
mtp gene	Mtp-261F: 5'-TTTTTAAGATCTCATGTACCGGTTCGCGTG-3' Mtp-261R: 5'-TTTTTTAAGCTTGGCACGGGAGCGTAAATCTG-3'	60

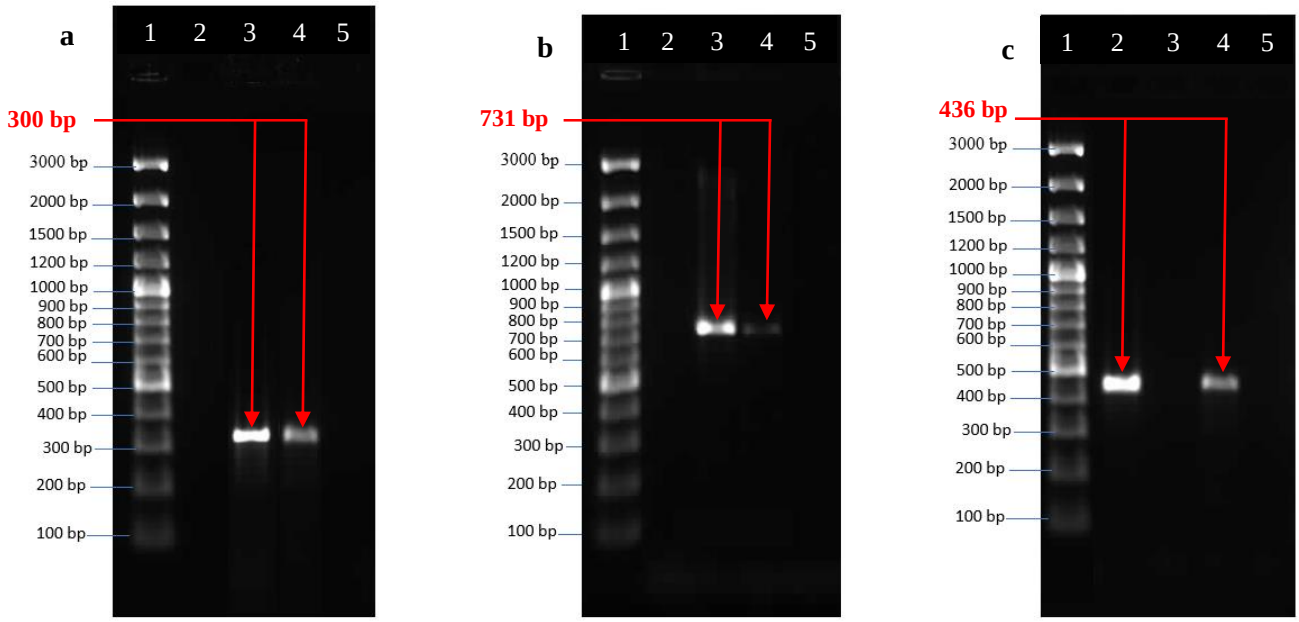

Figure C1. Gel electrophoresis images of PCR products confirming bacterial strains run at 70V for 3 hours on a 1.5% agarose gel using 100 bp (New England BioLabs, MA, USA) marker. (a) PCR targeting a region of hygromycin resistance (hyg^R) cassette, (b) PCR targeting upstream allelic exchange substrate (AES) and (c) PCR targeting the *mtp* gene. (Lane 1) Molecular weight marker, (Lane 2) wild-type (V9124), (Lane 3) ∆*mtp*, (Lane 4) *mtp*-complement, (Lane 5) negative control. Expected band sizes: (a) 300 bp, (b) 731 bp, (c) 436 bp.

C2. Bacterial CFU counts and significance values

Broth cultures were revived and grown to an OD_{600nm} of 1 and plated to confirm that the *M. tuberculosis* cultures at this optical density were equivalent to approximately 1 X 10^8 CFU/mL (Larsen et al., 2007). The cultures were 10-fold serially diluted to determine CFU/mL for each strain (Table C2.1). Dilutions were prepared in Eppendorf tubes (Merck) by adding 100 µL of OD_{600nm} 1 bacterial suspensions to 900 µL of 7H9 broth. A volume of 100 µL was plated onto 7H11 agar plates. Plates were sealed in CO_2 permeable plastic bags and incubated at 37 °C for 3 weeks and colonies counted thereafter. GraphPad Prism version 8 software (GraphPad Software, La Jolla, CA, USA) was used to assess the significance levels between combinations of the three strains using non-parametric, unpaired Mann Whitney testing. All the *p*-values were above 0.05 hence the differences between the CFU/mL values were non-significant (Table C2.2). This confirms that any observations detected in the experimental results will be attributed to the deletion of *mtp* and not from any other variation in experimental conditions. Hence, OD_{600nm} of 1 cultures of each strain from the same stocks were used for experimental samples and pellet collection using two levels of standardisation; initial inoculum standardisation and subsequent OD_{600nm} standardisation using a range of 0.95 – 1.10. From the metabolomics data obtained, excellent separation

was observed between the strains, indicating that the resulting variation was due to group structure differences, i.e. metabolome differences, thereby validating the standardisation techniques used in this study.

Table C2.1. Colony forming units (CFUs) for each strain done in triplicate

Strain	Dilution	Colonies			CFU/mL
		Plate 1	Plate 2	Plate 3	
WT	neat	Lawn	Lawn	Lawn	-
	10^{-1}	Lawn	Lawn	Lawn	-
	10^{-2}	Lawn	Lawn	Lawn	-
	10^{-3}	TMTC	TMTC	TMTC	-
	10^{-4}	>200	>200	>200	-
	10^{-5}	151	118	156	1.41×10^{8}
Δ*mtp*	neat	Lawn	Lawn	Lawn	-
	10^{-1}	Lawn	Lawn	Lawn	-
	10-^{2}	Lawn	Lawn	Lawn	-
	10^{-3}	TMTC	TMTC	TMTC	-
	10^{-4}	>200	>200	>200	-
	10^{-5}	85	94	121	1.00×10^{8}
mtp-complement	neat	Lawn	Lawn	Lawn	-
	10^{-1}	Lawn	Lawn	Lawn	-
	10^{-2}	Lawn	Lawn	Lawn	-
	10^{-3}	TMTC	TMTC	TMTC	-
	10^{-4}	>200	>200	>200	-
	10^{-5}	82	137	122	1.14×10^{8}

TMTC = Too much to count

Table C2.2 Significance testing between the three *M. tuberculosis* strains

Strain comparison	*p*-value	Significance
WT and Δ*mtp*	0.200	None
Δ*mtp* and *mtp*-complement	0.700	None
WT and *mtp*-complement	0.400	None

C3. Bacterial inoculum standardization

Each bacterial strain was revived and grown to an OD_{600nm} (Lightwave II, Biochrom, Cambridge, UK) of approximately 1 (Table C3.1). These cultures were used to calculate and prepare the standardized bacterial inoculum for each strain (Table C3.1). Twelve flasks (Nest Biotechnology, Jiangsu, China) per strain were standardized to $OD600_{nm}$ (Lightwave II, Biochrom, Cambridge, UK) of 0.015 in a total volume of 40 mL. After standardized flasks were incubated, final $OD600_{nm}$ readings were reported in Table C3.2. Only ten cultures of each strain were sent for metabolite extraction, selected by the most suitable $OD600_{nm}$ readings (between the range 0.95 - 1.10) and pellet sizes (Table C3.2).

Bacterial standardization protocol:

1. The three strains of *M. tuberculosis* stocks were revived and grown for 7 - 8 days at 37 °C with shaking (I-26 Shaking Incubator, New Brunswick Scientific, Canada) at 100 rpm to reach OD_{600nm} of ~1.
2. The OD_{600nm} of each culture was measured (Lightwave II, Biochrom, Cambridge, UK) and used to calculate the OD units based on the amount of media present as follows:

(OD) X (Amount of Media (9 mL in this case)) X (dilution factor) = (Total OD Units)

3. Cultures were centrifuged (Mikro 200R, Hettich Zentrifugen, Tuttlingen, Germany) at 1792 x *g* for 10 min and the supernatant was discarded.
4. Pellets were resuspended in 8 mL of PBS (Sigma-Aldrich, St. Louis, MO, USA) containing 0.05 % Tween-80 (Sigma-Aldrich, St. Louis, MO, USA).
5. Pellets were mixed well and centrifuged (Mikro 200R, Hettich Zentrifugen, Tuttlingen, Germany) at 1792 x *g* for 10 min.
6. Supernatant was discarded and washing step was repeated.
7. Pellets were re-suspend in 1 mL of 7H9 (Difco, Becton-Dickinson, Franklin Lakes, NJ, USA) broth (supplemented with10 % OADC, 0.5 % glycerol and 0.05 % Tween-80).
8. Cultures were vortexed to achieve homogenous suspensions.
9. Cultures were back diluted to an OD_{600nm} of 0.015 (standardisation). For back dilutions, the following calculations were used:

(Total OD Units of Sample) (x) = (0.015) (Final Volume of Media (40 mL in this case))
x = the initial volume (mL) used to get an OD of 0.015 in the 9 mL
Multiply x by 1000 to get uL
Therefore, add x to (40 mL – x)

10. A total of 12 flasks were inoculated for each strain.
11. Flasks were incubated with shaking (I-26 Shaking Incubator, New Brunswick Scientific, Canada) (100 rpm) at 37 ºC until an OD_{600nm} ~ 1 was reached.
12. Thereafter, cultures were ready for metabolomic pellet collection and RNA extraction.

Table C3.1 Initial OD_{600nm} readings of bacterial cultures and calculations for bacterial standardization procedure

		Replicates									
		1	**2**	**3**	**4**	**5**	**6**	**7**	**8**	**9**	**10**
Wild-type	**$OD600_{nm}$**	1.10	1.10	1.07	1.01	1.07	1.06	1.06	0.98	1.03	1.10
	Weight (mg)	46.9	39.0	35.8	47.7	44.3	43.4	50.2	50.2	45.0	55.6
Δ*mtp*	**$OD600_{nm}$**	0.97	1.03	1.10	1.10	1.08	1.08	1.09	1.05	1.07	1.08
	Weight (mg)	43.5	42.5	43.9	41.3	41.6	42.6	40.6	44.6	43.8	43.6
***mtp*-complement**	**$OD600_{nm}$**	1.10	1.06	1.09	0.98	1.09	1.06	1.03	0.97	1.08	1.02
	Weight (mg)	55.2	40.4	44.0	38.9	47.1	44.6	56.6	53.1	42.3	38.4

Table C3.2. Final $OD600_{nm}$ readings and respective pellet weights for the 10 selected samples of each strain

Strain	Initial OD_{600nm}	OD units	Calculation to determine volume required to achieve OD_{600nm} 0.015	Volume required (µL)
Wild-type	1.430	12.870	$\frac{(0.015)(40)}{(12.870)} \times 1000$	46.62
Δ*mtp*	1.177	10.593	$\frac{(0.015)(40)}{(10.593)} \times 1000$	56.60
***mtp*-complement**	0.943	8.478	$\frac{(0.015)(40)}{(8.478)} \times 1000$	70.77

C4. RNA extraction data

RNA extraction (Larsen et al., 2007) was performed on all three strains from the same broth cultures used for pellet collection. The only modification to this protocol was the inclusion of an additional 70 % ethanol (Sigma-Aldrich, St. Louis, MO, USA) wash step. Concentration values and purity ratios are depicted in Tables C4.1 – 4.3. Highlighted in grey are the samples that were chosen for subsequent RT-qPCR analysis based on yield and purity. This was confirmed by running all the samples on a MOPS gel, further confirming the best samples (Figures C4.1 and 4.2).

Table C4.1 RNA concentrations and purity ratios obtained for WT after extraction

Sample (WT)	Concentration (ng/µL)	260/280	260/230
1	288.0	1.94	2.26
2	300.5	1.92	2.13
3	250.0	1.91	2.10
4	484.4	1.89	2.20
5	238.0	1.88	2.16
6	329.7	1.90	2.28
7	635.8	1.99	2.26
8	656.3	1.99	2.19
9	469.3	1.92	2.20
10	267.3	1.92	2.29

Table C4.2 RNA concentrations and purity ratios obtained for Δ*mtp* after extraction

Sample (Δ*mtp*)	Concentration (ng/µL)	260/280	260/230
11	208.6	1.88	2.19
12	209.9	1.96	2.06
13	197.0	1.89	2.14
14	287.9	2.02	2.11
15	298.3	2.01	2.12
16	239.1	1.89	2.26
17	318.3	1.92	2.01
18	414.9	1.93	2.01
19	348.7	1.93	2.12
20	561.5	1.96	2.00

Table C4.3 RNA concentrations and purity ratios obtained for *mtp*-complement after extraction

Sample (*mtp*-complement)	Concentration (ng/µL)	260/280	260/230
21	34.3	1.86	0.85
22	55.5	1.87	1.19
23	86.5	1.84	1.45
24	88.6	1.88	1.48
25	48.5	1.84	1.27
26	43.5	1.89	1.35
27	539.4	2.02	2.22
28	688.4	1.98	2.24
29	617.7	1.97	2.20
30	688.5	1.99	2.14

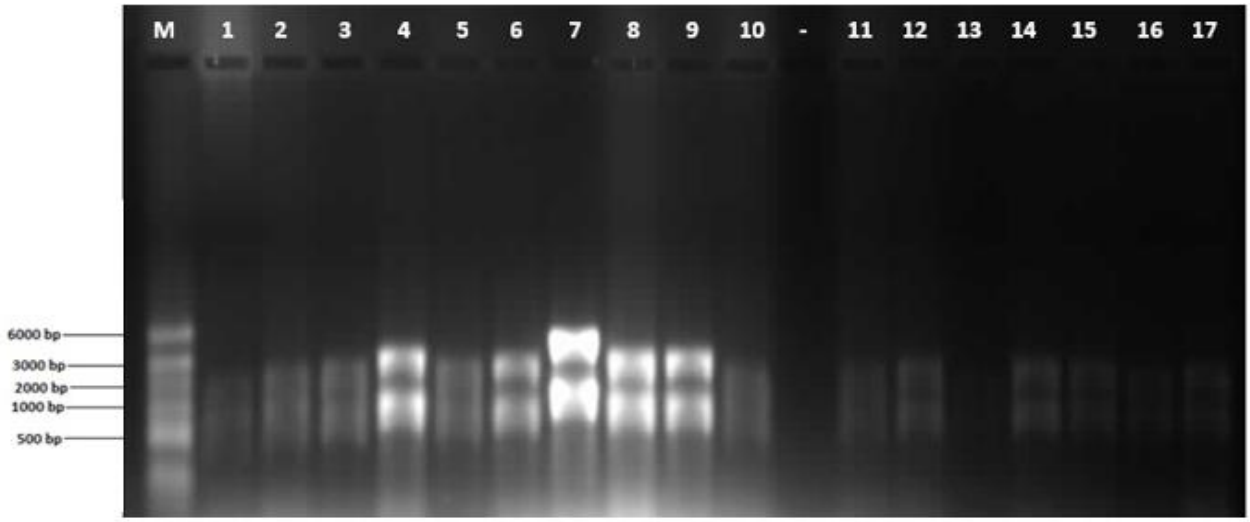

Figure C4.1. MOPS gel image of RNA extracted from *M. tuberculosis* WT and Δ*mtp* strains run at 70V for 3 hours on a 1.5% agarose gel. (M) represents the molecular weight marker. Lanes 1 – 10 correspond to the WT samples from Table C4.1 where samples 4, 6, 7, 8 and 9 have the best banding patterns. Lanes 11 – 17 correspond to the Δ*mtp* samples from Table C4.2 showing feint banding.

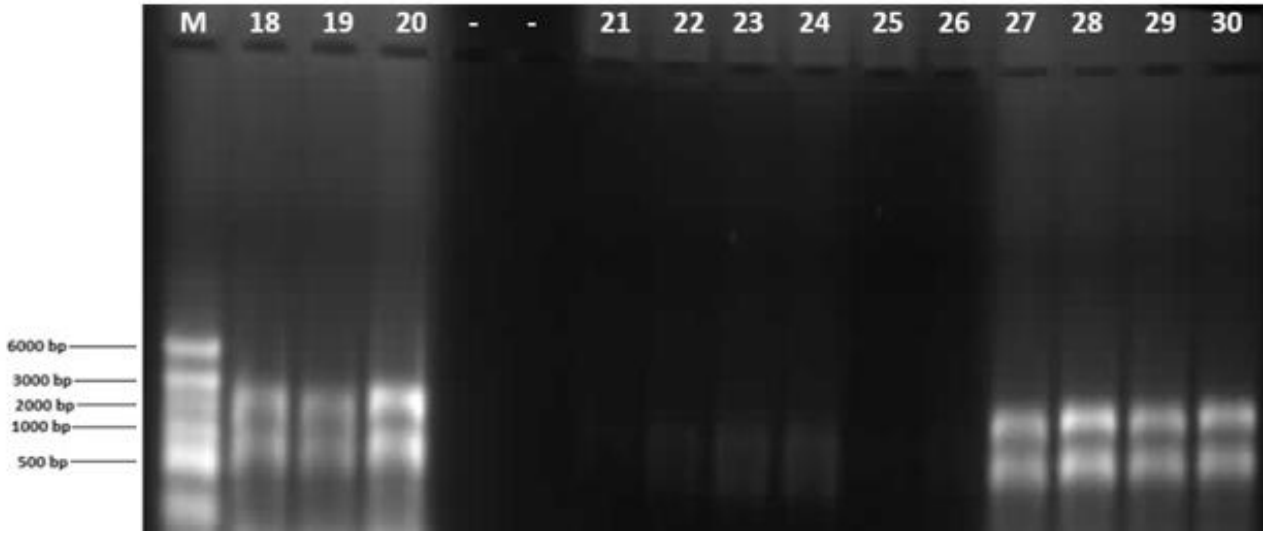

Figure C4.2. MOPS gel image of RNA extracted from *M. tuberculosis* Δ*mtp* and *mtp*-complemented strains run at 70V for 3 hours on a 1.5% agarose gel. (M) represents the molecular weight marker. Lanes 18 – 20 correspond to the remaining Δ*mtp* samples from Table C4.2 where all 4 samples showed the best banding patterns. Lanes 21 – 30 correspond to the *mtp*-complement samples with feint banding in Lanes 21 – 26 while the best banding was depicted in Lanes 27 – 30.

C5. RT-qPCR raw data

Primer efficiency calculations and dilutions

WT genomic DNA (507.5 ng/µL) previously extracted for the PCR confirmation of the strains was used to test primer efficiency. Firstly, the number of molecules in any piece of DNA was calculated. For the genome length, H37Rv was used as a reference strain. The genome length of H37Rv is 4411532 bp.

Number of copies = (ng of DNA x 6.022x10^23)/(genome length x 1x10^9 x 650)
= (507.5 x 6.022x10^23)/(4411532 bp x 1x10^9 x 650)
= 1.1 x 10^8 (number of genomes in 1 µL of DNA sample)

For primer efficiency, a 10-fold dilution series was made. To construct the first aliquot of the dilution series, a 50 µL volume is made using the following calculation:
C1V1 = C2V2
(1.1x10^8)V1 = (1x10^7)(50)
V1 = 4.5 µL

Primer efficiency was tested using the abovementioned calculations, and the mastermix in Table C5.2, prior to RT-qPCR to determine the ideal conditions for each primer set. It was found that all primers were efficient at an annealing temperature of 60˚C with excellent R^2 values (Table C5.1). Ct values are shown in Table C5.3 after the RT-qPCR run.

Table C5.1 Primer efficiency percentages and R^2 values for each primer

Gene	Primer efficiency (%)	R^2 value
glf	101.239	0.970
glmU	91.569	0.945
fadD32	101.599	0.974
fadE5	135.435	0.994
glpK	117.581	0.991
16S rRNA	175.01	0.983

Table C5.2 qPCR mastermix for a 10 µL reaction volume using the Ssoadvanced Universal SYBR Green Supermix kit(Bio-Rad, Hercules, CA, USA)

Reagent	X 1 reaction (µL)	X 10 reactions (µL)
SYBR Green	5	50
Primer (F)	1	10
Primer (R)	1	10
DNA	1	(1 µl added individually)
nH2O	2	20
Total	10	90

Table C5.3 Ct values obtained for each gene and sample after the RT-qPCR run

Replicate	Sample	Gene					
		glf	***glmU***	***fadd32***	***fadE5***	***glpK***	**16S rRNA**
1	WT1	23.321	26.194	17.696	19.173	22.672	6.841
	WT2	20.295	21.195	17.695	19.910	22.998	6.623
	WT3	19.615	20.064	17.636	19.220	23.753	7.530
	WT4	20.266	20.679	17.259	19.288	23.934	7.691
	M1	19.058	19.271	16.531	19.927	22.962	7.318
	M2	19.048	19.826	16.834	19.914	23.718	7.830
	M3	19.348	19.879	16.497	19.729	22.825	7.264
	M4	19.923	20.424	17.635	20.735	23.350	8.975
	C1	20.755	20.908	16.935	21.947	23.906	7.935
	C2	21.927	21.738	17.675	21.911	24.395	8.265
	C3	21.639	21.176	17.577	21.371	23.921	7.966
	C4	21.544	21.922	18.184	22.525	25.940	8.924
2	WT1	20.886	20.932	17.924	20.874	24.432	9.25
	WT2	21.284	21.074	18.087	20.784	24.275	9.36
	WT3	21.142	21.183	18.076	20.552	24.513	8.708
	WT4	21.123	21.636	18.185	20.94	25.375	9.67
	M1	20.289	20.35	17.329	20.673	23.739	8.924
	M2	20.956	21.059	17.944	21.963	24.844	10.182
	M3	19.803	20.075	16.871	21.068	23.922	9.057
	M4	21.144	21.103	17.969	21.806	24.601	10.125
	C1	21.505	20.986	17.512	21.993	23.315	9.614
	C2	22.407	21.475	17.878	22.16	24.951	10.064

	C3	21.931	21.185	17.252	22.325	24.315	9.826
	C4	22.209	21.411	17.693	22.144	25.15	10.201
3	WT1	19.48	20.256	17.195	20.673	24.454	6.699
	WT2	20.825	21.012	17.605	20.278	23.441	7.67
	WT3	18.898	19.652	17.443	18.989	23.548	9.094
	WT4	19.848	20.63	17.655	19.932	24.535	6.872
	M1	18.883	20.533	16.94	21.048	22.761	6.896
	M2	19.273	20.907	16.562	21.78	23.536	8.063
	M3	18.445	20.073	15.797	20.191	23.908	7.657
	M4	19.615	20.169	17.626	20.26	23.902	8.791
	C1	20.259	20.949	17.238	21.294	23.754	8.047
	C2	20.575	20.525	17.076	20.98	24.272	8.374
	C3	20.538	21.19	16.845	21.006	23.856	7.991
	C4	21.211	21.392	17.173	22.937	25.712	8.913

C6. Quality assurance for GCxGC-TOFMS analysis

To ensure analytical repeatability a quality control (QC) sample was injected intermittently throughout the GCxGC-TOFMS analysis. Principal Component Analysis (PCA), an unsupervised parametric projection approach used to summarize variation, depicted in the resulting scores plot (Figure C6.1). Scores represent samples (QC or grouped) as projected onto principal components (PC) or latent variables (LV) which were constructed as linear combinations of metabolites. The analysis was considered successful as the variability between experimental samples far exceeded the variability between QC sample analyses (Figure C6.1). Given that samples were replicates and the relatively small group sizes, outlier removal could not be justified.

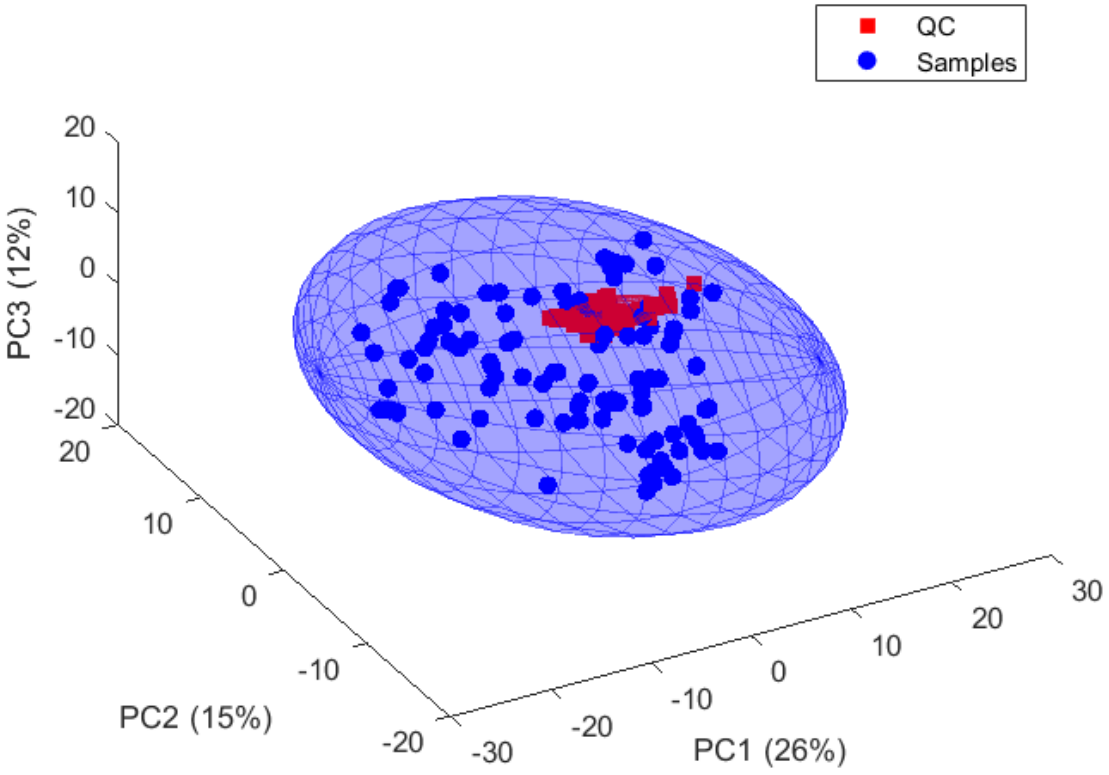

Figure C6. Quality assurance PCA scores plots. Projections of the QC samples (red) relative to the experimental samples (blue) with ellipses represent a 90% CI (confidence intervals) for experimental samples and 50% CI for QC injections.

C7. Principal Component Analysis (PCA) scores plots and Partial Least Squares Discriminant Analysis (PLS-DA) comparing the strains used in the study

The unsupervised PCA models generated from comparisons of WT to Δ*mtp* (Figure C7.1a) and WT to *mtp*-complemented (Figure C7.1c) strains illustrate good separation of data. The separation was reiterated by the supervised PLS-DA models generated from comparisons of WT to Δ*mtp* (Figure C7.1b) and WT to *mtp*-complemented (Figure C7.1d) strains.

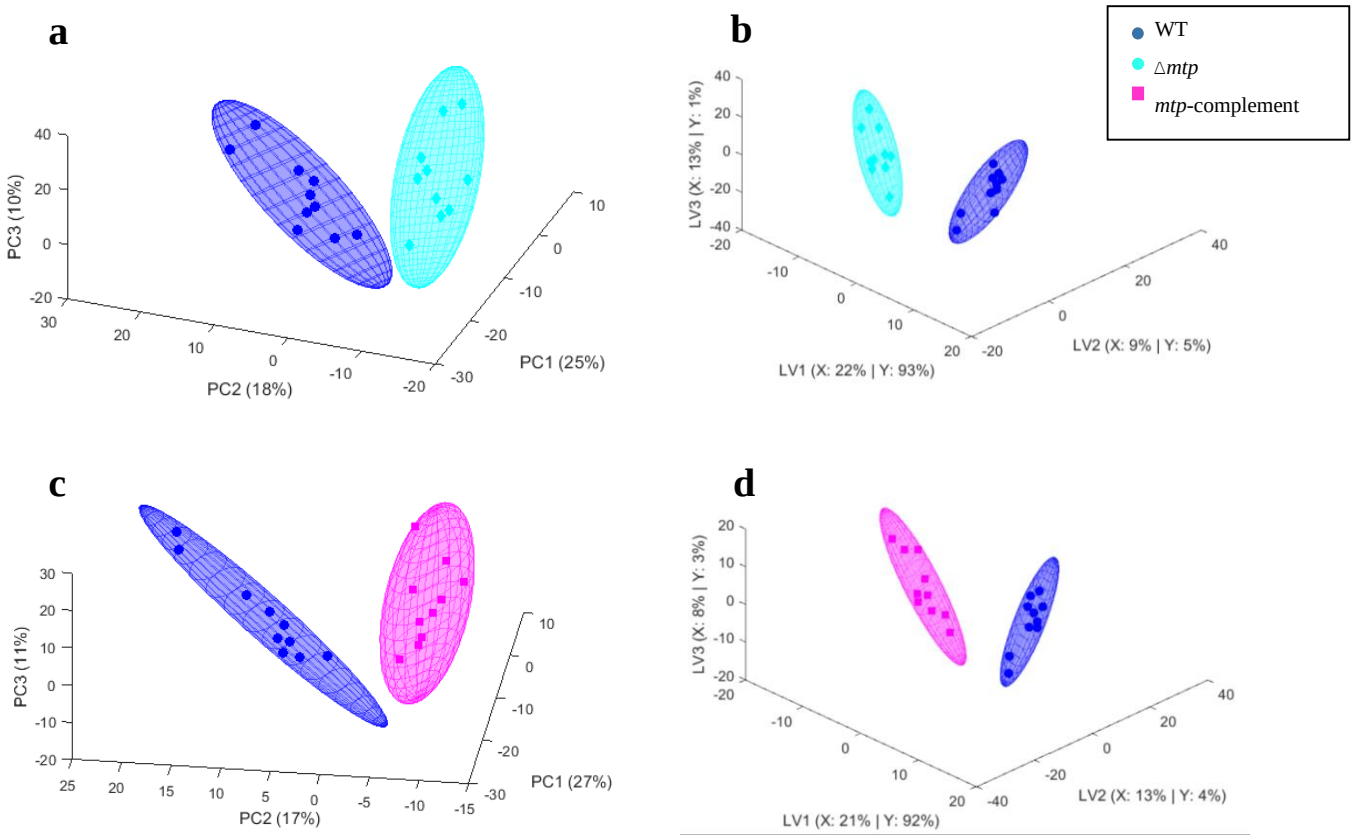

Figure C7. PCA and PLS-DA scores plot comparing the WT to the Δ*mtp* and *mtp*-complement. (a and c) PCA and (b and d) PLS-DA scores plots comparing (a and b) WT to Δ*mtp* and (c and d) WT to *mtp*-complement, respectively. WT metabolites (blue) are separated from those of Δ*mtp* (pink) and *mtp*-complement (cyan) in their respective models. All ellipses represent a 90% CI.

C8. Additional metabolites detected through two-dimensional gas chromatography coupled with time of flight mass spectrometry (GCxGC-TOFMS)

Statistically and biologically significant metabolites that met all selection criteria but were not supported by literature and analysis of metabolic metabolites and pathways using PubChem (Kim et al., 2019) and/or KEGG (Kanehisa et al., 2017), are indicated here. A total of 23 additional metabolites were detected in significantly varied relative concentrations between WT and Δ*mtp* are shown in Table C6.1. Majority of the detected metabolites were found in higher relative concentrations in the Δ*mtp* relative to the WT; six of the 23 metabolites, were found in lower relative concentrations. A total of nine additional metabolites were detected to be significantly different between WT and *mtp*-complement, shown in Table C6.2. Here, five metabolites were found in higher relative concentrations in the *mtp*- complement strain and four metabolites were found in relatively lower concentrations relative to the WT. Metabolites documented as analyte are those that were unknown metabolites.

References:

Larsen, M. H., Biermann, K., Tandberg, S., Hsu, T., and Jacobs Jr, W. R. (2007). Genetic manipulation of Mycobacterium tuberculosis. *Current Protocols in Microbiology*, *6*(1), 10A-2.

Ramsugit, S., Guma, S., Pillay, B., Jain, P., Larsen, M. H., Danaviah, S., et al. (2013). Pili contribute to biofilm formation *in vitro* in *Mycobacterium tuberculosis*. *Antonie Van Leeuwenhoek*, *104*(5), 725-735.

Table C8.1. Significant metabolites with unknown function between *M. tuberculosis* WT and Δ*mtp* strains selected as per multivariate and univariate selection criteria together with their respective mean relative concentration and standard deviation, fold change with respect to the WT, PLS-DA VIP value, effect size d-value and *p*-values

Metabolites	Mean relative concentration and standard deviation		Fold change	PLS-DA VIP	d-value	*p*-value
	WT	Δ*mtp*				
3-Nonanol	4.08E-04 (1.42E-04)	1.13E-03 (2.89E-04)	2.765	5.326	2.489	<0.001
3.5-Di-tert-butyl-4-trimethylsiloxy toluene	5.33E-04 (1.98E-04)	1.14E-03 (3.10E-04)	2.136	5.263	1.954	<0.001
2.4.6-Cycloheptatrien-1-one	4.75E-04 (1.74E-04)	1.37E-03 (4.17E-04)	2.888	5.138	2.149	<0.001
1-Trifluorosilyltridecane	3.66E-04 (2.45E-04)	1.46E-03 (5.17E-04)	3.987	5.009	2.117	<0.001
N-Trimethylsilylcyclohexylamine	1.73E-04 (1.50E-04)	5.39E-04 (1.80E-04)	3.117	4.423	2.028	<0.001
3.6.9.12-Tetraoxa-2.13-disilatetradecane	2.41E-03 (1.04E-03)	1.12E-03 (3.94E-04)	-2.148	2.681	1.245	0.003
Silane	1.91E-04 (1.73E-04)	5.24E-04 (2.67E-04)	2.746	2.084	1.247	0.005
Tetracosan-1-ol trimethylsilyl ether	1.42E-04 (6.31E-05)	2.86E-04 (1.36E-04)	2.010	1.775	1.059	0.010
Ethylbis(trimethylsilyl)amine	1.04E-04 (4.56E-05)	4.36E-05 (2.27E-05)	-2.377	1.415	1.317	0.003
Octadec-9Z-enol trimethylsilyl ether	5.97E-05 (1.36E-05)	4.06E-04 (1.87E-04)	6.800	1.073	1.849	<0.001
Camphoric acid	2.34E-04 (8.14E-05)	5.83E-05 (2.16E-05)	-4.013	7.550	2.160	<0.001
5-Nonanol	6.15E-05 (3.07E-05)	2.12E-04 (6.04E-05)	3.442	6.199	2.488	<0.001

Table C8.1. Significant metabolites with unknown function between *M. tuberculosis* WT and Δ*mtp* strains selected as per multivariate and univariate selection criteria together with their respective mean relative concentration and standard deviation, fold change with respect to the WT, PLS-DA VIP value, effect size d-value and *p*-values

Metabolites	Mean relative concentration and standard deviation		Fold change	PLS-DA VIP	d-value	*p*-value
	WT	Δ*mtp*				
2-O-Glycerol-à-d-galactopyranoside	1.58E-04 (5.70E-05)	5.07E-04 (6.32E-05)	-3.214	5.786	5.528	<0.001
á-D-(+)-Talopyranose	1.94E-04 (9.21E-05)	8.22E-04 (2.64E-04)	4.238	1.924	2.384	<0.001
E-7-Tetradecenol	6.64E-05 (1.6E-05)	3.63E-04 (2.08E-04)	5.456	1.553	1.425	0.002
Analyte 962	4.26E-04 (6.87E-05)	1.64E-04 (5.24E-05)	-2.604	8.854	3.825	<0.001
Analyte 667	8.85E-05 (4.84E-05)	2.03E-04 (6.21E-05)	2.299	6.382	1.852	<0.001
Analyte 696	5.58E-05 (1.51E-05)	3.22E-04 (7.75E-05)	5.761	4.673	3.432	<0.001
Analyte 178	1.40E-04 (4.98E-05)	6.66E-05 (3.06E-05)	-2.093	3.472	1.463	0.001
Analyte 659	3.32E-05 (1.00E-05)	9.28E-05 (3.85E-05)	2.794	1.806	1.547	0.001
Analyte 591	5.25E-04 (3.67E-04)	1.45E-03 (6.85E-04)	2.753	1.382	1.344	0.002
Analyte 730	7.78E-05 (3.61E-05)	3.16E-05 (1.81E-05)	-2.461	1.121	1.279	0.003

WT: wild-type; Δ*mtp*: *mtp*-gene knockout mutant strain; PLS-DA VIP: Partial Least Squares Discriminatory Analysis Variable in Projection value; Positive fold change = higher concentration in Δ*mtp*t; Negative fold change = higher concentration in WT.

Table C8.2. Significant metabolites with unknown function between *M. tuberculosis* WT and *mtp*-complemented strains selected as per multivariate and univariate selection criteria together with their respective mean relative concentration and standard deviation, fold change with respect to the WT, PLS-DA VIP value, effect size d-value and *p*-values

Metabolites	Mean relative concentration and standard deviation		Fold change	PLS-DA VIP	d-value	*p*-value
	WT	*mtp*-complement				
2-O-Glycerol-α-d-galactopyranoside	6.77E-05 (2.93E-05)	4.58E-04 (1.94E-04)	6.761	3.976	2.009	<0.001
2-Monopalmitoylglycerol	1.62E-04 (4.18E-05)	3.32E-04 (1.12E-04)	2.044	1.875	1.513	<0.001
3.6.10.13-Tetraoxa-2.14-disilapentadecane	1.89E-04 (5.76E-05)	7.14E-05 (2.61E-05)	-2.648	3.980	2.044	<0.001
2-Amino-4.6-dihydroxypyrimidine	1.65E-04 (1.37E-04)	6.4E-05 (4.56E-05)	-2.581	2.755	0.740	0.048
1.8-cis-Undecadien-5-yne 3.7-bis-trimethylsilyl ether	0.001 (5.35E-04)	7.10E-04 (1.94E-04)	-2.043	6.366	1.386	0.002
9-Tetradecenoic acid	0.002 (6.69E-04)	0.007 (0.002)	3.183	2.129	2.321	<0.001
α-D-(+)-Talopyranose	5.58E-04 (3.35E-04)	0.002 (3.52E-04)	2.713	1.671	2.272	<0.001
Allonic acid	2.78E-04 (1.75E-04)	8.07E-04 (1.74E-04)	2.903	4.777	3.021	<0.001
Analyte 1031	3.57E-04 (1.01E-04)	1.77E-04 (5.22E-05)	-2.020	5.239	1.791	0<.001

WT: wild-type; *mtp*-complement: *mtp*-complemented strain; PLS-DA VIP: Partial Least Squares Discriminatory Analysis Variable in Projection value; Positive fold change = higher concentration in *mtp*-complement; Negative fold change = higher concentration in WT.

Appendix D: Chapter 3 Supplementary Material

D1. Pilot study – Determination of optimal time point for infection

Four infection time points were investigated; 2, 4, 8 and 24 hr. Mid-log phase cultures of WT, Δ*mtp* and *mtp*-complement were used to infect A549 cells at an MOI of 5 and incubated (Shel Lab CO_2 Incubator, Cornelius, OR, USA) 37˚C, 5% CO_2 and 95% humidity for the respective time points. Uninfected A549 cells subjected to the same conditions were used as a control. After each time point, the flasks underwent a washing procedure with PBS, and the pellet was collected and weighed. For the remaining flasks (8 hr and 24 hr), extracellular bacteria were removed by washing twice with PBS (Sigma-Aldrich, St. Louis, MO, USA) after infection at 4 hr. Fresh 20 mL EMEM (Lonza, Basel, Switzerland) (10% FBS (BioWest, Nuaille, France)) was replaced and flasks were incubated (Shel Lab CO_2 Incubator, Cornelius, OR, USA) at 37˚C, 5% CO_2 and 95% humidity for the 8 hr and 24 hr time points. The resulting pellets were subjected to metabolite extraction, GCxGC-TOFMS analyses and statistical testing.

The final dataset used consisted of 16 samples with 579 variables for A549 cells. These were the variables deemed significant out of the ± 1000 metabolites detected from the total number of metabolites found per time point (Figure D1.1). The 24 hr time point produced the highest number of compounds, followed by the 8 hr, 2 hr and 4 hr time points (Figure D1.1). The following statistical tests focused on the 2 and 4 hr time points as they were more closely associated with the biological question of the study, i.e. the MTP adhesin, which is involved in the first point of contact to a host cell to establish infection. Hence, the aim was to determine the more optimal time point for infection between the 2 and 4 hrs. Batch effect correction using quality control samples and mean scaling was done to correct for any analytical or technical variation. Univariate comparisons to time 0 considered an independent samples *t*-test *p*-value to assess statistical significance and Cohen's d-value as effect size to establish practical relevance. The volcano plot shows the scatter of the metabolites (Figure D1.2). The red dots in particular that are located above the horizontal red line represents both statistical and practical relevance. The 2 hr plot (Figure D1.2a) displayed a greater number of differentiating metabolites of statistical and practical significance, compared to the 4 hr plot (Figure D1.2b). The 3D PCA and PLS-DA plots were generated to show group observations. For the PCA, the 2 hr plot (Figure D1.3a) showed clearer separation compared to the 4 hr plot (Figure D1.3b). For the PLS-DA plots, there is clear separation between both groups of time points (Figure D1.4). The 2 and 4 hr time points detected almost similar numbers of metabolites (Figure D1.1), but the 2 hr consisted of more practically and statistically significant metabolites (Figure D1.2), and additionally had better separation of infected and uninfected groups (Figures D1.3 and D1.4). Collectively, this validated the 2 hr time point as the optimal time point for infection.

Figure D1.1 Bar graph showing total counts of compounds extracted for each incubation time period and the control. Overall, the number of compounds differed slightly between the four time points tested. The 24 hr time point produced the highest number of compounds, followed by the 8 hr, 2 hr and 4 hr time points. All time points produced a greater but comparable number of compounds compared to the control group.

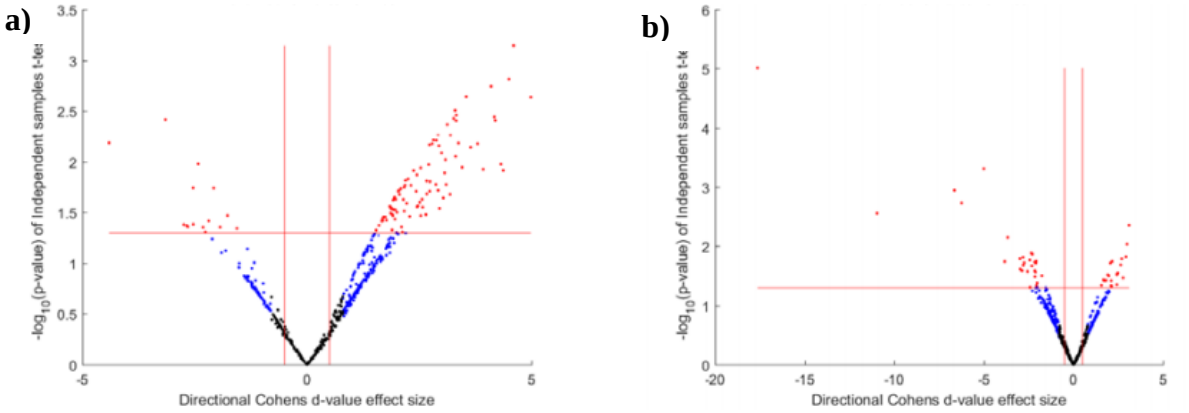

Figure D1.2 Volcano plots showing parametric univariate spread of data across *M. tuberculosis*-infected A549 epithelial cells for a 2 hr (a) and 4 hr (b) incubation period. Practical (blue), statistical and practical (red) or neither (black) significance is depicted by the dots. The horizontal threshold (red line) represents a 5 % significance level, while the vertical thresholds (red lines) represent a |Cohen's d-value| = 0.5. There is a larger number of variables in the 2 hr plot compared to the 4 hr plot.

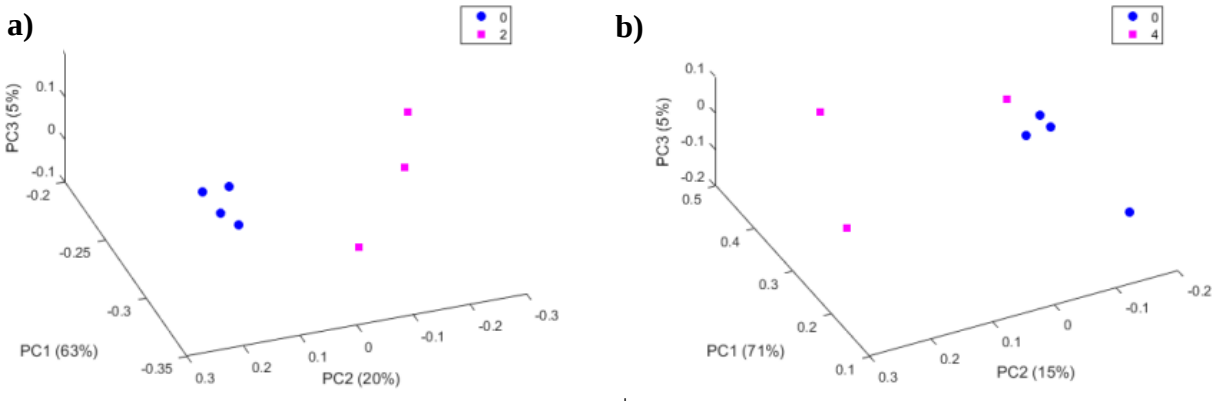

Figure D1.3 Three-dimensional PCA scores plots for uninfected and *M. tuberculosis*-infected A549 epithelial cells at a 2 hr (a) and 4 hr (b) incubation period. Clear separation of groups can be seen between the uninfected and infected A549 epithelial cells at 2 hrs (a) compared to the 4 hr plot (b).

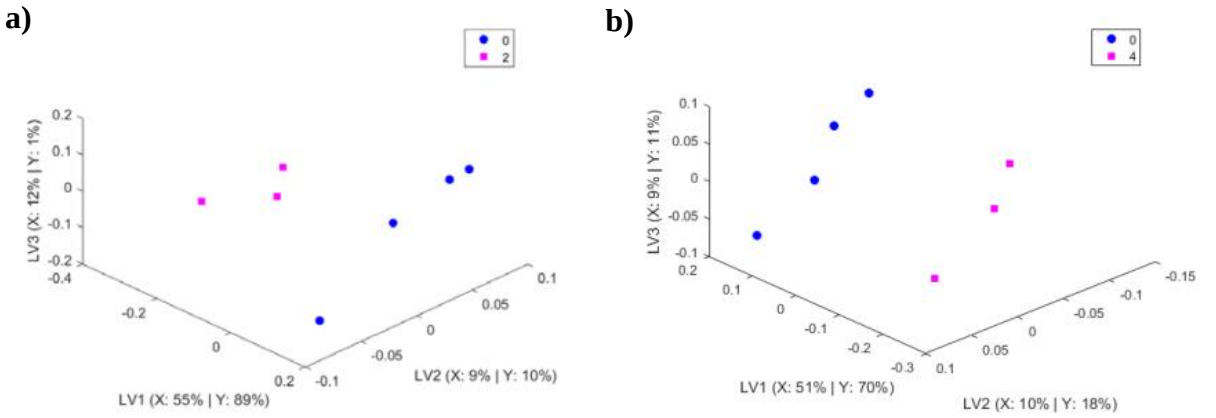

Figure D1.4 Three-dimensional PLS-DA scores plots for uninfected and *M. tuberculosis*-infected A549 epithelial cells at a 2 hr (a) and 4 hr (b) incubation period. Clear separation of groups can be seen between the uninfected and infected A549 epithelial cells at 2 hrs (a) and at 4 hrs (b).

D2. Bacterial CFU counts and significance values

After the bacterial inocula were prepared and added to the respective flasks (Nest Biotechnology, Jiangsu, China) for infection, an aliquot of the inoculum of each strain was used to determine the multiplicity of infection (MOI) and the colony forming units (CFU)/mL at the time of infection. The cultures were 10-fold serially diluted in microcentrifuge tubes (Merck, Dermstadt, Germany) by adding 100 µL of OD_{600nm} 1 (Lightwave II, Biochrom, Cambridge, UK) bacterial inoculum to 900 µL of 7H9

(Difco, Becton-Dickinson, Franklin Lakes, NJ, USA) broth. A volume of 100 µL was plated onto 7H11 (Difco, Becton-Dickinson, Franklin Lakes, NJ, USA) agar plates. Plates were sealed in CO_2 permeable plastic bags and incubated (Shel Lab CO_2 Incubator, Cornelius, OR, USA) at 37°C for 3 weeks and colonies were then counted (Table D2.1). Formulae for MOI and CFU/mL are shown below. GraphPad Prism version 8 software (GraphPad Software, La Jolla, CA, USA) was used to assess the significance levels between combinations of the three strains using non-parametric, unpaired Mann Whitney testing. All the *p*-values were above 0.05 hence the differences between the CFU/mL values of the strains were non-significant (Table D2.2). Hence, any observations detected in the experimental results were attributed to the deletion of *mtp* and not from any other variation in experimental conditions.

After the 2 hr infection period and Triton-X 100 (Millipore, Merck, Dermstadt, Germany) treatment, the same serial dilution method as above was used to determine the CFU/mL for each strain after infection (Table D2.3). After significance testing using GraphPad Prism, there were significant differences between WT and Δ*mtp,* and between Δ*mtp* and *mtp*-complement, with no significant differences between WT and *mtp*-complement (Table D2.4). This was expected as the deletion of *mtp* in the mutant strain resulted in less adhesion and decreased invasion (0.840×10^5 CFU/mL) of *M. tuberculosis* (Ramsugit et al., 2016). The non-significance between the WT and *mtp*-complement was also expected which indicates that *mtp* was successfully knocked back in. The average CFU/mL for the complemented strain (1.288×10^5 CFU/mL) was slightly higher than the WT (1.174×10^5 CFU/mL) possibly due to the overexpressing *mtp* gene in the complemented strain. Table D2.5 displays the weights of the pellet collected for each of the 10 replicates for each infected and uninfected sample.

$$\text{MOI} = \frac{(\text{Average bacterial CFU/mL}) \times (\text{volume of inoculum in mL})}{(\text{Host cell count at the time of infection in CFU/mL}) \times (\text{total cell count volume in mL})}$$

$$\text{CFU/mL} = \frac{(\text{Average number of colonies})}{(\text{volume plated in mL}) \times (\text{dilution factor})}$$

Table D2.1 Colony forming units (CFU) and multiplicity of infection (MOI) values for each strain done in triplicate at the time of infection

Strain	Dilution	Rep 1	Rep 2	Rep 3	CFU/mL	MOI
WT	-4	>200	>200	>200	[(85+82+89)/3] x (10 x 10^5) = 8.53 x 10^7	(8.53x 10^7 x 1)/ (4.45 x 10^6 x 4) = 4.79
	-5	85	82	89		
	-6	8	13	12		
Δ*mtp*	-4	>200	>200	>200	[(36+37+48)/3] x (10 x 10^5) = 4.03 x 10^7	(4.03x 10^7 x 1.1)/ (2.6 x 10^6 x 4) = 4.27
	-5	36	37	48		
	-6	1	3	2		
***mtp*-complement**	-4	>200	>200	>200	[(37+44+41)/3] x (10 x 10^5) = 4.07 x 10^7	(4.07x 10^7 x 0.9)/ (2.1 x 10^6 x 4) = 4.36
	-5	37	44	41		
	-6	2	5	3		

Rep = replicate; CFU = colony forming units; MOI = multiplicity of infection

Table D2.2 Significance testing between the three *M. tuberculosis* strains at the time of infection

Strain comparison	*p*-value	Significance
WT and Δ*mtp*	0.1000	None
Δ*mtp* and *mtp*-complement	0.8000	None
WT and *mtp*-complement	0.1000	None

Table D2.3 Average colony forming units (CFU) for each infected strain after the 2 hour infection period

Flask	WT (CFU/ml)	Δ*mtp* (CFU/ml)	*mtp*-complement (CFU/ml)
1	1.15 x 10^5	0.82 x 10^5	1.14 x 10^5
2	1.40 x 10^5	0.88 x 10^5	1.22 x 10^5
3	1.22 x 10^5	0.90 x 10^5	1.27 x 10^5
4	1.27 x 10^5	1.06 x 10^5	1.17 x 10^5
5	1.29 x 10^5	0.80 x 10^5	1.31 x 10^5
6	1.11 x 10^5	0.85 x 10^5	1.27 x 10^5
7	1.16 x 10^5	0.77 x 10^5	1.14 x 10^5
8	0.99 x 10^5	0.74 x 10^5	1.23 x 10^5
9	1.19 x 10^5	0.87 x 10^5	1.53 x 10^5
10	0.96 x 10^5	0.71 x 10^5	1.60 x 10^5
Average	1.174 x 10^5	0.840 x 10^5	1.288 x 10^5

Table D2.4 Significance testing between the three *M. tuberculosis* strains infecting A549 epithelial cells after the 2 hour infection period

Strain comparison	*p*-value	Significance
WT and Δ*mtp*	< 0.0001	Yes
Δ*mtp* and *mtp*-complement	< 0.0001	Yes
WT and *mtp*-complement	0.1704	None

Table D2.5 Pellet weight (mg) collected for the three *M. tuberculosis*-infected A549 epithelial cells after the 2 hour infection period for uninfected and infected samples for the 10 replicates

Sample	Replicate	WT (mg)	Δ*mtp* (mg)	*mtp*-complement (mg)
Uninfected	1	30.3	47.9	40.4
	2	31.6	37.8	40.3
	3	28.4	42.4	43.4
	4	35.5	36.9	45.0
	5	28.2	44.1	41.6
	6	33.1	43.5	38.0
	7	29.7	47.5	44.7
	8	33.3	38.4	42.9
	9	27.9	35.6	35.9
	10	28.5	41.3	36.7
Infected	1	32.4	43.8	37.5
	2	31.1	38.5	36.9
	3	29.9	47.6	54.3
	4	31.2	33.4	45.8
	5	31.2	37.8	47.9
	6	33.7	35.9	37.1
	7	33.5	42.6	38.7
	8	26.3	45.0	37.0
	9	30.2	42.8	50.5
	10	30.0	37.9	35.6

D3. Supplementary statistical data and calculations

To ensure analytical repeatability, a quality control (QC) sample was injected intermittently throughout the GCxGC-TOFMS analysis. The analysis was considered successful as the variability between experimental samples far exceeded the variability between QC sample analyses. Principal Component Analysis (PCA), an unsupervised parametric projection approach used to summarize variation, was employed. Figure D3 displays the resulting scores plot. Scores represent samples (QC or grouped) as projected onto principal components (PC) or latent variables (LV) which were constructed as linear combinations of metabolites.

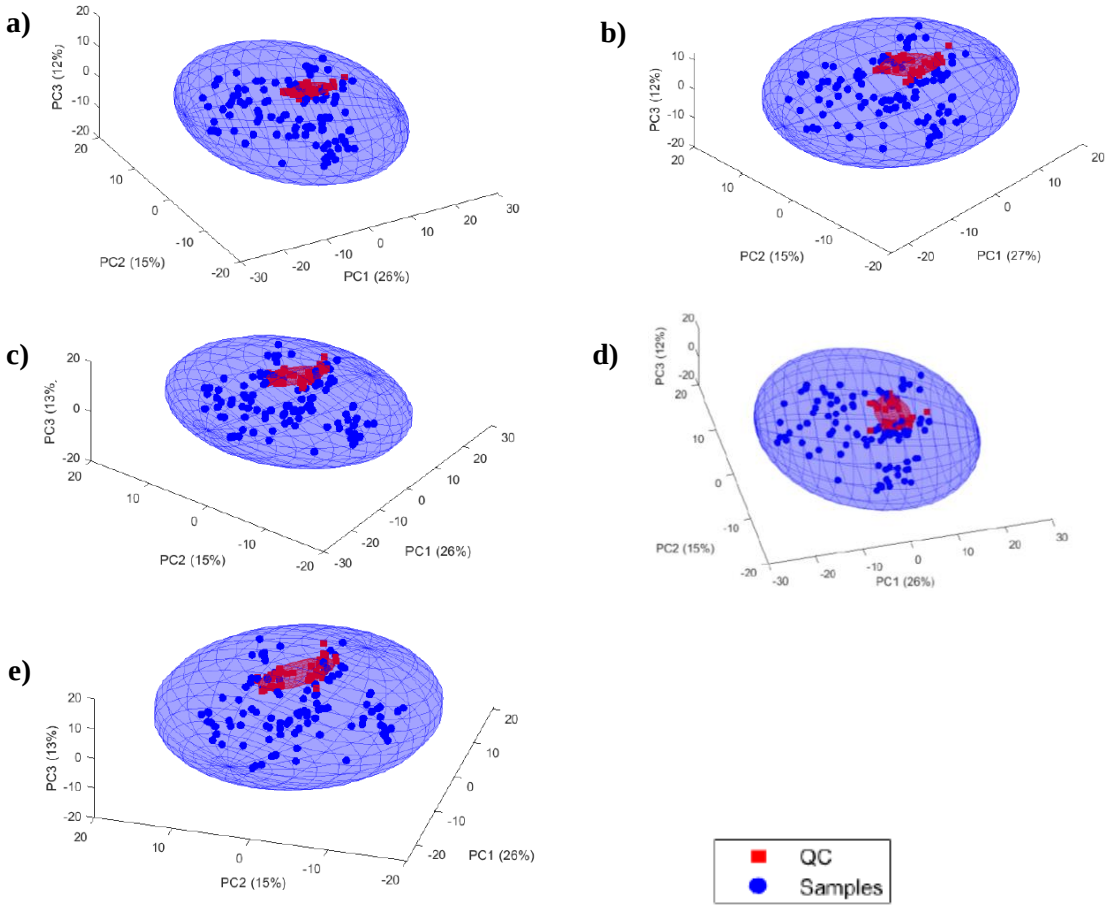

Figure D3. Quality assurance PCA scores plots showing projections of the QC samples relative to the experimental samples. Ellipses represent a 95 % CI (confidence interval) for experimental samples and 50 % CI for QC injections. Comparisons between WT-infected and WT-uninfected A549 cells (a), Δ*mtp*-infected and Δ*mtp*-uninfected A549 cells (b), *mtp*-complement-infected and *mtp*-complement-uninfected A549 cells (c), WT-infected and Δ*mtp*-infected A549 cells (d), and lastly, WT-infected and *mtp*-complement-infected A549 cells (e), all show that the signal outweighs the noise.

Additional statistical calculations:

1. The coefficient of variation (CV) assesses repeatability and provides a way to quantify signal to noise. This was calculated as follows:

$$\left(\frac{sd(X_I)}{\bar{X}_I}\right).100\%$$

where *sd* represents the standard deviation of infected replicates and $\overline{X}_I$ represents the average at a give incubation time (*I*).

2. Cohen's d-value or effect size is calculated as follows:

$$\frac{|\overline{X}_1 - \overline{X}_2|}{\max(s_1; s_2)}$$

where $\overline{X}_1$ and $\overline{X}_2$ represent the means while s_1 and s_2 represent the standard deviations of the respective groups.

3. Fold change (FC) values are also included in the sheet to provide an additional measure of practical significance. FC values were calculated as follows:

$$sign(\bar{X}_1 - \bar{X}_2).\, 2^{|\log_2(\bar{X}_1) - \log_2(\bar{X}_2)|}$$

where the sign of the difference between the means are added after calculation and indicates the direction of the change (up- or down-regulated).

D4. Additional metabolites from the models in this investigation

Four of the five models tested in this investigation did not validate. A few metabolites were detected but lacked statistical rigour to be classified as potential metabolites and were omitted from further inspection. These metabolites included aucubin and niacin for all four models (WT-infected vs. uninfected; Table D4.1), in addition to, 1.2,3-butanetriol and allonic acid between the Δ*mtp*-infected and Δ*mtp*-uninfected A549 cell model (Table D4.2), 5-dodecenoic acid between the *mtp*-complement-infected and *mtp*-complement-uninfected A549 cell model (Table D4.3) and 5-dodecenoic acid, hydracrylic acid and L-aspartic between the WT-infected and *mtp*-complement-infected A549 cells (Table D4.4).

The WT-infected and Δ*mtp*-infected model did validate. Only those metabolites that met all four selection criteria were included in the investigation. Metabolites that met less than four of the selection criteria or those with limited or no biological function are listed in Table D4.5. In addition, duplicated metabolites were excluded. From the duplicated metabolites, the metabolite with better discriminatory ability (based on the more optimal selection criteria values) were selected for the main analysis.

Table D4.1 Metabolites between *M. tuberculosis* WT-uninfected A549 epithelial cells and WT-infected A549 epithelial cells selected as per multivariate and univariate selection criteria together with their respective mean relative concentration and standard deviation, fold change with respect to the WT, effect size d-value and *p*-values

Metabolite	Mean relative concentration and standard deviation		Fold change	Effect size	*p*-value
	Uninfected A549	WT-infected A549			
Aucubin	0.013 (0.0391)	1.014 (0.340)	77.674	3.57	>0.001
Niacin	14.537 (4.086)	49.097 (13.990)	3.377	3.79	>0.001

Table D4.2 Metabolites between *M. tuberculosis* Δ*mtp*-uninfected A549 epithelial cells and Δ*mtp*-infected A549 epithelial cells selected as per multivariate and univariate selection criteria together with their respective mean relative concentration and standard deviation, fold change with respect to the WT, effect size d-value and *p*-values

Metabolite	Mean relative concentration and standard deviation		Fold change	Effect size	*p*-value
	Uninfected A549	ΔMTP-infected A549			
Niacin	9.451 (3.434)	30.960 (5.507)	-3.276	3.42	>0.001
Aucubin	0	0.803 (0.370)	-	2.66	>0.001
1.2,3-Butanetriol	0	1.751 (1.613)	-	1.13	0.01
Allonic acid, ç-lactone	0.094 (0.195)	0.650 (0.697)	-6.939	0.79	0.05

Table D4.3 Metabolites between *M. tuberculosis mtp*-complement-uninfected A549 epithelial cells and *mtp*-complement-infected A549 epithelial cells selected as per multivariate and univariate selection criteria together with their respective mean relative concentration and standard deviation, fold change with respect to the WT, effect size d-value and *p*-values

Metabolite	Mean relative concentration and standard deviation		Fold change	Effect size	*p*-value
	Uninfected A549	cMTP-infected A549			
Niacin	16.866 (5.008)	143.032 (43.550)	-8.481	6.75	>0.001
Aucubin	0	3.836 (1.513)	-	4.61	>0.001
5-Dodecenoic acid	19.165 (9.612)	9.511 (3.267)	2.015	1.06	0.02

Table D4.4 Metabolites between *M. tuberculosis* WT-infected A549 epithelial cells and *mtp*-complement-infected A549 epithelial cells selected as per multivariate and univariate selection criteria together with their respective mean relative concentration and standard deviation, fold change with respect to the WT, effect size d-value and *p*-values

Metabolite	Mean relative concentration and standard deviation		Fold change	Effect size	*p*-value
	WT-infected A549	cMTP-infected A549			
Aucubin	1.014 (0.340)	3.836 (1.513)	3.785	2.643	>0.001
Niacin	49.097 (13.990)	143.032 (43.550)	2.913	3.422	>0.001
5-Dodecenoic acid	21.972 (9.504)	9.511 (3.267)	-2.310	1.348	0.004
Hydracrylic acid	8.876 (4.378)	3.672 (1.214)	-2.417	1.312	0.004
L-Aspartic acid	0.108 (0.323)	0.645 (0.433)	6.002	1.260	0.009

Table D4.5 Additional metabolites between *M. tuberculosis* WT-infected A549 epithelial cells and Δ*mtp*-infected A549 epithelial cells selected as per multivariate and univariate selection criteria together with their respective mean relative concentration and standard deviation, fold change with respect to the WT, PLS-DA VIP value, effect size d-value and *p*-values

Metabolite	Mean relative concentration and standard deviation		Fold change	PLS-DA VIP	d-value	*p*-value
	WT-infected A549	ΔMTP-infected A549				
9H-Purin-6-ol	1984.958 (452.048)	68.304 (249.204)	-2.909	1.906	1.870	<0.001
2-(Methylamino)ethanol	93.639 (4.182)	8.181 (10.005)	-11.445	1.7179	2.590	<0.001
Isoserine	14.482 (4.314)	0.668 (0.811)	-21.687	1.702	6.450	<0.001
meso-Erythritol	47.440 (12.962)	12.014 (3.755)	-3.949	1.639	4.030	<0.001
Methane	16.173 (9.311)	2.108 (2.574)	-7.673	1.450	2.980	<0.001
S-[2-[N,N-Dimethylamino]ethyl]N,N-dimethylcarbamoyl thiocarbohydroximate	956.945 (408.358)	297.797 (143.504)	-3.213	1.341	2.210	<0.001
N-(Trimethylsilyl)hexanamide	74.969 (43.628)	28.431 (28.150)	-2.637	1.297	0.990	0.020
Pseudo uridine penta	83.146 (24.768)	35.820 (32.746)	-2.321	1.243	0.980	0.020
Triethylamine	8.105 (5.959)	2.126 (2.802)	-3.812	1.180	1.610	<0.001
2-Amino-1-methyl-1H-imidazol-4-ol	175.057 (66.965)	20.947 (7.901)	-8.357	1.137	4.460	<0.001
L-Glutamic acid	2943.834 (935.964)	1171.391 (556.274)	-2.513	1.078	0.760	0.050
7-(Trimethylsilyl)-2,6-bis[(trimethylsilyl)oxy]-7H-purine	130.889 (35.720)	63.233 (29.380)	-2.070	1.040	0.940	0.020
Asparagine	526.793 (132.550)	170.150 (64.799)	-3.096	0.993	2.080	<0.001
Glycine	6273.537 (3415.854)	1834.543 (1147.27)	-3.420	0.971	1.840	<0.001

Table D4.5 Additional metabolites between *M. tuberculosis* WT-infected A549 epithelial cells and Δ*mtp*-infected A549 epithelial cells selected as per multivariate and univariate selection criteria together with their respective mean relative concentration and standard deviation, fold change with respect to the WT, PLS-DA VIP value, effect size d-value and *p*-values

Metabolite	Mean relative concentration and standard deviation		Fold change	PLS-DA VIP	d-value	*p*-value
	WT-infected A549	ΔMTP-infected A549				
N-acetyl aspartic acid	149.713 (66.127)	15.305 (7.897)	-9.783	1.938	2.692	<0.0001
L-Proline	6394.195 (1254.392)	3228.925 (1444.828)	-1.980	1.823	0.646	0.160
Niacinamide	294.041 (102.351)	31.766 (11.381)	-7.839	1.769	4.272	<0.0001
Pyroglutamic acid	910.118 (243.443)	270.484 (84.187)	-3.365	1.687	3.947	<0.0001
Doconexent	195.806 (74.338)	332.464 (123.114)	1.698	1.246	1.364	0.020
Phenylalanine	1519.419 (345.257)	907.344 (345.259)	-1.753	1.214	1.767	<0.0001
Palmitelaidic acid	618.152 (153.823)	1029.649 (173.692)	1.665	1.192	2.077	<0.0001
Propanal	1033.288 (307.364)	227.584 (47.767)	-4.452	1.186	4.589	<0.0001
L-Lysine	1253.447 (369.372)	847.162 (363.143)	-1.480	1.185	0.639	0.170
Arachidonic acid	454.390 (128.121)	744.116 (188.414)	1.637	1.183	1.839	<0.0001
á-Alanine	208.955 (128.126)	28.533 (22.324)	-7.323	1.178	1.631	0.010
L-Tyrosine	1756.203 (396.027)	1084.737 (395.464)	-1.619	1.128	1.152	0.020
Octopamine	18.226 (9.663)	4.942 (2.674)	-3.687	1.123	1.848	<0.0001
Phosphoric acid	19.028 (6.074)	35.221 (5.165)	1.851	1.113	1.912	<0.0001
L-Valine	2979 (743.357)	2007.646 (813.405)	-1.483	1.080	0.640	0.170
Linolenic acid	216.224 (85.571)	330.927 (90.256)	1.530	0.981	1.262	0.020
Pyrimidine	70.599 (18.605)	40.660 (10.278)	-1.736	0.979	1.784	<0.0001
Eicosapentanoic acid	326.572 (77.470)	509.426 (187.755)	1.559	0.911	1.311	0.020
Heptadecanoic acid	140.067 (36.630)	213.200 (51.674)	1.522	0.892	1.617	0.010
Oleic acid	2532.639 (720.243)	3976.911 (1215.284)	1.570	0.881	1.275	0.020
L-Methionine	580.628 (126.268)	373.348 (147.672)	-1.555	0.874	1.168	0.020
Octadecanoic acid	2263.082 (648.600)	3191.089 (816.195)	1.410	0.815	1.213	0.040
L-Tryptophan	158.199 (43.016)	103.860 (21.564)	-1.523	0.636	1.467	0.010
Pentanedioic acid	2.352 (1.328)	0.285 (0.444)	-8.251	0.622	1.773	<0.0001
Tetradecanoic acid	721.967 (138.152)	989.812 (256.144)	1.371	0.541	1.251	0.030
Glyceric acid	60.972 (18.540)	90.527 (28.859)	1.485	0.524	1.210	0.030
L-Threonine	929.949 (216.722)	635.233 (143.201)	-1.464	0.425	1.590	0.010
Niacin	49.097 (13.990)	30.960 (5.507)	-1.586	0.289	1.384	0.010

Table D4.5 Additional metabolites between *M. tuberculosis* WT-infected A549 epithelial cells and Δ*mtp*-infected A549 epithelial cells selected as per multivariate and univariate selection criteria together with their respective mean relative concentration and standard deviation, fold change with respect to the WT, PLS-DA VIP value, effect size d-value and *p*-values

Metabolite	Mean relative concentration and standard deviation		Fold change	PLS-DA VIP	d-value	*p*-value
	WT-infected A549	ΔMTP-infected A549				
4-Hydroxybutanoic acid	9.834 (4.629)	2.923 (2.026)	-3.363	0.776	1.61	<0.001
L-Ornithine	79.450 (26.956)	25.297 (3.140)	-3.140	0.767	1.54	<0.001
1-Decanamine	7.596 (2.584)	3.133 (1.345)	-2.424	0.758	2.25	<0.001
Phosphorylethanolamine	269.487 (218.840)	66.943 (62.230)	-4.025	0.748	1.69	<0.001
L-(-)-Sorbose	50.396 (27.620)	11.303 (7.773)	-4.458	0.633	1.59	<0.001
Hydracrylic acid	8.876 (4.378)	3.090 (0.717)	-2.872	0.626	1.55	<0.001
Pentanedioic acid	2.352 (1.328)	0.285 (0.444)	-8.251	0.622	1.77	<0.001
Allonic acid, ç-lactone	8.894 (7.712)	0.649 (0.697)	-13.689	0.961	1.99	<0.001
Octanoic acid	6.302 (5.713)	2.258 (1.031)	-2.790	0.948	1.10	0.010
N-Acetyl-D-glucosamine	23.879 (9.895)	5.673 (3.898)	-4.208	0.937	1.83	<0.001
1,2-Dihydroxy-4-Methylpentane	3.020 (2.148)	1.067 (1.492)	-2.830	0.845	1.21	0.02
Glycine	5605.814 (2729.198)	1529.161(1110.116)	-3.665	0.830	1.38	0.01
Phosphoethanolamine	447.512 (217.014)	133.829 (104.548)	-3.343	0.829	1.35	<0.001
Ribitol	74.990 (39.358)	34.694 (42.643)	-2.161	0.789	1.17	0.010
4-Hydroxyphenyllactic acid	4.244 (1.641)	0.080 (0.240)	-52.899	0.602	3.36	<0.001
Lactic acid	186.778 (94.538)	54.730 (15.606)	-3.412	0.570	2.30	<0.001
Citric acid	2.466 (1.269)	0.907 (0.265)	-2.718	0.411	1.05	0.010
Homoserine	0.326 (0.350)	0	-	0.283	1.09	0.010
Butanedioic acid	3.521 (1.160)	1.548 (0.414)	-2.273	0.232	176	<0.001

Appendix E: Turnitin Reports

(attached after this page)

Introduction and Literature Review

ORIGINALITY REPORT

8%	3%	3%	6%
SIMILARITY INDEX	INTERNET SOURCES	PUBLICATIONS	STUDENT PAPERS

PRIMARY SOURCES

1	Submitted to University of KwaZulu-Natal Student Paper	2%
2	apps.who.int Internet Source	1%
3	Submitted to North West University Student Paper	1%
4	Saiyur Ramsugit, Balakrishna Pillay, Manormoney Pillay. "Evaluation of the role of Mycobacterium tuberculosis pili (MTP) as an adhesin, invasin, and cytokine inducer of epithelial cells", The Brazilian Journal of Infectious Diseases, 2016 Publication	1%
5	Kuan, Chee Sian, Chai Ling Chan, Su Mei Yew, Yue Fen Toh, Jia-Shiun Khoo, Jennifer Chong, Kok Wei Lee, Yung-Chie Tan, Wai-Yan Yee, Yun Fong Ngeow, and Kee Peng Ng. "Genome Analysis of the First Extensively Drug-Resistant (XDR) Mycobacterium tuberculosis in Malaysia Provides Insights into the Genetic Basis of Its	<1%

Deletion of M. tuberculosis curli pili (MTP) reveals alterations in cell wall biogenesis, fatty acid metabolism and amino acid synthesis in a metabolomics investigation using GCxGC-TOFMS

ORIGINALITY REPORT

8%	2%	5%	6%
SIMILARITY INDEX	INTERNET SOURCES	PUBLICATIONS	STUDENT PAPERS

PRIMARY SOURCES

1	Submitted to University of KwaZulu-Natal Student Paper	1%
2	Submitted to North West University Student Paper	1%
3	academicjournals.org Internet Source	1%
4	Submitted to University of Pretoria Student Paper	1%
5	Du Toit Loots, Conrad C. Swanepoel, Mae Newton-Foot, Nicolaas C. Gey van Pittius. "A metabolomics investigation of the function of the ESX-1 gene cluster in mycobacteria", Microbial Pathogenesis, 2016 Publication	<1%
6	Reinart J. Meissner-Roloff, Gerhard Koekemoer, Robert M. Warren, Du Toit Loots. "A metabolomics investigation of a hyper- and	<1%

M. tuberculosis curli pili (MTP) is associated with significant host metabolic pathways in an A549 epithelial cell infection model and contributes to the pathogenicity of M. tuberculosis

ORIGINALITY REPORT

5%	1%	3%	3%
SIMILARITY INDEX	INTERNET SOURCES	PUBLICATIONS	STUDENT PAPERS

PRIMARY SOURCES

1	Submitted to University of KwaZulu-Natal Student Paper	2%
2	Saiyur Ramsugit, Balakrishna Pillay, Manormoney Pillay. "Evaluation of the role of Mycobacterium tuberculosis pili (MTP) as an adhesin, invasin, and cytokine inducer of epithelial cells", The Brazilian Journal of Infectious Diseases, 2016 Publication	1%
3	Sinthujan Jegaskanda, Hillary A Vanderven, Hyon-Xhi Tan, Sheilajen Alcantara et al. "Influenza infection enhances antibody-mediated NK cell functions via Type I interferon dependent pathways", Journal of Virology, 2018 Publication	<1%
4	Korea, C. G., G. Balsamo, A. Pezzicoli, C. Merakou, S. Tavarini, F. Bagnoli, D. Serruto, and M. Unnikrishnan. "Staphylococcal Esx Proteins Modulate Apoptosis and Release of	<1%